

# Biocatalysis and biotransformation guided by protein engineering

**Edited by**

Hui-Min Qin, Masaru Tanokura, Weidong Liu  
and Rey-Ting Guo

**Published in**

Frontiers in Bioengineering and Biotechnology



## FRONTIERS EBOOK COPYRIGHT STATEMENT

The copyright in the text of individual articles in this ebook is the property of their respective authors or their respective institutions or funders. The copyright in graphics and images within each article may be subject to copyright of other parties. In both cases this is subject to a license granted to Frontiers.

The compilation of articles constituting this ebook is the property of Frontiers.

Each article within this ebook, and the ebook itself, are published under the most recent version of the Creative Commons CC-BY licence. The version current at the date of publication of this ebook is CC-BY 4.0. If the CC-BY licence is updated, the licence granted by Frontiers is automatically updated to the new version.

When exercising any right under the CC-BY licence, Frontiers must be attributed as the original publisher of the article or ebook, as applicable.

Authors have the responsibility of ensuring that any graphics or other materials which are the property of others may be included in the CC-BY licence, but this should be checked before relying on the CC-BY licence to reproduce those materials. Any copyright notices relating to those materials must be complied with.

Copyright and source acknowledgement notices may not be removed and must be displayed in any copy, derivative work or partial copy which includes the elements in question.

All copyright, and all rights therein, are protected by national and international copyright laws. The above represents a summary only. For further information please read Frontiers' Conditions for Website Use and Copyright Statement, and the applicable CC-BY licence.

ISSN 1664-8714  
ISBN 978-2-83251-804-5  
DOI 10.3389/978-2-83251-804-5

## About Frontiers

Frontiers is more than just an open access publisher of scholarly articles: it is a pioneering approach to the world of academia, radically improving the way scholarly research is managed. The grand vision of Frontiers is a world where all people have an equal opportunity to seek, share and generate knowledge. Frontiers provides immediate and permanent online open access to all its publications, but this alone is not enough to realize our grand goals.

## Frontiers journal series

The Frontiers journal series is a multi-tier and interdisciplinary set of open-access, online journals, promising a paradigm shift from the current review, selection and dissemination processes in academic publishing. All Frontiers journals are driven by researchers for researchers; therefore, they constitute a service to the scholarly community. At the same time, the *Frontiers journal series* operates on a revolutionary invention, the tiered publishing system, initially addressing specific communities of scholars, and gradually climbing up to broader public understanding, thus serving the interests of the lay society, too.

## Dedication to quality

Each Frontiers article is a landmark of the highest quality, thanks to genuinely collaborative interactions between authors and review editors, who include some of the world's best academicians. Research must be certified by peers before entering a stream of knowledge that may eventually reach the public - and shape society; therefore, Frontiers only applies the most rigorous and unbiased reviews. Frontiers revolutionizes research publishing by freely delivering the most outstanding research, evaluated with no bias from both the academic and social point of view. By applying the most advanced information technologies, Frontiers is catapulting scholarly publishing into a new generation.

## What are Frontiers Research Topics?

Frontiers Research Topics are very popular trademarks of the *Frontiers journals series*: they are collections of at least ten articles, all centered on a particular subject. With their unique mix of varied contributions from Original Research to Review Articles, Frontiers Research Topics unify the most influential researchers, the latest key findings and historical advances in a hot research area.

Find out more on how to host your own Frontiers Research Topic or contribute to one as an author by contacting the Frontiers editorial office: [frontiersin.org/about/contact](https://frontiersin.org/about/contact)

# Biocatalysis and biotransformation guided by protein engineering

## Topic editors

Hui-Min Qin — Tianjin University of Science and Technology, China

Masaru Tanokura — The University of Tokyo, Japan

Weidong Liu — Tianjin Institute of Industrial Biotechnology, Chinese Academy of Sciences (CAS), China

Rey-Ting Guo — Hubei University, China

## Citation

Qin, H.-M., Tanokura, M., Liu, W., Guo, R.-T., eds. (2023). *Biocatalysis and biotransformation guided by protein engineering*. Lausanne: Frontiers Media SA. doi: 10.3389/978-2-83251-804-5

## Table of contents

- 05 Editorial: Biocatalysis and biotransformation guided by protein engineering  
Chao Li, Keke Yang, Heyue Li, Minze Jia, Lijun Guan and Hui-Min Qin
- 07 Immobilized  $\text{Fe}_3\text{O}_4$ -Polydopamine-*Thermomyces lanuginosus* Lipase-Catalyzed Acylation of Flavonoid Glycosides and Their Analogs: An Improved Insight Into Enzymic Substrate Recognition  
Zhaoyu Wang, Yang Li, Mingyi Li, Xiaohui Zhang, Qingxia Ji, Xiaojuan Zhao, Yanhong Bi and Si Luo
- 15 Biochemical and Structural Characterization of a Novel Bacterial Tannase From *Lachnospiraceae bacterium* in Ruminant Gastrointestinal Tract  
Lijun Guan, Kunlun Wang, Yang Gao, Jialei Li, Song Yan, Nina Ji, Chuanying Ren, Jiayou Wang, Ye Zhou, Bo Li and Shuwen Lu
- 25 Effects of Pore Size and Crosslinking Methods on the Immobilization of Myoglobin in SBA-15  
Hengmin Miao, Maosheng Li, Xiaochun Sun, Jikun Xia, Yanqing Li, Jiao Li, Fang Wang and Jiakun Xu
- 33 Improving Thermostability of Chimeric Enzymes Generated by Domain Shuffling Between Two Different Original Glucoamylases  
Zhongxiu Chen, Longbin Wang, Yuyu Shen, Dunji Hu, Liying Zhou, Fuping Lu and Ming Li
- 44 Characterization of D-Allulose-3-Epimerase From *Ruminiclostridium papyrosolvens* and Immobilization Within Metal-Organic Frameworks  
Jiaming Yang, Dexun Fan, Fengguang Zhao, Ying Lin, Suiping Zheng and Shuangyan Han
- 53 Improving Thermostability and Catalytic Activity of Glycosyltransferase From *Panax ginseng* by Semi-Rational Design for Rebaudioside D Synthesis  
Meiqi Chen, Fangwei Song, Yuxi Qin, Shuangyan Han, Yijian Rao, Shuli Liang and Ying Lin
- 65 Surface Functionalization of SBA-15 for Immobilization of Myoglobin  
Hengmin Miao, Maosheng Li, Fang Wang, Jiao Li, Ying-Wu Lin and Jiakun Xu
- 72 Molecular and Biochemical Differences of the Tandem and Cold-Adapted PET Hydrolases Ple628 and Ple629, Isolated From a Marine Microbial Consortium  
Ingrid E. Meyer Cifuentes, Pan Wu, Yipei Zhao, Weidong Liu, Meina Neumann-Schaal, Lara Pfaff, Justyna Barys, Zhishuai Li, Jian Gao, Xu Han, Uwe T. Bornscheuer, Ren Wei and Başak Öztürk



- 85 **Feasible Cluster Model Method for Simulating the Redox Potentials of Laccase CueO and Its Variant**  
Qixuan Jiang, Ziheng Cui, Ren Wei, Kaili Nie, Haijun Xu and Luo Liu
- 91 **Characterization and application of a novel xylanase from *Halolactibacillus miurensis* in wholewheat bread making**  
Yaping Zhang, Chun Liu, Manli Yang, Zuyun Ou, Ying Lin, Fengguang Zhao and Shuangyan Han
- 103 **<sup>1</sup>Progress, applications, challenges and prospects of protein purification technology**  
Miao Du, Zhuru Hou, Ling Liu, Yan Xuan, Xiaocong Chen, Lei Fan, Zhuoxi Li and Benjin Xu



## OPEN ACCESS

EDITED AND REVIEWED BY  
Georg M. Guebitz,  
University of Natural Resources and Life  
Sciences Vienna, Austria

\*CORRESPONDENCE  
Hui-Min Qin,  
✉ huiminqin@tust.edu.cn

SPECIALTY SECTION  
This article was submitted  
to Industrial Biotechnology,  
a section of the journal  
Frontiers in Bioengineering  
and Biotechnology

RECEIVED 06 February 2023  
ACCEPTED 10 February 2023  
PUBLISHED 16 February 2023

CITATION  
Li C, Yang K, Li H, Jia M, Guan L and  
Qin H-M (2023), Editorial: Biocatalysis  
and biotransformation guided by  
protein engineering.  
*Front. Bioeng. Biotechnol.* 11:1159555.  
doi: 10.3389/fbioe.2023.1159555

COPYRIGHT  
© 2023 Li, Yang, Li, Jia, Guan and Qin.  
This is an open-access article distributed  
under the terms of the [Creative  
Commons Attribution License \(CC BY\)](#).  
The use, distribution or reproduction in  
other forums is permitted, provided the  
original author(s) and the copyright  
owner(s) are credited and that the original  
publication in this journal is cited, in  
accordance with accepted academic  
practice. No use, distribution or  
reproduction is permitted which does not  
comply with these terms.

# Editorial: Biocatalysis and biotransformation guided by protein engineering

Chao Li<sup>1</sup>, Keke Yang<sup>1</sup>, Heyue Li<sup>1</sup>, Minze Jia<sup>2</sup>, Lijun Guan<sup>3</sup> and  
Hui-Min Qin<sup>1\*</sup>

<sup>1</sup>Key Laboratory of Industrial Fermentation Microbiology of the Ministry of Education, Tianjin Key Laboratory of Industrial Microbiology, College of Biotechnology, National Engineering Laboratory for Industrial Enzymes, Tianjin University of Science and Technology, Tianjin, China, <sup>2</sup>Beijing Chengzhi Life Science Co., Ltd., Beijing, China, <sup>3</sup>Institute of Food Processing, Heilongjiang Academy of Agricultural Sciences, Harbin, China

## KEYWORDS

biocatalysts, enzymatic properties, enzyme immobilization, structural analysis, protein design and engineering

## Editorial on the Research Topic

### Biocatalysis and biotransformation guided by protein engineering

Enzyme-based processing technologies have attracted much attention for their wide-ranging applications in the sustainable synthesis of industrially useful products in various fields, including pharmaceuticals, food, feed, chemicals, detergents, and biofuels. Enzymes have significant industrial potential as biocatalysts which display high levels of activity and stereocontrol, function under mild conditions, and can, in principle, be readily modified for industrial uses *via* genetic engineering. Additionally, enzymes have demonstrated their enormous potential for use in green technology as promising alternatives to traditional inorganic catalysts due to the benefits of being sustainable, clean, highly specific, and energy-efficient. Unfortunately, high-performance enzymes are quite scarce in nature, which has severely limited their use in practical synthetic applications. As a result, it has been emphasized that researching and developing highly active and robust biocatalysts that are specifically designed for the biosynthesis of target products is an essential advance. It is extremely valuable to both scientific and industrial interests. Protein engineering based on rational design and directed evolution has been developed as a potent tool to tailor natural enzymes for industrial applications. The substitution of amino acid residues in the protein sequence would induce the redistribution of the conformational ensemble, which can potentially fine-tune the catalytic performance of the enzyme. Meanwhile, enzyme immobilization, which could improve the catalytic properties, recovery, and reusability of enzymes, was also designed for the manufacture of diverse bio-products in large-scale industrial applications to reduce process costs.

This Research Topic has compiled a broad range of original research and reviews to provide readers with an overview of the most recent approaches to biocatalysis and biotransformation guided by protein engineering. Overall, 11 articles on this Research Topic have been published, including 1 review article and 10 research articles. The published articles are briefly highlighted in the following.

Du et al. offered an extensive summary of the principle and process of protein purification, the recent advances and applications of protein purification technologies in

the life and health fields, and their wide-ranging effects, which advance the research of protein structure and function, drug development, and precision medicine and provide fresh perspectives to researchers in related fields. Guan et al. developed a novel tannase (TanALb) with comprehensive biochemical and structural characterization to facilitate the biosynthesis of gallic acid by catalyzing the hydrolysis of ester and depside bonds present in hydrolyzable tannins. A new glycosyltransferase (PgUGT) for the production of rebaudioside D was described by Chen et al. Based on two kinds of structure modeling (homology modeling and deep-learning-based modeling), PgUGT was semi-rationally designed using FireProt to enhance its activity and thermostability. Similarly, Chen et al. attempted to improve the enzymatic properties of glucoamylases by domain shuffling between two different original glucoamylases, in which two novel thermostability chimeric glucoamylases were created. Zhang et al. identified a new xylanase from *H. miurensis* (Hmxyn) with wheat arabinoxylan hydrolysis activity. The water-unextractable arabinoxylan was significantly degraded by the use of recombinant Hmxyn, which also enhanced the dough's organizational structure, air-holding capability, and expansion rate. Two tandem PETase-like hydrolases (Ples), Ple628 and Ple629, were examined in terms of their kinetic characteristics, degradation products, and activity by Cifuentes et al. Structural analysis revealed that two enzymes were classified as member of the PETases IIa subclass,  $\alpha/\beta$  hydrolase superfamily since their structures were similar to other PETases. Jiang et al. developed a procedure for the type 1 copper site active center cluster model to determine the redox potentials of copper efflux oxidase. The target cluster model structures were designed using the equilibrium structures from the dynamics simulations, whose oxidized and reduced states were geometrically optimized independently in the solvated environment at the B3LYP-D3(BJ)/6-311G\* level. Yang et al. improved the reusability of a novel D-allulose-3-epimerase (RpDAE) by *in situ* encapsulation within the microporous zeolite imidazolate framework at room temperature. Wang et al. optimized the conversion of flavonoid glycosides and their analogs to their lipophilic ester derivatives using immobilized *Thermomyces lanuginosus* lipase (TLL) as nanobiocatalysts, in which TLL was immobilized on polydopamine-functionalized magnetic Fe<sub>3</sub>O<sub>4</sub> nanoparticles. Miao et al. successfully immobilized myoglobin (Mb) using mesoporous silica sieves

(SBA-15), which were synthesized with various pore sizes using a hydrothermal process. The immobilized Mb, especially the crosslinked version, showed good reusability and stability. It showed great significance to the industrial application. Additionally, Miao et al. further optimized the protein loading capacity, thermostability, storage stability, and reusability of the SBA-15 by functionalizing the surface of the mesoporous molecular sieve.

We hope this Research Topic will benefit both the scientific and industrial communities to track the state-of-the-art in this enzymatic field, no matter whether the readers are at a beginner or professional level. Finally, we would also like to express our appreciation to all of the contributing authors for sharing their excellent scientific works, the reviewers for their insightful comments, as well as the editorial staffs of Frontiers in Bioengineering and Biotechnology for their unwavering support to ensure the success of this Research Topic.

## Author contributions

All authors listed have made a substantial, direct, and intellectual contribution to the work and approved it for publication.

## Conflict of interest

Author MJ was employed by Beijing Chengzhi Life Science Co., Ltd.

The remaining authors declare that the research was conducted in the absence of any commercial or financial relationships that could be construed as a potential conflict of interest.

## Publisher's note

All claims expressed in this article are solely those of the authors and do not necessarily represent those of their affiliated organizations, or those of the publisher, the editors and the reviewers. Any product that may be evaluated in this article, or claim that may be made by its manufacturer, is not guaranteed or endorsed by the publisher.



# Immobilized Fe<sub>3</sub>O<sub>4</sub>-Polydopamine-*Thermomyces lanuginosus* Lipase-Catalyzed Acylation of Flavonoid Glycosides and Their Analogs: An Improved Insight Into Enzymic Substrate Recognition

Zhaoyu Wang, Yang Li, Mingyi Li, Xiaohui Zhang, Qingxia Ji, Xiaojuan Zhao, Yanhong Bi\* and Si Luo

School of Life Science and Food Engineering, Huaiyin Institute of Technology, Huai'an, China

## OPEN ACCESS

### Edited by:

Hui-Min Qin,  
Tianjin University of Science and  
Technology, China

### Reviewed by:

Ming-Dong Yao,  
Tianjin University, China  
Zhenlin Han,  
University of Hawaii at Manoa,  
United States

### \*Correspondence:

Yanhong Bi  
xy\_7881@126.com

### Specialty section:

This article was submitted to  
Bioprocess Engineering,  
a section of the journal  
Frontiers in Bioengineering and  
Biotechnology

**Received:** 20 October 2021

**Accepted:** 28 October 2021

**Published:** 16 November 2021

### Citation:

Wang Z, Li Y, Li M, Zhang X, Ji Q,  
Zhao X, Bi Y and Luo S (2021)  
Immobilized Fe<sub>3</sub>O<sub>4</sub>-Polydopamine-  
*Thermomyces lanuginosus* Lipase-  
Catalyzed Acylation of Flavonoid  
Glycosides and Their Analogs: An  
Improved Insight Into Enzymic  
Substrate Recognition.  
Front. Bioeng. Biotechnol. 9:798594.  
doi: 10.3389/fbioe.2021.798594

The conversion of flavonoid glycosides and their analogs to their lipophilic ester derivatives was developed by nanobiocatalysts from immobilizing *Thermomyces lanuginosus* lipase (TLL) on polydopamine-functionalized magnetic Fe<sub>3</sub>O<sub>4</sub> nanoparticles (Fe<sub>3</sub>O<sub>4</sub>-PDA-TLL). The behavior investigation revealed that Fe<sub>3</sub>O<sub>4</sub>-PDA-TLL exhibits a preference for long chain length fatty acids (i.e., C10 to C14) with higher reaction rates of 12.6–13.9 mM/h. Regarding the substrate specificity, Fe<sub>3</sub>O<sub>4</sub>-PDA-TLL showed good substrate spectrum and favorably functionalized the primary OH groups, suggesting that the steric hindrances impeded the secondary or phenolic hydroxyl groups of substrates into the bonding site of the active region of TLL to afford the product.

**Keywords:** flavonoid glycosides, immobilized enzyme, magnetic nanoparticle, *Thermomyces lanuginosus* lipase, substrate recognition

## INTRODUCTION

Ever since the groundbreaking work of Klivanov in the early 1980s (Zaks and Klivanov, 1984), nonaqueous enzymology has represented a significant extension of organic synthetic processes that come with more challenges—or that is even impossible—compared with traditional chemical approaches (Hughes and Lewis, 2018; van Schie et al., 2021). Studies over the past 30 years have revealed that enzymatic catalysis shows unusual abilities and can be a powerful tool for synthesizing fine chemicals in the pharmaceutical, food, and cosmetic industries (Sheldon and Pereira, 2017; SÁ et al., 2017).

Flavonoid glycosides and their analogs are a large group of well-known natural plant secondary metabolites that are of great academic and industrial interest because of their potentially beneficial biological, pharmacological, and medicinal properties (Chen et al., 2018; Yang et al., 2018). Because of their active polyhydroxyl structure, however, these compounds usually exert a moderately hydrophilic nature and instability, which limits their primary application in lipophilic systems (Xin et al., 2018; Yang et al., 2018). Recently, selective structural and functional modifications of natural flavonoid glycosides and their analogs based on their basic flavonoid skeletons by fatty acid acylation have been demonstrated not only to improve their physicochemical properties, but also to enrich new drug design and discovery strategies (Newman and Cragg, 2016). For example, de Araújo

et al. recently comprehensively reviewed the preferable biological benefits of the flavonoid ester derivatives (de Araújo et al., 2017).

Over the past few years and compared with the arduous and harsh chemical method, an enzymatic methodology in nonaqueous systems to form diverse natural product acylates has proved to be greatly beneficial, featuring mild condition processing, environmental benignancy, and adjustable selectivity (Sheldon and Pereira, 2017). However, the drawbacks of the enzyme catalyst, such as poor organic solvent tolerance, low reusability, and unsatisfied continuous operability in industrial enzymatic processes, may still be unavoidable (Gonçalves Filho et al., 2019; Liang et al., 2020). In this context, chemists have been committed to overcoming these shortcomings by exploring solvent engineering, substrate engineering, or enzyme engineering strategies. Recently, with the rapid development of nanotechnology, magnetic nanoparticles incorporated with biodegradable mussel-inspired polydopamine (PDA) nanocarriers, cellulose nanocrystals (CNCs), and biopolymer nanogels have generated intense interest and been successfully introduced to immobilize enzymes; these processes are characterized by superior enzyme loading capacity, high enzyme activity recovery, long-term operational stability, and facilitated separation for reuse (Bilal et al., 2020; Wang et al., 2020b; Liang et al., 2020). For example, a considerable amount of studies on constructing enzyme-immobilized magnetic nanosystem *via* a simple method have been successfully performed by Lou et al., and the results showed that both the magnetic Fe<sub>3</sub>O<sub>4</sub>-CNC-papain and Fe<sub>3</sub>O<sub>4</sub>-PDA-lipase improved the performance of enhanced enzyme loading, catalytic efficiency, and solvent tolerance compared with their free forms (Cao et al., 2016; Liang et al., 2020).

Up to now, although magnetic nanostructures have drawn extensive attention and much work has been reported, no substantial empirical rules can be followed to facilitate the immobilization of various enzymes and guide their application in the manufacturing of enzyme-processed products (Bi et al., 2020; Liang et al., 2020). Most of the studies were usually carried out using a trial-and-error method. To some extent, this phenomenon might be attributed to the absence of a detailed discussion of the molecular mechanisms of catalytic behaviors of the nanocatalyst. For these reasons, in the current study, the acylation of flavonoid glycosides and their analogs catalyzed with Fe<sub>3</sub>O<sub>4</sub>-PDA-*Thermomyces lanuginosus* lipase (Fe<sub>3</sub>O<sub>4</sub>-PDA-TLL) was selected as a model reaction to elucidate the catalytic performance of the nanocatalyst, here based on revealing the molecular basis of substrate recognition specificity by using a substrate engineering strategy; doing this may provide some valuable information for constructing an enzyme-immobilized magnetic nanosystem.

## MATERIALS AND METHODS

### Catalysts and Chemicals

CALB (powder, lipase from *Candida antarctica* B), TLL (powder, lipase from *Thermomyces lanuginosus*), RML (powder, lipase from *Rhizomucor miehei*), TLIM (lipase from *Thermomyces lanuginosus*, immobilized on granulated silica), and MML

(powder, lipase from *Mucor miehei*) were purchased from Novozymes Co., Ltd, China. PEL (powder, lipase from *Penicillium expansum*) and ANL (powder, lipase from *Aspergillus niger*) were obtained from Leveking Bioengineering Co., Ltd, Shenzhen, China. Polydatin, arbutin, helicid, dihydromyricetin, dopamine hydrochloride, and 2-methyltetrahydrofuran (MeTHF) were provided by Aladdin. Hyperoside, vinyl sorbate, and vinyl laurate were obtained from Sigma-Aldrich. Vinyl butyrate, vinyl hexanoate, vinyl octanoate, vinyl decanoate, vinyl myristate, vinyl palmitate, vinyl pivalate, vinyl 2-ethylhexanoate, vinyl stearate, vinyl benzoate, vinyl crotonate, and vinyl undecenoate were from TCI. Quercimetrin, isoquercetin, astragaline, myricetrin, taxifolin, gastrodin, and baicalin were from Yihe Biotechnology Co., Ltd, Shanghai, China. All other chemicals were also from commercial sources and of the highest purity available.

### Preparation of Immobilized Lipase

Magnetic Fe<sub>3</sub>O<sub>4</sub> nanoparticles were fabricated by a coprecipitation method per the methods reported previously (Abbaszadeh and Hejazi, 2019). To prepare PDA-coated Fe<sub>3</sub>O<sub>4</sub>, a certain amount of dopamine hydrochloride was added into deionized water containing an equivalent molar quantity of magnetic Fe<sub>3</sub>O<sub>4</sub> nanoparticles, which were dispersed and sonicated for 10 min before usage. The pH of the mixture was adjusted to 8.5 by the addition of a 1.5 M NaOH solution. After stirring for 24 h, a polydopamine-coated magnetic nanoparticle (Fe<sub>3</sub>O<sub>4</sub>-PDA) was formed and collected through a permanent magnet and washed three times with deionized water. In the next step, an aqueous solution of TLL was prepared by dissolving the TLL powder in phosphate buffer (260 mg/ml). Then, 2.4 ml of a TLL solution and 0.4 g of Fe<sub>3</sub>O<sub>4</sub>-PDA were added into 12 ml of a phosphate buffer (50 mM, pH 8.5) in a 25°C water bath. After stirring at 200 rpm for 4.0 h, the immobilized TLL was separated and continuously washed with the above buffer until no TLL was detected in the supernatant. The TLL-loaded Fe<sub>3</sub>O<sub>4</sub>-PDA was named Fe<sub>3</sub>O<sub>4</sub>-PDA-TLL.

### Assaying of Enzyme Esterification Activity

An immobilized TLL lipase assay was performed using the *p*-nitrophenyl palmitate (*p*-NPP) method (Soni et al., 2018). The substrate solution contained 30 mg of *p*-NPP in 10 ml of isopropanol. To initiate the reaction, 0.1 g of Fe<sub>3</sub>O<sub>4</sub>-PDA-TLL was added to the mixture of the substrate solution (0.1 ml) and Tris-HCl buffer (0.9 ml, 50 mM, pH 8.0) and incubated at 37°C for 10 min; here, absorbance was measured at 410 nm in a spectrophotometer. One unit of activity (U) was defined as the amount of enzyme required to produce 1.0 μmol *p*-nitrophenol (*p*-NP) in 1.0 min under the above conditions. The specific activities of Fe<sub>3</sub>O<sub>4</sub>-PDA-TLL, TLL, TLIM, CALB, RML, MML, ANL, and PEL were 8,022, 3,921, 9,750, 10,200, 2,575, 2033, 2,100, and 1990 U/g, respectively.

### Enzymatic Synthesis of Ester Derivatives

The reaction was carried out in 3.0 ml pure organic solvent, which was dried over 4 Å molecular sieves before usage, with each containing 0.03 mmol substrate, 0.33 mmol vinyl decanoate,

**TABLE 1** | Regioselective decanoylation of polydatin catalyzed by various lipases.:

Enzyme	Source	$V_0$ (mM/h)	Time (h)	$C^a$ (%)	OH <sup>b</sup> -regioselectivity <sup>c</sup> (%)
TLL	<i>Thermomyces lanuginosus</i>	3.7 ± 0.1	9.0	35.4 ± 0.3	100
Fe <sub>3</sub> O <sub>4</sub> -PDA-TLL	<i>Thermomyces lanuginosus</i>	12.6 ± 0.3	14.0	98.7 ± 0.4	100
TLIM	<i>Thermomyces lanuginosus</i>	9.7 ± 0.2	14.0	94.1 ± 0.3	100
RML	<i>Rhizomucor miehei</i>	2.1 ± 0.1	6.0	20.5 ± 0.4	100
CALB	<i>Candida antarctica</i> B	3.8 ± 0.2	14.0	31.6 ± 0.5	100
PEL	<i>Penicillium expansum</i>	2.1 ± 0.2	6.0	17.3 ± 0.3	100
ANL	<i>Aspergillus niger</i>	2.4 ± 0.1	6.0	21.8 ± 0.4	100
MML	<i>Mucor miehei</i>	0.4 ± 0.1	6.0	11.1 ± 0.5	100
Control	—	n.d. <sup>d</sup>	4.0	—	—

The reactions were carried out at 55°C and 200 rpm by adding 0.03 mmol polydatin, 0.33 mmol vinyl decanoate, 180 mg enzyme into 3.0 ml anhydrous MeTHF.

<sup>a</sup>Maximum substrate conversion.

<sup>b</sup>Primary hydroxyl.

<sup>c</sup>Regioselectivity was defined as the ratio of the concentration of the indicated product to that of all the products formed.

<sup>d</sup>Not detected.

and 180 mg Fe<sub>3</sub>O<sub>4</sub>-PDA-TLL. The reaction mixture was put in a 10 ml Erlenmeyer shaking flask at 55°C and at 200 rpm. Aliquots were withdrawn from the reaction mixture at specified time intervals and then diluted 50-fold with mobile phase before being analyzed by HPLC. The above experiment was conducted in triplicate.

## HPLC Analysis of Ester Derivatives

The reaction mixtures were analyzed by a HPLC (Agilent 1,200) system containing an XDB-C18 column (4.6 mm × 250 mm, 5 μm, Agilent) and an ultraviolet detector. Samples (20 μL) were eluted by a mixture of water and methanol at a rate of 1.0 ml/min, and detected at wavelengths of 360 (quercetrin, isoquercetrin, hyperoside, astragaline, and myricetrin), 282 (arbutin), 220 (gastrodin), 278 (baicalin), 270 (helicidin), and 280 nm (polydatin, dihydromyricetin, and taxifolin), respectively (see **Supplementary material**).

## Determination of the Chemical Structure of Ester Derivatives

After the reactions, the immobilized enzyme was removed by filtration. Then, the filtrates were evaporated under vacuum. The products were separated and purified by silica gel chromatography with an eluent consisting of petroleum ether (PE) and ethyl acetate (EA) for the mobile phase. The chemical structures of the purified products were determined by <sup>1</sup>H NMR and <sup>13</sup>C NMR in DMSO-*d*<sub>6</sub> using a Bruker DRX-400 NMR spectrometer at 400 and 100 MHz, respectively. The results from the NMR spectroscopy are given in the supplementary material.

## RESULTS AND DISCUSSION

### Influence of Enzyme Source

The catalytic behavior of the enzyme depends strongly on its source, which is well-known as the vital influence factor of the catalytic procedure and manipulates the catalytic activity, selectivity, and effectiveness (Littlechild, 2017; Gonçalves Filho

et al., 2019; Wang et al., 2020a). Among the enzymes widely used in acylating polyhydroxy compounds, lipases have been shown to have preferential catalytic characteristics over the other kinds of enzymes (Xin et al., 2019). Therefore, comparative experiments were initially devoted to an enzyme screening based on the decanoylation of polydatin as a model reaction. The results are summarized in **Table 1**.

For the enzymes, we screened six lipases, either in their free form or supported on different carriers; as expected, two supported lipases possessed an excellent ability to acylate polydatin with vinyl decanoate. For example, the nanocatalyst TLL, which was immobilized on nano-Fe<sub>3</sub>O<sub>4</sub>-PDA (Fe<sub>3</sub>O<sub>4</sub>-PDA-TLL), afforded the highest initial reaction rates of 12.6 mM/h and substrate conversions of 98.7%, while the other examined free enzymes were hardly available. Moreover, TLL immobilized on magnetic Fe<sub>3</sub>O<sub>4</sub>-PDA makes the isolation of product very easy as the catalyst can be removed from the reaction with the help of a magnet.

Regarding the position of the acylation, all of the investigated lipases preferentially acylated the more active and less steric hindrance primary hydroxyl group in polydatin and formed monoester derivatives by NMR spectra analysis. Particularly for *T. lanuginosus* lipase, the immobilized supports, including Fe<sub>3</sub>O<sub>4</sub>-PDA and granulated silica, did not change the enzyme's selectivity toward the OH position. In the acylation of polyhydroxy nucleosides reported by Li and our group (Li et al., 2009a; Wang et al., 2011), however, TLIM was been found to be superior to other enzymes when it came to functionalizing its favorable secondary hydroxyl group. X-ray crystallographic studies have shown that the amphiphilic active center of TLL contains a large hydrophobic acyl chain-binding groove and a smaller hydrophilic pocket in which the alcohol moiety and Tyr 21 bind (Noinville et al., 2002). Therefore, this distinctive binding model might be beneficial for increasing the hydrogen-bond interactions between the phenolic hydroxyl groups of the substrate with amino acid residue Tyr 21, thus stabilizing the conformation of the acylation transition state and enhancing the primary hydroxyl regioselectivity.



**TABLE 2 |** Effect of organic solvents on Fe<sub>3</sub>O<sub>4</sub>-PDA-TLL-catalyzed decanoylation of polydatin.:

Solvent	Log <i>p</i>	V <sub>0</sub> (mM/h)	Time (h)	C (%)	OH <sup>a</sup> -regioselectivity (%)
Dioxane	−1.10	9.4 ± 0.3	14.0	94.7 ± 0.05	100
DMSO	−1.00	—	15.0	3.1 ± 0.1	100
Acetone	−0.23	11.3 ± 0.5	14.0	98.0 ± 0.4	100
THF	0.49	10.8 ± 0.4	14.0	98.2 ± 0.3	100
<i>t</i> -Butanol	0.60	7.2 ± 0.2	16.0	90.0 ± 0.5	100
MeTHF	0.99	12.6 ± 0.6	14.0	98.7 ± 0.3	100

The reactions were carried out at 55°C and 200 rpm by adding 0.03 mmol polydatin, 0.33 mmol vinyl decanoate, 180 mg Fe<sub>3</sub>O<sub>4</sub>-PDA-TLL, into 3.0 ml anhydrous solvent.

<sup>a</sup>Primary hydroxyl.

## Influence of Reaction Medium

The reaction solvents used in nonaqueous biocatalysis can modulate the catalyst's catalytic activity, selectivity, substrate specificity, and stability (Pätzold et al., 2019; van Schie et al., 2021). However, no theory of experience can be applied for solvent choice, even to this day, and trial-and-error experiments still are inevitable for the given biocatalytic reaction. As can be seen in **Table 2**, apart from the case of polar DMSO (which can lead to an increase in the internal rigidity of the enzyme protein and result in enzyme inactivation by stripping the essential water layer off the enzyme molecules), Fe<sub>3</sub>O<sub>4</sub>-PDA-TLL presented substantial acylation activity and an excellent conversion (90.0–98.7%) in all the tested media. Compared with the other traditional organic solvents, the biomass-derived MeTHF always displayed excellent biocompatibility and contributed the highest initial rate and polydatin conversion.

However, the influence of thermodynamic parameter log *p* on enzyme behavior is rather unpredictable, in one case possessing a low log *p* value of −1.1 (e.g., dioxane); here, the catalytic efficiency may be satisfied, yet in another one (e.g., DMSO), the opposite may be observed. This is similar to the enzyme-mediated acylation nucleosides found by our group (Bi et al., 2014). In addition to the solvent polarity, a computer simulation study revealed that different solvent molecule with various spatial structures and sizes would exert a different ability to occupy the substrate binding site in active region of the enzyme (Yang et al., 2004), thus leading to further disruption of the enzymatic process.

## Influence of the Acyl Donor

A variety of acyl donors, such as saturated, unsaturated, branched, or aromatic, were chosen to evaluate the recognition regularity of the immobilized Fe<sub>3</sub>O<sub>4</sub>-PDA-TLL. Among the acyl donors investigated, 11 of the 14 vinyl esters could be introduced into polydatin, and the regioselectivity was overwhelming toward the primary hydroxyl position. Interestingly, when straight-chain saturated fatty acid vinyl esters (C4–C18) (Entries 1, 4, 7, 9, and 11–14, **Table 3**) were used for polydatin ester synthesis, Fe<sub>3</sub>O<sub>4</sub>-PDA-TLL may exhibit a slight preference to the long-chain fatty acids (e.g., C10 to C14) with the relative higher reaction rates of 12.6–13.9 mM/h. The reason might be attributed to the hydrophobic, crevice-like binding site of the *T. lanuginosus* lipase (Pleiss et al., 1998), in which in the longer the carbon

chain of the acyl donor, a stronger hydrophobic interaction was produced, thus being more favorable for forming an acylation transition state and improving the enzymatic catalytic efficiency.

As predicted, no reactions occurred using branched vinyl donors such as vinyl pivalate (Entry 3, **Table 3**) and vinyl 2-ethylhexanoate (Entry 8, **Table 3**) because of the presence of a severe steric hindrance between the branched chain of the acyl donor and the large hydrophobic acyl chain-binding pocket (Yang et al., 2010). For the unsaturated and aromatic acyl donors, a significant variation of the initial rates and conversions were obtained during acylation. As shown in **Table 3**, Fe<sub>3</sub>O<sub>4</sub>-PDA-TLL displayed no or low activity using vinyl benzoate, vinyl crotonate, and vinyl sorbate (Entries two and 5–6, **Table 3**), while the reactions were smooth in the reaction systems containing vinyl undecenoate (Entry 10, **Table 3**). The resonance effect stemming from the interaction between the conjugated α-double bond of the acyl chain and carbonyl carbon may strengthen the electron cloud density of the carbonyl group and reduce the flexibility of the aliphatic chain (Kobayashi et al., 2003), thereby resulting in more difficulty in the conformation of an acylation transition state. When the C–C double bond in the acyl moiety is far away from the carbonyl group, this resonance effect on acylation is insignificant; in addition, the performance of the Fe<sub>3</sub>O<sub>4</sub>-PDA-TLL was similar to those in lauroylation (Entry 13, **Table 3**).

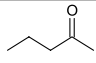
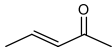
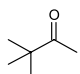
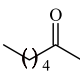
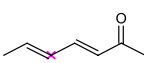
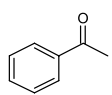
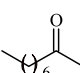
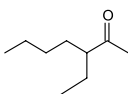
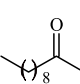
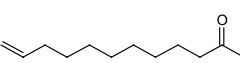
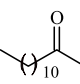
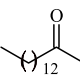
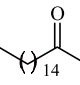
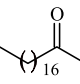
## Influence of the Substrate Structure

For an in-depth insight into the universal applicability of the immobilized nanocatalyst, 12 flavonoid glycosides and their analogs possessing various positions and numbers of primary, secondary, and tertiary hydroxyl requirements for regioselective catalysis by Fe<sub>3</sub>O<sub>4</sub>-PDA-TLL were established. As can be seen from **Table 4**, eight flavonoid glycosides (Entries 1–4 and 8–11, **Table 4**) could be converted into the desired products in excellent conversion (94.1–99.7%), indicating the good substrate spectrum of the immobilized Fe<sub>3</sub>O<sub>4</sub>-PDA-TLL.

Regarding the regioselectivity, all the finished acylations took place in the primary OH of the glucose moiety of the examined acylating substrates and produced monoester derivatives, except for the case of gastrodin, which has two more active primary OH and afforded the domain diester product with a regioselectivity of 82% (Entry 8, **Table 4**). However, the reaction rates were significantly higher for gastrodin, polydatin, helicid, and arbutin (Entries 8–11, **Table 4**) than for the other active



**TABLE 3 |** Effect of acyl donor structure on the acylation of polydatin catalyzed by Fe<sub>3</sub>O<sub>4</sub>-PDA-TLL.

Entry	Acyl donor	Acyl group	V <sub>0</sub> (mM/h)	Time (h)	C (%)	OH <sup>a</sup> -regioselectivity (%)
1	Vinyl butyrate		9.8 ± 0.4	14.0	98.1 ± 0.1	100
2	Vinyl crotonate		4.7 ± 0.1	18.0	90.1 ± 0.2	100
3	Vinyl pivalate		n.d	6.0	—	—
4	Vinyl hexanoate		12.3 ± 0.4	14.0	98.1 ± 0.4	100
5	Vinyl sorbate		6.3 ± 0.2	18.0	91.3 ± 0.3	100
6	Vinyl benzoate		n.d	6.0	—	—
7	Vinyl octanoate		12.4 ± 0.3	14.0	98.4 ± 0.2	100
8	Vinyl 2-ethylhexanoate		n.d	6.0	—	—
9	Vinyl decanoate		12.6 ± 0.4	14.0	98.7 ± 0.5	100
10	Vinyl undecenoate		13.9 ± 0.5	14.0	98.8 ± 0.6	100
11	Vinyl laurate		13.7 ± 0.6	14.0	99.1 ± 0.5	100
12	Vinyl myristate		12.8 ± 0.3	14.0	97.5 ± 0.3	100
13	Vinyl palmitate		12.6 ± 0.2	14.0	97.5 ± 0.4	100
14	Vinyl stearate		11.2 ± 0.3	14.0	96.0 ± 0.5	100

The reactions were carried out at 55°C and 200 rpm by adding 0.03 mmol polydatin, 0.33 mmol vinyl donor, 180 mg Fe<sub>3</sub>O<sub>4</sub>-PDA-TLL, into 3.0 ml anhydrous MeTHF.

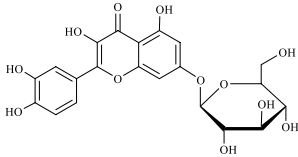
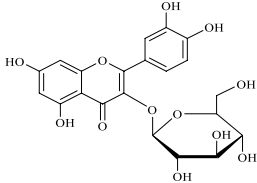
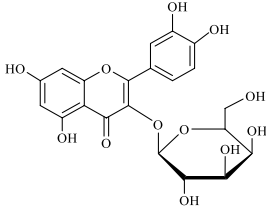
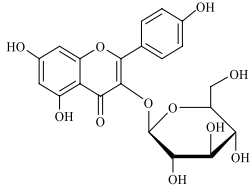
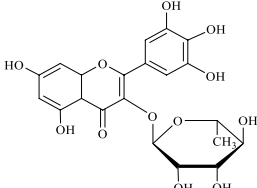
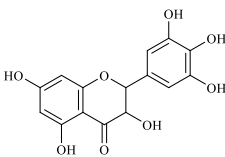
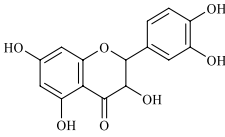
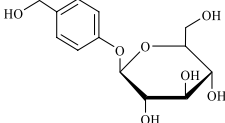
<sup>a</sup>Primary hydroxyl.

compounds (Entries 1–4, **Table 4**). The reason might be that their relatively simple aglycone structures may enter into the active site more easily to attack the acyl-enzyme intermediate and prepare various glycoside ester derivatives, thus shortening the reaction time.

Surprisingly, although baicalin (Entry 12, **Table 4**) seemed to be less hindered than quercimetrin, isoquercetin, and hyperoside (Entries 1–3, **Table 4**) because of the presence of more phenolic hydroxyl groups in the aglycones in latters, no esterification product was found in the acylation. The differences in the spatial structure among them derived from the different

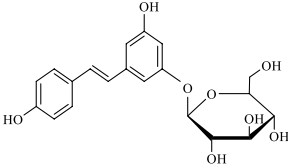
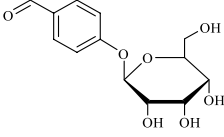
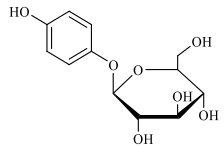
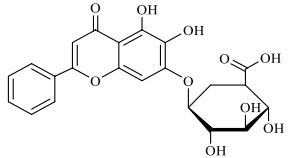
bonding paths between the aglycone and glucose moiety may be responsible for this phenomenon (Li et al., 2009b). To verify the possibility of secondary OH groups acylated in the tested glycosides, their aglycone analogs, such as dihydromyricetin (Entry 6, **Table 4**) and taxifolin (Entry 7, **Table 4**), were selected as the acylation substrates. However, Fe<sub>3</sub>O<sub>4</sub>-PDA-TLL did not display the capacity for acylating the secondary OH groups in not only the glucose moiety, but also the aglycone structure. Most studies have suggested that the steric hindrance in the substrate structure blocked the secondary OH group in the

**TABLE 4 |** Effect of chemical construction of substrate on the acylation catalyzed by Fe<sub>3</sub>O<sub>4</sub>-PDA-TLL.

Entry	Substrate	Structure	V <sub>0</sub> (mM/h)	Time (h)	C (%)	OH <sup>a</sup> -regioselectivity (%)
1	Quercimetrin		6.5 ± 0.2	16.0	94.1 ± 0.5	100
2	Isoquercetin		6.8 ± 0.3	16.0	95.1 ± 0.3	100
3	Hyperoside		6.5 ± 0.3	16.0	97.5 ± 0.7	100
4	Astragaline		6.4 ± 0.3	16.0	95.3 ± 0.5	100
5	Myricetrin		n.d	8.0	—	—
6	Dihydromyricetin		n.d	8.0	—	—
7	Taxifolin		n.d	8.0	—	—
8	Gastrodin		13.0 ± 0.5	10.0	99.7 ± 0.6	82

(Continued on following page)

**TABLE 4 |** (Continued) Effect of chemical construction of substrate on the acylation catalyzed by Fe<sub>3</sub>O<sub>4</sub>-PDA-TLL.

Entry	Substrate	Structure	V <sub>0</sub> (mM/h)	Time (h)	C (%)	OH <sup>a</sup> -regioselectivity (%)
9	Polydatin		12.6 ± 0.4	12.0	98.7 ± 0.5	100
10	Helicid		14.6 ± 0.5	10.0	99.3 ± 0.5	100
11	Arbutin		14.5 ± 0.3	14.0	99.6 ± 0.4	100
12	Baicalin		n.d	8.0	—	—

The reactions were carried out at 55°C and 200 rpm by adding 0.03 mmol polydatin, 0.33 mmol vinyl decanoate, 180 mg Fe<sub>3</sub>O<sub>4</sub>-PDA-TLL, into 3.0 ml anhydrous MeTHF.

<sup>a</sup>Primary hydroxyl.

bonding site to form the tetrahedral intermediate and product (Li et al., 2009b; Bi et al., 2014).

## CONCLUSION

In the present work, more insight into the substrate recognition law of the nanobiocatalyst of Fe<sub>3</sub>O<sub>4</sub>-PDA-TLL through a rational substrate engineering strategy was gained. The unexpected yet satisfactory results improved and extended the application of the magnetic nanoparticles for immobilizing TLL lipase in regioselectively acylating active polyhydroxy natural compounds in nonaqueous systems, which was demonstrated by receiving the higher catalytic activity, excellent selectivity, and good substrate specificity of Fe<sub>3</sub>O<sub>4</sub>-PDA-TLL. Based on these observations, the biocompatible Fe<sub>3</sub>O<sub>4</sub> magnetic nanoparticles modified by biodegradable polydopamine (Fe<sub>3</sub>O<sub>4</sub>-PDA) can act as an alternative immobilized support for useful enzymes, indicating great potential for industrial applications.

## DATA AVAILABILITY STATEMENT

The original contributions presented in the study are included in the article/**Supplementary Material**, further inquiries can be directed to the corresponding author.

## AUTHOR CONTRIBUTIONS

YB and SL gave the idea for this project and helped in the case of scientific problems. ZW was responsible for planning and performing the experiments as well as writing the main part of the manuscript. ML, XZ, and QJ helped with the experiments operation and data collation. YL and XZ supervised the study and revised the manuscript.

## FUNDING

This work was financially supported by the National Natural Science Foundation of China (21676114), Qing Lan Project of Jiangsu Province of China, Six Talent Peaks Project in Jiangsu Province (SWYY-011; YY-061) and Natural Science Research Project of Higher Education of Jiangsu Province (18KJD530002) for financial support.

## SUPPLEMENTARY MATERIAL

The Supplementary Material for this article can be found online at: <https://www.frontiersin.org/articles/10.3389/fbioe.2021.798594/full#supplementary-material>

## REFERENCES

- Abbaszadeh, M., and Hejazi, P. (2019). Metal Affinity Immobilization of Cellulase on Fe<sub>3</sub>O<sub>4</sub> Nanoparticles with Copper as Ligand for Biocatalytic Applications. *Food Chem.* 290, 47–55. doi:10.1016/j.foodchem.2019.03.117
- Bi, Y.-H., Du, W.-Y., Wang, Z.-Y., Chen, X.-M., Nie, L.-H., and Zong, M.-H. (2014). Understanding the Behavior of *Thermomyces Lanuginosus* Lipase in Acylation of Pyrimidine Nucleosides Possessing 2'-Substituent. *Appl. Biochem. Biotechnol.* 174, 556–563. doi:10.1007/s12010-014-1096-7
- Bi, Y., Wang, Z., Tian, Y., Fan, H., Huang, S., Lu, Y., et al. (2020). Highly Efficient Regioselective Decanoylation of Hyperoside Using Nanobiocatalyst of Fe<sub>3</sub>O<sub>4</sub>@PDA-*Thermomyces Lanuginosus* Lipase: Insights of Kinetics and Stability Evaluation. *Front. Bioeng. Biotechnol.* 8, 485. doi:10.3389/fbioe.2020.00485
- Bilal, M., Wang, Z., Cui, J., Ferreira, L. F. R., Bharagava, R. N., and Iqbal, H. M. N. (2020). Environmental Impact of Lignocellulosic Wastes and Their Effective Exploitation as Smart Carriers - A Drive towards Greener and Eco-Friendlier Biocatalytic Systems. *Sci. Total Environ.* 722, 137903. doi:10.1016/j.scitotenv.2020.137903
- Cao, S., Xu, P., Ma, Y., Yao, X., Yao, Y., Zong, M., et al. (2016). Recent Advances in Immobilized Enzymes on Nanocarriers. *Chin. J. Catal.* 37, 1814–1823. doi:10.1016/S1872-2067(16)62528-7
- Chen, L., Teng, H., Xie, Z., Cao, H., Cheang, W. S., Skalicka-Woniak, K., et al. (2018). Modifications of Dietary Flavonoids towards Improved Bioactivity: An Update on Structure-Activity Relationship. *Crit. Rev. Food Sci. Nutr.* 58, 513–527. doi:10.1080/10408398.2016.1196334
- de Araújo, M., Franco, Y., Messias, M., Longato, G., Pamphile, J., and Carvalho, P. (2017). Biocatalytic Synthesis of Flavonoid Esters by Lipases and Their Biological Benefits. *Planta Med.* 83, 7–22. doi:10.1055/s-0042-118883
- Filho, D. G., Silva, A. G., and Guidini, C. Z. (2019). Lipases: Sources, Immobilization Methods, and Industrial Applications. *Appl. Microbiol. Biotechnol.* 103, 7399–7423. doi:10.1007/s00253-019-10027-6
- Hughes, G., and Lewis, J. C. (2018). Introduction: Biocatalysis in Industry. *Chem. Rev.* 118, 1–3. doi:10.1021/acs.chemrev.7b00741
- Kobayashi, T., Adachi, S., and Matsuno, R. (2003). Lipase-catalyzed Condensation of *p*-Methoxyphenethyl Alcohol and Carboxylic Acids with Different Steric and Electrical Properties in Acetonitrile. *Biotechnol. Lett.* 25, 3–7. doi:10.1023/A:1021799825272
- Li, N., Zong, M.-H., and Ma, D. (2009b). *Thermomyces Lanuginosus* Lipase-Catalyzed Regioselective Acylation of Nucleosides: Enzyme Substrate Recognition. *J. Biotechnol.* 140, 250–253. doi:10.1016/j.jbiotec.2009.02.003
- Li, N., Zong, M.-H., and Ma, D. (2009a). Unexpected Reversal of the Regioselectivity in *Thermomyces Lanuginosus* Lipase-Catalyzed Acylation of Floxuridine. *Biotechnol. Lett.* 31, 1241–1244. doi:10.1007/s10529-009-0001-x
- Liang, S., Wu, X.-L., Xiong, J., Zong, M.-H., and Lou, W.-Y. (2020). Metal-organic Frameworks as Novel Matrices for Efficient Enzyme Immobilization: an Update Review. *Coord. Chem. Rev.* 406, 213149. doi:10.1016/j.ccr.2019.213149
- Littlechild, J. A. (2017). Improving the 'tool Box' for Robust Industrial Enzymes. *J. Ind. Microbiol. Biot.* 44, 711–720. doi:10.1007/s12025-017-1920-5
- Newman, D. J., and Cragg, G. M. (2016). Natural Products as Sources of New Drugs from 1981 to 2014. *J. Nat. Prod.* 79, 629–661. doi:10.1021/acs.jnatprod.5b01055
- Noinville, S., Revault, M., Baron, M.-H., Tiss, A., Yapoudjian, S., Ivanova, M., et al. (2002). Conformational Changes and Orientation of *Humicola Lanuginosa* Lipase on a Solid Hydrophobic Surface: an *In Situ* Interface Fourier Transform Infrared-Attenuated Total Reflection Study. *Biophysical J.* 82, 2709–2719. doi:10.1016/S0006-3495(02)75612-9
- Pätzold, M., Siebenhaller, S., Kara, S., Liese, A., Syldatk, C., and Holtmann, D. (2019). Deep Eutectic Solvents as Efficient Solvents in Biocatalysis. *Trends Biotechnol.* 37, 943–959. doi:10.1016/j.tibtech.2019.03.007
- Pléiss, J., Fischer, M., and Schmid, R. D. (1998). Anatomy of Lipase Binding Sites: the Scissile Fatty Acid Binding Site. *Chem. Phys. Lipids* 93, 67–80. doi:10.1016/S0009-3084(98)00030-9
- Sá, A. G. A., Meneses, A. C. d., Araújo, P. H. H. d., and Oliveira, D. d. (2017). A Review on Enzymatic Synthesis of Aromatic Esters Used as Flavor Ingredients for Food, Cosmetics and Pharmaceuticals Industries. *Trends Food Sci. Tech.* 69, 95–105. doi:10.1016/j.tifs.2017.09.004
- Sheldon, R. A., and Pereira, P. C. (2017). Biocatalysis Engineering: the Big Picture. *Chem. Soc. Rev.* 46, 2678–2691. doi:10.1039/C6CS00854B
- Soni, S., Dwivedee, B. P., and Chand Banerjee, U. (2018). Facile Fabrication of a Recyclable Nanobiocatalyst: Immobilization of *Burkholderia Cepacia* Lipase on Carbon Nanofibers for the Kinetic Resolution of a Racemic Atenolol Intermediate. *RSC Adv.* 8, 27763–27774. doi:10.1039/C8RA05463K
- van Schie, M. M. C. H., Spöring, J.-D., Bocla, M., Domínguez de María, P., and Rother, D. (2021). Applied Biocatalysis beyond Just Buffers - from Aqueous to Unconventional media. Options and Guidelines. *Green. Chem.* 23, 3191–3206. doi:10.1039/D1GC00561H
- Wang, F., Zhu, M., Song, Z., Li, C., Wang, Y., Zhu, Z., et al. (2020a). Reshaping the Binding Pocket of Lysine Hydroxylase for Enhanced Activity. *ACS Catal.* 10, 13946–13956. doi:10.1021/acscatal.0c03841
- Wang, X., Lan, P. C., and Ma, S. (2020b). Metal-Organic Frameworks for Enzyme Immobilization: Beyond Host Matrix Materials. *ACS Cent. Sci.* 6, 1497–1506. doi:10.1021/acscentsci.0c00687
- Wang, Z.-Y., Bi, Y.-H., and Zong, M.-H. (2011). Highly Regioselective Synthesis of 3'-O-Acyl-Trifluridines Catalyzed by *Pseudomonas cepacia* Lipase. *Appl. Biochem. Biotechnol.* 165, 1161–1168. doi:10.1007/s12010-011-9333-9
- Xin, X., Zhang, M., Li, X.-F., and Zhao, G. (2019). Biocatalytic Synthesis of Lipophilic Baicalin Derivatives as Antimicrobial Agents. *J. Agric. Food Chem.* 67, 11684–11693. doi:10.1021/acs.jafc.9b04667
- Xin, X., Zhang, M., Li, X., Lai, F., and Zhao, G. (2018). Biocatalytic Synthesis of Acylated Derivatives of Troxerutin: Their Bioavailability and Antioxidant Properties *In Vitro*. *Microb. Cell Fact.* 17, 130. doi:10.1186/s12934-018-0976-x
- Yang, B., Liu, H., Yang, J., Gupta, V. K., and Jiang, Y. (2018). New Insights on Bioactivities and Biosynthesis of Flavonoid Glycosides. *Trends Food Sci. Tech.* 79, 116–124. doi:10.1016/j.tifs.2018.07.006
- Yang, L., Dordick, J. S., and Garde, S. (2004). Hydration of Enzyme in Nonaqueous media Is Consistent with Solvent Dependence of its Activity. *Biophysical J.* 87, 812–821. doi:10.1529/biophysj.104.041269
- Yang, R.-L., Li, N., Li, R.-F., Smith, T. J., and Zong, M.-H. (2010). A Highly Regioselective Route to Arbutin Esters by Immobilized Lipase from *Penicillium expansum*. *Bioresour. Tech.* 101, 1–5. doi:10.1016/j.biortech.2009.07.067
- Zaks, A., and Klibanov, A. M. (1984). Enzymatic Catalysis in Organic Media at 100°C. *Science* 224, 1249–1251. doi:10.1126/science.6729453

**Conflict of Interest:** The authors declare that the research was conducted in the absence of any commercial or financial relationships that could be construed as a potential conflict of interest.

**Publisher's Note:** All claims expressed in this article are solely those of the authors and do not necessarily represent those of their affiliated organizations, or those of the publisher, the editors and the reviewers. Any product that may be evaluated in this article, or claim that may be made by its manufacturer, is not guaranteed or endorsed by the publisher.

Copyright © 2021 Wang, Li, Li, Zhang, Ji, Zhao, Bi and Luo. This is an open-access article distributed under the terms of the Creative Commons Attribution License (CC BY). The use, distribution or reproduction in other forums is permitted, provided the original author(s) and the copyright owner(s) are credited and that the original publication in this journal is cited, in accordance with accepted academic practice. No use, distribution or reproduction is permitted which does not comply with these terms.



# Biochemical and Structural Characterization of a Novel Bacterial Tannase From *Lachnospiraceae* bacterium in Ruminant Gastrointestinal Tract

Lijun Guan<sup>1,2\*</sup>, Kunlun Wang<sup>1,2</sup>, Yang Gao<sup>1,2</sup>, Jialei Li<sup>1,2</sup>, Song Yan<sup>1,2</sup>, Nina Ji<sup>3</sup>, Chuanying Ren<sup>1,2</sup>, Jiayou Wang<sup>4</sup>, Ye Zhou<sup>1,2</sup>, Bo Li<sup>1,2</sup> and Shuwen Lu<sup>1,2\*</sup>

<sup>1</sup>Institute of Food Processing, Heilongjiang Academy of Agricultural Sciences, Harbin, China, <sup>2</sup>Heilongjiang Province Key Laboratory of Food Processing, Harbin, China, <sup>3</sup>Soybean Institute, Heilongjiang Academy of Agricultural Sciences, Harbin, China, <sup>4</sup>Biotechnology Research Institute, Heilongjiang Academy of Agricultural Sciences, Harbin, China

## OPEN ACCESS

### Edited by:

Weidong Liu,  
Tianjin Institute of Industrial  
Biotechnology (CAS), China

### Reviewed by:

Fei Wang,  
Jiangxi Agricultural University, China  
Fenghua Wang,  
Tianjin University of Science and  
Technology, China

### \*Correspondence:

Lijun Guan  
qqaipph@sina.com  
Shuwen Lu  
shuwenl@sina.com

### Specialty section:

This article was submitted to  
Industrial Biotechnology,  
a section of the journal  
Frontiers in Bioengineering and  
Biotechnology

**Received:** 01 November 2021

**Accepted:** 17 November 2021

**Published:** 15 December 2021

### Citation:

Guan L, Wang K, Gao Y, Li J, Yan S,  
Ji N, Ren C, Wang J, Zhou Y, Li B and  
Lu S (2021) Biochemical and Structural  
Characterization of a Novel Bacterial  
Tannase From *Lachnospiraceae*  
bacterium in Ruminant  
Gastrointestinal Tract.  
Front. Bioeng. Biotechnol. 9:806788.  
doi: 10.3389/fbioe.2021.806788

Tannases are a family of esterases that catalyze the hydrolysis of ester and depside bonds present in hydrolyzable tannins to release gallic acid. Here, a novel tannase from *Lachnospiraceae* bacterium (TanA<sub>LB</sub>) was characterized. The recombinant TanA<sub>LB</sub> exhibited maximal activity at pH 7.0 and 50°C, and it maintained more than 70% relative activity from 30°C to 55°C. The activity of TanA<sub>LB</sub> was enhanced by Mg<sup>2+</sup> and Ca<sup>2+</sup>, and was dramatically reduced by Cu<sup>2+</sup> and Mn<sup>2+</sup>. TanA<sub>LB</sub> is capable of degrading esters of phenolic acids with long-chain alcohols, such as lauryl gallate as well as tannic acid. The Km value and catalytic efficiency ( $k_{cat}/K_m$ ) of TanA<sub>LB</sub> toward five substrates showed that tannic acid (TA) was the favorite substrate. Homology modeling and structural analysis indicated that TanA<sub>LB</sub> contains an insertion loop (residues 341–450). Based on the molecular docking and molecular dynamics (MD) simulation, this loop was observed as a flap-like lid to interact with bulk substrates such as tannic acid. TanA<sub>LB</sub> is a novel bacterial tannase, and the characteristics of this enzyme make it potentially interesting for industrial use.

**Keywords:** bacterial tannase, biochemical characterization, kinetic analysis, homology modeling, structural analysis

## INTRODUCTION

Tannins are water-soluble polyphenolic compounds that constitute the fourth most abundant class of plant biomass components, richly secreted by defensive systems in wood, fruits, roots, and seeds (White, 1957; Smeriglio et al., 2016; Maisetta et al., 2019). Tannins and their derivatives are the key compounds of the astringent taste of tea, fruits, and vegetables, and determine the quality of their production such as muddy and astringency problem of juice and beer (Charlton et al., 2002). In addition, tannins inhibit the growth of microbes, exert antinutritional effect on animals and are even toxic to the human body in that they possess the capacity to bind and precipitate proteins and to bind iron, which could lead to many biological process disorders (McDonald et al., 1996; Baxter et al., 1997; Chung et al., 1998; Aguilar et al., 2007; Smeriglio et al., 2016). During millions of years of biological evolution, various microorganisms have adapted to utilize tannins as carbon and/or energy sources for growth and development using enzymes such as tannin acyl hydrolases, generally known as

tannases (Lekha and Lonsane, 1997; Aguilar et al., 2007). Tannases (EC 3.1.1.20) catalyze the hydrolysis of ester and depside bonds present in gallotannins, complex tannins, and gallic acid esters, resulting in the release of glucose and gallic acid (Govindarajan et al., 2016). Tannase have broad practical applications in the food, feed, beverage, pharmaceutical, agricultural, and the leather industries. Compared with chemical hydrolysis methods catalyzed by HCl, nucleophiles and precious metals, the bio-hydrolysis of tannins has unique advantages due to its low environmental impact (Aharwar and Parihar, 2018). Thus, there is an increasing demand for tannases with desirable biochemical properties in industry.

Most tannases that are biochemically studied and characterized in detail come from fungi (Aboubakr et al., 2013), but not much is known about tannase of bacteria or yeasts living under extreme conditions, which are considered to be the potential of tannases with unexpected characteristics (Dhiman et al., 2018; Tomás-Cortázar, 2018). The studied tannases in bacteria are almost from the rumen, gut, oral cavity microbiota, or soils (Noguchi et al., 2007; Wu et al., 2014; Chaitanyakumar and Anbalagan, 2016; Tomás-Cortázar et al., 2018). Recently, it is reported that plant tannase was first identified from leaves of tea, strawberry, and crops, which hydrolyze tannin compounds, glycosides, and phenolic glycosides to produce toxic small molecule phenolic compounds, so as to protect plants from attack by microorganisms and herbivore (Dai et al., 2020).

Tannase includes extracellular tannases encoded by the tanA gene and intracellular tannases encoded by tanB gene, with molecular size of 66 and 50 kDa, respectively (Tomás-Cortázar et al., 2018). Exceptionally, TanB<sub>SS</sub> encoded by a tanB gene from *Streptomyces sviveus* was identified as an extracellular tannase (Wu et al., 2014). The optimum temperature and pH value for biochemical characteristics of bacterial tannases are 30°C–50°C and 3.0–7.0, respectively (Lekshmi et al., 2021). Up to now, two kinds of bacterial tannase belonging to probiotics (TanA<sub>Lp</sub>, *Lactobacillus plantarum*) and the oral bacteria (TanB<sub>Fnn</sub>, *Fusobacterium nucleatum*) have been structurally characterized by combining crystal structure, molecular dynamics, and mutation analysis, which confirmed the functional role of the flap domain and flap-like domain in the substrate recognition and specificity of tannase (Ren et al., 2013; Mancheño et al., 2020).

Here, a putative bacterial tannase from a species of *Lachnospiraceae bacterium* was characterized in detail. Recombinant TanA<sub>Lb</sub> was cloned, overexpressed, and purified in order to fully analyze the biochemical characteristics. To understand the biochemical characteristics of TanA<sub>Lb</sub>, three-dimensional structure of the enzyme was modeled. Assisted by molecular docking and MD simulation, the structure-oriented substrate specificity analysis was carried out. This work adds a new bacterial tannase with comprehensive biochemical and structural characterization to provide a platform for the manipulation of tannins in food and beverage products, or for transformation into biologically active products to benefit human health on the basis of specific requirements.

## MATERIALS AND METHODS

### Cloning and Expression of Tannase From *Lachnospiraceae Bacterium*

The coding sequence of TanA<sub>Lb</sub> (GenBank accession No. MBQ6323131.1) was codon optimized for *E. coli* and synthesized by Genewiz (Beijing, China). The purified PCR products were subcloned into the pET-28a (+) vector (Novagen, Madison, WI, USA) between the *Nde* I and *Eco*R I restriction sites, resulting in the addition of a 6×His tag at the N-terminus. The primer sequences are TanA<sub>Lb</sub>\_F (GGAATTCCATATGTCACAGTCAACAGCTACACGC) and TanA<sub>Lb</sub>\_R (GGAATTC AAGGCCAGCAGCTTTAAGGCG). *E. coli* BL21 (DE3) was transformed with the resulting expression vector pET-28a-TanA<sub>Lb</sub> and grown in Luria-Bertani (LB) broth medium with 50 µg/ml kanamycin overnight at 37°C. On the next day, a fresh culture in the same medium was inoculated, and when it reached 0.6–0.8, isopropyl β-D-1-thiogalactopyranoside (IPTG) was added to a final concentration of 0.5 mM, to induce the expression of pET-28a-TanA<sub>Lb</sub> at 16°C overnight. The cells were harvested by centrifugation for 15 min at 5,000 × g and 4°C, and washed with 0.9% NaCl solution.

### Purification of the Recombinant Tannase From *Lachnospiraceae bacterium*

The cells expressing recombinant TanA<sub>Lb</sub> were resuspended in lysis buffer [20 mM Tris-HCl, 20 mM imidazole, 500 mM NaCl, 1 mM dithiothreitol (DTT), pH 8.0] and ultrasonicated at 1.5-s pulse and 3-s output for 15 min. Then, the crude lysate was centrifuged at 40,000 × g and 4°C for 30 min, and the supernatant was bound to a 1 ml of Ni-NTA Superflow column (Qiagen, Hilden, Germany). After washing with 10 ml of wash buffer (20 mM Tris-HCl, 0.5 M NaCl, 1 mM DTT, 50 mM imidazole, pH 8.0), the TanA<sub>Lb</sub> protein was eluted with 10 ml of elution buffer (20 mM Tris-HCl, 0.3 M NaCl, 1 mM DTT, 0.5 M imidazole, pH 8.0). For further purification, the target protein was buffer exchanged into 20 mM Tris-HCl pH 8.0, 1 mM DTT, loaded onto a 5-ml MonoQ ion exchange column (GE Healthcare, Piscataway, NJ, USA), and eluted using a linear gradient using from 0 to 1 M NaCl. Then, gel filtration chromatography was used to determine the apparent mass of the TanA<sub>Lb</sub> protein using a Superdex 200 increase column (GE Healthcare, Piscataway, NJ, USA). The running buffer was 20 mM Tris-HCl (pH 8.0, containing 150 mM NaCl and 1 mM DTT), and the flow rate was 0.5 ml/min. Finally, the purified protein was stored at 4°C until further analysis. The molecular mass and purity of the target protein were assessed by SDS-PAGE.

### Enzyme Activity Assay

The enzyme activity of TanA<sub>Lb</sub> was determined using the rhodamine assay published by Inoue and Hagerman (Jiménez et al., 2014). TanA<sub>Lb</sub> (100 µg) in 700 µl of 50 mM phosphate buffer, pH 6.5, was incubated with 40 µl of 25 mM methyl gallate (final substrate concentration 1 mM), for 5 min at 37°C. After



incubation, 150  $\mu$ l of 0.667% rhodamine in 100% methanol was added to the mixture. After incubation at 30°C for 5 min, 100  $\mu$ l of 0.5 M KOH was added and incubated for an additional 5–10 min, after which the absorbance was measured at 520 nm using a spectrophotometer. A standard curve was prepared using gallic acid solutions ranging from 0.125 to 1 mM. One unit of TanA<sub>Lb</sub> activity was defined as the amount of enzyme that releases 1  $\mu$ M gallic acid per minute under the described assay conditions. The concentration of TanA<sub>Lb</sub> was determined using a BCA Protein Assay Kit (Solarbio, China).

To determine the substrate specificity of TanA<sub>Lb</sub>, 1 mM methyl gallate (MG), ethyl gallate (EG), propyl gallate (PG), lauryl gallate (LG) and tannic acid (TA) were used as the substrate, and enzyme activity was measured at 50°C and pH 7.0. The kinetic parameters of the purified enzymes were determined by assaying the activity on various substrate concentrations. MG, EG, PG, LG (0.2–5 mM) and tannic acid (0.01–0.05 mM) were incubated with appropriate amount of enzyme to calculate the kinetics. The amount of gallic acid which was formed by the catalysis of tannase was calibrated using the absorbance at 520 nm. Kinetic parameters were obtained according to the Line-weaver and Burk method. Each measurement was conducted three times. All calculations were performed using the Origin 9.0 software.

## Effects of Temperature, pH, and Additives on the Activity and Stability of the Enzyme

The optimal temperature of TanA<sub>Lb</sub> was determined by measuring the relative activities in the range of 20°C–70°C in 20 mM phosphate buffer saline at pH 7.0. To evaluate the thermal stability of TanA<sub>Lb</sub>, the residual activity was measured after pre-incubation in 20 mM phosphate buffer saline buffer (pH 7.0) at 20°C, 30°C, 40°C, 50°C, 60°C, and 70°C, respectively. Samples were taken every 30 min for 5 h.

Different buffers were used to assess the optimal pH of TanA<sub>Lb</sub> at 50°C, with methyl gallate as the substrate. The pH value was varied from 2.5 to 10 using 20 mM glycine-HCl buffer (pH 2.5–5.5), 20 mM 4-morpholineethanesulfonic acid (MES) (pH 5.5–6.5), 20 mM phosphate buffer saline (pH 6.5–8.0), 20 mM Tris-HCl (pH 8.0–9.5), and 20 mM glycine-NaOH (pH 9.5–10.0). In order to determine the pH stability of TanA<sub>Lb</sub>, the enzyme was incubated in the indicated buffers (pH 2.5–10.0) at 50°C for 30 min, and the residual activity was measured under the standard conditions.

The effects of various metal ions on the purified recombinant TanA<sub>Lb</sub> were investigated by measuring the relative enzyme activity in the presence of 1 mM K<sup>+</sup>, Ca<sup>2+</sup>, Co<sup>2+</sup>, Mn<sup>2+</sup>, Mg<sup>2+</sup>, Zn<sup>2+</sup>, and Cu<sup>2+</sup>, respectively. The enzyme activity was measured at pH 7.0 and 50°C. Additionally, the enzyme was incubated in 20 mM phosphate saline buffer pH 7.0 with 1 mM ethylene diamine tetraacetic acid (EDTA), sodium dodecyl sulfate (SDS), Tween-80, dimethyl sulfoxide (DMSO), and TritonX-100 at 25°C for 1.0 h to investigate the effect of a chelating agent. The activity without adding any additives was defined as 100%.

## Homology Modeling of Tannase From *Lachnospiraceae bacterium*

Modeller 9.9 software (<http://salilab.org/modeller/>) was used to generate a homology model of TanA<sub>Lb</sub> (Gao et al., 2012). The crystal structure of a homologous protein from *Fusobacterium nucleatum* subsp. *nucleatum* (PDB ID: 6YQ4), which has 42.9% sequence identity with the target protein TanA<sub>Lb</sub>, was chosen as template. A sequence alignment between TanB<sub>Fnn</sub> and TanA<sub>Lb</sub> was generated automatically using the align2d command. Subsequently, homology modeling was executed using the auto-model command. The best model was chosen based on the MODELLER objective function values and the DOPE assessment scores. Quality of the predicted 3D structural model was assessed by the PROCHECK (<https://servicesn.mbi.ucla.edu/PROCHECK>). The constructed model structure was visualized and analyzed using PyMOL software (<http://www.pymol.org>).

## Molecular Docking

MOE package (Molecular Operating Environment, 1010 Sherbooke St. West, Suite #910, Montreal, QC, Canada, H3A 2R7, 2018) was used for molecular docking of TanA<sub>Lb</sub> with five ligands and predicting the binding affinity, respectively. The 2D structure of ligands were downloaded from the PubChem web site (<http://pubchem.ncbi.nlm.nih.gov>) and converted to 3D in MOE through energy minimization. Then the protonation state of target and the orientation of the hydrogens were optimized by LigX, at the PH of 7 and temperature of 300 K. Prior to docking, the force field of AMBER10:EHT and the implicit solvation model of Reaction Field (R-field) were selected (Case et al., 2008). The position of the native ligand (SPD) in the X-ray structure of 6YQ4 which is selected as the homology template of TanA<sub>Lb</sub> was defined as the binding site. The docking workflow followed the “induced fit” protocol, in which the side chains of the receptor pocket were allowed to move according to ligand conformations, with a constraint on their positions. The weight used for tethering side chain atoms to their original positions was 10. All docked poses of molecules were ranked by London dG scoring first, and then a force field refinement was carried out on the top 30 poses followed by a rescoring of GBVI/WSA dG.

## Molecular Dynamics (MD) Simulation

For the complex structure of TanA<sub>Lb</sub> and tannic acid, whose structure was neutralized by adding sodium/chlorine counter ions and solvated in a cuboid box of TIP3P water molecules with solvent layers 12 Å between the box edges and solute surface.

All MD simulations were performed using AMBER20 (Case et al., 2021). The AMBER FF19SB and gaff2 force fields were applied, and the SHAKE algorithm was used to restrict all covalent bonds involving hydrogen atoms with a time step of 2 fs. The Particle mesh Ewald (PME) method was employed to treat long-range electrostatic interactions. For the solvated system, two steps of minimization were performed before the heating step. The first 4,000 cycles of minimization were performed with all heavy atoms restrained with 50 kcal/





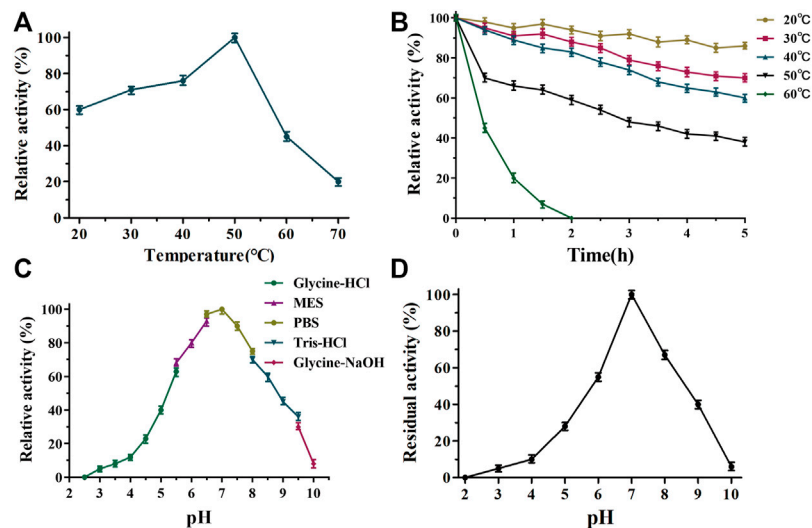


**FIGURE 3 |** Determination of the optimal temperature (A), thermostability (B), pH optimum (C), and pH stability (D) of TanA<sub>LB</sub>.

**TABLE 1 |** Effects of metal ions, inhibitors, and surfactants on the activity of tannase from *Lachnospiraceae bacterium* (TanA<sub>LB</sub>).

		Residual activity (%) *
Metal ions	Control	100
	K <sup>+</sup>	72
	Ca <sup>2+</sup>	115
	Co <sup>2+</sup>	80
	Mn <sup>2+</sup>	51
	Mg <sup>2+</sup>	124
	Zn <sup>2+</sup>	75
	Cu <sup>2+</sup>	33
Surfactant and inhibitor	Control	100
	SDS	105
	DMSO	133
	Tween-80	127
	Triton X-100	122
	EDTA	78

(Supplementary Figure S1). The sequence alignment results revealed that TanA<sub>LB</sub> showed 42.9% sequence similarity with TanB<sub>Fnn</sub> from *Fusobacterium nucleatum* subsp. *nucleatum* (GenBank Accession No. ALQ42581.1) (Mancheño et al., 2020) and 40.4% with TanASl from *Staphylococcus lugdunensis* (GenBank Accession No. BAF03594.1) (Rusniok et al., 2010). However, it showed only 24% sequence similarity with TanB<sub>Lp</sub> from *Lactobacillus plantarum* (GenBank Accession No. AB379685.1) (Matoba et al., 2013). TanA<sub>LB</sub> exhibited the conserved catalytic triad (Ser205, His614, Asp582) typical for the tannase family (Supplementary Figure S1). Furthermore, TanA<sub>LB</sub> also contained the conserved motif Gly203-X-Ser205-X-Gly207, which is typical of serine hydrolases (Ren et al., 2013). A phylogenetic analysis of TanA<sub>LB</sub> and previously identified tannases indicated that TanA<sub>LB</sub> is more similar with TanA<sub>SI</sub>

**TABLE 2 |** Kinetic parameters of TanA<sub>LB</sub>.

Substrate	$K_m$ (mM)	$k_{cat}$ (s <sup>-1</sup> )	$k_{cat}/K_m$ (mM <sup>-1</sup> s <sup>-1</sup> )
MG	2.8 ± 0.35	82.5 ± 6.3	36.4 ± 4.4
EG	2.6 ± 0.19	78.8 ± 10.4	33.3 ± 7.3
PG	2.0 ± 0.22	44.2 ± 3.6	24.5 ± 4.0
LG	1.8 ± 0.26	24.6 ± 5.2	15.3 ± 2.1
TA	0.47 ± 0.12	82.1 ± 11.6	192.51 ± 4.3

than the other investigated enzymes (Figure 1). Multiple sequence alignment and phylogenetic analysis, therefore, both indicated that TanA<sub>LB</sub> may have tannase activity.

TanA<sub>LB</sub> was purified using Ni-NTA affinity chromatography, ion exchange (Figure 2A) and size-exclusion chromatography (Figure 2B) of which the purification multiple was probably 6.9. The purified TanA<sub>LB</sub> was analyzed via SDS-PAGE and showed a single protein band with an apparent molecular weight of approximately 68 kDa (Figure 2C), which was in agreement with the predicted molecular weight. Furthermore, size-exclusion chromatography of purified TanA<sub>LB</sub> was performed to determine its native state in solution. A single peak was observed between the peaks of the standard protein markers actin from rabbit muscle (43 kDa) and conalbumin (75 kDa), which indicated that TanA<sub>LB</sub> was a monomer in solution (Figure 2B).

## Biochemical Characterization of Tannase From *Lachnospiraceae Bacterium*

Since tannic acid is almost exclusively formed from poly-galloyl glucose derivatives, it was used as substrate to assess if TanA<sub>LB</sub> can catalyze the hydrolysis of natural tannin. The gallic acid resulting from the degradation was identified using the rhodamine method, which indicated that tannic acid was hydrolyzed by TanA<sub>LB</sub>.

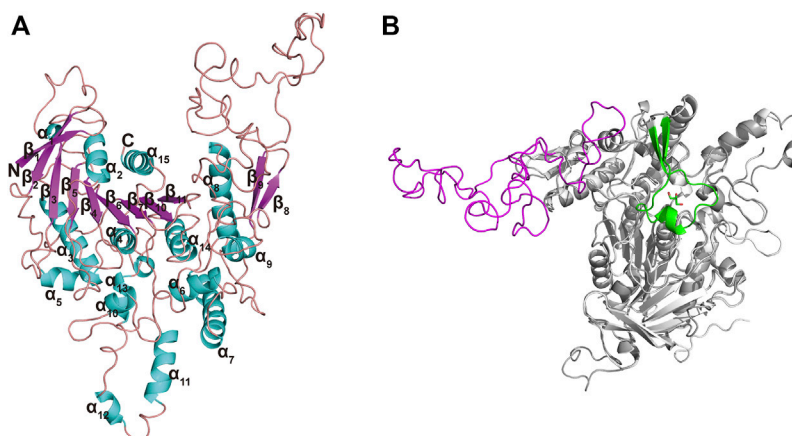


**FIGURE 4 |** Ribbon representation of the TanA<sub>Lb</sub> homology model. **(A)** The modeled 3D-structure of TanA<sub>Lb</sub> based on the crystal structure of TanB<sub>Fnn</sub> from *Fusobacterium nucleatum* subsp. *Polymorphum* (PDB code, 6YQ4). **(B)** Superimposition of the structures of TanA<sub>Lb</sub> (gray, ribbon model) and TanB<sub>Fnn</sub> (white, ribbon model) reveals significant differences between both proteins predominantly found in the flap region. The flap lid in TanB<sub>Fnn</sub> is shown in green and the hypothetic one in TanA<sub>Lb</sub> is shown in magenta.

**TABLE 3 |** The docking score of ligands with TanA<sub>Lb</sub>.

Receptor	Ligand	Docking score (Kcal/mol)
TanA <sub>Lb</sub>	EG	-4.38
TanA <sub>Lb</sub>	MG	-4.19
TanA <sub>Lb</sub>	PG	-4.64
TanA <sub>Lb</sub>	LG	-5.58
TanA <sub>Lb</sub>	TA	-11.39

The biochemical properties of TanA<sub>Lb</sub> were characterized using methyl gallate (MG) as the substrate. The temperature–activity profile revealed that the purified TanA<sub>Lb</sub> displayed the highest activity at 50°C, which was determined by incubating the TanA<sub>Lb</sub> in 20 mM phosphate buffer saline at pH 7.0. TanA<sub>Lb</sub> maintained more than 70% relative activity in a rather wide temperature range from 30°C to 55°C. However, the activity of TanA<sub>Lb</sub> decreased dramatically at temperatures over 60°C. (**Figure 3A**). Furthermore, the thermostability of the purified TanA<sub>Lb</sub> was also measured by pre-incubation at different temperatures in the range of 20°C–60°C. After pre-incubation of the enzyme between 20°C and 40°C, it maintained more than 70% residual activity, which indicated that TanA<sub>Lb</sub> was stable at moderate temperatures. However, incubation at temperature 60°C induced a dramatic decrease in TanA<sub>Lb</sub> activity within 30 min, and the enzyme was completely inactivated after 2 h (**Figure 3B**). Thus, TanA<sub>Lb</sub> was highly active in a wider range of temperatures, from 20°C to 50°C, exhibiting much higher thermostability than the previously reported tannases from *L. plantarum* (Curiel et al., 2009) and *B. subtilis* (Jana et al., 2013).

TanA<sub>Lb</sub> exhibited measurable activity toward methyl gallate at pH 2.5–10, with optimal activity in 20 mM phosphate buffer at pH 7.0. Furthermore, it maintained more than 80% of the maximal activity at pH 5.5–7.5 (**Figure 3C**). TanA<sub>Lb</sub> was also incubated for 2 h in different buffers to investigate its pH stability. Over 80% of the initial enzyme activity remained after incubation

for 2 h at pH 6.5–7.5 (**Figure 3D**), while the residual activity decreased dramatically at pH values from 2–6.5 and 6.5–10.0.

The enzymatic activity of TanA<sub>Lb</sub> in the presence of various additives was determined by pre-incubating the enzyme at 50°C for 1.0 h, and the effects on the activity of TanA<sub>Lb</sub> are shown in **Table 1**. When Mg<sup>2+</sup> and Ca<sup>2+</sup> ions were added, the relative activity of TanA<sub>Lb</sub> was enhanced by 130% and 122%, respectively. Zn<sup>2+</sup> and Co<sup>2+</sup> had a weak influence on the activity of TanA<sub>Lb</sub>, while Cu<sup>2+</sup> and Mn<sup>2+</sup> had a strong inhibitory effect. Additionally, the enzyme activity was increased by surfactants, such as SDS, Tween-80, DMSO, and TritonX-100, while decreased by the metal chelating agent EDTA.

## Kinetic Analysis on Substrate Preference of Tannase From *Lachnospiraceae* bacterium

Tannase catalyzes the hydrolysis of the galloyl ester bond, liberating gallic acid. Accordingly, tannase activity can be determined by measuring the concentration of gallic acid formed by the enzyme. In order to investigate the substrate specificity of TanA<sub>Lb</sub> different esters of gallic acid, methyl gallate (MG), ethyl gallate (EG), propyl gallate (PG), lauryl gallate (LG), and tannic acid (TA) were transformed into gallic acid by TanA<sub>Lb</sub> under the optimal catalytic conditions. The *K<sub>m</sub>* and *k<sub>cat</sub>* value were always used to compare the substrate specificity of enzymes. *K<sub>m</sub>* values of five kinds of substrates showed that tannic acid (TA) had the highest affinity, laurate gallate (LG) had lower activity than tannic acid, and methyl gallate (MG) had the lowest affinity for the TanA<sub>Lb</sub> (**Table 2**). The activity assay also showed that the catalytic efficiency (*k<sub>cat</sub>*/*K<sub>m</sub>*) of TanA<sub>Lb</sub> toward tannic acid (TA) was 5.3- to 12.5-fold larger than that toward the other four substrates. Analysis of catalytic efficiency implied that TanA<sub>Lb</sub> was conducive to using tannic acid (TA) as substrate. On the basis of these results, we can conclude that TanA<sub>Lb</sub> has high substrate affinity and catalytic efficiency for depside bonds. In addition, TanA<sub>Lb</sub> is capable of

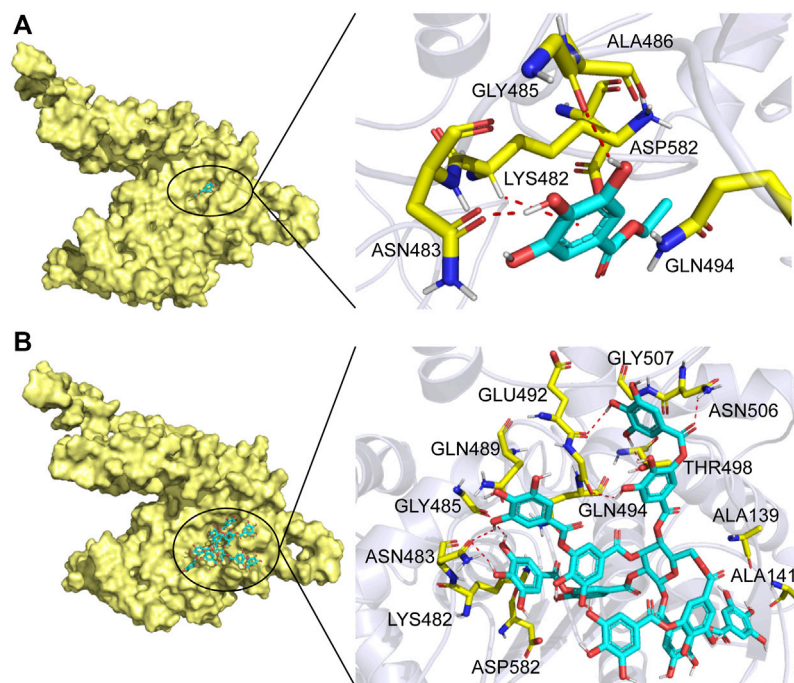


**FIGURE 5 |** Substrate binding mode to TanA<sub>Lb</sub>. **(A)** The binding model of ethyl gallate on molecular surface of TanA<sub>Lb</sub>. **(B)** The binding model of tannic acid on molecular surface of TanA<sub>Lb</sub>. Substrates are colored cyan, and the molecular surface of TanA<sub>Lb</sub> is colored pale yellow. The residues involved in binding are shown in yellow sticks.

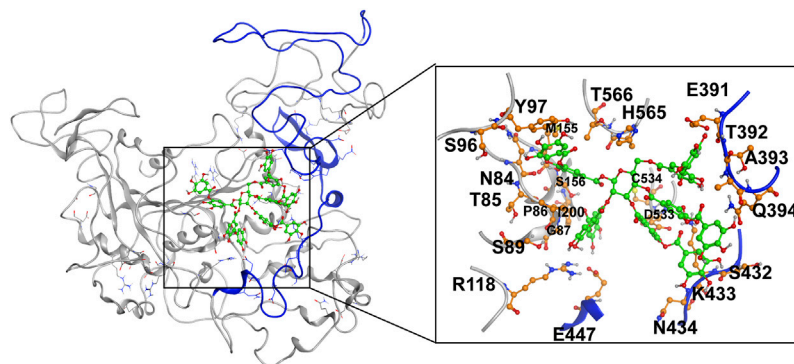


**FIGURE 6 |** The final stable structure model after 500-ns molecular dynamics (MD) simulation. The sequence from 341 to 450 is highlighted with blue color. The atoms in tannic acid in binding area are depicted as green, and the residues in TanA<sub>Lb</sub> involved in binding are depicted as orange.

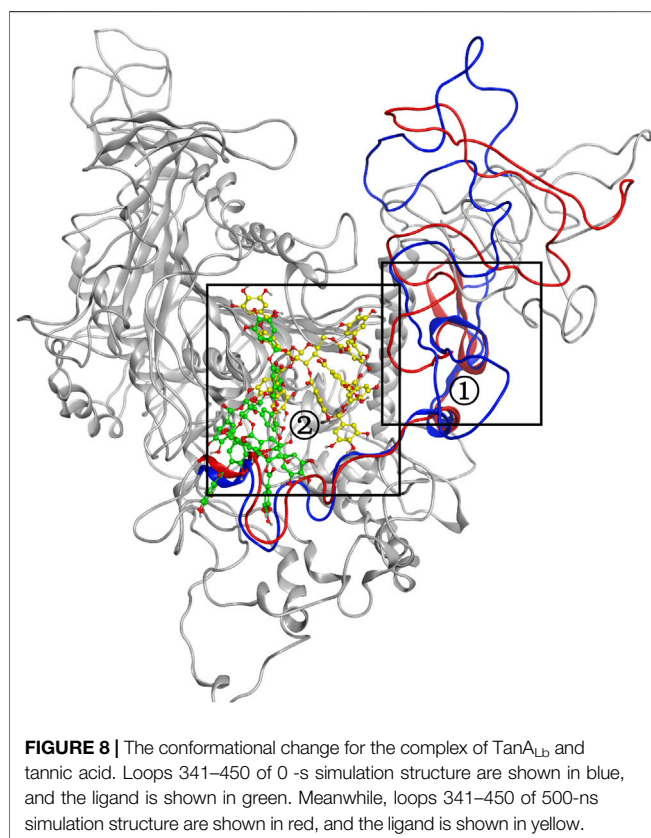
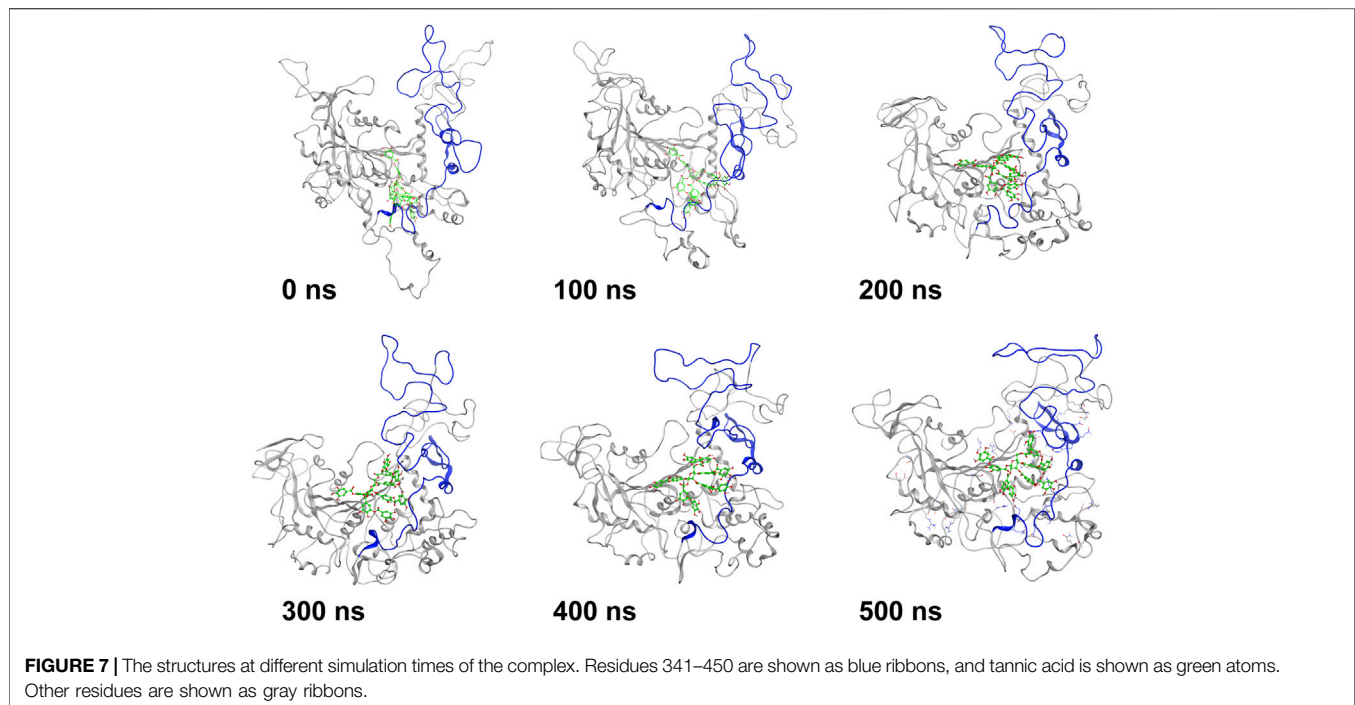
degrading not only esters of phenolic acid with short chain aliphatic alcohols but also esters of phenolic acids with long chain alcohols such as lauryl gallate, similar to TanB<sub>Fnp</sub> and TanB<sub>Fnn</sub> (Tomás-Cortázar et al., 2018; Mancheño et al., 2020).

### Molecular Structure Simulation and Structural Analysis of Tannase From *Lachnospiraceae* bacterium

The Ramachandran plot (Supplementary Figure S2) for TanA<sub>Lb</sub> showed that 98% residues were in allowed regions, indicating that

the 3D structure of the model was reasonable. The structure of TanA<sub>Lb</sub> was composed of nine  $\beta$ -strands and six  $\alpha$ -helices. The  $\beta$ -strands formed a twisted  $\beta$ -sheet, in which  $\beta$ 2 runs antiparallel to the other  $\beta$ -strands, similar to the crystal structure of TanB<sub>Fnn</sub>. Furthermore, the structure of TanA<sub>Lb</sub> exhibited an almost parallel six-strand  $\beta$ -sheet surrounded by five  $\alpha$  helices, two of which were located on the concave side of the sheet ( $\alpha$ 2 and  $\alpha$ 15) and three on the convex side ( $\alpha$ 3,  $\alpha$ 4, and  $\alpha$ 14), to form a central cavity (Figure 4A). In agreement with the sequence alignment, the structural characterization, therefore, indicated that TanA<sub>Lb</sub> belongs to the  $\alpha/\beta$ -hydrolase superfamily (Remington et al.,





1992). It is worth noting that the TanA<sub>Lb</sub> contained an insertion of a 109 residue stretch (residues 341–450) (**Figure 4B**), which is the largest structural deviation and may assume the role of the

flap covering the active site of the enzyme (Mancheño et al., 2020).

## Molecular Docking and Molecular Dynamics Simulation

In order to further understand the mechanism of action of TanA<sub>Lb</sub>, molecular docking and MD simulation were carried out. In the overall docking conformation of TanA<sub>Lb</sub>, the substrates have formed a suitable steric complementarity with the binding site of TanA<sub>Lb</sub>. The docking scores (**Table 3**), the more negative, the better binding with protein, were consistent with the kinetic analysis. The contact residues during docking of ligands on the predicted structure of TanA<sub>Lb</sub> are presented in **Figure 5** and **Supplementary Figures S3–S5**. Concretely, hydrogen bond interactions and H- $\pi$  stacking were formed between TanA<sub>Lb</sub> and ethyl gallate. The oxygen atom of ethyl gallate, regarded as hydrogen bond donor, forms a hydrogen bond with the oxygen atom of backbone of Gly485 and the oxygen atom of side chain of Asn483. The benzene ring of ethyl gallate, forms a CH- $\pi$  stacking with the alpha carbon atom of Lys482 (**Figure 5A**). The other three phenolic acid esters had similar binding modes (**Supplementary Figures S3–S5**). For the most suitable and largest substrate, the oxygen atom of the propyl group in tannic acid, regarded as hydrogen bond donor, forms hydrogen bonds with Gly485, Glu492, Gly493, Thr498, and Asn506. In addition, the two oxygen atoms of the phenolic hydroxyl group in tannic acid form two hydrogen bonds with the oxygen atom of the side chain of Asn483. VDW interactions were also formed between ethyl gallate and the surrounding residues (**Figure 5B**). These docking simulations may provide insights into the substrate specificity of TanA<sub>Lb</sub>, although the exact enzyme structures were not obtained (Wang et al., 2020).

MD simulation was carried out to explore the role of the insertion part (residue 341–450). The results showed that the root means square deviation (RMSD) of heavy atoms of TanA<sub>Lb</sub> was less than 10.0 Å, that of tannic acid was less than 5.0 Å, and the system achieved equilibrium within 150 ns (**Supplementary Figure S6**). The final stable 3D structure binding model of the complex of TanA<sub>Lb</sub> and tannic acid is shown in **Figure 6** and the binding energy of key residues are listed in **Supplementary Tables S1, S2**. During the MD simulation, tannic acid tended to approach the target loop structure (residue 341–450), and the other loop (residue 389–395) moved toward tannic acid to form a stable interaction (**Figure 7**). The main conformational change was the loop from amino acid 389 to 395, which swung like a pair of hands holding tannic acid. The remaining parts, which mainly interact with tannic acid, were the loop structures of 431–435 and 446–448, which were relatively stable here (**Figure 8**). It is supposed that the loop (residue 341–450) is a flap-like domain working for binding bulk substrates such as tannic acid, like the flexible structure in esterases (Truongvan et al., 2016).

## CONCLUSION

A novel bacterial tannase from a species of *Lachnospiraceae* has been cloned and overexpressed in *E. coli* BL21 (DE3), purified, and characterized. It exhibited maximal activity at pH 7.0 and 50°C, and retained more than 70% relative activity from 30°C to 55°C. The enzyme retained more than 80% of the initial activity after incubation for 2 h in the pH range 6.5–7.5. TanA<sub>Lb</sub> is stable in the presence of surfactants such as SDS, DMSO, and TritonX-100. TanA<sub>Lb</sub> has broad substrate specificity, and investigating the detailed kinetic characteristics of TanA<sub>Lb</sub> advances our knowledge about this bacterial tannase at the molecular level. MD simulation revealed an assumed flap-like lid, which was beneficial to the interactions with the substrates. This may be helpful to guide the application of tannase and provide the theoretical basis for the modification of tannase. As a novel bacterial tannase, TanA<sub>Lb</sub> has demonstrated superior properties that may help improve the industrial biodegradation or bioconversion of tannins. Moreover, TanA<sub>Lb</sub> is from *Lachnospiraceae* bacterium in ruminant gastrointestinal tract, and the research probably helps to increase our understanding of the relationship between tannases and gut microbiota and health.

## REFERENCES

- Aboubakr, H. A., El-Sahn, M. A., and El-Banna, A. A. (2013). Some Factors Affecting Tannase Production by *Aspergillus niger* Van Tieghem. *Braz. J. Microbiol.* 44 (2), 559–567. doi:10.1590/s1517-83822013000200036
- Aguiar, C. N., Rodríguez, R., Gutiérrez-Sánchez, G., Augur, C., Favela-Torres, E., Prado-Barragan, L. A., et al. (2007). Microbial Tannases: Advances and Perspectives. *Appl. Microbiol. Biotechnol.* 76 (1), 47–59. doi:10.1007/s00253-007-1000-2
- Aharwar, A., and Parihar, D. K. (2018). Tannases: Production, Properties, Applications. *Biocatal. Agric. Biotechnol.* 15, 322–334. doi:10.1016/j.bcab.2018.07.005
- Baxter, N. J., Lilley, T. H., Haslam, E., and Williamson, M. P. (1997). Multiple Interactions between Polyphenols and a Salivary Proline-Rich Protein Repeat

## DATA AVAILABILITY STATEMENT

The original contributions presented in the study are included in the article/**Supplementary Material**. Further inquiries can be directed to the corresponding authors.

## AUTHOR CONTRIBUTIONS

LG contributed to conception and design of the study. Experiments were conceived and supervised by LG and performed by KW, YG, JL, JW, and SY. Data were analyzed by LG and JW. The manuscript was initially drafted by LG and then revised by CR and SL. NJ, CR, and JW coordinated the project. YZ contributed to project administration. BL and SL took charge of the conceptualization and funding acquisition. All authors read and approved the final manuscript.

## FUNDING

This research was funded by the National Natural Science Foundation of China (31600642), the Agricultural Science and Technology Innovation Project of Heilongjiang Academy of Agricultural Sciences (HNK2019CX19), and the Excellent Young Scholars Fund of Heilongjiang Academy of Agricultural Sciences (2020JCQN004).

## ACKNOWLEDGMENTS

The authors thank Haibo Liu from the Chinese Academy of Medical Sciences for providing the aforementioned modeling software and Wecomput Technology for providing computation consulting.

## SUPPLEMENTARY MATERIAL

The Supplementary Material for this article can be found online at: <https://www.frontiersin.org/articles/10.3389/fbioe.2021.806788/full#supplementary-material>

Result in Complexation and Precipitation. *Biochemistry* 36 (18), 5566–5577. doi:10.1021/bi9700328

- Case, D. A., Aktulga, H. M., Belfon, K., Ben-Shalom, I. Y., Brozell, S. R., Cerutti, D. S., et al. (2021). *Amber 2021*. California, USA: University of California Press.
- Case, D. A., Darden, T. A., Cheatham, T. E., Simmerling, C. L., Wang, J., Duke, R. E., et al. (2008). *Amber 10*. San Francisco CA: University of California.
- Chaitanyakumar, A., and Anbalagan, M. (2016). Expression, Purification and Immobilization of Tannase from *Staphylococcus Lugdunensis* MTCC 3614. *AMB Expr.* 6 (1), 89. doi:10.1186/s13568-016-0261-5
- Charlton, A. J., Baxter, N. J., Khan, M. L., Moir, A. J. G., Haslam, E., Davies, A. P., et al. (2002). Polyphenol/Peptide Binding and Precipitation. *J. Agric. Food Chem.* 50 (6), 1593–1601. doi:10.1021/jf010897z
- Chung, K.-T., Wong, T. Y., Wei, C.-I., Huang, Y.-W., and Lin, Y. (1998). Tannins and Human Health: A Review. *Crit. Rev. Food Sci. Nutr.* 38 (6), 421–464. doi:10.1080/10408699891274273

- Curiel, J. A., Rodríguez, H., Acebrón, I., Mancheño, J. M., De Las Rivas, B., and Muñoz, R. (2009). Production and Physicochemical Properties of Recombinant *Lactobacillus Plantarum* Tannase. *J. Agric. Food Chem.* 57 (14), 6224–6230. doi:10.1021/jf901045s
- Dai, X., Liu, Y., Zhuang, J., Yao, S., Liu, L., Jiang, X., et al. (2020). Discovery and Characterization of Tannase Genes in Plants: Roles in Hydrolysis of Tannins. *New Phytol.* 226 (4), 1104–1116. doi:10.1111/nph.16425
- Dhiman, S., Mukherjee, G., and Singh, A. K. (2018). Recent Trends and Advancements in Microbial Tannase-Catalyzed Biotransformation of Tannins: A Review. *Int. Microbiol.* 21 (4), 175–195. doi:10.1007/s10123-018-0027-9
- Gao, S., Wang, J., Wu, M., Zhang, H., Yin, X., and Li, J. (2012). Engineering Hyperthermostability into a Mesophilic Family 11 Xylanase from *Aspergillus Oryzae* by In Silico Design of N-Terminus Substitution. *Biotechnol. Bioeng.* 110 (4), 1028–1038. doi:10.1002/bit.24768
- Govindarajan, R., Revathi, S., Rameshkumar, N., Krishnan, M., and Kayalvizhi, N. (2016). Microbial Tannase: Current Perspectives and Biotechnological Advances. *Biocatal. Agric. Biotechnol.* 6, 168–175. doi:10.1016/j.bcab.2016.03.011
- Jana, A., Maity, C., Halder, S. K., Das, A., Pati, B. R., Mondal, K. C., et al. (2013). Structural Characterization of Thermotable, Solvent Tolerant, Cytosafe Tannase from *Bacillus Subtilis* PAB2. *Biochem. Eng. J.* 77, 161–170. doi:10.1016/j.bej.2013.06.002
- Jiménez, N., Esteban-Torres, M., Mancheño, J. M., Rivas, B. D., and Muñoz, R. (2014). Tannin Degradation by a Novel Tannase Enzyme Present in Some *Lactobacillus Plantarum* Strains. *Appl. Environ. Microbiol.* 80 (10), 2991–2997. doi:10.1128/aem.00324-14
- Lekha, P., and Lonsane, B. (1997). Production and Application of Tannin Acyl Hydrolase: State of the Art. *Adv. Appl. Microbiol.* 44, 215–260. doi:10.1016/s0065-2164(08)70463-5
- Lekshmi, R., Nisha, S. A., Vasan, P. T., and Kaleeswaran, B. (2021). A Comprehensive Review on Tannase: Microbes Associated Production of Tannase Exploiting Tannin Rich Agro-Industrial Wastes with Special Reference to its Potential Environmental and Industrial Applications. *Environ. Res.* 201, 111625. doi:10.1016/j.envres.2021.111625
- Maisetta, G., Batoni, G., Caboni, P., Esin, S., Rinaldi, A. C., and Zucca, P. (2019). Tannin Profile, Antioxidant Properties, and Antimicrobial Activity of Extracts from Two Mediterranean Species of Parasitic Plant *Cytinus*. *BMC Complement. Altern. Med.* 19 (1), 82. doi:10.1186/s12906-019-2487-7
- Mancheño, J. M., Atondo, E., Tomás-Cortázar, J., Lavín, J. L., Plaza-Vinuesa, L., Martín-Ruiz, I., et al. (2020). A Structurally Unique *Fusobacterium Nucleatum* Tannase Provides Detoxicant Activity against Gallotannins and Pathogen Resistance. *Microb. Biotechnol.*, 1–20. [Epub ahead of print]. doi:10.1111/1751-7915.13732
- Matoba, Y., Tanaka, N., Noda, M., Higashikawa, F., Kumagai, T., and Sugiyama, M. (2013). Crystallographic and Mutational Analyses of Tannase from *Lactobacillus Plantarum*. *Proteins* 81 (11), 2052–2058. doi:10.1002/prot.24355
- Mcdonald, M., Mila, I., and Scalbert, A. (1996). Precipitation of Metal Ions by Plant Polyphenols: Optimal Conditions and Origin of Precipitation. *J. Agric. Food Chem.* 44 (2), 599–606. doi:10.1021/jf950459q
- Noguchi, N., Ohashi, T., Shiratori, T., Narui, K., Hagiwara, T., Ko, M., et al. (2007). Association of Tannase-Producing *Staphylococcus Lugdunensis* with colon Cancer and Characterization of a Novel Tannase Gene. *J. Gastroenterol.* 42 (5), 346–351. doi:10.1007/s00535-007-2012-5
- Remington, S. J., Franken, S. M., Sussman, J., Frolov, F., Ollis, D., Verschueren, K., et al. (1992). The Alpha/beta Hydrolase Fold. *Prot. Eng.* 5, 197–211. doi:10.1093/protein/5.3.197
- Ren, B., Wu, M., Wang, Q., Peng, X., Wen, H., McKinstry, W., et al. (2013). Crystal Structure of Tannase from *Lactobacillus Plantarum*. *J. Mol. Biol.* 425, 2737–2751. doi:10.1016/j.jmb.2013.04.032
- Roe, D. R., and Cheatham, T. E., III (2013). PTRAJ and CPPTRAJ: Software for Processing and Analysis of Molecular Dynamics Trajectory Data. *J. Chem. Theory Comput.* 9 (7), 3084–3095. doi:10.1021/ct400341p
- Rusniok, C., Couvé, E., Cunha, V. D., Gana, R. E., Zidane, N., Bouchier, C., et al. (2010). Genome Sequence of *Streptococcus Gallolyticus*: Insights into its Adaptation to the Bovine Rumen and its Ability to Cause Endocarditis. *J. Bacteriol.* 192 (8), 2266–2276. doi:10.1128/jb.01659-09
- Smeriglio, A., Barreca, D., Bellocchio, E., and Trombetta, D. (2016). Proanthocyanidins and Hydrolysable Tannins: Occurrence, Dietary Intake and Pharmacological Effects. *Br. J. Pharmacol.* 174 (11), 1244–1262. doi:10.1111/bph.13630
- Tomás-Cortázar, J., Plaza-Vinuesa, L., Rivas, B. D., Lavín, J. L., Barriales, D., Abecia, L., et al. (2018). Identification of a Highly Active Tannase Enzyme from the Oral Pathogen *Fusobacterium Nucleatum* Subsp. *Polymorphum*. *Microb. Cell. Fact.* 17 (1). doi:10.1186/s12934-018-0880-4
- Truongvan, N., Jang, S., and Lee, C. (2016). Flexibility and Stability Trade-Off in Active Site of Cold-Adapted *Pseudomonas Mandelii* Esterase EstK. *Biochemistry* 55 (25), 3542–3549. doi:10.1021/acs.biochem.6b00177
- Wang, F., Zhu, M., Song, Z., Li, C., Wang, Y., Zhu, Z., et al. (2020). Reshaping the Binding Pocket of Lysine Hydroxylase for Enhanced Activity. *ACS Catal.* 10 (23), 13946–13956. doi:10.1021/acscatal.0c03841
- White, T. (1957). Tannins—their Occurrence and Significance. *J. Sci. Food Agric.* 8 (7), 377–385. doi:10.1002/jsfa.2740080702
- Wu, M., Wang, Q., McKinstry, W. J., and Ren, B. (2014). Characterization of a Tannin Acyl Hydrolase from *Streptomyces Viscus* with Substrate Preference for Digalloyl Ester Bonds. *Appl. Microbiol. Biotechnol.* 99 (6), 2663–2672. doi:10.1007/s00253-014-6085-9

**Conflict of Interest:** The authors declare that the research was conducted in the absence of any commercial or financial relationships that could be construed as a potential conflict of interest.

**Publisher's Note:** All claims expressed in this article are solely those of the authors and do not necessarily represent those of their affiliated organizations, or those of the publisher, the editors, and the reviewers. Any product that may be evaluated in this article, or claim that may be made by its manufacturer, is not guaranteed or endorsed by the publisher.

Copyright © 2021 Guan, Wang, Gao, Li, Yan, Ji, Ren, Wang, Zhou, Li and Lu. This is an open-access article distributed under the terms of the Creative Commons Attribution License (CC BY). The use, distribution or reproduction in other forums is permitted, provided the original author(s) and the copyright owner(s) are credited and that the original publication in this journal is cited, in accordance with accepted academic practice. No use, distribution or reproduction is permitted which does not comply with these terms.





# Effects of Pore Size and Crosslinking Methods on the Immobilization of Myoglobin in SBA-15

Hengmin Miao<sup>1,2</sup>, Maosheng Li<sup>2,3</sup>, Xiaochun Sun<sup>4</sup>, Jikun Xia<sup>2,5</sup>, Yanqing Li<sup>2,6</sup>, Jiao Li<sup>1\*</sup>, Fang Wang<sup>2\*</sup> and Jiakun Xu<sup>2\*</sup>

<sup>1</sup>School of Materials Science and Engineering, Shandong University of Technology, Zibo, China, <sup>2</sup>Key Lab of Sustainable Development of Polar Fisheries, Lab for Marine Drugs and Byproducts of Pilot National Lab for Marine Science and Technology, Yellow Sea Fisheries Research Institute, Chinese Academy of Fishery Sciences, Qingdao, China, <sup>3</sup>School of Food Science and Engineering, Qilu University of Technology (Shandong Academy of Sciences), Jinan, China, <sup>4</sup>Marine Science Research Institute of Shandong Province, Qingdao, China, <sup>5</sup>College of Marine Science and Biological Engineering, Qingdao University of Science and Technology, Qingdao, China, <sup>6</sup>College of Food Science and Technology, Shanghai Ocean University, Shanghai, China

## OPEN ACCESS

### Edited by:

Hui-Min Qin,  
Tianjin University of Science and  
Technology, China

### Reviewed by:

Chunjie Gong,  
Hubei University of Technology, China  
Yunjie Xiao,  
Tianjin University, China

### \*Correspondence:

Jiao Li  
haiyan9943@163.com  
Fang Wang  
wendywf2002@163.com  
Jiakun Xu  
xujk@ysfri.ac.cn

### Specialty section:

This article was submitted to  
Industrial Biotechnology,  
a section of the journal  
Frontiers in Bioengineering and  
Biotechnology

**Received:** 02 December 2021

**Accepted:** 20 December 2021

**Published:** 28 January 2022

### Citation:

Miao H, Li M, Sun X, Xia J, Li Y, Li J,  
Wang F and Xu J (2022) Effects of Pore  
Size and Crosslinking Methods on the  
Immobilization of Myoglobin in SBA-  
15.  
Front. Bioeng. Biotechnol. 9:827552.  
doi: 10.3389/fbioe.2021.827552

A series of stable mesoporous silica sieves (SBA-15) with different pore sizes (9.8, 7.2, and 5.5 nm) were synthesized using a hydrothermal method. The resulting mesoporous material was then utilized for protein immobilization using myoglobin (Mb) as the target protein. The effects of pore size and adsorption methods on the immobilization efficiency of Mb in a mesoporous material were studied. The SBA-15 with a pore size of 7.2 nm showed the best loading capacity, reaching 413.8 mg/g. The SBA-15 with a pore size of 9.8 nm showed the highest retained catalytic ability (92.36%). The immobilized enzyme was more stable than the free enzyme. After seven consecutive assay cycles, Mb adsorbed by SBA-15 (Mb/SBA-15) and Mb adsorbed by SBA-15 and crosslinked with glutaraldehyde (Mb/G/SBA-15) retained 36.41% and 62.37% of their initial activity, respectively.

**Keywords:** myoglobin, SBA-15, immobilization, catalytic activity, reusability

## INTRODUCTION

Conventional enzymes are especially effective when catalyzing a series of reactions under mild conditions. However, under cruel conditions, conventional enzymes have obvious limitations in practical applications due to insufficient stability (Schmid et al., 2001; Sheldon, 2007; Wang and Hsieh, 2008; Badgujar and Bhanage, 2015). Most enzymes are unstable and lose their activity easily in organic solvents or high-temperature conditions, and they are difficult to be recycled, so they are not always ideal for industrial applications. These disadvantages would be overcome by immobilizing enzymes on solid supports (Hartmann, 2005; Clark et al., 2006; Vinu et al., 2006; Cipolatti et al., 2014; Eş et al., 2015). Over the past few decades, great efforts were devoted to constructing immobilized protein for improved efficiency and stability (Bezbradica et al., 2006; Zheng et al., 2006). To date, several new types of carriers and technologies on immobilization have been developed to enhance the loading and stability of enzymes, which could reduce the cost of enzyme biocatalysts for industrial applications. These include crosslinked enzyme aggregates, microwave-assisted immobilization, mesoporous supports, and click chemistry technology (Xu et al., 2014). Mesoporous silica materials have gathered significant attention in both academic and industrial areas due to their well-ordered and adjustable pore structures as well as abundant hydroxyl groups, accompanied by a series of advantages, such as cost-effectiveness, simple process, readily available raw materials, easy purification of products, low cost, and long guarantee period (Salis et al., 2005). There are

mainly three kinds of immobilization methods: physical adsorption, where van der Waals forces, hydrogen bonding, and electrostatic force exist between the support and enzyme; crosslinking adsorption, where the active group of the enzyme reacts with a crosslinking agent to form crosslinked aggregates; and covalent adsorption, where chemical bonds are formed between support and enzyme. Physical adsorption is one of the most widely used methods due to its simplicity, and it typically does not change the native structure of the enzyme (Li et al., 2009; Jesionowski et al., 2014).

SBA-15 is a form of mesoporous silica nanoparticle with uniform pore size and long-range ordered pore structure. The morphology, pore size, and pore structure of mesoporous silica can be freely designed and controlled. SBA-15 has been extensively investigated as a catalyst supporting absorbents and drug delivery due to its simple preparation, uniform pore structures, diverse morphology, and well-modified surface properties. On the one hand, the large surface area and high pore volume of SBA-15 not only can promote the immobilization of enzyme molecules but also can protect the enzyme and enhance its operational stability (Lynch et al., 2016). On the other hand, in the process of adsorption, too large a pore may make the proteins easier to leach out from the channels, resulting in a decrease in enzyme loading (Kang et al., 2007). According to reports, the ratio of pore size to the size of the enzyme may greatly affect the adsorption of the enzyme (Lü et al., 2008), mainly because the smaller pore size makes it difficult for proteins to enter the channel, resulting in a low enzyme loading. However, in some other cases, the nature of the pores, total pore volume, and surface area have no obvious effects on the enzyme immobilization process (Serra et al., 2008).

Although the physical adsorption method is simple, the stability of the immobilized enzyme might be poor due to the leaching of adsorbed enzymes. For instance, Serra et al. studied the loss of physical adsorption lipase and found that nearly 30% of the enzyme was leached from the support silica. Hydroxyl groups are the only existing groups on the surface of silica; the silica support generally requires further modification with functional groups (like  $-NH_2$  or  $-CHO$  groups) to generate chemical bonds for enzyme immobilization, but it required harsh conditions and multistep synthetic processes (Hong et al., 2008). Crosslinking adsorption and covalent adsorption are common methods to overcome this drawback. Compared with covalent adsorption, crosslinking adsorption is simpler and easier to operate, and this method depends on the use of coupling reagents (such as polyamines, polyethyleneimine, and various phosphates) to crosslink the enzyme molecules. Chemical means of crosslinking normally involve covalent bonding between enzymes by using reagents such as glutaraldehyde or toluene diisocyanate. Glutaraldehyde is a common crosslinking agent, and its aldehyde group could react with the amino groups in enzyme molecules to realize the crosslinking between immobilization enzymes. Kim et al. (2010) adsorbed the enzyme onto mesoporous silica and then add glutaraldehyde to crosslink the enzymes with the improved recovery of immobilized enzyme. Gao et al. (2010) used glutaraldehyde as a crosslinking agent to adsorb lipase on

SBA-15; the immobilized lipase retained 80.5% activity after repeated use for 6 times.

Myoglobin (Mb), having molecular dimensions of  $4.5 \times 3.5 \times 2.5$  nm (Wüstneck et al., 1989), is a heme protein that originally functions as oxygen storage and transportation. Mb can be transformed into peroxidase by protein engineering, which can catalyze various reactions such as oxidation of guaiacol and indole (Xu et al., 2012; Liao et al., 2020) and decolorization of industrial dyes (Zhang et al., 2019). In this study, three different pore diameters of SBA-15 (5.5, 7.2, and 9.8 nm) were prepared using a reported method (Zhao et al., 1998a; Zhao et al., 1998b) and characterized by means of scanning electron microscopy (SEM), Fourier transform IR (FTIR) spectroscopy, small-angle X-ray diffraction (SAXRD), and nitrogen adsorption-desorption experiments. The synthesized SBA-15 was then used for Mb immobilization. The influences of pore size and surface area of SBA-15 on the protein immobilization were investigated. Glutaraldehyde as a crosslinking agent has been utilized in the immobilization process, which effectively prevented the loss of enzyme molecules from the pore channels of mesoporous materials.

## MATERIALS AND METHODS

### Materials

1,3,5-Trimethylbenzene (TMB) and P123 triblock copolymer (poly(ethylene oxide)-block-poly(propylene oxide)-block-poly(ethylene oxide), EO20-PO70-EO20,  $M_n = 5,800$ ), and tetraethyl orthosilicate (TEOS) were purchased from HI-LEAD BIO-TECHNOLOGY, Qingdao, China. Guaiacol was purchased from TCI, Shanghai, China. H64D/V68I Mb was expressed in *Escherichia coli* BL21 (DE3) cells and purified using the procedure described previously.

### Methods

#### Synthesis of SBA-15

The SBA-15 mesoporous materials were synthesized using a previously reported method (Zhao et al., 1998a; Zhao et al., 1998b), with P123 as a structure-directing agent and the TMB as a pore dilator agent. First, 4 g of P123 was dissolved in 104 ml of water and 20 ml of 2 M HCl by stirring at 35°C. Then, an appropriate amount of TMB was added to adjust the final target pore size. A total of 8.5 g of TEOS was then added to the solution and stirred at 35°C for 24 h. This resulting solution was transferred into a Teflon-lined autoclave and heated to 100°C for 24 h. Finally, the solid products were filtered and washed with deionized water, air-dried at room temperature, calcined at 500°C for 6 h at a heating rate of  $1^\circ\text{C min}^{-1}$  in a tube furnace, and returned to room temperature at a cooling rate of  $5^\circ\text{C min}^{-1}$ .

#### Characterization of SBA-15

SEM micrographs were obtained on a Zeiss Merlin compact field-emission SEM (Carl Zeiss, Oberkochen, Germany). Nitrogen adsorption-desorption experiments were

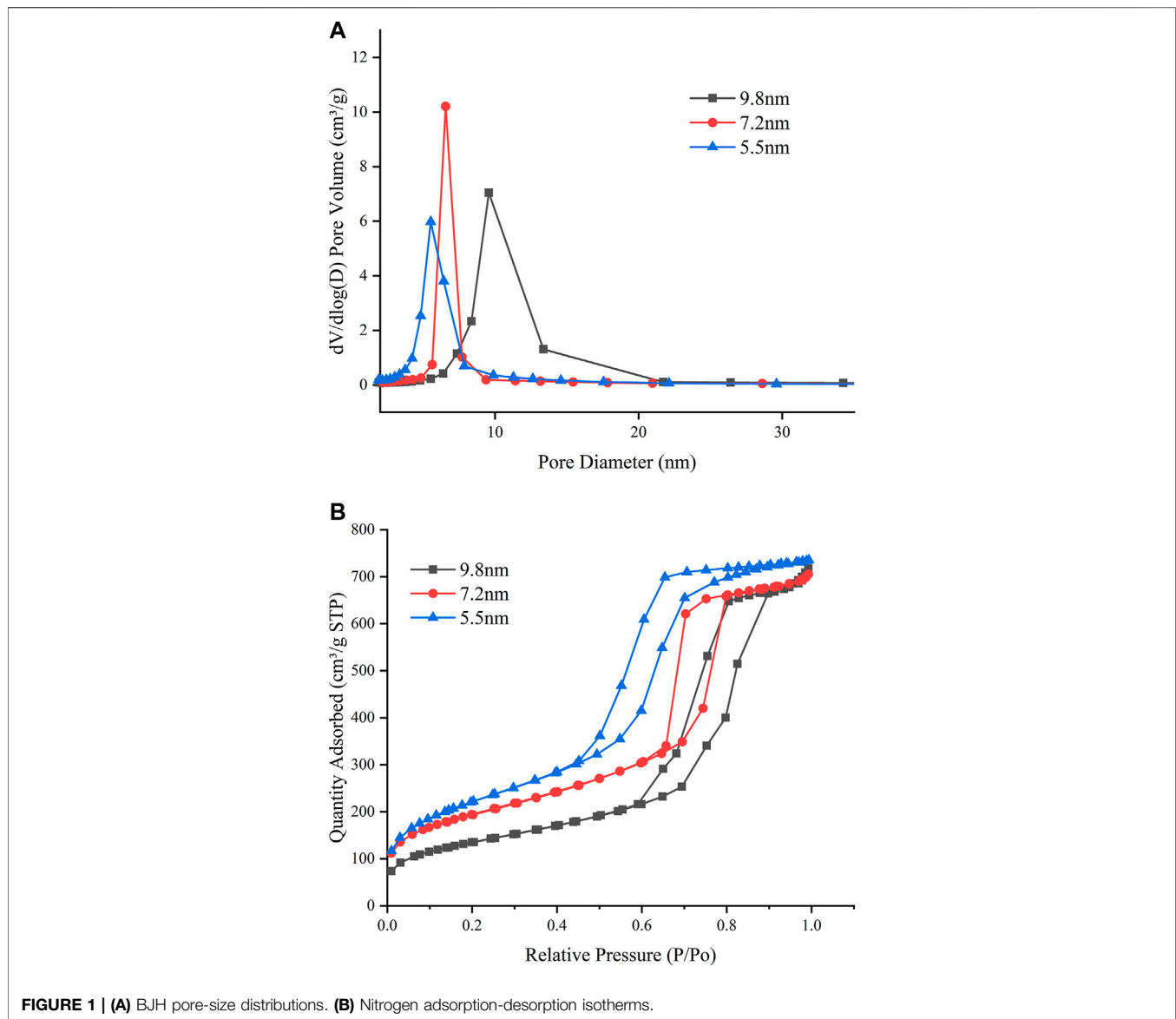


**FIGURE 1 | (A)** BJH pore-size distributions. **(B)** Nitrogen adsorption-desorption isotherms.

performed using an ASAP 2460 Micromeritics System, Micromeritics instrument Ltd, America. Before the measurement, samples were degassed in a vacuum at  $200^\circ\text{C}$  for 2 h. The surface areas were calculated using the Brunauer–Emmett–Teller (BET) method based on the desorption isotherms, and the pore diameter distributions were calculated from desorption branches using the Barrett–Joyner–Halenda (BJH) method. The small-angle X-ray powder diffraction patterns were obtained using Cu K $\alpha$  radiation on a Bruker D8 Advance diffractometer (Bruker, Kontich, Belgium). The data were collected from  $0.5^\circ$  to  $10^\circ$  with a step size of  $0.5^\circ$ . The IR spectra were recorded in diffuse reflectance mode (spectral resolution  $4\text{ cm}^{-1}$ , 100 scans) using FTIR spectroscopy (Shimadzu 8201 PC spectrophotometer in the region  $400\text{--}4,000\text{ cm}^{-1}$ ; Shimadzu Corp., Kyoto, Japan). The samples were prepared using the standard KBr disk method. All analyses were conducted under dry conditions.

### Adsorption of Myoglobin on SBA-15

The optimal conditions for adsorption were obtained by changing the immobilization time, shaking speed, temperature, and pH. The adsorption experiments were performed by mixing 5 mg of SBA-15 and 1 ml of protein solution (2 mg/ml) and stirring at  $25^\circ\text{C}$  for 15 h in 2 ml of phosphate buffer (50 mM, pH 6). Then, the reaction mixture was centrifuged, the supernatant was removed, and 1 ml of phosphate buffer (50 mM, pH 6) was added to the precipitate. The mixture was stirred for 1 h to wash the SBA-15 and centrifuged, and the supernatant was removed. This last wash step was repeated three times. The UV absorption value of the supernatant was measured at 470 nm to determine the concentration of protein in the supernatant. The final products were identified as Mb/SBA-15. The kinetics of the adsorption process was investigated by testing the relationship between the loading amount of Mb enzyme originally added and time.

**TABLE 1** | Detailed structural features of SBA-15.

BJH pore diameter (nm)	BJH pore volume (cm <sup>3</sup> /g)	BET surface area (m <sup>2</sup> /g)
9.8	1.08	484.133
7.2	1.05	612.911
5.5	1.02	803.489

Note. BJH, Barrett–Joyner–Halenda; BET, Brunauer–Emmett–Teller.

**TABLE 2** | The maximum adsorption amount and retained activity of Mb onto SBA-15.

BJH pore diameter (nm)	BET surface area (m <sup>2</sup> /g)	Adsorption proteins (mg/g)	Retained activity (%)
9.8	484.133	359.6 ± 10.73	93.24 ± 1.36
7.2	612.911	413.8 ± 9.86	90.10 ± 1.57
5.5	803.489	381.8 ± 9.4	86.13 ± 1.62

Note. BJH, Barrett–Joyner–Halenda; BET, Brunauer–Emmett–Teller.

To determine the crosslinking adsorption of Mb onto SBA-15, 2.0 wt% of glutaraldehyde was added to the solution after 15 h of Mb protein physical adsorption, and the mixture was stirred for 30 min at 25°C to crosslink the adsorbed protein. The final product was identified as Mb/G/SBA-15. To determine the effect of glutaraldehyde dosage on the activity of the immobilized enzyme, different volumes of glutaraldehyde were used in the protocol described for enzyme crosslinking, and the activity was compared with that of Mb/SBA-15. To determine the effect of pH on protein adsorption, 0.5 mg of SBA-15 and 1 ml of protein solution were added to 2 ml of buffer (pH 3–5, 50 mM, citrate buffer; pH 6–9, 50 mM, phosphate buffer) following the procedure described above.

### Catalytic Activity of Free Myoglobin and Immobilized Myoglobin

The assays comparing the catalytic activity of free Mb and immobilized Mb were performed using the oxidation of guaiacol and the product by UV absorption at 470 nm (Zhang et al., 2020). The reaction mixture (50 mM of phosphate buffer, 1 μM of Mb, 2.5 mM of guaiacol) was incubated at 25°C for 15 min, and the reaction was initiated by the addition of H<sub>2</sub>O<sub>2</sub> (final concentration 10 mM). The effect of pore size on the activity of the immobilized enzyme was determined by the retained activity, which is the percentage of activity that is maintained in the immobilized enzyme compared with the free enzyme activity.

### Operational Stability Test for Free and Immobilized Myoglobin

To assess the stability of the immobilized protein, the influence of metal ions (Ba<sup>2+</sup>, Ca<sup>2+</sup>, Mg<sup>2+</sup>, Mn<sup>2+</sup>, and Al<sup>3+</sup>), organic solvents (methanol, ethanol, isopropanol, glycol, and formic acid), storage time, and temperature on Mb activity were studied. The reactions were carried out in 50 mM, pH 6, of phosphate buffer.

The experiment to study the effect of metal ions on Mb activity was performed as follows: free Mb, Mb/SBA-15, and Mb/G/SBA-15 were incubated for 1 h in a buffer solution (phosphate buffer, 50 mM, pH 6) containing different metal ions (10 mM), with a control group containing solely buffer solution. Then, the enzyme activity was tested using the method described in *Catalytic Activity*

*of Free Myoglobin and Immobilized Myoglobin*. The effect of organic solvents (10% v/v) was investigated in the same way. The effect of temperature on the activity of free and immobilized Mb was examined by incubation for 1 h in phosphate buffer (50 mM, pH 6) in a temperature range between 10°C and 60°C. The effect of storage time was tested by determining the residual activity after storing the Mb in phosphate buffer (50 mM, pH 6) for different time periods of 30 days at 25°C. The activity was assayed every 5 days.

### Reusability Test for Myoglobin/SBA-15 and Myoglobin/G/SBA-15

The proteins were physically adsorbed onto the SBA-15 with different pore sizes, and then the catalytic activities were tested by measuring the oxidation of guaiacol. After centrifugation of the reaction solution, the supernatant was tested using UV, and the precipitate was washed three times with phosphate buffer (50 mM, pH 6). The above method was used to test the reusability of Mb/SBA-15 for seven consecutive assays. The remaining activity was calculated by comparing it with the first assay. The leaching amount of protein in the supernatant of the assays for Mb/SBA-15 and Mb/G/SBA-15 was determined to calculate the protein leaching rate (leaching amount of protein/initial total amount of immobilized protein) after each reaction.

## RESULTS AND DISCUSSION

### Structural Characteristics of the SBA-15

The BJH pore-size distributions and nitrogen adsorption–desorption isotherms of materials are shown in **Figure 1**. The BJH pore-size distributions show that the pore sizes of the three samples are 9.8, 7.2, and 5.5 nm. The nitrogen adsorption–desorption isotherms of the three samples can be classified as type IV and exhibit an H1-type hysteresis loop at high relative pressure, which is a typical feature of hexagonal cylindrical pore mesoporous materials (Shah et al., 2008). Detailed structural features are shown in **Table 1**.

SAXRD patterns of the SBA-15 show three well-resolved peaks (**Supplementary Figure S1**) that are indexed as (100), (110), and (200) reflections. These three peaks are the characteristic of

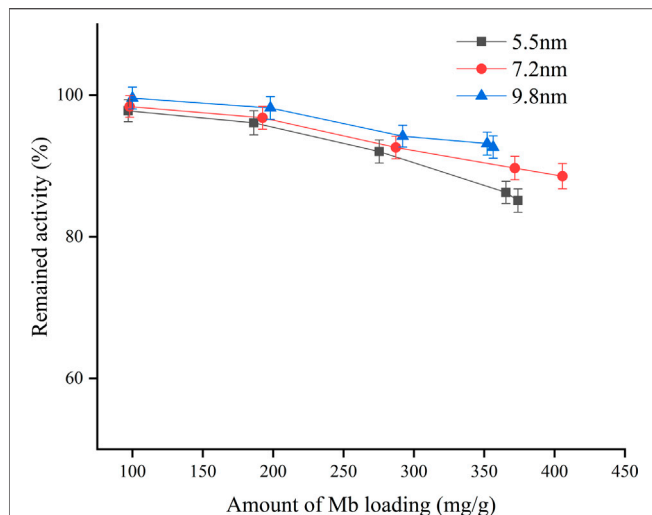


**FIGURE 2 |** Effect of pore size and amount of Mb loading on remained activity.

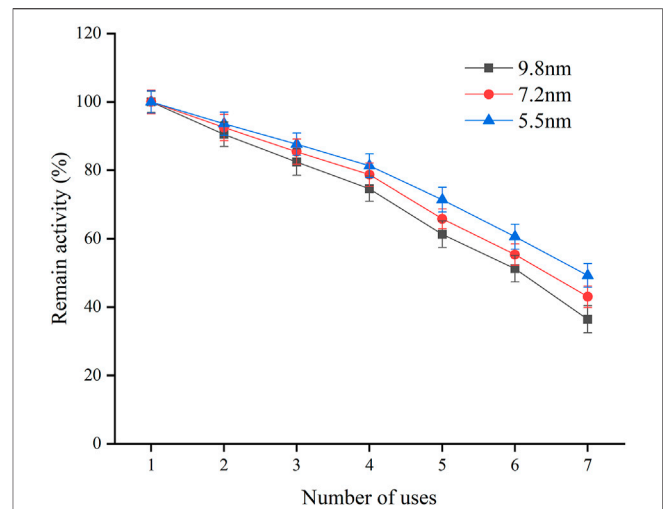


**FIGURE 4 |** Reusability of immobilized Mb on SBA-15 with different pore diameter.

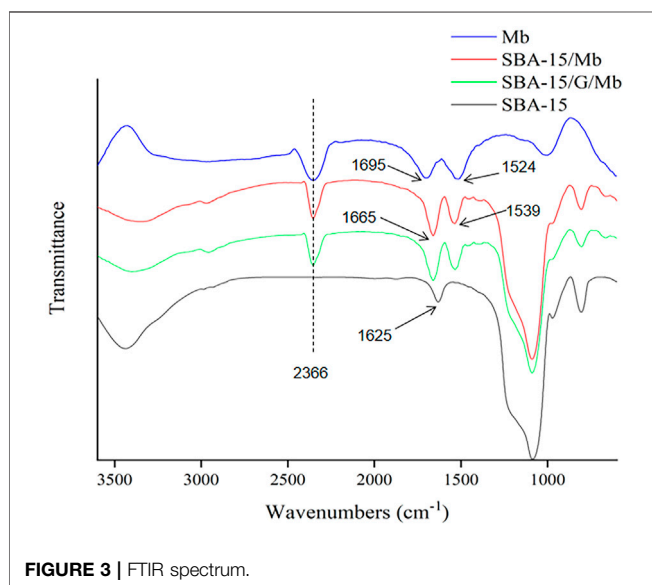


**FIGURE 3 |** FTIR spectrum.

hexagonal mesoporous structures, are associated with p6mm hexagonal symmetry (Zhao et al., 1998a), and indicate that the structure of the SBA-15 is actually representative of a long-range order.

The SEM images of SBA-15 are shown in **Supplementary Figure S2**, showing that the structures of the three samples are the same. The structure of materials is rod-shaped; meanwhile, they consist of many rod-shaped domains with relatively uniform sizes.

## Immobilization of Myoglobin on the SBA-15 Using Physical Adsorption

We assessed the effect of SBA-15 pore diameter (5.5, 7.2, and 9.8 nm) on the immobilization efficiency and activity of Mb compared with free Mb using a physical adsorption method.

The influence of pore size on Mb loadings on the SBA-15 is shown in **Supplementary Figure S3**. As shown in **Supplementary Figure S3A**, the SBA-15 with a larger pore diameter showed much higher adsorption efficiency, indicating that the material with larger pores is more efficient for protein adsorption, whereas the smaller pore size is not conducive to the entry of protein molecules into its channels and thus limits the spread of the enzymes (Bonzom et al., 2018). Apparently, it takes slightly more time for the adsorbed Mb to move into the channels of the SBA-15. The SBA-15 with a pore diameter of 7.2 nm had better protein adsorption capacity than the other two, with the loading amount reaching 413.9 mg/g, whereas the adsorption capacity of the SBA-15 with pore diameters of 5.5 and 9.8 nm was 381.8 and 359.6 mg/g, respectively (**Table 2**, initial Mb concentration: 3 mg/ml). This result suggests that the protein immobilized on the material with a larger pore size (9.8 nm) might easily leak out from the SBA-15 during the immobilization process. **Supplementary Figure S3B** shows that the amount of protein loaded increased with the increase in protein concentration, and the adsorption equilibrium was reached when the protein concentration was more than 2 mg/ml. Although the SBA-15 with a pore size of 7.2 nm was best for adsorption of Mb, the Mb immobilized on the SBA-15 of pore diameter 9.8 nm showed the best remaining enzymatic activity (93.24%). Consistent with the report by Serra (Serra et al., 2008), we also found that the surface area of the SBA-15 had no significant effect on the adsorption capacity.

As shown in **Figure 2**, the retained activity of the immobilized protein was affected by the pore size, and the SBA-15 with a larger pore size was best for the enzymatic reaction. On the other hand, the enzymatic activity of immobilized Mb decreased as the amount of Mb loading increased. It is likely that as more and more Mb diffused into the pores of the SBA-15, some might get aggregated and did not distribute as a one layer at the inner surface of the channels, leading to a decrease in enzyme activity per gram due to the non-contact with substrates of the bottom layer Mb (Gao et al.,



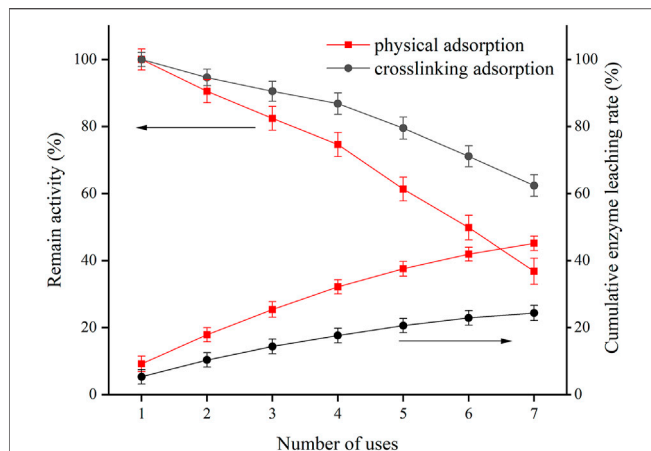


**FIGURE 5 |** Reusability of immobilized Mb with different methods and immobilized Mb leaching ration.

**TABLE 3 |** The enzyme activity loss rate and leaching rate after repeated use for seven times with different adsorption methods.

Adsorption method	Enzyme activity loss rate (%)	Enzyme leaching rate (%)
Physical adsorption	63.59 ± 1.46	45.12 ± 1.34
Crosslinking adsorption	37.63 ± 1.38	24.31 ± 1.27

2010). Considering the effect of pore size on loading capacity and retained activity, the SBA-15 with a pore size of 9.8 nm was the most suitable for enzyme immobilization. Therefore, it was chosen as the representative support for the rest of the study.

## Crosslinking Adsorption of Myoglobin Onto SBA-15

To solve the leaching problem of the adsorbed enzyme, the SBA-15 with a pore size of 9.8 nm was used for crosslinking. Glutaraldehyde was used as a crosslinking agent for adsorption. The addition of glutaraldehyde could reduce the leaching of the enzyme and make the adsorption capacity of the SBA-15 with the 9.8-nm pore diameter reach 471.3 mg/g (Mb/G/SBA-15), which was 31.06% higher than physical adsorption. This is because the aldehyde group of the glutaraldehyde molecule reacts with the amino group of Mb through a Schiff's base reaction (Chui and Wan, 1997) so that multiple protein molecules are crosslinked to form a whole, which makes it difficult for the protein to leach from the pore. The amount of glutaraldehyde in the absorption process was optimized (Supplementary Figure S4). When the amount of glutaraldehyde was less than 400  $\mu$ l, the enzyme activity after crosslinking adsorption was the same as that after physical adsorption. However, the enzyme activity was inhibited when the amount of glutaraldehyde solution was more than 400  $\mu$ l. Therefore, we chose 400  $\mu$ l of glutaraldehyde solution (2.0 wt%) for the crosslinking adsorption of Mb onto the SBA-15. Too much crosslinking agent could result in a distortion of the enzyme

structure (Chui and Wan, 1997), which would lead to the decrease of the catalytic activity.

## Fourier Transform IR Spectrum

To confirm that Mb was immobilized on the SBA-15, the FTIR spectra of Mb, SBA-15, SBA-15/Mb, and SBA-15/G/Mb were studied. As shown in Figure 3, in the FTIR spectra of Mb, the peak at 2,366  $\text{cm}^{-1}$  corresponds to the secondary amine salt, and the peaks at 1,695 and 1,524  $\text{cm}^{-1}$  correspond to amide I and N-H bending vibrations, respectively (Nguyen et al., 2008; Kijima et al., 2018). Compared with that of SBA-15, the absorption of SBA-15/Mb has the characteristic peaks of Mb. The absorption band at about 1,625  $\text{cm}^{-1}$  can be attributed to the stretching vibration of Si-OH at the surface of the SBA-15 (Li et al., 2009) because the absorption band of amide I is also near this position. Thus, the two absorption bands overlap, and only one absorption band is evident. FTIR shows that the protein was immobilized to SBA-15/Mb. Meanwhile, the protein was also immobilized on SBA-15/G/Mb, but the characteristic absorption peak of glutaraldehyde was not observed. This may be because the aldehyde group reacts with the amino group in Mb, which also proves the feasibility of glutaraldehyde crosslinking.

## Stability of Free and Immobilized Myoglobin

Supplementary Figure S5 shows the stability of free Mb, Mb/SBA-15, and Mb/G/SBA-15 tested under different conditions. Supplementary Figure S5A shows the thermal stability of both the free and immobilized Mb. The optimum reaction temperature of free Mb was 25°C, whereas both Mb/SBA-15 and Mb/G/SBA-15 showed maximum activities at a higher temperature of 30°C. At 60°C, Mb/SBA-15 and Mb/G/SBA-15 retained 52.98% and 57.5% of the relative activity, respectively, whereas free Mb retained only 31.02%, which proved that the immobilized Mb has higher temperature stability.

The effect of storage time on the relative activity of the free and immobilized Mb is shown in Supplementary Figure S5B. Although the enzyme activity decreased with the increase of storage time, Mb/SBA-15 and Mb/G/SBA-15 retained over 51.5% and 58.9% of the relative activity, respectively, after 30 days, whereas free Mb retained only 33.68%. Thus, the immobilized Mb exhibited better storage stability than free Mb.

Supplementary Figures S5C,D show the effects of metal ions and organic solvents on the activity of free and immobilized Mb, respectively. Considering the effect of metal ions on the enzyme activity, we found that  $\text{Ba}^{2+}$ ,  $\text{Ca}^{2+}$ ,  $\text{Mg}^{2+}$ , and  $\text{Mn}^{2+}$  could improve the enzyme activity. Mb/SBA-15 and Mb/G/SBA-15 still retained 19.97% and 21.48% of relative activity, respectively, in the presence of 10 mM of  $\text{Al}^{3+}$ , whereas free Mb was completely inactivated under the same condition. As for the influence of organic solvents on the activity of free and immobilized Mb, the methanol solution could improve the enzyme activity. Ethanol, isopropanol, glycol, and formic acid solutions could inhibit the activity of free and immobilized Mb. The relative activities of Mb/SBA-15 and Mb/G/SBA-15 were higher than those of free Mb under the same conditions. The comparison of the immobilized Mb and free Mb revealed that the relative activity of Mb/SBA-15 was increased by 8.73%, 9.86%, 9.16%, and 30.84% in ethanol,

isopropanol, glycol, and formic acid solutions, respectively. Mb/G/SBA-15 retained higher relative activity and increased by 9.2%, 11.64%, 10.28%, and 32.7% in the above solutions. It has been previously observed that Mb immobilized on SBA-15 is protected from metal ions and organic solutions, and the addition of crosslinking agent can further increase the stability of the enzyme.

## Reusability of Myoglobin/SBA-15 and Myoglobin/G/SBA-15

The reusability of immobilized enzymes is very important for their practical application. **Figure 4** shows the remaining activity of Mb immobilized on SBA-15 with different pore diameters after seven consecutive uses. The Mb immobilized on SBA-15 with different pore sizes of 5.5, 7.2, and 9.8 nm retained 49.26%, 43.02%, and 36.41% of its original activities after seven consecutive uses, respectively. The SBA-15 with a smaller pore diameter retained the most activity, which could be attributed to the easy leaking out of the enzyme from SBA-15 with a large pore diameter during the reuse process (Dettori et al., 2018).

As shown in **Figure 5**, the crosslinked adsorption proteins retain more activity, effectively improving enzyme reusability. A total of 62.37% of initial activity was retained after seven consecutive assays, which proved that the addition of glutaraldehyde can reduce the leaching of the enzyme and improve the reusability of the enzyme. As shown in **Table 3**, the catalytic activity loss of physical adsorption and crosslinking adsorption was 63.59% and 37.63%, respectively. Assessment of the protein content in the supernatant of the eluate revealed that some Mb was leached from the immobilized Mb during the reuse process. The protein leaching rate for Mb/SBA-15 and Mb/G/SBA-15 was 45.12% and 24.31%, respectively. The catalytic activity loss rate was greater than the corresponding protein leaching rate. Therefore, the loss of catalytic activity of immobilized Mb in reuse was caused by protein leaching and partial inactivation of the protein. Thus, crosslinking is a useful method for protein immobilization, which could not only increase the loading ability but also increase the stability of the immobilized protein.

As shown in **Supplementary Figure S6**, the changes in pH have a large influence on the adsorption capacity by the method of physical adsorption. The reason is that electrostatic force is included in the adsorption process, and the isoelectric points of SBA-15 and Mb are 3.8 and 7, respectively (Essa et al., 2007; Jin et al., 2020). In the zone pI (SBA-15) and pI (Mb), the charges are complementary, and there is an electrostatic attraction between protein and carrier materials, which is conducive to the adsorption of protein on the carrier. As the pH increased from 7 to 9, the overall charge of the protein and SBA-15 is the same, so the protein easily leaches due to electrostatic repulsion. After crosslinking, the effect of pH on protein

adsorption decreases, which proves that protein leaching could be reduced by crosslinking.

## CONCLUSION

We successfully synthesized SBA-15 with different pore diameters using a hydrothermal method. The pore size of the SBA-15 showed significant effects on the immobilization of Mb: a large pore size was conducive to the rapid adsorption of Mb with a better-retained activity. Among the SBA-15 materials used, the SBA-15 with a pore diameter of 9.8 nm was more suitable for the immobilization of Mb. The immobilized Mb showed improved stability against metal ions, organic solutions, and temperature than the free enzyme. The addition of glutaraldehyde for crosslinking during the adsorption process increased the adsorption capacity of SBA-15, improving the stability and reusability of immobilized protein. The immobilized Mb, especially the crosslinked version, showed good reuse performance and stability, which is of great significance to the industrial application of Mb.

## DATA AVAILABILITY STATEMENT

The original contributions presented in the study are included in the article/**Supplementary Material**. Further inquiries can be directed to the corresponding authors.

## AUTHOR CONTRIBUTIONS

HM: data curation and writing—original draft. ML: data analysis. XS: writing—review, and data analysis. JX: data curation. YL: data curation. JL: supervision. FW: data analysis. JX: supervision, writing—review and editing.

## FUNDING

This work was supported by the National Natural Science Foundation of China (32171263) and Special Project of Major Scientific and Technological Innovation in Shandong Province (2018SDKJ0303-1-2223).

## SUPPLEMENTARY MATERIAL

The Supplementary Material for this article can be found online at: <https://www.frontiersin.org/articles/10.3389/fbioe.2021.827552/full#supplementary-material>

## REFERENCES

Badgujar, K. C., and Bhanage, B. M. (2015). Immobilization of Lipase on Biocompatible Co-polymer of Polyvinyl Alcohol and Chitosan for Synthesis

of Laurate Compounds in Supercritical Carbon Dioxide Using Response Surface Methodology. *Process Biochem.* 50 (8), 1224–1236. doi:10.1016/j.procbio.2015.04.019

Bezbradica, D., Mijin, D., Siler-Marinkovic, S., and Knezevic, Z. (2006). The Candida Rugosa Lipase Catalyzed Synthesis of Amyl Isobutyrate in Organic



- Solvent and Solvent-free System: A Kinetic Study. *J. Mol. Catal. B: Enzym.* 38 (1), 11–16. doi:10.1016/j.molcatb.2005.10.004
- Bonzom, C., Schild, L., Gustafsson, H., and Olsson, L. (2018). Feruloyl Esterase Immobilization in Mesoporous Silica Particles and Characterization in Hydrolysis and Transesterification. *BMC Biochem.* 19 (1), 1. doi:10.1186/s12858-018-0091-y
- Chui, W. K., and Wan, L. S. C. (1997). Prolonged Retention of Cross-Linked Trypsin in Calcium Alginate Microspheres. *J. Microencapsulation* 14 (1), 51–61. doi:10.3109/02652049709056467
- Cipolatti, E. P., Silva, M. J. A., Klein, M., Feddern, V., Feltes, M. M. C., Oliveira, J. V., et al. (2014). Current Status and Trends in Enzymatic Nanoimmobilization. *J. Mol. Catal. B: Enzym.* 99, 56–67. doi:10.1016/j.molcatb.2013.10.019
- Clark, J. H., Macquarrie, D. J., and Tavener, S. J. (2006). The Application of Modified Mesoporous Silicas in Liquid Phase Catalysis. *Dalton Trans.* 36, 4297–4309. doi:10.1039/b607831a
- Dettori, L., Vibert, F., Guaiavarc'h, Y., Delaunay, S., Humeau, C., Blin, J. L., et al. (2018). N- $\alpha$ -acylation of Lysine Catalyzed by Immobilized Aminoacylases from *Streptomyces Ambofaciens* in Aqueous Medium. *Microporous Mesoporous Mater.* 267, 24–34. doi:10.1016/j.micromeso.2018.03.018
- Eş, I., Vieira, J. D. G., and Amaral, A. C. (2015). Principles, Techniques, and Applications of Biocatalyst Immobilization for Industrial Application. *Appl. Microbiol. Biotechnol.* 99 (5), 2065–2082. doi:10.1007/s00253-015-6390-y
- Essa, H., Magner, E., Cooney, J., and Hodnett, B. K. (2007). Influence of pH and Ionic Strength on the Adsorption, Leaching and Activity of Myoglobin Immobilized onto Ordered Mesoporous Silicates. *J. Mol. Catal. B: Enzym.* 49 (1–4), 61–68. doi:10.1016/j.molcatb.2007.07.005
- Gao, S., Wang, Y., Diao, X., Luo, G., and Dai, Y. (2010). Effect of Pore Diameter and Cross-Linking Method on the Immobilization Efficiency of *Candida Rugosa* Lipase in SBA-15. *Bioresour. Technol.* 101 (11), 3830–3837. doi:10.1016/j.biortech.2010.01.023
- Hartmann, M. (2005). Ordered Mesoporous Materials for Bioadsorption and Biocatalysis. *Chem. Mater.* 17 (18), 4577–4593. doi:10.1021/cm0485658
- Hong, J., Xu, D., Gong, P., Yu, J., Ma, H., and Yao, S. (2008). Covalent-bonded Immobilization of Enzyme on Hydrophilic Polymer Covering Magnetic Nanogels. *Microporous Mesoporous Mater.* 109 (1–3), 470–477. doi:10.1016/j.micromeso.2007.05.052
- Jesionowski, T., Zdarta, J., and Krajewska, B. (2014). Enzyme Immobilization by Adsorption: a Review. *Adsorption* 20 (5–6), 801–821. doi:10.1007/s10450-014-9623-y
- Lee, J. G., Lannigan, K., Shelton, W. A., Meissner, J., and Bharti, B. (2020). Adsorption of Myoglobin and Corona Formation on Silica Nanoparticles. *Langmuir* 36 (47), 14157–14165. doi:10.1021/acs.langmuir.0c01613
- Kang, Y., He, J., Guo, X., GuoSong, Z., and Song, Z. (2007). Influence of Pore Diameters on the Immobilization of Lipase in SBA-15. *Ind. Eng. Chem. Res.* 46 (13), 4474–4479. doi:10.1021/ie061440n
- Kijima, J., Shibuya, Y., Katayama, K., Itoh, T., Iwase, H., Fukushima, Y., et al. (2018). Structural Characterization of Myoglobin Molecules Adsorbed within Mesoporous Silicas. *J. Phys. Chem. C* 122 (27), 15567–15574. doi:10.1021/acs.jpcc.8b04356
- Kim, M. I., Kim, J., Lee, J., Jia, H., Na, H. B., Youn, J. K., et al. (2010). Crosslinked Enzyme Aggregates in Hierarchically-Ordered Mesoporous Silica: A Simple and Effective Method for Enzyme Stabilization. *Biotechnol. Bioeng.* 96 (2), 210–218. doi:10.1002/bit.21107
- Li, Y., Zhou, G., Li, C., Qin, D., Qiao, W., Chu, B., et al. (2009). Adsorption and Catalytic Activity of Porcine Pancreatic Lipase on Rod-like SBA-15 Mesoporous Material. *Colloids Surf. A: Physicochem. Eng. Aspects* 341 (1–3), 79–85. doi:10.1016/j.colsurfa.2009.03.041
- Liao, F., Xu, J.-K., Luo, J., Gao, S.-Q., Wang, X.-J., and Lin, Y.-W. (2020). Bioinspired Design of an Artificial Peroxidase: Introducing Key Residues of Native Peroxidases into F43Y Myoglobin with a Tyr-Heme Cross-Link. *Dalton Trans.* 49, 5029–5033. doi:10.1039/D0DT00875C
- Lü, Y., Guo, Y., Wang, Y., Liu, X., Wang, Y., Guo, Y., et al. (2008). Immobilized Penicillin G Acylase on Mesoporous Silica: The Influence of Pore Size, Pore Volume and Mesophases. *Microporous Mesoporous Mater.* 114 (1–3), 507–510. doi:10.1016/j.micromeso.2007.12.027
- Lynch, M. M., Liu, J., Nigra, M., and Coppens, M.-O. (2016). Chaperonin-Inspired pH Protection by Mesoporous Silica SBA-15 on Myoglobin and Lysozyme. *Langmuir* 32 (37), 9604–9610. doi:10.1021/acs.langmuir.6b02832
- Nguyen, T. P. B., Lee, J.-W., Shim, W. G., and Moon, H. (2008). Synthesis of Functionalized SBA-15 with Ordered Large Pore Size and its Adsorption Properties of BSA. *Microporous Mesoporous Mater.* 110 (2–3), 560–569. doi:10.1016/j.micromeso.2007.06.054
- Salis, A., Meloni, D., Ligas, S., Casula, M. F., Monduzzi, M., Solinas, V., et al. (2005). Physical and Chemical Adsorption of Mucor Javanicus Lipase on SBA-15 Mesoporous Silica. Synthesis, Structural Characterization, and Activity Performance. *Langmuir* 21 (12), 5511–5516. doi:10.1021/la047225y
- Schmid, A., Dordick, J. S., Hauer, B., Kiener, A., Wubbolts, M., and Witholt, B. (2001). Industrial Biocatalysis Today and Tomorrow. *Nature* 409 (6817), 258–268. doi:10.1038/35051736
- Serra, E., Mayoral, Á., Sakamoto, Y., Blanco, R. M., and Díaz, I. (2008). Immobilization of Lipase in Ordered Mesoporous Materials: Effect of Textural and Structural Parameters. *Microporous Mesoporous Mater.* 114 (1–3), 201–213. doi:10.1016/j.micromeso.2008.01.005
- Shah, P., Sridevi, N., Prabhune, A., and Ramaswamy, V. (2008). Structural Features of Penicillin Acylase Adsorption on APTES Functionalized SBA-15. *Microporous Mesoporous Mater.* 116 (1–3), 157–165. doi:10.1016/j.micromeso.2008.03.030
- Sheldon, R. A. (2007). Enzyme Immobilization: The Quest for Optimum Performance. *Adv. Synth. Catal.* 349 (8–9), 1289–1307. doi:10.1002/adsc.200700082
- Vinu, A., Miyahara, M., and Ariga, K. (2006). Assemblies of Biomaterials in Mesoporous Media. *J. Nanosci. Nanotech.* 6 (6), 1510–1532. doi:10.1166/jnn.2006.253
- Wang, Y., and Hsieh, Y.-L. (2008). Immobilization of Lipase Enzyme in Polyvinyl Alcohol (PVA) Nanofibrous Membranes. *J. Membr. Sci.* 309 (1–2), 73–81. doi:10.1016/j.memsci.2007.10.008
- Wüstneck, R., Buder, E., Wetzel, R., and Hermel, H. (1989). The Modification of the Triple Helical Structure of Gelatin in Aqueous Solution 3. The Influence of Cationic Surfactants. *Colloid Polym. Sci.* 267 (5), 429–433. doi:10.1007/BF01410188
- Xu, J., Shoji, O., Fujishiro, T., Ohki, T., Ueno, T., and Watanabe, Y. (2012). Construction of Biocatalysts Using the Myoglobin Scaffold for the Synthesis of Indigo from Indole. *Catal. Sci. Technol.* 2 (4), 739–744. doi:10.1039/C2CY00427E
- Xu, J., Sun, J., Wang, Y., Sheng, J., Wang, F., and Sun, M. (2014). Application of Iron Magnetic Nanoparticles in Protein Immobilization. *Molecules* 19 (8), 11465–11486. doi:10.3390/molecules190811465
- Zhang, P., Xu, J., Wang, X.-J., He, B., Gao, S.-Q., and Lin, Y.-W. (2019). The Third Generation of Artificial Dye-Decolorizing Peroxidase Rationally Designed in Myoglobin. *ACS Catal.* 9, 7888–7893. doi:10.1021/acscatal.9b02226
- Zhang, P., Yuan, H., Xu, J., Wang, X.-J., Gao, S.-Q., Tan, X., et al. (2020). A Catalytic Binding Site Together with a Distal Tyr in Myoglobin Affords Catalytic Efficiencies Similar to Natural Peroxidases. *ACS Catal.* 10, 891–896. doi:10.1021/acscatal.9b05080
- Zhao, D., Huo, Q., Feng, J., Chmelka, B. F., and Stucky, G. D. (1998a). Nonionic Triblock and Star Diblock Copolymer and Oligomeric Surfactant Syntheses of Highly Ordered, Hydrothermally Stable, Mesoporous Silica Structures. *J. Am. Chem. Soc.* 120 (24), 6024–6036. doi:10.1021/ja974025i
- Zhao, D., Feng, J., Huo, Q., Melosh, N., Fredrickson, G. H., Chmelka, B. F., et al. (1998b). Triblock Copolymer Syntheses of Mesoporous Silica with Periodic 50 to 300 Ångström Pores. *Science* 279 (5350), 548–552. doi:10.1126/science.279.5350.548
- Zheng, L., Zhang, S., Zhao, L., Zhu, G., Yang, X., Gao, G., et al. (2006). Resolution of N-(2-ethyl-6-methylphenyl)alanine via Free and Immobilized Lipase from *Pseudomonas cepacia*. *J. Mol. Catal. B: Enzym.* 38 (3–6), 119–125. doi:10.1016/j.molcatb.2005.12.003

**Conflict of Interest:** The authors declare that the research was conducted in the absence of any commercial or financial relationships that could be construed as a potential conflict of interest.

**Publisher's Note:** All claims expressed in this article are solely those of the authors and do not necessarily represent those of their affiliated organizations, or those of the publisher, the editors, and the reviewers. Any product that may be evaluated in this article, or claim that may be made by its manufacturer, is not guaranteed or endorsed by the publisher.

Copyright © 2022 Miao, Li, Sun, Xia, Li, Li, Wang and Xu. This is an open-access article distributed under the terms of the Creative Commons Attribution License (CC BY). The use, distribution or reproduction in other forums is permitted, provided the original author(s) and the copyright owner(s) are credited and that the original publication in this journal is cited, in accordance with accepted academic practice. No use, distribution or reproduction is permitted which does not comply with these terms.



# Improving Thermostability of Chimeric Enzymes Generated by Domain Shuffling Between Two Different Original Glucoamylases

Zhongxiu Chen<sup>1,2†</sup>, Longbin Wang<sup>1,2†</sup>, Yuyu Shen<sup>1,2</sup>, Dunji Hu<sup>1,2</sup>, Liying Zhou<sup>1,2</sup>, Fuping Lu<sup>1,2,3\*</sup> and Ming Li<sup>1,2,3\*</sup>

<sup>1</sup>Key Laboratory of Industrial Fermentation Microbiology (Tianjin University of Science and Technology), Ministry of Education, Tianjin, China, <sup>2</sup>College of Biotechnology, Tianjin University of Science and Technology, Tianjin, China, <sup>3</sup>Tianjin Key Laboratory of Industrial Microbiology, Tianjin, China

## OPEN ACCESS

### Edited by:

Weidong Liu,  
Tianjin Institute of Industrial  
Biotechnology (CAS), China

### Reviewed by:

Qilin Yu,  
Nankai University, China  
Yun Zhang,  
IMCAS, China

### \*Correspondence:

Fuping Lu  
lfp@tust.edu.cn  
Ming Li  
liming09@tust.edu.cn

<sup>†</sup>These authors have contributed  
equally to this work

### Specialty section:

This article was submitted to  
Industrial Biotechnology,  
a section of the journal  
Frontiers in Bioengineering and  
Biotechnology

Received: 22 February 2022

Accepted: 08 March 2022

Published: 05 April 2022

### Citation:

Chen Z, Wang L, Shen Y, Hu D,  
Zhou L, Lu F and Li M (2022) Improving  
Thermostability of Chimeric Enzymes  
Generated by Domain Shuffling  
Between Two Different  
Original Glucoamylases.  
Front. Bioeng. Biotechnol. 10:881421.  
doi: 10.3389/fbioe.2022.881421

In order to improve enzymatic properties of glucoamylases, six recombinant genes GA1–GA6 were created by domain shuffling of glucoamylase genes GAA1 from *Aspergillus niger* Ld418AI and GATE from *Talaromyces emersonii* Ld418 TE using overlap extension PCR and were expressed in *Saccharomyces cerevisiae* W303-1B; only activities of GA1 and GA2 in the fermentation broth were higher than those of GAA1 but less than those of GATE. Further research results of GA1 and GA2 indicated that chimeric glucoamylases GA1 and GA2 revealed increased thermostability compared with GAA1 and GATE, although with a slight change in the activity and optimal temperature. However, GA1 had almost the same catalytic efficiency as GATE, whereas the catalytic efficiency of GA2 was slightly less than that of GATE, but still higher than that of GAA1. The structural analysis showed that the change of enzymatic properties could be caused by the increased and extended  $\alpha$ -helix and  $\beta$ -sheet, which change the secondary and tertiary structures of chimeric glucoamylases. These results demonstrated that domain shuffling was feasible to generate a chimeric enzyme with novel properties.

**Keywords:** glucoamylase, domain shuffling, chimeric enzyme, thermostability, enzymatic properties

## INTRODUCTION

Glucoamylase (GA) ( $\alpha$ -1, 4-glucan glucohydrolase, EC 3.2.1.3) plays an important role in the fermentation and food industries for saccharification of starch/amylopectin (Kumar and Satyanarayana, 2009; Zong et al., 2022). It can catalyze hydrolysis of  $\alpha$ -1,4 glycosidic bonds to release D-glucose residues from the non-reducing ends of starch and related oligo- and polysaccharide chains and also has limited ability to hydrolyze amylopectin  $\alpha$ -1,6 linkages resulting in glucose (Sauer et al., 2000). Although glucoamylases can be produced by many fungal species (Norouzian et al., 2006), commercial or industrial glucoamylases with moderate thermostability and high activity are mainly derived from *Aspergillus niger* (Norouzian et al., 2006), *Rhizopus oryzae* (Wang et al., 2020), and *Talaromyces emersonii* (Nielsen et al., 2002) due to the conversion of starch to glucose (Zong et al., 2022). Because the saccharification processes are usually followed by a liquefaction process of starch and are performed at 60°C for 48–72 h, the glucoamylases required in starch industrials have to possess good thermostability and catalytic activities (Lim and Oslan, 2021; Tong et al., 2021). So, searching for a new source of glucoamylase with potentially

applicable properties encompassing elevated temperature, extreme pH, high salinity, organic solvents, surfactants, and specificities (substrate and product) is still of considerable importance (Schmidt et al., 2019). Although some novel glucoamylases have been found and characterized for industrial applications (Guo et al., 2019; Karim et al., 2019; Lincoln et al., 2019; Zhang et al., 2019; Wang et al., 2020; Lago et al., 2021; Wayllace et al., 2021), they did not achieve industrially desirable traits.

In addition to exploring novel enzymes with desirable properties in nature, attempts are being made to improve the properties of the existing enzymes by protein engineering techniques to make them suitable for industrial applications (Parashar and Satyanarayana, 2016; Sharma et al., 2019). These techniques mainly include rational design, semi-rational design, directed evolution (error prone PCR and DNA shuffling), and fusion (Schmidt et al., 2019; Sharma et al., 2019; Lim and Oslan, 2021; Tong et al., 2021). However, the design of chimeric enzymes by fusing different domains from native enzymes is considered to be a straightforward method for generating a novel enzyme with improved catalytic properties (Parashar and Satyanarayana, 2016; Ali et al., 2020). Many chimeric enzymes have enhanced thermostability, catalytic efficiency, substrate specificity, and product selectivity (Parashar and Satyanarayana, 2016; Parashar and Satyanarayana, 2017; Peng et al., 2018). For example, Parashar et al. constructed a chimeric  $\alpha$ -amylase by fusing the domains of amylases from *Bacillus acidicola* and *Geobacillus thermoleovorans*, which showed enhanced thermostability and catalytic efficiency (Parashar and Satyanarayana, 2016).

In general, the GA from filamentous fungi consists of three regions: the N-terminal catalytic domain (CD), C-terminal starch-binding domain (SBD), and a linker composed primarily of serine and threonine residues between the CD and SBD (Sauer et al., 2000; Guo et al., 2019). Studies have showed that the CD, linker, and SBD sequences of glucoamylase from *A. niger*, respectively, contain residues 1–471, 472–508, and 509–616 (Lee and Paetzel, 2011; Suyama et al., 2017). Of course, a few glucoamylases lack the SBD; however, it has almost the same hydrolytic rate against soluble starch as the average GA, but against insoluble starch, it has a much less hydrolytic rate than the average GA (Sauer et al., 2000; Cornett et al., 2003; Hostinova et al., 2003). The study of the three structural domains of glucoamylase has been carried out, and the results indicated that the positioning of the SBD related to the catalytic domain had an effect on soluble starch/insoluble starch; the effect on soluble starch was much less than that on insoluble starch (Cornett et al., 2003). Moreover, the presence/absence of O-glycosylated linker connecting the CD and SBD of glucoamylase also affected the hydrolysis of insoluble starch (Sauer et al., 2001; Lin et al., 2007).

Domain shuffling is a method to generate chimeric proteins with novel structural and functional properties by fusing domains of different proteins (Cornett et al., 2003; Marin-Navarro et al., 2011; Gomis-Cebolla et al., 2020). In our laboratory, there are two industrial strains, *Aspergillus niger* Ld418A1 and *Talaromyces emersonii* Ld418 TE, producing glucoamylases GAA1 and GATE

which are used in saccharification processes of starch. GAA1 has a good thermostability, but its optimal temperature is lower than that of GATE. On the contrary, glucoamylase GATE has a higher optimal temperature, but its thermostability is lower than that of GAA1. We aim to create a chimeric glucoamylase combining their positive characteristics using the domain shuffling method. So, the three domains from the two glucoamylase genes GAA1 and GATE were amplified and then shuffled by overlap PCR to generate six glucoamylase genes: GA1–GA6. The chimeric GA1 and GA2 obtained enhanced thermostability and had almost the same catalytic efficiency as GATE.

## MATERIALS AND METHODS

### Strains, Plasmids, and Medium

*Aspergillus niger* Ld418A1 and *Talaromyces emersonii* Ld418 TE were used as donors of glucoamylase genes and cultivated in a PDA medium. Cloning was done in *Escherichia coli* DH5 $\alpha$ , and *Saccharomyces cerevisiae* W303-1B (Xu et al., 2010) was used as a host strain for the expression of glucoamylase genes, which were grown in an LB medium and a YPD medium, respectively.

The pUCm-T vector was purchased from TaKaRa (Dalian, Liaoning, China), and the pYPGE15 vector (Xu et al., 2010) was provided by East China Normal University (Shanghai, China). The restriction endonucleases and DNA ligases involved in the molecular manipulation were bought from Fermentas (Tianjin, China). The SC-U plate containing 0.67% YNB, 0.115% mixture of basic amino acids, and adenine without uracil, 2% glucose, and 2% agar was used for screening yeast transformants. The YWSX (SC-U without glucose, 1% soluble starch, 0.02% trypan blue) plate was used for testing the expression of transformants.

## METHODS

### Cloning Glucoamylase Genes

Filamentous fungi Ld418A1 and Ld418 TE were, respectively, cultivated in 50 ml PDA medium at 28°C for three days. The total RNA was extracted by the TRIzol method using a TRIquick reagent (Solarbio Science and Technology Co., Ltd., Beijing China) and processing as per the instructions. The cDNA was obtained by reverse transcription using RNase inhibitor, dNTP, M-MLV, and the primers ANR TER (Table 1), which were designed and synthesized according to the mRNA sequence of glucoamylase genes from *A. niger* in the NCBI database (GenBank Accession No. BD087377) and *T. emersonii* in the NCBI database (GenBank Accession No. AJ304803.1). The glucoamylase genes GAA1 and GATE were synthesized by PCR using the obtained cDNA as a template.

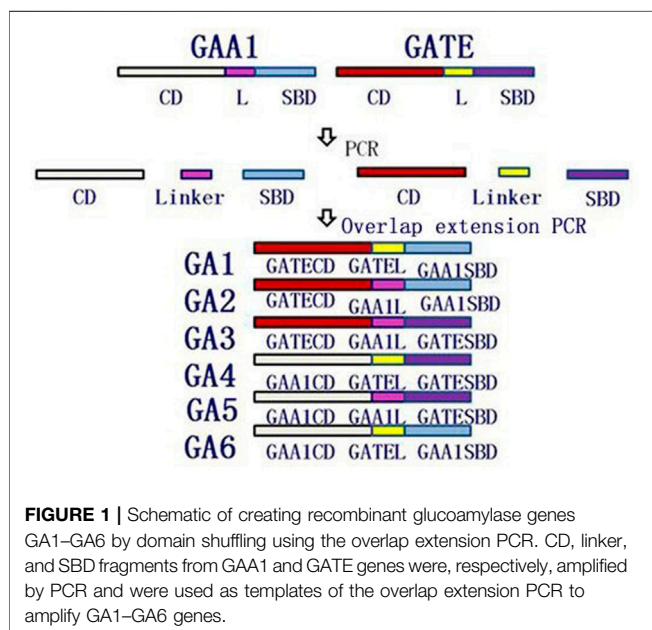
### Domain Shuffling

The different domains (CD, linker, and SBD) were amplified by PCR using glucoamylase genes GAA1 and GATE as templates and corresponding primers, which are listed in Table 1. Domain shuffling was conducted, as shown in Figure 1, using the overlap extension PCR. For example, recombinant gene GA1 was

**TABLE 1** | Sequences of the primers used for this research.

Primer	Primer sequence (5-3')	Restriction enzyme
ANF	ATGTCGTTCCGATCTCTACTCGCC	
ANR	TCACAGTGTACATACCAGAGCGGG	
TEF	ATGGCGTCCCTCGTTGCTGGC	
TER	TCACTGCCAACTATCGTCAAGAATG	
ANWF	CGGAATTCATGTCGTTCCGATCTCTACTCGCC	<i>EcoR</i> I
ANWR	CCGCTCGAGTCACAGTGACATACCAGAGCGGG	<i>Xho</i> I
TEWF	GCTCTAGAATGGCGTCCCTCGTTGCTGGC	<i>Xba</i> I
TEWR	CCGCTCGAGTCACGTCGCAACTATCGTCAAGAATG	<i>Xho</i> I
GAA1F	GCTACCAACACCGTCTGGCCAAGCATCGTGGCTACTGGCGGCACCACTA	
GAA1R	GGTTGTTGAGCTGCCAGAGCCAGAACTCGGCCACGAGGTGACAGTCAC	
GAA2F	GTCAGCACCAGTTACGGGGAGACATGTACCACTCCCAACCGCGTGGCTG	
GAA2R	GGGGATCGAGCCGGCCAGGTAGATGGAGTTGATGACGTAAGTGGTGCTG	
GATE1F	GTGACTGTACCTCGTGGCCGAGTTCTGGCTCTGGCAGCTCAACAACC	
GATE1R	TAGTGGTGCCGCCAGTAGCCACGATGCTTGGCCAGACGGTGTGGTAGC	
GATE2F	CAGCACCAGTACGTATCAACCTCCATCTACCTGGCCGGCTCGATCCCC	
GATE2R	CAGCCACGGCGGTGGGAGTGGTACATGTCTCCCGTAAGTGGTGCTGAC	

The fragments (CD, SBD, or linker) amplified for each primer pairs: ANF/ANR, GAA1; TEF/TER, GATE; ANWF/ANWR, GAA1; TEWF/TEWR, GATE; ANWF/GAA1R, CD, of GAA1; GAA1F/GAA2R, linker of GAA1; GAA2F/ANWR, SBD, of GAA1; TEWF/GATE1R, CD, of GATE; GATE1F/GATE2R, linker of GATE; GATE2F/TEWR, SBD, of GATE.



amplified by overlap extension PCR using CD and linker fragments from GATE and SBD fragments from GAA1 as templates and TEWF/ANWR as primes. Six recombinant genes GA1–GA6 were generated similar to GA1 by overlap extension PCR.

The overlap extension PCR was carried out under the following conditions: the first step was initial denaturation at 95°C for five min, followed by six cycles of 95°C for 45 s, 72°C for three min, six cycles of 95°C for 45 s, 55°C for 45 s, and 72°C for four min, 20 cycles at 95°C for 45 s, 60°C for 45 s, and 72°C for four min, and the final extension was carried out at 72°C for ten min.

## Construction and Transformation of Recombinant Expression Vectors

The genes GAA1, GATE, and GA1–GA6 were, respectively, ligated into pYPGE15 and transformed into *E. coli* DH5α by  $\text{CaCl}_2$  transformation. The recombinant expression vectors were identified by the digestion of restriction enzymes and sequencing by Shengsong Biotech Company. The *S. cerevisiae* W303-1B was transformed with the constructed vectors pYPGE15-GAA1, pYPGE15-GATE, and pYPGE15-GA1–pYPGE15-GA6 by using the electroporation method and was then inoculated into the SC-U plate for screening transformants.

## Expression, Activity Assay, and Purification of GAs

The monoclonal transformants on the SC-U plate were inoculated into the YWSX plate and incubated for 60 h at 30°C in order to screen the high-level GA expression strain by determination of the ratio (DH/DC) of the hydrolysis circle diameter (DH) and colony diameter (DC). The engineered strains with higher ratios were inoculated into shake flasks and fermented for three days at 30°C for the activity assay and purification of GAs.

The GA activity in the fermentation supernatant was determined according to a modified method (Miller, 1959). With this method, 25 ml soluble starch (20 g/L) was mixed with 5 ml 0.05 mol/L sodium acetate buffer (pH 4.5) and then incubated at 40°C for five min in a tube. Furthermore, 2 ml standard diluted enzyme solution was added into the tube and incubated at 40°C for 30 min. Then, 0.2 ml NaOH (200 g/L) was added. Finally, the diluted solution (diluted ten times) and 1.5 ml DNS (3, 5-dinitrosalicylic acid) was mixed in the tube and immediately transferred to boiling water for five min to end the reaction. The absorbance of these mixtures was measured at a wavelength of 520 nm with sterile water as the control. One unit (U) of the enzyme activity was defined as the amount that



catalyzes soluble starch and produces 1  $\mu\text{mol}$  glucose per minute at 40°C, pH 4.5.

The purification of the GAs was performed as previously reported with minor modifications (Cornett et al., 2003). The fermentation supernatant collected by centrifugation was filtered through  $\Phi 0.45\text{-}\mu\text{m}$  filter membrane and further concentrated through a 10-kDa cutoff Amicon ultrafiltration system, followed by diafiltration with three times its wash/diafiltration buffer (0.1 mol/L sodium acetate, pH 4.3/1.5 mol/L NaCl). The crude GAs were further purified through acarbose affinity chromatography. The purity of the recombinant GAs was examined by SDS-PAGE.

### Effects of Temperature on the GA Activity and Stability

The optimum temperature of the GAs was evaluated by measuring the enzyme activity at different temperatures (35–80°C) at pH 4.5. The effect of temperature on enzyme stability was determined by measuring the residual activity after being kept at different temperatures (45–80°C) for six h and cooled down rapidly on ice, and the residual enzyme activity of the recombinant GAs was individually measured at pH 4.5. A stability curve of temperature was plotted when the enzyme activity at optimal temperature was set as 100%.

### Effects of pH on the GA Activity and Stability

The optimum pH of the GA was measured by varying the pH of the reaction buffer using 0.05 mol/L sodium acetate buffer at desired pH (from 3.0 to 6.5) at 40°C. In order to test the stability of GA in different pH, the GA solution was adjusted to the desired pH (3.0–6.5) using acetic acid and was kept at 4°C for 6 h, and then the residual enzyme activity of the recombinant GAs was individually measured at 40°C. A stability curve of pH was plotted when the uninsulated enzyme activity at the optimal pH was set as 100%.

### Determination of Kinetic Parameters

Kinetic studies were performed in 0.05 mol/L sodium acetate at 40°C, pH 4.5 using soluble starch as the substrate with concentrations ranging from 0.125 km to 8 km. The  $K_m$  and  $K_{cat}$  values of the purified GAs were calculated using the Lineweaver–Burk plot method.

### Structural Analysis of Chimeric Glucoamylases GA1 and GA2

The homologous analysis of DNA and the amino acid sequence alignment of recombinant GAs were conducted using the tool DNAMAN. The tool PSIPRED (Jones, 1999) was used to predict the secondary structure of recombinant GAs. The tertiary structure of recombinant glucoamylases was predicted by SWISS-MODEL (Arnold et al., 2006). All pieces of software were used to make a comparison of the structure between GAA1 and GATE, and GA1 and GA2, and the change of structure was also discussed.

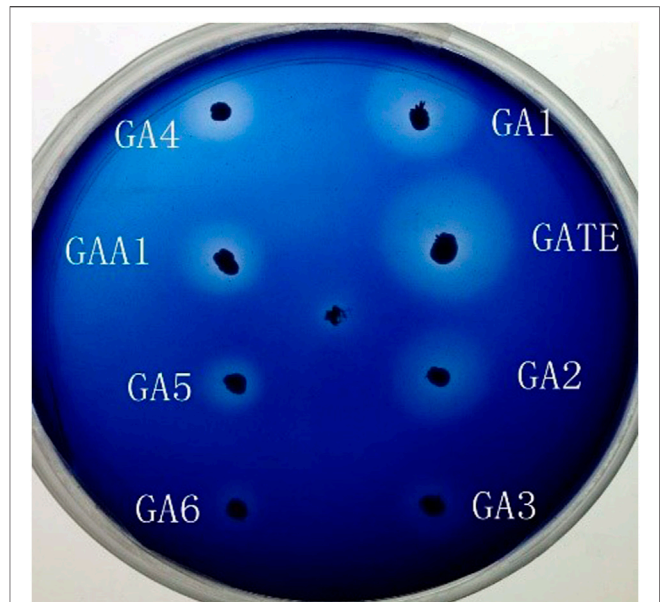


**FIGURE 2 |** Transparent hydrolysis circle test of the recombinant strains expressing chimeric glucoamylases GAA1, GATE, GA1, GA2, GA3, GA4, GA5, and GA6, respectively.

## RESULTS

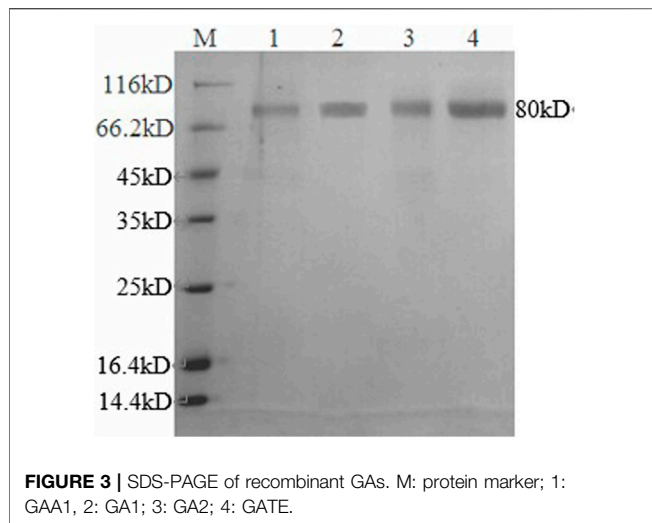
### Cloning GAA1 and GATE and Rearranging Domains

The glucoamylase genes GAA1 and GATE were, respectively, cloned and sequenced. According to the results, the size of genes GAA1 and GATE were 1776 bp and 1857 bp, respectively, consistent with the reported sequences. As shown in **Figure 1**, CD, linker, and SBD regions of genes GAA1 and GATE were, respectively, amplified by PCR. Then, six recombinant genes GA1 (GATECD + GATEL + GAA1SBD), GA2 (GATECD + GAA1L + GAA1SBD), GA3 (GATECD + GAA1L + GATESBD), GA4 (GAA1CD + GATEL + GATESBD), GA5 (GAA1CD + GAA1L + GATESBD), and GA6 (GAA1CD + GATEIL + GAA1SBD) were obtained by overlap extension PCR and further identified by sequencing; the lengths of these were GA1 as 1776 bp, GA2 as 1791 bp, GA3 as 1872 bp, GA4 as 1857 bp, GA5 as 1842 bp, and GA6 as 1761 bp.

### Construction and Screening of Engineered Strains

The recombinant expression vectors pYPGE15-GA1, pYPGE15-GA2, pYPGE15-GA3, pYPGE15-GA4, pYPGE15-GA5, and pYPGE15-GA6; the control vectors pYPGE15-GAA1 and pYPGE15-GATE were constructed and transformed into *S. cerevisiae* W303-1B; and the possible positive transformants were selected from the SC-U plate and inoculated to the YWSX plate to screen the recombinant strains which could express high-level GAs. The engineered strains YGAA1, YGATE, YGA1, YGA2, YGA3, YGA4, YGA5, and YGA6





could produce transparent hydrolysis circles around their colonies on the YWSX plate, and it is found by calculating the ratio of the diameters of hydrolysis circles and colonies, and the ratios produced by the engineered strains YGAA1, YGATE, YGA1, and YGA2 were obviously higher than those produced by the other engineered strains (Figure 2). It is generally believed that the higher the ratio was, the stronger the ability that strains produce GAs will be. So, the three strains with the highest ratio in each class of engineered strains were inoculated into flasks for fermentation, and GA activities in the fermentation broth were determined.

## Enzymatic Activity Assay and SDS-PAGE of Recombinant GAs

The enzyme activity was determined, and GATE had the highest enzyme activity (73.4 IU/ml), followed by the recombinant GA1 (62.8 IU/ml), GA2 (31.6 IU/ml), and the original GAA1 (27.6 IU/ml), and the activities of the other four recombinants GA3, GA4, GA5, and GA6 were, respectively, 6.1, 21.1, 16.7, and 19.7 IU/ml, which had even lower enzyme activity than GAA1. It showed that domain shuffling could affect the expression and activity of glucoamylase. So, GA1 and GA2 with higher activity than the original GAA1 were purified for the analysis of their enzymatic properties. The SDS-PAGE result indicated that apparent molecular weights of the recombinant GAs were about 80 kDa (Figure 3), which were all larger than their theoretical molecular weights. It is possible that the recombinant GAs were glycosylated due to presence of O-glycosylated linker. The result also showed that their purity reached electrophoretic purity.

## Analysis of Enzymatic Properties of Recombinant Glucoamylases GA1 and GA2 Optimal Temperature and Thermal Stability

The results (Figure 4A) showed that the optimal temperature of GATE, GA1, GA2, and GAA1 was 70°C, 65°C, 60°C, and 60°C, respectively. Under the optimum temperature of GATE, GA1,

GA2, and GAA1, the enzyme activities of the fermentation broth were 163.08 IU/ml, 140.36 IU/ml, 62.81 IU/ml, and 47.53 IU/ml, respectively. The results (Figure 4B) showed that the activity of recombinant GA declined after being preserved at different temperatures for six h. The activity of GATE, GA1, GA2, and GAA1 decreased to 73, 90, 86, and 80% at 50°C, and 53, 78, 72, and 66% at 60°C, respectively. The results revealed that the activities of recombinant GATE and GAA1 decreased much faster than those of recombinant GA1 and GA2, where the thermostability of GA1 was the highest, followed by GA2. Both were higher than the original GAA1 and GATE, indicating that the thermostability of GA could be enhanced by domain shuffling.

## The Optimum pH and pH Stability

According to Figure 4C, the optimum pH of the original GAA1 and GATE and the recombinant GA1 and GA2 was pH 4.5. Under the optimum pH, the activity of GATE was the highest, followed by GA1, and the activity of GA2 was higher than that of GAA1. Figure 4D illustrates that the relative activity of GA1, preserved at pH 4.5, 40°C for six h, was still 98%, which was higher than that of GATE, GAA1, and GA2 (88, 94, and 92%, respectively). The activity of the recombinant GAs was decreased when the pH was far away from the optimum pH. However, the reduced rate of GA1 was slower than that of others, indicating that the pH stability of GA1 was higher than that of GAA1, GA2, and GATE.

## Determination of Kinetic Parameters

The kinetic parameters of the recombinant GAs are shown in Table 2. The  $K_m$  values of GATE, GA1, GA2, and GAA1 were  $32.58 \text{ s}^{-1}$ ,  $30.01 \text{ s}^{-1}$ ,  $26.29 \text{ s}^{-1}$ , and  $18.71 \text{ s}^{-1}$ , respectively, showing that the affinity of GA1 to the substrates was similar to that of GATE; however, the affinity of GA2 to substrates was lower than that of GATE but superior to the affinity of GAA1 to substrates. By the analysis of their  $K_{cat}$  values, it was found that  $K_{cat}$  values of GA1 (0.15 mg/ml) and GA2 (0.15 mg/ml) were very similar to those of GATE (0.16 mg/ml) but outclassed GAA1 (0.12 mg/ml), indicating that  $K_{cat}$  values may be related to the SBD of glucoamylases. As for  $K_{cat}/K_m$ ,  $K_{cat}/K_m$  values of GATE, GA1, GA2, and GAA1 were, respectively, 203.62 mg/mL/s, 200.07 mg/mL/s, 175.27 mg/mL/s, and 155.92 mg/mL/s, indicating that GATE and GA1 had almost the same catalytic efficiency. Nevertheless, the catalytic efficiency of GA2 was less than that of GATE but higher than that of GAA1. These results revealed that domain shuffling could still influence catalytic efficiency.

## Structural Analysis of Chimeric Glucoamylases GA1 and GA2

### Analysis of the Primary Structure

Through the similarity comparison of amino acid sequences between recombinant GAs and original GAs, GAA1 and GATE had a similarity of 55.11%, GATE and GA1, GA2 had a similarity of 86.88 and 84.19%, respectively, GA1 and GA2 was 94.30%. Marin-Navarro (Marin-Navarro et al., 2011) indicated

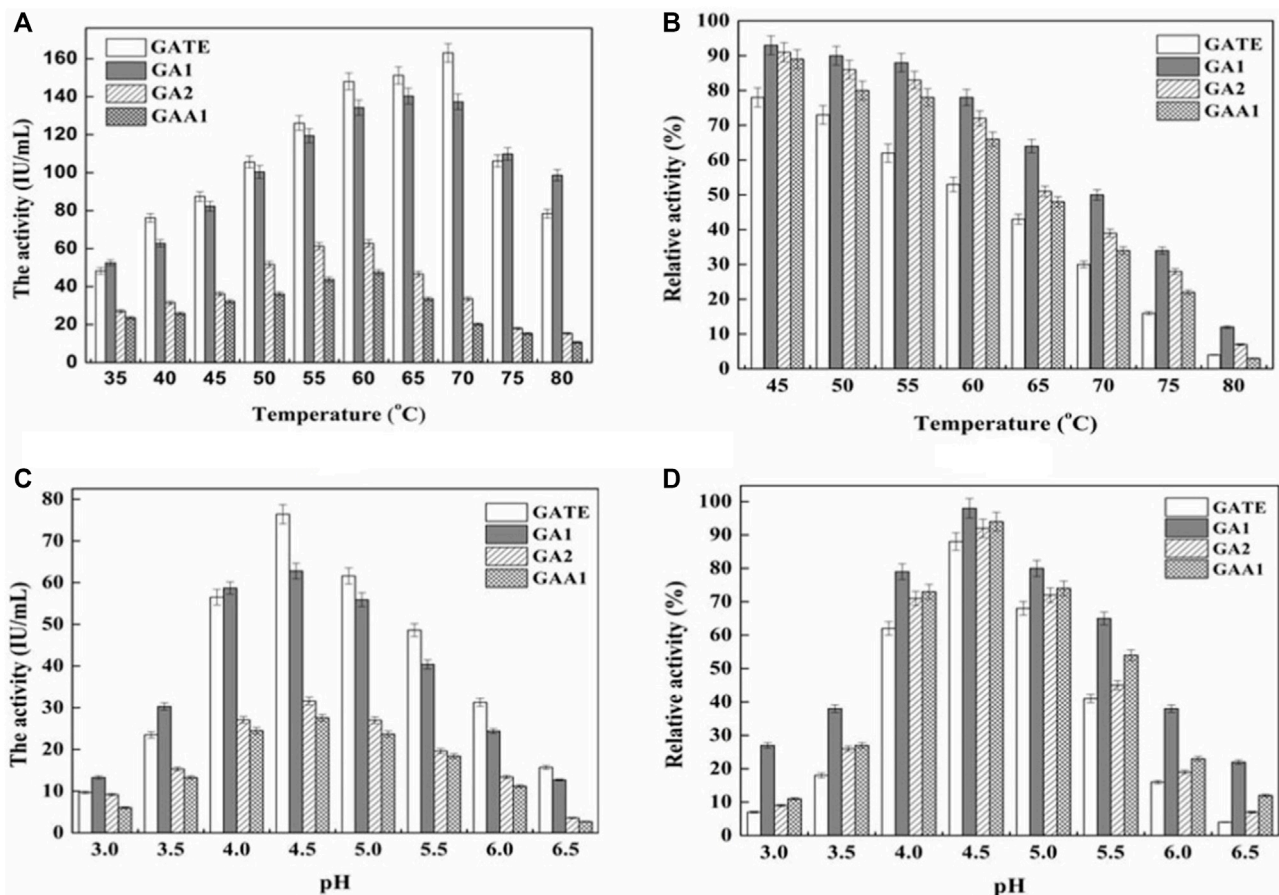


**FIGURE 4 |** Effect of temperature and pH on activities and stabilities of recombinant GAs. **(A)** Effect of temperature on the activity of the GA. GA activity was measured at various temperatures (35–80°C) at pH 4.5. **(B)** Thermal stability of the purified GA. After being kept at different temperatures (45–80°C) for six h and cooled down rapidly on ice, the residual enzyme activity of GA was measured at pH 4.5. The enzyme activity at optimal temperature was set as 100%. At 50°C, the relative activity of GATE, GA1, GA2, and GAA1 was 73, 90, 86, and 80%, respectively, corresponding to 100%. At 60°C, the relative activity of GATE, GA1, GA2, and GAA1 was 53, 78, 72, and 66%, respectively, corresponding to 100%. **(C)** Effect of pH on GA activity. GA activity was measured in the pH range of 3.0–6.5 at 40°C. The maximum activity was obtained at pH 4.5. **(D)** pH stability of the GA. GA activity was determined after being kept at various pH values (3.0–6.5) for 6 h at 40°C. A stability curve of pH was plotted when the enzyme activity at optimal pH was set as 100%. The relative activity of GA1, GATE, GAA1, and GA2 was 98, 88, 94, and 92%, respectively.

**TABLE 2 |** Kinetic parameters of recombinant GAs.

Enzyme	Kcat (/s)	Km (mg/ml)	Kcat/Km (mg/mL/s)
GAA1	18.71 ± 1.81	0.12 ± 0.02	155.92 ± 8.91
GATE	32.58 ± 1.52	0.16 ± 0.03	203.62 ± 6.28
GA1	30.01 ± 1.22	0.15 ± 0.06	200.07 ± 7.68
GA2	26.29 ± 1.38	0.15 ± 0.05	175.27 ± 5.98

that domain shuffling of different enzymes might evolve new enzymes and improve the enzymatic properties due to possible changes in the secondary and tertiary structures of the enzymes.

### Prediction of the Secondary Structure

According to the analysis result of PSIPRED (Jones, 1999) (Figure 5), the number of  $\alpha$ -helices of GA1 and GA2 did not change, but the length of some  $\alpha$ -helices changed. Compared

with GATE, the length of  $\alpha$ -helices at seven regions (98, 273–281, 300–305, 344, 378–384, 396–420, and 433–460, amino acid number) increased and extended, especially at the regions (396–420 and 433–460). The longer the  $\alpha$ -helix is, the higher the thermal stability will be (Stoffer et al., 1993). Figure 5 also shows that both the number and length of the  $\beta$ -sheet of GA1 and GA2 changed compared with GATE. GA1 had nine  $\beta$ -sheets, which was three  $\beta$ -sheets less than GATE, and formed one new  $\beta$ -sheet (516–518 region), which did not exist in GATE and GAA1. The length of the  $\beta$ -sheet of GA1 increased at the 514–524 regions and decreased at 328–332 and 565–569 regions, which were the same as those of GAA1. However, GA2 had ten  $\beta$ -sheets, which was two  $\beta$ -sheets less than GATE, and formed two new  $\beta$ -sheets (200–209 and 516–518 regions) which only existed in GAA1. The length of the  $\beta$ -sheet of GA1 increased at the 134–139 and 530–537 regions and decreased at the 328–332 and 565–569 regions,



**FIGURE 5 |** Prediction and comparison of secondary structures of GA1, GA2, GATE, and GAA1 using the tool PSIPRED. The yellow arrow means  $\beta$ -sheet, and the circular column means  $\alpha$ -helix.

which were consistent with GAA1. These differences might cause GA1 and GA2 to have a more stable structure than GATE and GAA1. The 179 and 400 sites of amino acids in GA from *A. niger* have been identified as the catalytic sites (Frandsen et al., 1994; Sierks et al., 1990; Svensson et al., 1990), so a change in the second structure near these catalytic sites might affect their activities. GA1, GA2, and GATE shared the same CD sequences only because their linker and/or SBD sequences were different. Their second

structures in the CD showed significant differences. Moreover, there was an increasing frequency at the C-terminal near the CD domain, which indicated that the linker and SBD near the CD domain might influence the secondary structure of the CD domain. The linker and SBD of GATE contained more numbers of  $\beta$ -sheets than those of GAA1, GA1, and GA2. These  $\beta$ -sheets might influence the secondary structure of GATE'CD domain and strengthen the binding of the enzyme with the substrate (Coutinho and Reilly,



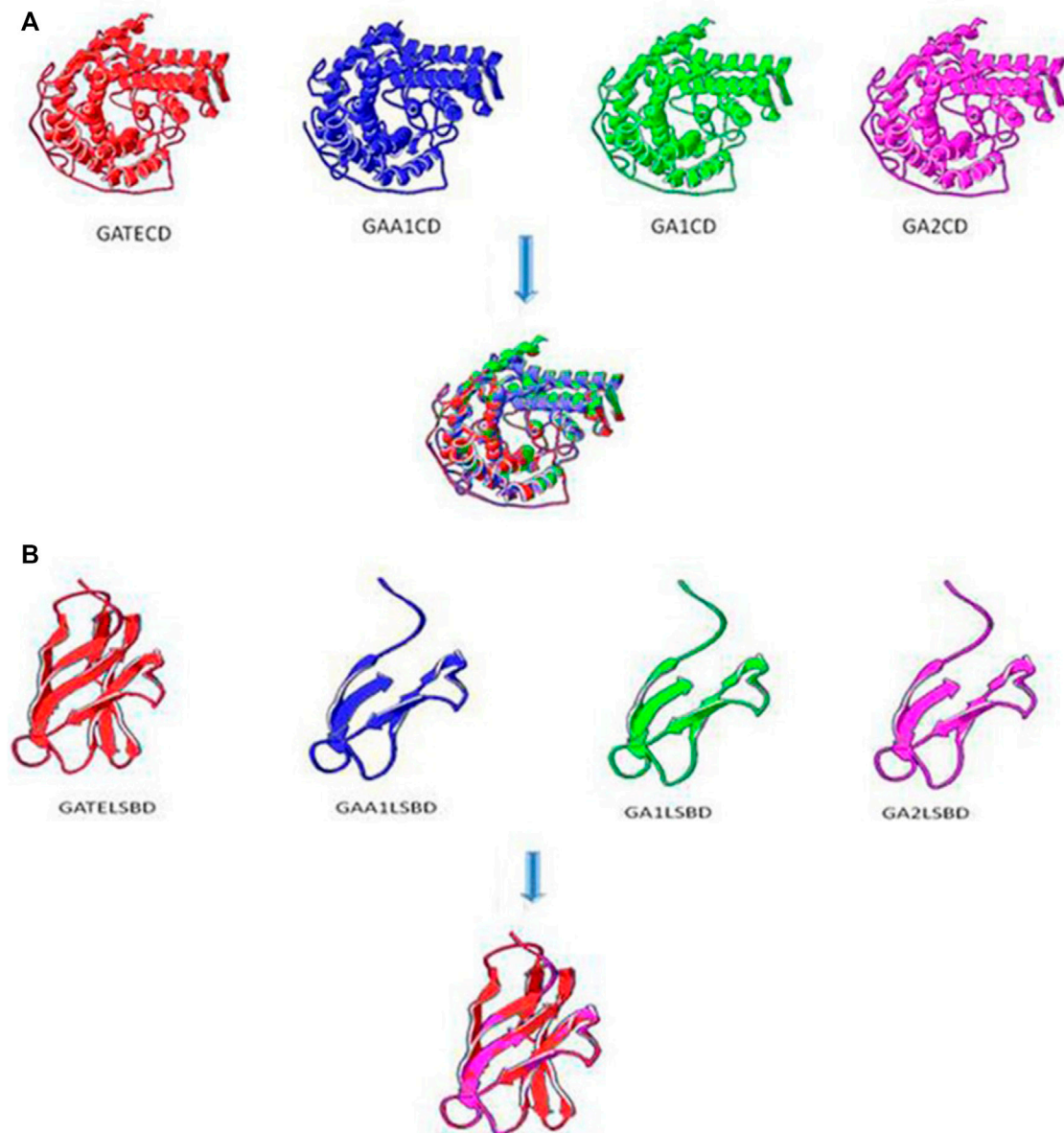


**FIGURE 6 |** Tertiary structure prediction of CD and SBD. **(A)** Tertiary structure prediction of CD domains. The homology modeling template of GAA1CD had a high-degree homology to PDB: 3eqaA protein and GATECD, GA1CD, and GA2CD were non-high-degree homology to PDB: lgaIA protein. **(B)** Tertiary structure prediction of SBD domains with Linker. The homology modeling template of GAA1SBD, GATESBD, GA1SBD, and GA2SBD were all PDB: 11acoA protein.

1994a). Jia et al. (2004) indicated that there was no complete correspondence between the amino acid sequence and conformation of the protein. Luo and Dong (1988) also showed that the amino acids near the CD domain played a decisive role in the formation of the secondary structure, which mainly had effects on the specificity and catalytic activity of enzymes. The structural differences of the  $\alpha$ -helix and  $\beta$ -sheet between chimeric GA1, GA2, and the original GATE and GAA1 contributed to knowing the higher structure of GA and the action mechanism of GA to the substrate (Coutinho and Reilly, 1994b).

### Prediction of the Tertiary Structure

The tertiary structure of chimeric glucoamylases was predicted by SWISS-MODEL (Arnold et al., 2006). The CD domains are described in Figure 6A, and the three-dimensional conformation of GATECD, GAA1CD, GA1CD, and GA2CD had a similarity. The homology modeling template of GAA1CD had a high-degree homology to the PDB: 3eqaA protein and GATECD, GA1'CD, and GA2CD had a non-high-degree homology to the PDB: lgaIA protein. As Figure 6A shows, the C-terminal  $\alpha$ -helix structure sited on the outside of the catalytic activity between GATE and GAA1 was different, whereas that of GA1, GA2, and GATE was alike. The GA2

had a  $\beta$ -sheet near the center of the CD domain compared with GA1 and GATE and had no difference with GAA1 in the same domain, which might have influenced the activity of GA2. This was consistent with the prediction of the secondary structure.

The tertiary structures of the SBD domain are shown in **Figure 6B**. The homology modeling templates of GAA1SBD, GATESBD, GA1SBD, and GA2SBD were all PDB: 1lacoA protein. However, there was a high-degree homology on the SBD domain between GAA1, GA1, GA2, and the template but only a certain homology between GATE and the template.

## DISCUSSION

Recombination of the existing protein domain is a straightforward method for the creation of new proteins and obtainment of some positive trait strains (Marin-Navarro et al., 2011; Parashar and Satyanarayana, 2016). This study used two chimeric glucoamylases, GA1 and GA2, with higher thermostability and similar catalytic efficiency. As for the enzyme activities, GATE, GA1, GA2, and GAA1 were 163.08 IU/ml, 140.36 IU/ml, 62.81 IU/ml, and 47.53 IU/ml, respectively. According to the results, GA1, GA2, and GA3 shared the same CD as GATE, while GA4, GA5, and GA6 shared the same CD as GAA1, but the enzyme activity of the former, except for GA3, was much higher than the latter. This demonstrated that the CD was a key factor for determining the enzyme activity. The difference between the recombinant GA1 and original GATE was the application of the SBD of GAA1, and the enzyme activity was approximate (only decreased 14%), showing that the change in the SBD had a slight influence on enzyme activity, which agreed with an earlier study (Cornett et al., 2003). The difference in the enzyme activity between GA1 and GA2 was caused by the different application of linker. The recombinant GA3 shared the same CD and SBD with the original GATE and the same Linker with the original GAA1, but its enzyme activity dropped significantly (decreased 92%), which further indicated the influence of linker on the change of the enzyme activity. The reason for this may be that different linkers changed the structure of the CD and SBD. Some studies have shown that the CD and SBD of fungal GAs are functionally independent, the connective function of the linker is not dependent on a special sequence, and different O-glucosylation patterns of linker influence the stability and secretion of GAs and digestion of raw starch (Coutinho and Reilly, 1994a). So, we speculated that linker affected the activities of chimeric GAs by changing the structure of the CD and SBD, which was consistent with the structural predict of recombinant GAs (**Figures 5, 6**).

Above all, although each domain of glucoamylase could affect the enzyme activity more or less, the influence of the CD on the enzyme activity was the greatest, followed by linker, and the influence of the SBD on the enzyme activity was weak.

The properties of the recombinant GA1 and GA2 and the original GATE and GAA1 were further analyzed. The optimal temperature of chimeric GA1 was 65°C, which was lower than that of GATE (70°C) but higher than that of GAA1 (60°C), and the optimal temperature of recombinant GA2 was the same as GAA1,

but the thermostability of GA1 and GA2 was higher than that of the original GAs, suggesting the domain shuffling of GAs could change the thermal stability, although with a slight decrease in the enzyme activity. The reason for the higher stability of GA1 and GA2, according to the analysis of the secondary structure, may be the increased and extended  $\alpha$ -helix of GA1 and GA2, especially at the 396–420 and 433–460 regions; the longer  $\alpha$ -helix is, the higher the thermostability will be (Stoffer et al., 1993). Through the analysis of the tertiary structures, it could be seen that the SBD of GATE had four additional structures constructed by the  $\beta$ -sheet. This complex structure might make GATE easier to bind with substrates.

## CONCLUSION

This study has successfully obtained six chimeric glucoamylase genes by domain shuffling of two glucoamylase genes with different enzymatic properties using overlap extension PCR. Of the six chimeric glucoamylases, only GA1 and GA2 revealed higher enzyme activities than the original GAA1 in the fermentation broth. Meanwhile, GA1 and GA2 also showed enhanced thermostability. Moreover, GA1 had the same catalytic efficiency as GATE. GA2 was slightly less than GATE but still higher than GAA1 in terms of catalytic efficiency. The prediction of the secondary and tertiary structures indicated that the increased and extended  $\alpha$ -helix of GA1 and GA2, especially in the poor thermal stability and easily being broken region of the amino acid between 443 and 444, may lead to higher thermostability. In a word, by domain shuffling, two novel thermostability chimeric glucoamylases were created, which offered a feasibility to generate novel enzymes with enhanced properties.

## DATA AVAILABILITY STATEMENT

The original contributions presented in the study are included in the article/Supplementary Material, further inquiries can be directed to the corresponding authors.

## AUTHOR CONTRIBUTIONS

ML, FL, ZC, and LW designed the experiments. ZC and LW performed the experiments. ML, YS, and LZ analyzed the data. DH and LZ analyzed and predicted the structure of GAs. ML and FL supervised the study. ZC, LW, and DH wrote the manuscript with contributions from all authors. All authors contributed to the article and approved the submitted version.

## FUNDING

This work was supported by the National Key Research and Development Program of China (Nos. 2021YFC2100403 and 2021YFC2101802) and the National Natural Science Foundation of China (No. 32072161).



## REFERENCES

- Ali, M., Ishqi, H. M., and Husain, Q. (2020). Enzyme Engineering: Reshaping the Biocatalytic Functions. *Biotechnol. Bioeng.* 117, 1877–1894. doi:10.1002/bit.27329
- Arnold, K., Bordoli, L., Kopp, J., and Schwede, T. (2006). The Swiss-Model Workspace: A Web-Based Environment for Protein Structure Homology Modelling. *Bioinformatics* 22, 195–201. doi:10.1093/bioinformatics/bti770
- Cornett, C. A. G., Fang, T.-Y., Reilly, P. J., and Ford, C. (2003). Starch-binding Domain Shuffling in *Aspergillus niger* Glucoamylase. *Protein Eng. Des. Selection* 16, 521–529. doi:10.1093/protein/gzg066
- Coutinho, P. M., and Reilly, P. J. (1994a). Structural Similarities in Glucoamylases by Hydrophobic Cluster Analysis. *Protein Eng. Des. Sel* 7, 749–760. doi:10.1093/protein/7.6.749
- Coutinho, P. M., and Reilly, P. J. (1994b). Structure-function Relationships in the Catalytic and Starch Binding Domains of Glucoamylase. *Protein Eng. Des. Sel* 7, 393–400. doi:10.1093/protein/7.3.393
- Frandsen, T. P., Dupont, C., Lehmbeck, J., Stoffer, B., Sierks, M. R., Honzatko, R. B., et al. (1994). Site-Directed Mutagenesis of the Catalytic Base Glutamic Acid 400 in Glucoamylase from *Aspergillus niger* and of Tyrosine 48 and Glutamine 401, Both Hydrogen-Bonded to the  $\gamma$ -Carboxylate Group of Glutamic Acid 400. *Biochemistry* 33, 13808–13816. doi:10.1021/bi00250a035
- Gomis-Cebolla, J., Ferreira Dos Santos, R., Wang, Y., Caballero, J., Caballero, P., He, K., et al. (2020). Domain Shuffling between Vip3aa and Vip3ca: Chimera Stability and Insecticidal Activity against European, American, African, and Asian Pests. *Toxins* 12, 99. doi:10.3390/toxins12020099
- Guo, Y., Tu, T., Qiu, J., Tong, L., Luo, H., and Yao, B. (2019). Characterization and Structure of a Novel Thermostable Glucoamylase from *Talaromyces leycettanus* Jcm12802. *Sheng Wu Gong Cheng Xue Bao* 35, 616–625. doi:10.13345/j.cjb.180330
- Hosťinová, E., Solovíková, A., Dvorský, R., and Gašperíková, J. (2003). Molecular Cloning and 3D Structure Prediction of the First Raw-Starch-Degrading Glucoamylase without a Separate Starch-Binding Domain. *Arch. Biochem. Biophys.* 411, 189–195. doi:10.1016/s0003-9861(03)00003-1
- Jia, M., Luo, L., and Liu, C. (2004). The Relationship between Protein Secondary Structure and Messenger RNA Secondary Structure. *Acta Scientiarum Naturalium Universitatis NeiMongol* 35, 55–59.
- Jones, D. T. (1999). Protein Secondary Structure Prediction Based on Position-specific Scoring Matrices. *J. Mol. Biol.* 292, 195–202. doi:10.1006/jmbi.1999.3091
- Karim, K. M. R., Husaini, A., Sing, N. N., Tasnim, T., Mohd Sinang, F., Hussain, H., et al. (2019). Characterization and Expression in *Pichia pastoris* of a Raw Starch Degrading Glucoamylase (ga2) Derived from *Aspergillus flavus* Nsh9. *Protein Expr. Purif.* 164, 105462. doi:10.1016/j.pep.2019.105462
- Kumar, P., and Satyanarayana, T. (2009). Microbial Glucoamylases: Characteristics and Applications. *Crit. Rev. Biotechnol.* 29, 225–255. doi:10.1080/0738850903136076
- Lago, M. C., Santos, F. C., Bueno, P. S. A., Oliveira, M. A. S., and Barbosa-Tessmann, I. P. (2021). The Glucoamylase from *Aspergillus wentii*: Purification and Characterization. *J. Basic Microbiol.* 61, 443–458. doi:10.1002/jobm.202000595
- Lee, J., and Paetzel, M. (2011). Structure of the Catalytic Domain of Glucoamylase from *Aspergillus niger*. *Acta Cryst. Sect F* 67, 188–192. doi:10.1107/S1744309110049390
- Lim, S. J., and Oslan, S. N. (2021). Native to Designed: Microbial  $\alpha$ -amylases for Industrial Applications. *PeerJ* 9, e11315. doi:10.7717/peerj.11315
- Lin, S.-C., Liu, W.-T., Liu, S.-H., Chou, W.-I., Hsiung, B.-K., Lin, I.-P., et al. (2007). Role of the Linker Region in the Expression of *Rhizopus oryzae* Glucoamylase. *BMC Biochem.* 8, 9. doi:10.1186/1471-2091-8-9
- Lincoln, L., More, V. S., and More, S. S. (2019). Purification and Biochemical Characterization of Extracellular Glucoamylase from *Paenibacillus amylolyticus* strain. *J. Basic Microbiol.* 59, 375–384. doi:10.1002/jobm.201800540
- Luo, L., and Dong, Y. (1988). Statistical Analysis of Peptide Correlation and Prediction of Protein Conformation. *Chin. Biochem. J.* 4, 173–183. doi:10.13865/j.cnki.cjbmb.1988.02.012
- Marín-Navarro, J., Gurgu, L., Alamar, S., and Polaina, J. (2011). Structural and Functional Analysis of Hybrid Enzymes Generated by Domain Shuffling between *Saccharomyces cerevisiae* (Var. Diastaticus) Stal Glucoamylase and *Saccharomycopsis fibuligera* Bgl1  $\beta$ -glucosidase. *Appl. Microbiol. Biotechnol.* 89, 121–130. doi:10.1007/s00253-010-2845-3
- Miller, G. L. (1959). Use of Dinitrosalicylic Acid Reagent for Determination of Reducing Sugar. *Anal. Chem.* 31, 420–428. doi:10.1021/ac60147a030
- Nielsen, B. R., Lehmbeck, J., and Frandsen, T. P. (2002). Cloning, Heterologous Expression, and Enzymatic Characterization of a Thermostable Glucoamylase from *Talaromyces emersonii*. *Protein Expr. Purif.* 26, 1–8. doi:10.1016/s1046-5928(02)00505-3
- Norouzian, D., Akbarzadeh, A., Scharer, J. M., and Moo Young, M. (2006). Fungal Glucoamylases. *Biotechnol. Adv.* 24, 80–85. doi:10.1016/j.biotechadv.2005.06.003
- Parashar, D., and Satyanarayana, T. (2016). A Chimeric  $\alpha$ -amylase Engineered from *Bacillus acidicola* and *Geobacillus thermoleovorans* with Improved Thermostability and Catalytic Efficiency. *J. Ind. Microbiol. Biotechnol.* 43, 473–484. doi:10.1007/s10295-015-1721-7
- Parashar, D., and Satyanarayana, T. (2017). Engineering a Chimeric Acid-Stable  $\alpha$ -amylase-glucoamylase (Amy-Glu) for One Step Starch Saccharification. *Int. J. Biol. Macromolecules* 99, 274–281. doi:10.1016/j.ijbiomac.2017.02.083
- Peng, H., Li, R., Li, F., Zhai, L., Zhang, X., Xiao, Y., et al. (2018). Extensive Hydrolysis of Raw rice Starch by a Chimeric  $\alpha$ -amylase Engineered with  $\alpha$ -amylase (AmyP) and a Starch-Binding Domain from *Cryptococcus* Sp. S-2. *Appl. Microbiol. Biotechnol.* 102, 743–750. doi:10.1007/s00253-017-8638-1
- Sauer, J., Christensen, T., Frandsen, T. P., Mirgorodskaya, E., McGuire, K. A., Driguez, H., et al. (2001). Stability and Function of Interdomain Linker Variants of Glucoamylase 1 from *Aspergillus niger*. *Biochemistry* 40, 9336–9346. doi:10.1021/bi010515i
- Sauer, J., Sigurskjöld, B. W., Christensen, U., Frandsen, T. P., Mirgorodskaya, E., Harrison, M., et al. (2000). Glucoamylase: Structure/function Relationships, and Protein Engineering. *Biochim. Biophys. Acta (Bba) - Protein Struct. Mol. Enzymol.* 1543, 275–293. doi:10.1016/s0167-4838(00)00232-6
- Schmidt, A., Shvetsov, A., Soboleva, E., Kil, Y., Sergeev, V., and Surzhik, M. (2019). Thermostability Improvement of *Aspergillus awamori* Glucoamylase via Directed Evolution of its Gene Located on Episomal Expression Vector in *Pichia pastoris* Cells. *Protein Eng. Des. Sel* 32, 251–259. doi:10.1093/protein/gzz048
- Sharma, A., Gupta, G., Ahmad, T., Mansoor, S., and Kaur, B. (2019). Enzyme Engineering: Current Trends and Future Perspectives. *Food Rev. Int.* 37, 121–154. doi:10.1080/87559129.2019.1695835
- Sierks, M. R., Ford, C., Reilly, P. J., and Svensson, B. (1990). Catalytic Mechanism of Fungal Glucoamylase as Defined by Mutagenesis of Asp176, Glu179 and Glu180 in the Enzyme from *Aspergillus awamori*. *Protein Eng. Des. Sel* 3, 193–198. doi:10.1093/protein/3.3.193
- Stoffer, B., Frandsen, T. P., Busk, P. K., Schneider, P., Svendsen, I., and Svensson, B. (1993). Production, Purification and Characterization of the Catalytic Domain of Glucoamylase from *Aspergillus niger*. *Biochem. J.* 292 (Pt 1), 197–202. doi:10.1042/bj2920197
- Suyama, Y., Muraki, N., Kusunoki, M., and Miyake, H. (2017). Crystal Structure of the Starch-Binding Domain of Glucoamylase from *Aspergillus niger*. *Acta Cryst. Sect F* 73, 550–554. doi:10.1107/S2053230X17012894
- Svensson, B., Clarke, A. J., Svendsen, I., and Møller, H. (1990). Identification of Carboxylic Acid Residues in Glucoamylase G2 from *Aspergillus niger* that Participate in Catalysis and Substrate Binding. *Eur. J. Biochem.* 188, 29–38. doi:10.1111/j.1432-1033.1990.tb15367.x
- Tong, L., Zheng, J., Wang, X., Wang, X., Huang, H., Yang, H., et al. (2021). Improvement of Thermostability and Catalytic Efficiency of Glucoamylase from *Talaromyces leycettanus* Jcm12802 via Site-Directed Mutagenesis to Enhance Industrial Saccharification Applications. *Biotechnol. Biofuels* 14, 202. doi:10.1186/s13068-021-02052-3
- Wang, C., Yang, L., Luo, L., Tang, S., and Wang, Q. (2020). Purification and Characterization of Glucoamylase of *Aspergillus oryzae* from Luzhou-Flavour Daqu. *Biotechnol. Lett.* 42, 2345–2355. doi:10.1007/s10529-020-02956-4
- Waylace, N. M., Hedin, N., Busi, M. V., and Gomez-Casati, D. F. (2021). Characterization of Sdga, a Cold-Adapted Glucoamylase from *Saccharophagus degradans*. *Biotechnol. Rep.* 30, e00625. doi:10.1016/j.btre.2021.e00625

- Xu, K., Zhang, H., Blumwald, E., and Xia, T. (2010). A Novel Plant Vacuolar Na<sup>+</sup>/H<sup>+</sup> Antipporter Gene Evolved by DNA Shuffling Confers Improved Salt Tolerance in Yeast. *J. Biol. Chem.* 285, 22999–23006. doi:10.1074/jbc.M109.073783
- Zhang, M.-Y., Zhao, S., Ning, Y.-N., Fu, L.-H., Li, C.-X., Wang, Q., et al. (2019). Identification of an Essential Regulator Controlling the Production of Raw-Starch-Digesting Glucoamylase in *Penicillium oxalicum*. *Biotechnol. Biofuels* 12, 7. doi:10.1186/s13068-018-1345-z
- Zong, X., Wen, L., Wang, Y., and Li, L. (2022). Research Progress of Glucoamylase with Industrial Potential. *J. Food Biochem.* doi:10.1111/jfbc.14099

**Conflict of Interest:** The authors declare that the research was conducted in the absence of any commercial or financial relationships that could be construed as a potential conflict of interest.

**Publisher's Note:** All claims expressed in this article are solely those of the authors and do not necessarily represent those of their affiliated organizations, or those of the publisher, the editors, and the reviewers. Any product that may be evaluated in this article, or claim that may be made by its manufacturer, is not guaranteed or endorsed by the publisher.

Copyright © 2022 Chen, Wang, Shen, Hu, Zhou, Lu and Li. This is an open-access article distributed under the terms of the Creative Commons Attribution License (CC BY). The use, distribution or reproduction in other forums is permitted, provided the original author(s) and the copyright owner(s) are credited and that the original publication in this journal is cited, in accordance with accepted academic practice. No use, distribution or reproduction is permitted which does not comply with these terms.



# Characterization of D-Allulose-3-Epimerase From *Ruminiclostridium papyrosolvens* and Immobilization Within Metal-Organic Frameworks

Jiaming Yang<sup>1</sup>, Dexun Fan<sup>1</sup>, Fengguang Zhao<sup>2</sup>, Ying Lin<sup>1</sup>, Suiping Zheng<sup>1</sup> and Shuangyan Han<sup>1\*</sup>

<sup>1</sup>Guangdong Key Laboratory of Fermentation and Enzyme Engineering, School of Biology and Biological Engineering, South China University of Technology, Guangzhou, China, <sup>2</sup>School of Light Industry and Engineering, South China University of Technology, Guangzhou, China

## OPEN ACCESS

### Edited by:

Hui-Min Qin,  
Tianjin University of Science and  
Technology, China

### Reviewed by:

Shuhong Mao,  
Tianjin University of Science and  
Technology, China  
Wenli Zhang,  
Jiangnan University, China

### \*Correspondence:

Shuangyan Han  
syhan@scut.edu.cn

### Specialty section:

This article was submitted to  
Bioprocess Engineering,  
a section of the journal  
Frontiers in Bioengineering and  
Biotechnology

**Received:** 04 February 2022

**Accepted:** 23 February 2022

**Published:** 14 April 2022

### Citation:

Yang J, Fan D, Zhao F, Lin Y, Zheng S  
and Han S (2022) Characterization of  
D-Allulose-3-Epimerase From  
*Ruminiclostridium papyrosolvens* and  
Immobilization Within Metal-  
Organic Frameworks.  
Front. Bioeng. Biotechnol. 10:869536.  
doi: 10.3389/fbioe.2022.869536

D-allulose is one sort of C-3 epimer of D-fructose with the low calorie (0.4 kcal/g) and high sweetness (70% of the relative sweetness of sucrose), which can be biosynthesized by D-allulose-3-epimerase (DAE). In this work, we report the characterization of a novel DAE from *Ruminiclostridium papyrosolvens* (RpDAE) by genome mining approach. The activity of RpDAE reached maximum at pH 7.5 and 60°C, supplemented with 1 mM Co<sup>2+</sup>. Using D-fructose (500 g/L) as the substrate for epimerization reaction, RpDAE produced D-allulose (149.5 g/L). In addition, RpDAE was immobilized within the microporous zeolite imidazolate framework, ZIF67, by *in situ* encapsulation at room temperature. The synthesized bio-composites were characterized by powder X-ray diffraction and Fourier transform infrared spectroscopy. RpDAE-ZIF67 maintained 56% of residual activity after five reaction cycles. This study provides helpful guidance for further engineering applications and industrial production of D-allulose.

**Keywords:** allulose, metal-organic frameworks, enzyme immobilization, *ruminiclostridium papyrosolvens*, D-allulose 3-epimerase

## INTRODUCTION

Vascular risk factors, exemplified by type 2 diabetes, hypertension, and obesity, have become health concerns worldwide. The quantity of type 2 diabetes victims in 2017 is assessed to be 415 million, and 31.1% of adults (13.9 billion) have hypertension (Wyss et al., 2020). In addition, NCD Risk Factor Collaboration predicts that the global obesity incidence rate will reach 18% for men and 21% for women by 2025 under existing trends (Trends in Adult body-mass, 2016). Amassing proof demonstrates that excessive caloric intake contributes to the development of these chronic diseases (Xia et al., 2021) (Johnson et al., 2007). Thusly, developing and intaking low-calorie food supplements can be the practical methodology to defuse vascular risks (Chung et al., 2012). D-allulose (D-ribo-2-hexylose, C<sub>6</sub>H<sub>12</sub>O<sub>6</sub>), initially named D-psicose, is one sort of rare sugar. Because of its low bioavailability, D-allulose keeps up with 70% of the relative sweetness of sucrose (Chung et al., 2012) with energy of only 0.4 kcal/g. U.S. Food and Drug Administration has ratified D-allulose as “generally recognized as safe” since 2012 (GRN No. 400), which makes it an attractive sugar substitute. The presence of D-allulose in nature is very

scant, which is found in a small number of plants exemplified by wheat (Miller and Swain, 1960) and *Itea* (Ayers et al., 2014) and a few processed foods, such as commercial fructose syrup mixtures and steamed treated coffee (Oshima et al., 2006).

The scarcity of D-allulose in nature enormously limits its large-scale application. Chemical synthesis of D-allulose has many defects, including complex purification process, by-product formation, and chemical waste pollution (Chen et al., 2021). By comparison, the biosynthesis of D-allulose is more efficient, with mild reaction conditions, without by-product formation, which allows better sustainability to be achieved. All monosaccharides can be cyclically transformed by four kinds of enzymes, including polyol dehydrogenase, aldose isomerase, aldose reductase, and ketose-3-epimerase (KEase). D-allulose-3-epimerases (DAEs) are one type of KEase catalyzing reversible epimerization of D-fructose, the most abundant ketose in nature, into D-allulose (Mu et al., 2015). Promising progress has been noted in the biosynthesis of D-allulose, until now, approximately 20 DAEs from different strains have been characterized (Chen et al., 2021). Most DAEs discovered to date are of bacterial origin, mainly derived from soil bacteria, e.g., *A. tumefaciens* (Kim et al., 2006a), *C. cellulolyticum* (Mu et al., 2011), *Desmospora* sp. 8,437 (Zhang et al., 2013), and *N. thermophilus* (Jia et al., 2021). Most DAEs rely on  $\text{Co}^{2+}$  or  $\text{Mn}^{2+}$  as co-factor and are inactive in the absence of metal ions.

Although the use of enzyme is an environment-friendly strategy, the actual production of D-allulose by the enzyme faces the problems of high cost, and poor operation stability. Enzyme immobilization has been proved to be an effective way to improve robustness, ease of recovery, and continuous utilization of enzymes in industrial processes (Homaei et al., 2013). High porosity, tunable pore sizes, good thermostability, and opportune biocompatibility endow metal-organic frameworks (MOFs) with potential as matrices to immobilize biological macromolecules, such as enzymes (Liang et al., 2015). Among the various MOFs, zeolitic imidazolate frameworks (ZIFs), which are formed by self-assembly of tetrahedral metal clusters ( $\text{Zn}^{2+}$  or  $\text{Co}^{2+}$ ) and 2-methylimidazole ligands, have been extensively studied *in situ* encapsulation because of their mild synthetic conditions in aqueous solution (Gross et al., 2012). Lyu and colleagues (Lyu et al., 2014) pioneeringly employed this strategy with cytochrome c and ZIF8, obtaining Cyt c/ZIF8 bio-composite with 10-fold higher bioactivity over free enzyme. Rafiei and co-workers constructed lipase/ZIF67 composite and applied it in the transesterification of soybean oil to biodiesel. The biocatalytic composite maintained excellent enzymatic catalytic performance after six cycles (Rafiei et al., 2018).

In the present study, a putative DAE from *Ruminiclostridium papyrosolvans* C7 (RpDAE) was identified. The RpDAE was cloned and overexpressed as recombinant proteins in *E. coli* BL21 (DE3). The enzyme properties of purified RpDAE and its application in the biological production of D-allulose were studied. In addition, RpDAE was encapsulated by ZIF67 under mild conditions to enhance its thermal stability and reusability. The RpDAE-ZIF67 bio-composites were characterized by powder X-ray diffraction (PXRD) and Fourier transform infrared (FT-IR) spectroscopy, and the catalytic performance and reusability were also evaluated.

## MATERIALS AND METHODS

### Gene Cloning, Expression, and Purification of RpDAE

The gene sequence of RpDAE (NCBI ACCESSION: WP\_020816056.1) was codon-optimized for *E. coli* expression and fused with a modified His-based tag (HE tag) containing eight repeat histidine-glutamate residues (HEHEHEHEHEHEHEHE) at C-terminus, which is capable of immobilized metal ion affinity chromatography purification. The sequence was synthesized (GenScript, Nanjing, China) and subcloned into the pET-21a (+) between *Nde*I and *Xho*I restriction sites. Recombinant plasmid pET-RpDAE was cloned and transformed into *E. coli* BL21 (DE3) for protein expression.

Recombinant strains were inoculated into 10 ml of Luria-Bertani (LB) medium. When needed, ampicillin was added into LB medium at the concentration of 100 µg/ml. Then, strains were cultured at 37°C with shaking at 200 rpm overnight. The seed was transferred into 100 ml of LB medium and after cultivated at 37°C with shaking at 200 rpm. When cells grown to the proper optical density ( $\text{OD}_{600} = 0.7$ ), 0.5 mM isopropyl- $\beta$ -D-1-thiogalactopyranoside (IPTG) was added, and induced recombinant cells were further cultured at 15°C with shaking at 180 rpm for 16 h.

Recombinant cells were harvested by centrifugation at 8,000g for 5 min at 4°C. Subsequently, cells were washed thrice in lysis buffer (50 mM Tris-HCl, 100 mM NaCl, pH 7.5). Then, cells were lysed by sonication at 30 amplitudes (pulse on for 3 s and pulse off for 3 s) for 30 min over the ice. The cell debris was removed by centrifugation at 10,000g for 5 min at 4°C, and the supernatant was obtained for further purification. Enzyme with HE tag was trapped on His Trap™ FF column (Cytiva, MA, USA) at a flow rate of 0.5 ml/min. Wash buffer (50 mM Tris-HCl, 10 mM imidazole, 0.5 M NaCl, pH 7.5) was used to elute unbound proteins, and the target enzyme was eluted by elution buffer (50 mM Tris-HCl, 300 mM imidazole, 0.5 M NaCl, pH 7.5). Eluant was further dialyzed to remove imidazole with 50 mM Tris-HCl (pH 7.5) and concentrated by Amicon® Ultra filter (10 kDa) (Merck, USA). The protein concentration was measured by Bradford Assay (Thermo Fisher, MA, USA). The purified protein was loaded onto sodium dodecyl sulfate-polyacrylamide gel electrophoresis (SDS-PAGE) gel for the determination of molecular mass and purity.

### Enzyme Assay

The enzyme activity was determined by quantitative determination of product converted from the substrate. Data for this study was collected by high-performance liquid chromatography (HPLC) system, linked to a 2424 evaporative light scattering detector and an xBridge BEH amide column (all from Waters, MA, USA). The temperatures of the detector and column were set at 65°C and 35°C, respectively. The mobile phase was acetonitrile and water mixture (80:20, v/v, with 0.1% v/v ammonia added) at a

flow rate of 1 ml/min. The reaction system incorporated D-fructose (50 g/L), 1 mM  $\text{Co}^{2+}$ , appropriate amount of RpDAE or RpDAE-ZIF67, and 50 mM  $\text{KH}_2\text{PO}_4/\text{Na}_2\text{HPO}_4$  (pH 7.5). The reaction was performed at 60°C for 5 min and terminated by boiling for 5 min. One unit (U) of RpDAE activity was defined as the amount of enzyme required to catalyze 1  $\mu\text{mol}$  of D-allulose within the unit time (min) under the reaction condition.

## Effect of Metal Ions and Substrate Specificity

To determine the influence of metal ions on the RpDAE activity, the activity was examined under standard enzyme assay except for supplemented with different metal ions ( $\text{Mg}^{2+}$ ,  $\text{Cu}^{2+}$ ,  $\text{Co}^{2+}$ ,  $\text{Ni}^{2+}$ ,  $\text{Mn}^{2+}$ ,  $\text{Ca}^{2+}$ , and  $\text{Zn}^{2+}$ ) at the final concentration of 1 mM. The activity measured without metal ions was defined as 100% relative activity. The substrate specificity of RpDAE was tested by adding different ketoses (D-allulose, D-fructose, D-sorbose, and D-tagatose) into the reaction system as substrates. The reaction conditions were standard.

## Bioconversion of D-Allulose

To determine the bioconversion from D-fructose to D-allulose, 2  $\mu\text{M}$  purified RpDAE was added with 1 mM  $\text{Co}^{2+}$  and D-fructose (500 g/L) in 50 mM  $\text{KH}_2\text{PO}_4/\text{Na}_2\text{HPO}_4$  buffer (pH 7.5) at 50°C. Samples were taken at designated time intervals and diluted tenfold. The yields of the accumulative D-allulose were detected by HPLC.

## Effect of Temperature and pH

To study the effect of temperature on RpDAE activity, RpDAE was added in  $\text{KH}_2\text{PO}_4/\text{Na}_2\text{HPO}_4$  buffer (pH 7.5) at temperatures varying from 40°C to 80°C. To investigate the effect of the pH on the activity of RpDAE, the reaction was conducted at 60°C across a pH range of 6–10 in MES buffer (50 mM, pH 6.0) or  $\text{KH}_2\text{PO}_4/\text{Na}_2\text{HPO}_4$  buffer (50 mM, pH 7.0–10.0).

## Preparation and Characterization of RpDAE-ZIF67

RpDAE-ZIF67 was synthesized by *in situ* approach in the aqueous solution. Experimentally, 2 ml of purified RpDAE (2 mg/ml) and 2 ml of cobalt nitrate hexahydrate (0.04 M) were mixed with 2-methylimidazole (1.2 M, 2 ml) in distilled water and stirred for 1 h at ambient temperature. The sample solution was aged for 7 h and collected by centrifugation at 6,000 rpm for 20 min. Subsequently, samples were washed three times with distilled water. It was freeze-dried for 12 h. PXRD data were collected by SmartLab 9 kW X-ray diffractometer (Rigaku, Tokyo, Japan) with Cu-K $\alpha$  radiation at  $2\theta$  from 5° to 40°. FT-IR measured was performed by Nicolet iS20 spectroscopy (Thermo Scientific, MA, USA) in the range of 400–2,500  $\text{cm}^{-1}$ .

## RESULTS AND DISCUSSION

### Sequence Analysis of RpDAE

The genome mining approach has turned out to be a promising way toward the detection of novel industrial enzymes, such as lipase (Vorapreea et al., 2015),  $\beta$ -glucosidase (Zou et al., 2012), and laccase (Fang et al., 2011). To explore novel DAE applicable to biosynthesis D-allulose, the amino acid sequence of *Clostridium cellulolyticum* DAE (GenBank: ACL75304.1) with significant thermostability was chosen as the template to BLAST in the NCBI database. The sequence that encoded a deduced DAE (NCBI: WP\_020816056.1) from *Ruminiclostridium papyrosolvans* C7 with 59% amino acid identity with *C. cellulolyticum* DAE was selected. *R. papyrosolvans* strain was initially isolated from mud in Massachusetts, and its whole-genome shotgun sequence data was uploaded to NCBI database in 2013 (Zepeda et al., 2013), with the NCBI accession number PRJNA201398.

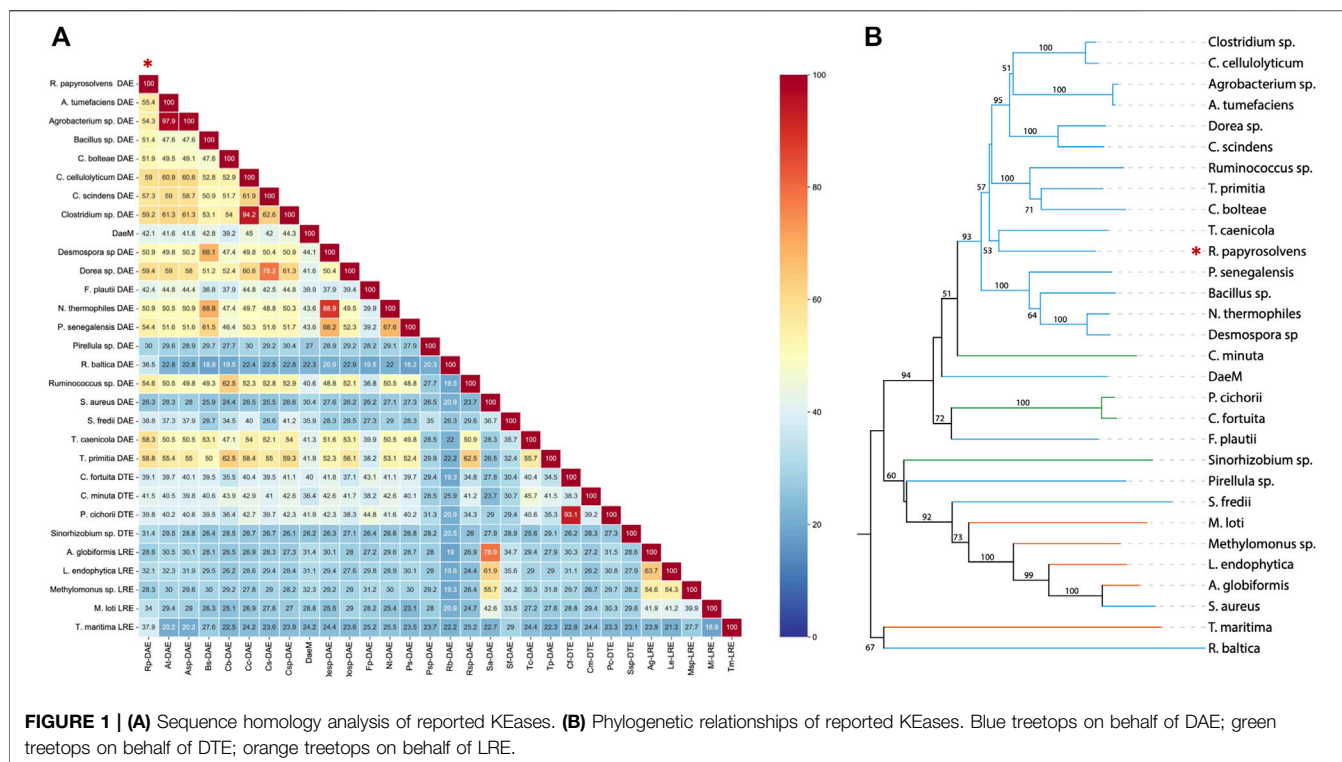
As presented in comparison of amino acid sequence (Figure 1A), deduced DAE from *R. Papyrosolvans* showed maximum homology identity with DAE from *Dorea* sp. (59.4%, GenBank: CDD07088.1), followed by DAE from *Clostridium* sp. (59.2%, GenBank: EDP19602.1). Except for DAEs from *Pirellula* sp., *R. baltica*, *S. aureus*, and *S. fredii* origin, there was more than 40% of homology identity between RpDAE and other characterized DAEs, while existed relatively low (less than 40%) homology identity with most D-tagatose-3-epimerases and L-ribulose-3-epimerases. Phylogenetic analysis with previously characterized KEases revealed its evolutionary relationship with DAE from genera of *T. caenicola* (Figure 1B).

So far, the crystal structures of *A. tumefaciens* ATCC33970 DAE (PDB: 2HK0) (Kim et al., 2006b) and *C. cellulolyticum* H10 DAE (PDB: 3VNI) (Chan et al., 2012) have been successfully resolved, and they are homotetramers with similar monomeric structures; each subunit possesses a distinct TIM barrel structure forming by eight  $\beta$ -sheets and  $\alpha$ -helices, and the catalytic activity center is strictly conserved (Jia et al., 2021). Multiple amino acid sequences alignment was performed between characterized DAEs and RpDAE (Figure 2). Crucial residues of RpDAE for the catalytic activity, including metal coordination sites (Glu150, Asp183, His209, and Glu244) and residues binding the O-1, O-2, O-3 of the substrate (Glu156, His186, and Arg215), were conserved with other reported DAEs. In general, these analyses indicate that RpDAE belongs to the DAE family.

### Expression and Purification of RpDAE

RpDAE fused with a modified histidine (HE) tag was recombinantly overexpressed in *E. coli* BL21 (DE3) by IPTG induction. HE tag can function as promoters of both affinity (Hofström et al., 2011) and solubility (Han et al., 2018). After cell disruption, the supernatants were purified by immobilized metal affinity chromatography. SDS-PAGE visualization confirmed expression and purification of proteins of about 35 kDa (Figure 3), which was in accordance with the theoretical molecular weight of RpDAE (34.89 kDa, containing HE tag).





Target proteins were mostly expressed in a soluble form under the conditions described above (Figure 3, Lane 2).

## Effect of Metal Ion and Substrate Specificity

To capture the effect of metal ions on RpDAE activity, diverse divalent metal ions were added into the reaction system at the final concentration of 1 mM. As illustrated in Figure 4A, RpDAE displayed activity in the absence of metal ions and enhanced in the presence of  $\text{Co}^{2+}$  and  $\text{Mn}^{2+}$ , by 1.78- and 1.56-fold, respectively. In contrast, the addition of  $\text{Cu}^{2+}$ ,  $\text{Ca}^{2+}$ ,  $\text{Zn}^{2+}$ , and  $\text{Ni}^{2+}$  inhibited enzyme activity, and the inhibitory effect of  $\text{Zn}^{2+}$  was the most significant, over 80%. Moreover,  $\text{Mg}^{2+}$  had little effect on the relative activity of RpDAE. Monosaccharide epimerase employing deprotonation/reprotonation mechanism often required metal ions as co-factor to participate in the catalysis (Van Overtveldt et al., 2015), and the optimum co-factor for RpDAE was determined to be  $\text{Co}^{2+}$ .

To explore the substrate specificity of RpDAE, four kinds of ketoses were used, containing D-allulose, D-fructose, D-tagatose, and D-sorbose. RpDAE displayed the highest activity in the presence of D-allulose, which was 40% higher in relation to D-fructose (Figure 4B). On the contrary, RpDAE displayed low epimerization activity toward D-tagatose and D-sorbose.

## Bioconversion of D-Allulose

The large-scale bioconversion of D-allulose was performed with D-fructose (500 g/L), 1 mM  $\text{Co}^{2+}$ , and 50 mM  $\text{KH}_2\text{PO}_4/\text{Na}_2\text{HPO}_4$  (pH 7.5), along with 0.2 g/L RpDAE at 50°C. The reaction rate for D-allulose production was 107.5 g/h for the first

hour. Finally, the equilibrium ratio of D-allulose and D-fructose was measured to be 29.9:70.1, and D-allulose (approximately 149.5 g/L) were obtained from D-fructose (500 g/L) without byproducts after 150 min (Figure 4C). At present, many multinational enterprises are researching and developing the biological production of D-allulose. In 2021, the European Food Safety Authority certified the safety of the two kinds of food enzyme DAEs, which were produced by genetically modified *E. coli* K-12 W3110 (pWKLP) strain (Matsutani Chemical Industry Co., Ltd.) (Lambré et al., 2021a) and *Corynebacterium Glutamicum* FIS002 strain (CJ-Tereos Sweeteners Europe SAS) (Lambré et al., 2021b), respectively. The efficiency of biocatalysts is crucial in industrial production. Generally, the conversion rates of different DAEs reported in the literature were between 22% and 32.9% (Jia et al., 2021), and the highest conversion yield was achieved by *A. tumefaciens* ATCC33970 DAE (Kim et al., 2006a). Compared to reported DAEs, the catalytic performance of RpDAE at the substrate scale of 500 g/L was at middle-upper levels, revealing as a potential candidate in the biological production of D-allulose.

## Effect of Temperature and pH on RpDAE

The enzyme activity of RpDAE was dependent on temperature and pH conditions. The influence of the temperatures on RpDAE activity was depicted in Figure 5A, and the activity was assayed with a temperature range of 40°C–80°C at pH 7.5. RpDAE displayed more than 82.9% relative activity at the temperature range between 55°C and 70°C. The maximum enzymatic activity of RpDAE was recorded at 60°C, which was higher than optimum temperature of *C.*

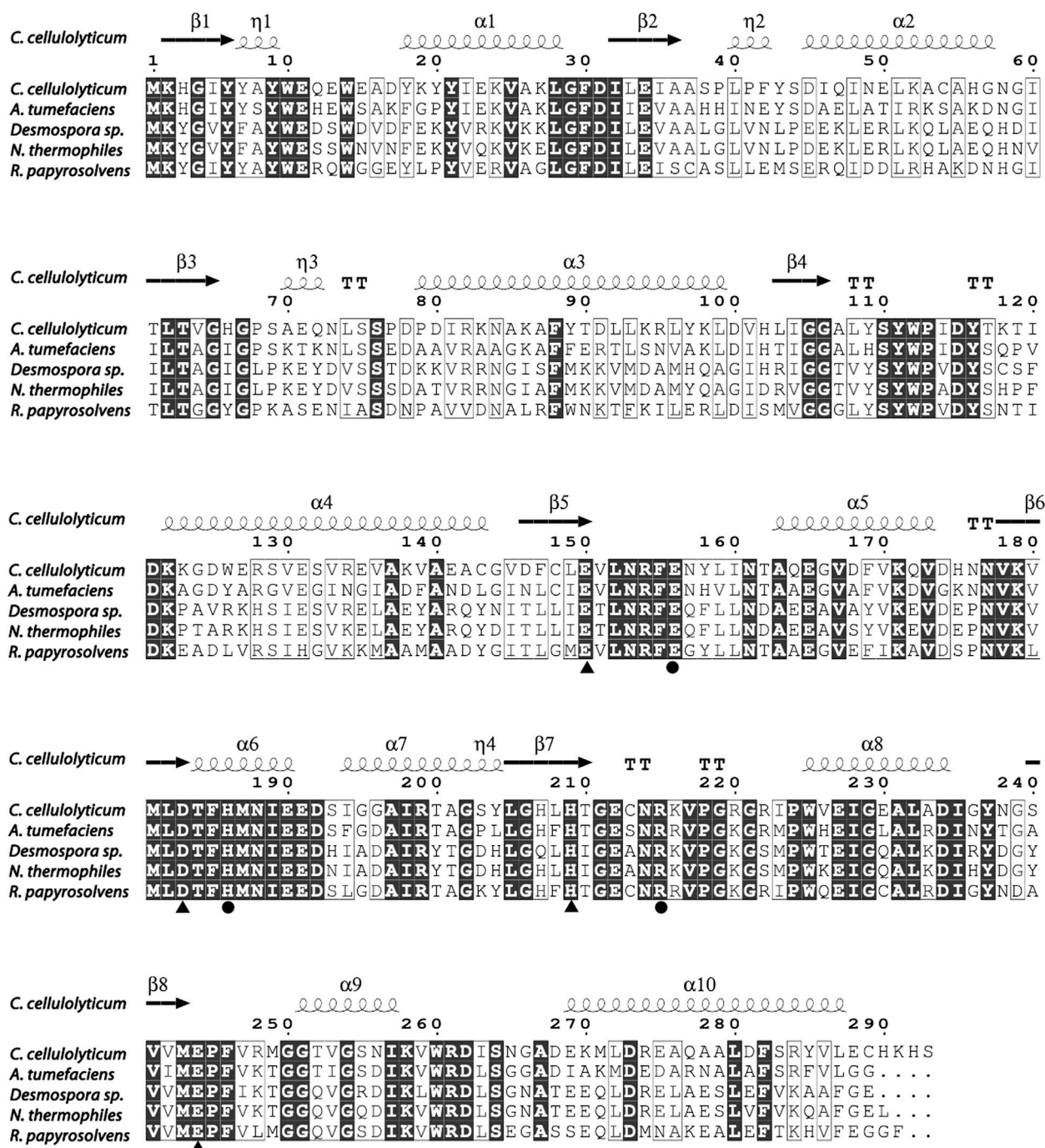


**FIGURE 2 |** Structure-based sequence alignment between *R. papyrosolvans* DAE and mentioned DAEs. The secondary structural elements of *C. cellulolyticum* (PDB: 3VNI) are presented. Identical and similar amino acid residues are marked in black and frame, respectively. Triangle mark as metal ions binding site, and circle mark as substrate (D-fructose) O-1, O-2, and O-3 binding sites.

*cellulolyticum* DAE (Mu et al., 2011). To further determine the activation energy ( $E_a$ ) of epimerization reaction at pH 7.5, activities measured at 40°C–60°C were plotted as  $\ln$  (relative activity) versus  $1000/T$ , and Arrhenius equation [ $\ln k = (-E_a/RT) + \ln A$ ] was used to calculate the  $E_a$  of 23.51 kJ/mol (illustration of Figure 5A).

The effect of pH on RpDAE was examined at 60°C over a pH range from 6.0 to 10.0, and the optimal pH occurred at a weak level of alkaline, which was pH 7.5 (Figure 5B). Most characterized DAEs showed optimum epimerization activity at pH 7.0 to 9.0, and the exception was *Dorea* sp. DAE with an optimal pH at 6.0

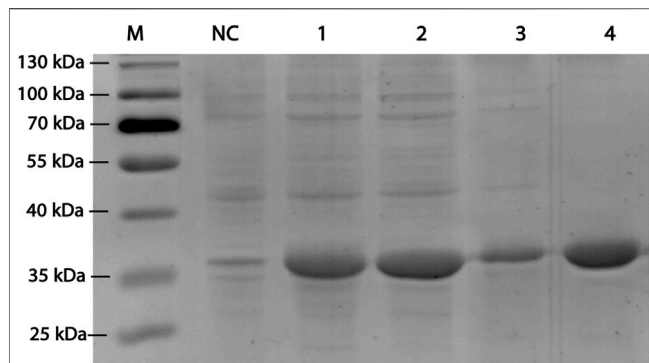


**FIGURE 3 |** SDS-PAGE analysis for RpDAE cloned in pET-21a (+) and expressed in *E. coli* BL21 (DE3). Lane M, protein marker; Lane NC, Cell lysate without induction; Lane 1, cell lysate with induction; Lane 2, supernatant of cell lysate with induction; Lane 3, debris of cell lysate with induction; Lane 4, purified protein.

(Zhang et al., 2015). RpDAE showed more than 87% of relative activity at pH 7.0, demonstrating application potentials in D-allulose production, because neutral conditions help to reduce browning of monosaccharide, thereby reducing yield loss.

## Preparation and Characterization of RpDAE-ZIF67

Immobilized enzymes are widely utilized in the food industry. On the one hand, immobilized enzymes are heterogeneous catalysts so that can be simply separated from the reaction medium and obtain a pure product without contamination. On the other hand, they can be applied multiple times to the production process, thus reducing costs (Yushkova et al., 2019). Benefiting from high biocompatibility and mild synthesis conditions, ZIFs are the most widely used *in situ* immobilization matrices (Lian et al., 2017). RpDAE-ZIF67 was synthesized through crystallization of ZIF67 around RpDAE in aqueous solution (Figure 6A), which is a straightforward, rapid, and cost-effective process (Patil and Yadav, 2018). To remove loosely attached RpDAE on the surface, the obtained RpDAE-ZIF67 particles were washed three times with deionized water. The synthesized ZIF67 and RpDAE-ZIF67 were characterized by PXRD. As shown in Figure 6B, the conspicuous reflections of synthesized ZIF67 at  $2\theta = 7.5^\circ, 10.5^\circ, 12.9^\circ, 14.8^\circ, 16.6^\circ, 18.1^\circ, 22.2^\circ, 24.6^\circ, 25.7^\circ, 26.8^\circ, 29.7^\circ, 30.7^\circ, 31.6^\circ, \text{ and } 32.5^\circ$  were associated with (0 1 1), (0 0 2), (1 1 2), (0 2 2), (0 1 3), (2 2 2), (1 1 4), (2 3 3), (2 2 4), (1 3 4), (0 4 4), (3 3 4), (2 4 4), and (2 3 5), respectively, of the simulated ZIF67 single-crystal planes (Banerjee et al., 2008) (Guo et al., 2016). Similar diffraction patterns were also observed in RpDAE-ZIF67,

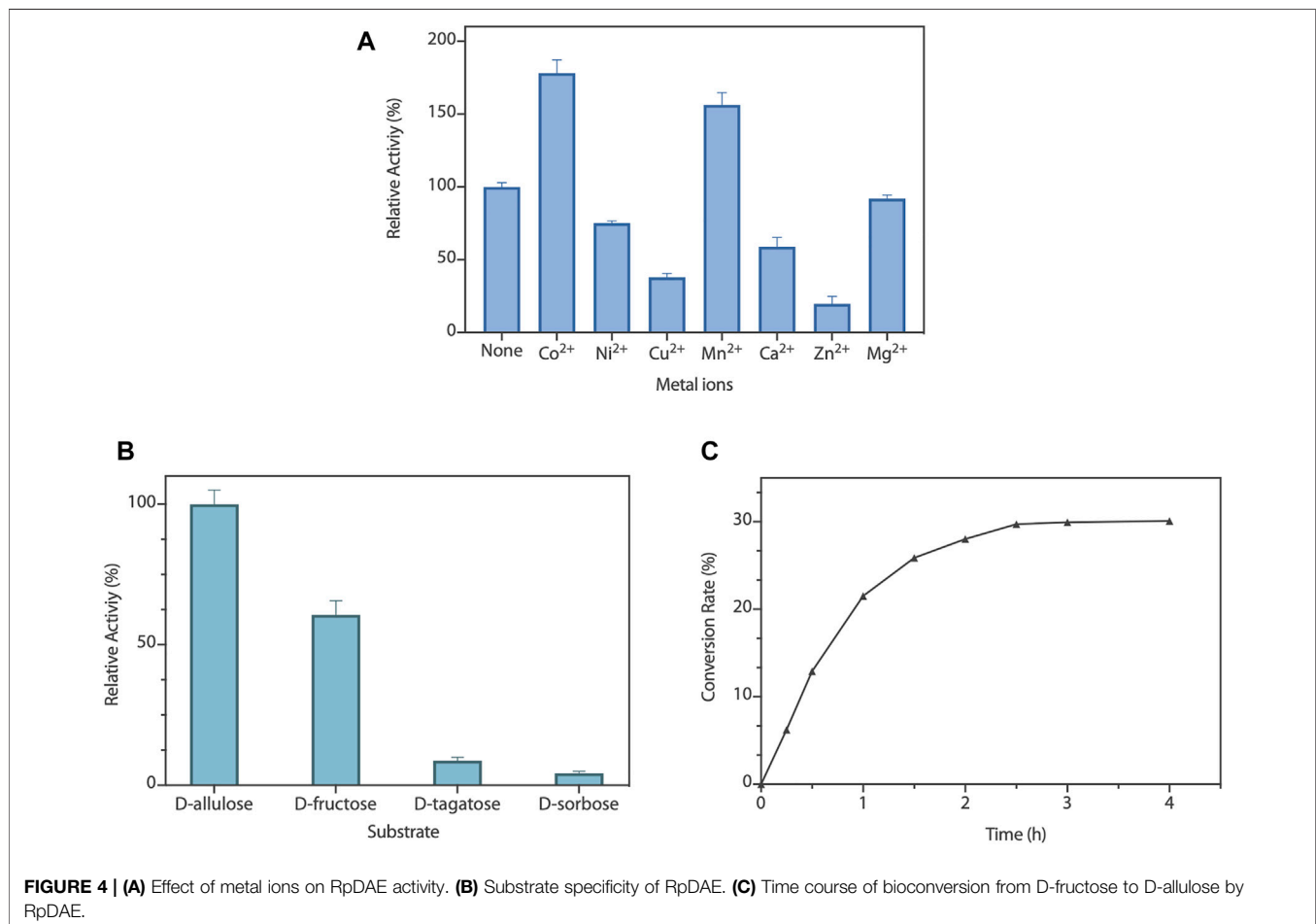


**FIGURE 4 |** (A) Effect of metal ions on RpDAE activity. (B) Substrate specificity of RpDAE. (C) Time course of bioconversion from D-fructose to D-allulose by RpDAE.

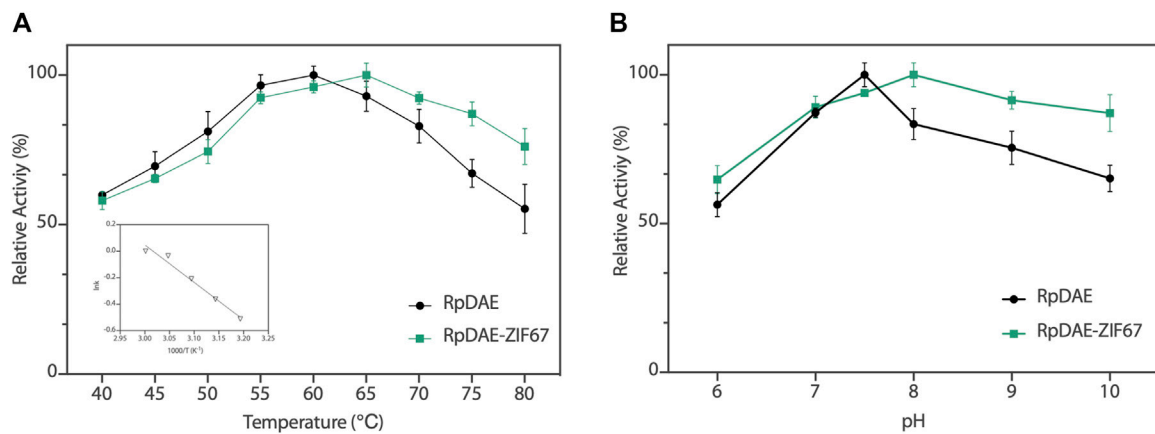


**FIGURE 5 | (A)** Temperature-activity profile of RpDAE and RpDAE-ZIF67. **(B)** pH-activity profile of RpDAE and RpDAE-ZIF67.

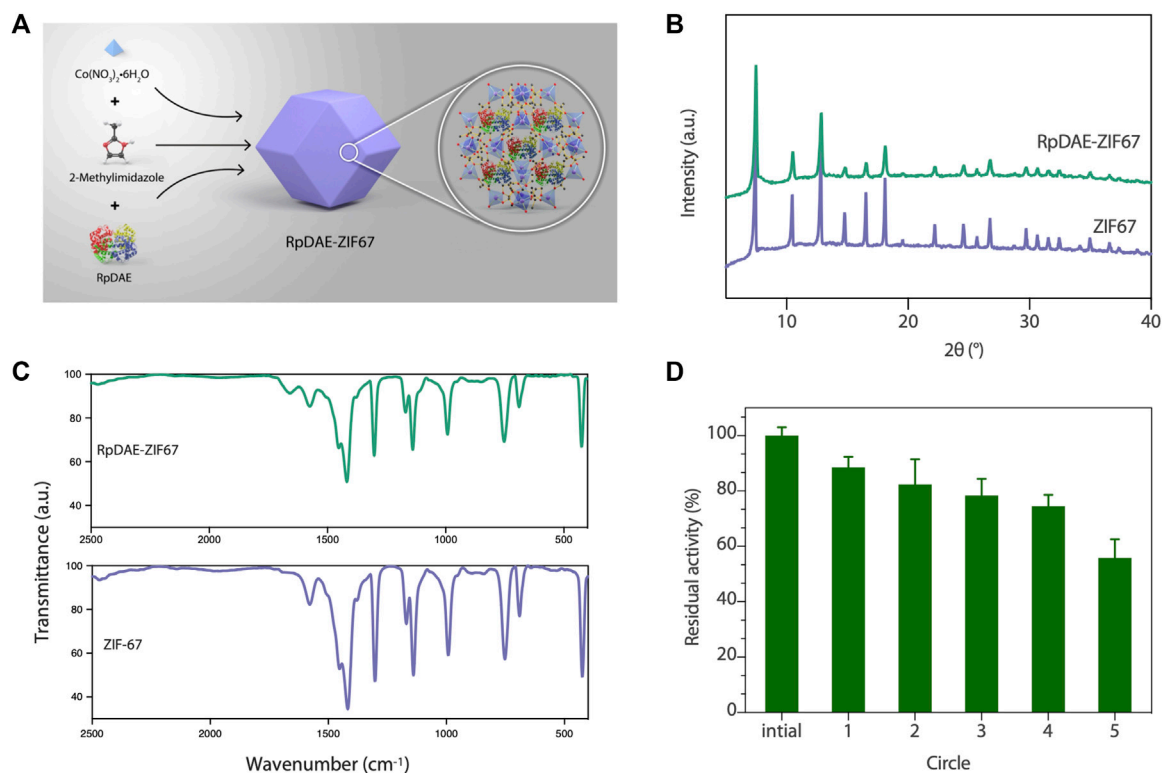


**FIGURE 6 | (A)** Scheme of synthesis of RpDAE-ZIF67 bio-composites. **(B)** PXRD patterns of RpDAE-ZIF67 and ZIF67. **(C)** FT-IR spectra of RpDAE-ZIF67 and ZIF67. **(D)** Cycle stability of RpDAE-ZIF67.

which indicated that the crystal structure of ZIF67 remained unaffected after the enzyme being incorporated. **Figure 6C** showed the FT-IR spectra of RpDAE and RpDAE-ZIF67. The vibrational bands of bare ZIF67 in the range of 600–1,500  $\text{cm}^{-1}$  correspond to the characteristic stretch and bending modes of imidazole rings. Furthermore, the band at 1,574  $\text{cm}^{-1}$  can be

attributed to the stretching mode of C=N in 2-methylimidazole. The above bands were all well represented in the spectrum of RpDAE-ZIF67. In addition, RpDAE-ZIF67 had a new absorption band at 1,658  $\text{cm}^{-1}$  compared to bare ZIF67, corresponding to the stretching vibration mode of C=O in the amide I bond, confirming the existence of DAE within ZIF67.



The relative activities of encapsulated DAE were evaluated, and **Figure 5A** demonstrated nearly identical activities of RpDAE and RpDAE-ZIF67 under 60°C. However, at higher temperatures (over 65°C), the encapsulated DAE displayed higher relative activity than free DAE. At 80°C, the free DAE showed only 55.3% of relative activity, whereas the encapsulated DAE retained 76.1% of relative activity. These results demonstrated that encapsulating enzymes in MOFs prevented conformational transitions at high temperatures and improved the thermostability. As shown in **Figure 5B**, encapsulated DAE reached maximum activity at pH 8.0 and showed the higher tolerance in alkaline compared with free DAE. Another purpose of immobilization is to make the biocatalyst easy to recover and reuse, which is a key factor for economic viability. Hence, the reusability of RpDAE was examined in consecutive epimerization reactions. Accordingly, the encapsulated DAE was separated from the reaction system by centrifugation. As shown in **Figure 6D**, the encapsulated DAE was successfully cycled for five times, and the residual activity was determined to be 56%. Wang et al. immobilized laccase within ZIF67 by the one-pot synthesis strategy, which maintained 59% residual enzyme activity after five reaction cycles (Wang et al., 2020). The gradual loss of activity during recycling may cause by mechanical damage to the enzyme. The reusability can be attributed to the small window size of the cages, physically preventing the leaching of the enzymes from ZIF67.

## CONCLUSION

In the present study, a novel RpDAE was identified, overexpressed in *E. coli*, purified, and characterized. RpDAE activity was not dependent on the presence of metal ions and can be enhanced by cobalt ions. The application potential was evaluated by large-scale bioconversion from D-fructose to D-allulose. Further, we pioneered the immobilization of DAE

within ZIF67 by *in situ* encapsulation strategy. Because of the shielding effect, the immobilized DAE exhibited reusability. These results provide an important reference for further research on the biological industrial production of D-allulose.

## DATA AVAILABILITY STATEMENT

The datasets presented in this study can be found in online repositories. The names of the repository/repositories and accession number(s) can be found in the article/Supplementary Material.

## AUTHOR CONTRIBUTIONS

All authors contributed to the background research and writing of the article, as well as the editing. In addition, all authors have read and approved the final version of this manuscript. Specific contributions are as follows: JY: experimental verification, data curation, and writing—reviewing and editing; DF: experiment performing and draft preparation; FZ: experimental assistance and software; SZ: methodology; YL: supervision; SH: conceptualization and funding acquisition.

## FUNDING

1: Key-Area Research and Development Program of Guangdong Province (No. 2020B020226007); 2: National Key R&D Program of China (No. 2021YFC2100400).

## REFERENCES

- Ayers, B. J., Hollinshead, J., Saville, A. W., Nakagawa, S., Adachi, I., Kato, A., et al. (2014). Itamine, the First Alkaloid Isolated from *Itea Virginica* L. Inflorescence. *Phytochemistry* 100, 126–131. doi:10.1016/j.phytochem.2014.01.012
- Banerjee, R., Phan, A., Wang, B., Knobler, C., Furukawa, H., O’Keeffe, M., et al. (2008). High-Throughput Synthesis of Zeolitic Imidazolate Frameworks and Application to CO<sub>2</sub> Capture. *Science* 319 (5865), 939–943. doi:10.1126/science.1152516
- Chan, H.-C., Zhu, Y., Hu, Y., Ko, T.-P., Huang, C.-H., Ren, F., et al. (2012). Crystal Structures of D-Psicose 3-epimerase from *Clostridium Cellulolyticum* H10 and its Complex with Ketohexose Sugars. *Protein Cell* 3 (2), 123–131. doi:10.1007/s13238-012-2026-5
- Chen, D., Chen, J., Liu, X., Guang, C., Zhang, W., and Mu, W. (2021). Biochemical Identification of a Hyperthermostable L-Ribulose 3-epimerase from *Labeledella Endophytica* and its Application for D-Allulose Bioconversion. *Int. J. Biol. Macromolecules* 189, 214–222. doi:10.1016/j.jbiomac.2021.08.131
- Chung, M.-Y., Oh, D.-K., and Lee, K. W. (2012). Hypoglycemic Health Benefits of D-Psicose. *J. Agric. Food Chem.* 60 (4), 863–869. doi:10.1021/jf204050w
- Cree, G. M., and Perlin, A. S. (1968). O-isopropylidene Derivatives of D-Allulose (D-Psicose) and D-Erythro-Hexopyranos-2,3-Diulose. *Can. J. Biochem.* 46 (8), 765–770. doi:10.1139/o68-117
- EFSA Panel on Food Contact Materials, Enzymes and Processing Aids (CEP) Lambré, C., Barat Baviera, J. M., Bolognesi, C., Cocconcelli, P. S., Crebelli, R., Gott, D. M., et al. (2021a). Safety Evaluation of the Food Enzyme D-psicose 3-epimerase from the Genetically Modified *Escherichia coli* Strain K-12 W3110 (pWKLp). *EFS* 19 (4), 6870. doi:10.2903/j.efsa.2021.6870
- EFSA Panel on Food Contact Materials, Enzymes and Processing Aids (CEP) Lambré, C., Barat Baviera, J. M., Bolognesi, C., Cocconcelli, P. S., Crebelli, R., Gott, D. M., et al. (2021b). Safety Evaluation of the Food Enzyme D-psicose 3-epimerase from the Genetically Modified *Corynebacterium Glutamicum* Strain FIS002. *EFS* 19 (10), 6870. doi:10.2903/j.efsa.2021.6870
- Emmadi, M., and Kulkarni, S. S. (2014). Recent Advances in Synthesis of Bacterial Rare Sugar Building Blocks and Their Applications. *Nat. Prod. Rep.* 31 (7), 870–879. doi:10.1039/c4np00003j
- Fang, Z., Li, T., Wang, Q., Zhang, X., Peng, H., Fang, W., et al. (2011). A Bacterial Laccase from marine Microbial Metagenome Exhibiting Chloride Tolerance and Dye Decolorization Ability. *Appl. Microbiol. Biotechnol.* 89 (4), 1103–1110. doi:10.1007/s00253-010-2934-3
- Gross, A. F., Sherman, E., and Vajo, J. J. (2012). Aqueous Room Temperature Synthesis of Cobalt and Zinc Sodalite Zeolitic Imidazolate Frameworks. *Dalton Trans.* 41 (18), 5458. doi:10.1039/c2dt30174a
- Guo, X., Xing, T., Lou, Y., and Chen, J. (2016). Controlling ZIF-67 Crystals Formation through Various Cobalt Sources in Aqueous Solution. *J. Solid State. Chem.* 235, 107–112. doi:10.1016/j.jssc.2015.12.021
- Han, Y., Guo, W., Su, B., Guo, Y., Wang, J., Chu, B., et al. (2018). High-level Expression of Soluble Recombinant Proteins in *Escherichia coli* Using an HE-Maltotriose-Binding Protein Fusion Tag. *Protein Expr. Purif.* 142, 25–31. doi:10.1016/j.pep.2017.09.013



- Hofström, C., Orlova, A., Altai, M., Wängsell, F., Gräslund, T., and Tolmachev, V. (2011). Use of a HEHEHE Purification Tag Instead of a Hexahistidine Tag Improves Biodistribution of Affibody Molecules Site-Specifically Labeled with  $^{99m}\text{Tc}$ ,  $^{111}\text{In}$ , and  $^{125}\text{I}$ . *J. Med. Chem.* 54 (11), 3817–3826.
- Homaei, A. A., Sariri, R., Vianello, F., and Stevanato, R. (2013). Enzyme Immobilization: an Update. *J. Chem. Biol.* 6 (4), 185–205. doi:10.1007/s12154-013-0102-9
- Jia, D.-X., Sun, C.-Y., Jin, Y.-T., Liu, Z.-Q., Zheng, Y.-G., Li, M., et al. (2021). Properties of D-Allulose 3-epimerase Mined from *Novibacillus Thermophilus* and its Application to Synthesis of D-Allulose. *Enzyme Microb. Technology* 148, 109816. doi:10.1016/j.enzymtec.2021.109816
- Johnson, R. J., Segal, M. S., Sautin, Y., Nakagawa, T., Feig, D. I., Kang, D.-H., et al. (2007). Potential Role of Sugar (Fructose) in the Epidemic of Hypertension, Obesity and the Metabolic Syndrome, Diabetes, Kidney Disease, and Cardiovascular Disease. *Am. J. Clin. Nutr.* 86 (4), 899–906. doi:10.1093/ajcn/86.4.899
- Kim, H.-J., Hyun, E.-K., Kim, Y.-S., Lee, Y.-J., and Oh, D.-K. (2006). Characterization of an Agrobacterium Tumefaciens D -Psicose 3-Epimerase that Converts D -Fructose to D -Psicose. *Appl. Environ. Microbiol.* 72 (2), 981–985. doi:10.1128/aem.72.2.981-985.2006
- Kim, K., Kim, H.-J., Oh, D.-K., Cha, S.-S., and Rhee, S. (2006). Crystal Structure of D-Psicose 3-epimerase from Agrobacterium Tumefaciens and its Complex with True Substrate D-Fructose: A Pivotal Role of Metal in Catalysis, an Active Site for the Non-phosphorylated Substrate, and its Conformational Changes. *J. Mol. Biol.* 361 (5), 920–931. doi:10.1016/j.jmb.2006.06.069
- Lian, X., Fang, Y., Joseph, E., Wang, Q., Li, J., Banerjee, S., et al. (2017). Enzyme-MOF (Metal-organic Framework) Composites. *Chem. Soc. Rev.* 46 (11), 3386–3401. doi:10.1039/c7cs00058h
- Liang, K., Ricco, R., Doherty, C. M., Styles, M. J., Bell, S., Kirby, N., et al. (2015). Biomimetic Mineralization of Metal-Organic Frameworks as Protective Coatings for Biomacromolecules. *Nat. Commun.* 6 (1), 7240. doi:10.1038/ncomms8240
- Lyu, F., Zhang, Y., Zare, R. N., Ge, J., and Liu, Z. (2014). One-Pot Synthesis of Protein-Embedded Metal-Organic Frameworks with Enhanced Biological Activities. *Nano Lett.* 14 (10), 5761–5765. doi:10.1021/nl5026419
- Miller, B. S., and Swain, T. (1960). Chromatographic Analyses of the Free Amino-Acids, Organic Acids and Sugars in Wheat Plant Extracts. *J. Sci. Food Agric.* 11 (6), 344–348.
- Mu, W., Chu, F., Xing, Q., Yu, S., Zhou, L., and Jiang, B. (2011). Cloning, Expression, and Characterization of a D-Psicose 3-Epimerase from *Clostridium Cellulolyticum* H10. *J. Agric. Food Chem.* 59 (14), 7785–7792. doi:10.1021/jf201356q
- Mu, W., Yu, L., Zhang, W., Zhang, T., and Jiang, B. (2015). Isomerases for Biotransformation of D-Hexoses. *Appl. Microbiol. Biotechnol.* 99 (16), 6571–6584. doi:10.1007/s00253-015-6788-6
- Oshima, H., Kimura, I., and Zumori, K. (2006). Psicose Contents in Various Food Products and its Origin. *Food Sci. Technol. Res.* 12 (2), 137–143.
- Patil, P. D., and Yadav, G. D. (2018). Rapid *In Situ* Encapsulation of Laccase into Metal-Organic Framework Support (ZIF-8) under Biocompatible Conditions. *ChemistrySelect* 3 (17), 4669–4675. doi:10.1002/slct.201702852
- Rafiei, S., Tangestaninejad, S., Horcajada, P., Moghadam, M., Mirkhani, V., Mohammadpoor-Baltork, I., et al. (2018). Efficient Biodiesel Production Using a lipase@ZIF-67 Nanobioreactor. *Chem. Eng. J.* 334, 1233–1241. doi:10.1016/j.cej.2017.10.094
- Trends in Adult Body-Mass (2016) index in 200 Countries from 1975 to 2014: a Pooled Analysis of 1698 Population-Based Measurement Studies with 19.2 Million Participants. *Lancet*, 387 (10026), 1377–1396. doi:10.1016/S0140-6736(16)30054-X
- Van Overtveldt, S., Verhaeghe, T., Joosten, H.-J., van den Bergh, T., Beerens, K., and Desmet, T. (2015). A Structural Classification of Carbohydrate Epimerases: From Mechanistic Insights to Practical Applications. *Biotechnol. Adv.* 33 (8), 1814–1828. doi:10.1016/j.biotechadv.2015.10.010
- Vorapreeda, T., Thammarongtham, C., Cheevadhanarak, S., and Laoteng, K. (2015). Genome Mining of Fungal Lipid-Degrading Enzymes for Industrial Applications. *Microbiology* 161 (8), 1613–1626. doi:10.1099/mic.0.000127
- Wang, Z., Ren, D., Yu, H., Jiang, S., Zhang, S., and Zhang, X. (2020). Study on Improving the Stability of Adsorption-Encapsulation Immobilized Laccase@ZIF-67. *Biotechnol. Rep.* 28, e00553. doi:10.1016/j.btre.2020.e00553
- Wyss, F., Coca, A., Lopez-Jaramillo, P., Ponte-Negretti, C., Wyss, F. S., Restrepo, G., et al. (2020). Position Statement of the Interamerican Society of Cardiology (IASC) on the Current Guidelines for the Prevention, Diagnosis and Treatment of Arterial Hypertension 2017–2020. *Int. J. Cardiol. Hypertens.* 6, 100041. doi:10.1016/j.ijch.2020.100041
- Xia, Y., Cheng, Q., Mu, W., Hu, X., Sun, Z., Qiu, Y., et al. (2021). Research Advances of D-Allulose: An Overview of Physiological Functions, Enzymatic Biotransformation Technologies, and Production Processes. *Foods* 10 (9), 2186. doi:10.3390/foods10092186
- Yoshida, H., Yoshihara, A., Gullapalli, P. K., Ohtani, K., Akimitsu, K., Izumori, K., et al. (2018). X-ray Structure of *Arthrobacter Globiformis* M30 Ketose 3-epimerase for the Production of D-Allulose from D-Fructose. *Acta Cryst. Sect F* 74 (10), 669–676. doi:10.1107/s2053230x18011706
- Yushkova, E. D., Nazarova, E. A., Matyuhina, A. V., Noskova, A. O., Shavronskaya, D. O., Vinogradov, V. V., et al. (2019). Application of Immobilized Enzymes in Food Industry. *J. Agric. Food Chem.* 67 (42), 11553–11567. doi:10.1021/acs.jafc.9b04385
- Zepeda, V., Dassa, B., Borovok, I., Lamed, R., Bayer, E. A., and Cate, J. H. (2013). Draft Genome Sequence of the Cellulolytic Bacterium *Clostridium Papyrosolvens* C7 (ATCC 700395). *Genome Announc* 1 (5), e00698–13. doi:10.1128/genomeA.00698-13
- Zhang, W., Fang, D., Zhang, T., Zhou, L., Jiang, B., and Mu, W. (2013). Characterization of a Metal-dependent D-Psicose 3-Epimerase from a Novel Strain, *Desmospora* Sp. 8437. *J. Agric. Food Chem.* 61 (47), 11468–11476. doi:10.1021/jf4035817
- Zhang, W., Li, H., Zhang, T., Jiang, B., Zhou, L., and Mu, W. (2015). Characterization of a D-Psicose 3-epimerase from *Dorea* Sp. CAG317 with an Acidic pH Optimum and a High Specific Activity. *J. Mol. Catal. B: Enzymatic* 120, 68–74. doi:10.1016/j.molcatb.2015.05.018
- Zou, Z.-Z., Yu, H.-L., Li, C.-X., Zhou, X.-W., Hayashi, C., Sun, J., et al. (2012). A New Thermostable  $\beta$ -glucosidase Mined from *Dictyoglomus Thermophilum*: Properties and Performance in Octyl Glucoside Synthesis at High Temperatures. *Bioresour. Technology* 118, 425–430. doi:10.1016/j.biortech.2012.04.040

**Conflict of Interest:** The authors declare that the research was conducted in the absence of any commercial or financial relationships that could be construed as a potential conflict of interest.

**Publisher's Note:** All claims expressed in this article are solely those of the authors and do not necessarily represent those of their affiliated organizations or those of the publisher, the editors, and the reviewers. Any product that may be evaluated in this article, or claim that may be made by its manufacturer, is not guaranteed or endorsed by the publisher.

Copyright © 2022 Yang, Fan, Zhao, Lin, Zheng and Han. This is an open-access article distributed under the terms of the Creative Commons Attribution License (CC BY). The use, distribution or reproduction in other forums is permitted, provided the original author(s) and the copyright owner(s) are credited and that the original publication in this journal is cited, in accordance with accepted academic practice. No use, distribution or reproduction is permitted which does not comply with these terms.



# Improving Thermostability and Catalytic Activity of Glycosyltransferase From *Panax ginseng* by Semi-Rational Design for Rebaudioside D Synthesis

Meiqi Chen<sup>1</sup>, Fangwei Song<sup>1</sup>, Yuxi Qin<sup>1</sup>, Shuangyan Han<sup>1</sup>, Yijian Rao<sup>2</sup>, Shuli Liang<sup>1\*</sup> and Ying Lin<sup>1\*</sup>

<sup>1</sup>Guangdong Key Laboratory of Fermentation and Enzyme Engineering, School of Biology and Biological Engineering, South China University of Technology, Guangzhou, China, <sup>2</sup>Key Laboratory of Carbohydrate Chemistry and Biotechnology, Ministry of Education, School of Biotechnology, Jiangnan University, Wuxi, China

## OPEN ACCESS

### Edited by:

Weidong Liu,  
Chinese Academy of Sciences (CAS),  
China

### Reviewed by:

Xu Han,  
Chinese Academy of Sciences (CAS),  
China

Shuhong Mao,

Tianjin University of Science and  
Technology, China

### \*Correspondence:

Shuli Liang  
shuli@scut.edu.cn  
Ying Lin  
feylin@scut.edu.cn

### Specialty section:

This article was submitted to  
Industrial Biotechnology,  
a section of the journal  
Frontiers in Bioengineering and  
Biotechnology

**Received:** 27 February 2022

**Accepted:** 25 March 2022

**Published:** 27 April 2022

### Citation:

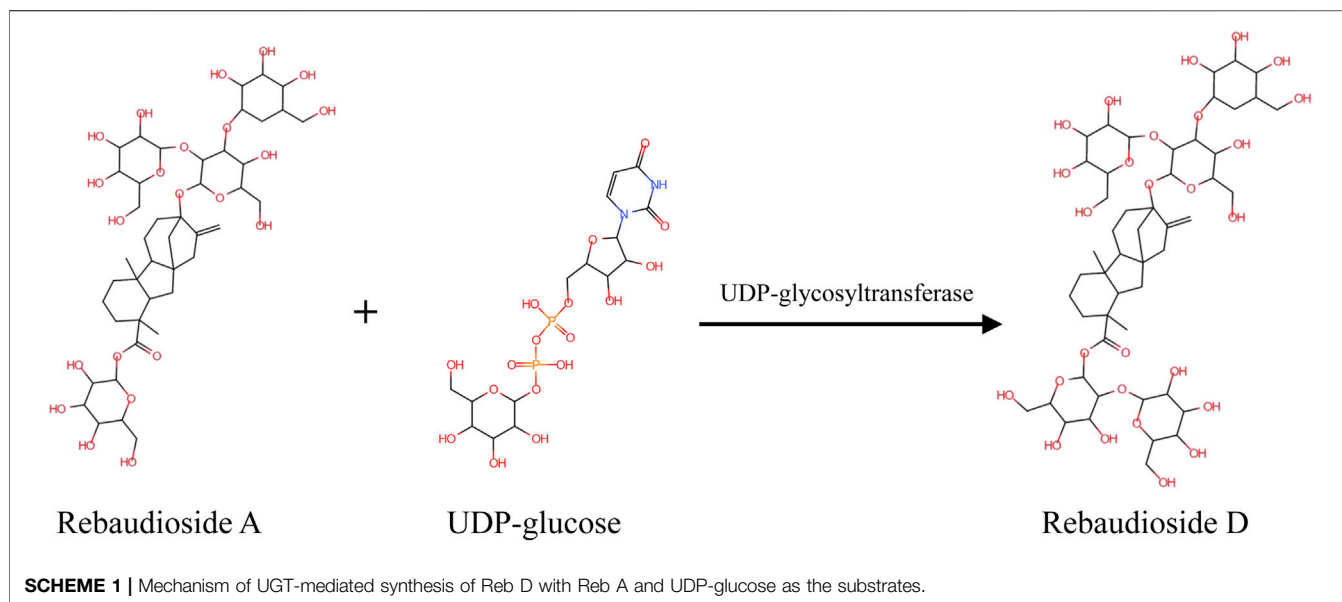
Chen M, Song F, Qin Y, Han S, Rao Y,  
Liang S and Lin Y (2022) Improving  
Thermostability and Catalytic Activity of  
Glycosyltransferase From *Panax*  
*ginseng* by Semi-Rational Design for  
Rebaudioside D Synthesis.  
Front. Bioeng. Biotechnol. 10:884898.  
doi: 10.3389/fbioe.2022.884898

As a natural sweetener and sucrose substitute, the biosynthesis and application of steviol glycosides containing the component rebaudioside D have attracted worldwide attention. Here, a glycosyltransferase PgUGT from *Panax ginseng* was first reported for the biosynthesis of rebaudioside D. With the three-dimensional structures built by homology modeling and deep-learning-based modeling, PgUGT was semi-rationally designed by FireProt. After detecting 16 site-directed variants, eight of them were combined in a mutant Mut8 with both improved enzyme activity and thermostability. The enzyme activity of Mut8 was 3.2-fold higher than that of the wild type, with an increased optimum reaction temperature from 35 to 40°C. The activity of this mutant remained over 93% when incubated at 35°C for 2 h, which was 2.42 times higher than that of the wild type. Meanwhile, when the enzymes were incubated at 40°C, where the wild type was completely inactivated after 1 h, the residual activity of Mut8 retained 59.0% after 2 h. This study would provide a novel glycosyltransferase with great potential for the industrial production of rebaudioside D and other steviol glycosides.

**Keywords:** glycosyltransferase, rebaudioside D, semi-rational design, thermostability, enzyme activity

## INTRODUCTION

Sweetness is an indispensable component of modern day life. Considering the health concerns caused by excessive intake of sucrose, the present trend of the prevailing market indicates that natural sucrose alternatives were appealing to consumers (Hagger et al., 2017; Archer, 2018; Mora and Dando, 2021). As one of the most widely used natural sweeteners, steviol glycosides (SGs) were low-calorie and zero glycemic indexes (Ceunen and Geuns, 2013; Castro-Munoz et al., 2022). SGs present positive effects on human health, including the improvement of metabolic health, assistance in weight control, and the benefits of lowering blood glucose, which attract the interest of many companies (Castro-Munoz et al., 2022). Excellent thermal (up to 80°C) and pH (2–10) stability allows them to be applied in the food and beverage industries (Kroyer, 2010). SGs contain a variety of sweet components, the highest levels of which are steviosides (St), followed by rebaudioside A (Reb A). The price of SG components is directly related to the nature and difficulty of extraction. Presently, with St



as the substrate, a high yield of valuable Reb A was efficiently synthesized *via* biocatalysts (Chen et al., 2021). Among the SGs, rebaudioside D (Reb D) is one of the most important components, which has a much better flavor and higher sweetness than most other SGs, including Reb A and St (Kovacevic et al., 2018). However, the low content (0.42–0.5% w/w) of Reb D in the dry leaves of *Stevia rebaudiana* (*S. rebaudiana*) leads to difficulties in extraction and isolation, resulting in a high price (Hanson, 2016).

In a previous study, Reb D could be synthesized with Reb A as the substrate (Mohamed et al., 2011; Olsson et al., 2016). Glucose from UDP-glucose was transferred by specific  $\beta$  (1–2) glycosylation to the glucose on the C19-carboxylate of Reb A by UDP-glycosyltransferases (UGTs) (Zhang et al., 2021). Three UGTs were found to act as catalysts in the production of Reb D from Reb A (Scheme 1). The UGT91D2 from *S. rebaudiana* was the original enzyme for Reb D synthesis (Olsson et al., 2016). EUGT11 from *Oryza sativa* was heterologously expressed in *Pichia pastoris* to provide a whole-cell biocatalyst technology (Wang et al., 2020). Meanwhile, a computational strategy was developed to promote the activity of EUGT11 (Lin et al., 2020). In addition, the UGTSL2 from *Solanum lycopersicum* was applied for Reb D synthesis by expressing both in yeast and *Escherichia coli*, along with RM2 as a side product (Prakash et al., 2014; Chen et al., 2018). To promote the product specificity of UGTSL2, a mutant of UGSL2 was constructed as well (Chen L. et al., 2020). The synthesis of Reb D with enzymatic techniques was more efficient and environmentally friendly for the industry.

Nowadays, a biocatalyst is applied for the synthesis of complex compounds in a variety of fields. However, natural enzymes, without evolving for industrial environments, were often challenging for application (Foo et al., 2012). For biocatalytic reactions, the properties of enzymes play an important role in the cost and process of the entire industrial production process (Kirk et al., 2002). To improve the low activity and instability of

enzymes, protein engineering was developed as a powerful tool to modify the structure (Xiong et al., 2021). The semi-rational design strategy combined the benefits of directed evolution and rational design (Chica et al., 2005; Sheldon and Pereira, 2017). Two distinct methodologies were involved in the semi-rational design: sequence-based enzyme redesign and structure-based enzyme redesign (Xiong et al., 2021). Proteins without a crystal structure or high-throughput determination methods could be redesigned for higher activity and better thermal stability by semi-rational design strategies (Nakano et al., 2018; Cheng et al., 2020).

In this study, a UDP-glycosyltransferase PgUGT from *Panax ginseng* (*P. ginseng*) catalyzing the bioconversion of Reb A to Reb D was first reported. The three-dimensional structure of PgUGT was modeled and redesigned by a semi-rational design strategy. Consequently, a mutant Mut8 containing eight altered residues was constructed with greater enzyme activity and enhanced thermostability after confirming the site-directed mutagenesis of selective noncatalytic residues.

## MATERIALS AND METHODS

### Chemicals and Reagents

All reagent grade chemicals were purchased from Sigma-Aldrich (Steinheim, Germany). Restriction enzymes, DNA polymerase, and T4 DNA ligase were purchased from Thermo Scientific (United States). Standard samples of Reb A (97%) and Reb D (97%) were purchased from Qingdao Runde Biotechnology Company.

### Strains, Plasmids, and Culture Conditions

*E. coli* Top10 was used as the host strain for plasmid storage. The strain used for protein expression was *E. coli* BL21 (DE3) with pET30a (Invitrogen, Waltham, MA, United States) as vectors.

The genes encoding EUGT11 (XP\_015629141.1), LsUGT1 (XP\_023735445.1), CsUGT1 (ALO19883.1), HaUGT1 (XP\_022009959.1), AsUGT1 (AZQ26909.1), AtUGT1 (XP\_020148974.1), PgUGT (A0A0A6ZFY4.1), ZmUGT1 (NP\_001150595.1), EUGT11 (XP\_015629141.1), UGTSL2 (XP\_004250485.1), and UGT94-28-3 (Itkin et al., 2016) were retrieved from the NCBI database and articles, synthesized by Generay (Shanghai Generay Biotech Co. Ltd, China). The gene sequences were constructed into the pET30a vector.

The bacteria were cultivated in Luria–Bertani (LB) medium (1% NaCl, 0.5% yeast extract, and 1% tryptone) containing 50 µg/ml kanamycin in a shaking incubator.

## Cell-Free Protein Synthesis System for Protein Production

The cell extract of *E. coli* BL21 (DE3) was prepared and quantified using the reported protocol (Karim and Jewett, 2016).

Cell-free protein synthesis (CFPS) was carried out in a 1.5-ml centrifuge tube containing 60 µl volumes at 37°C for 16 h. Each reaction consisted of ATP (1.8 mM), GTP (1.3 mM), UTP (1.3 mM), CTP (1.3 mM), nicotinamide adenine dinucleotide (NAD; 0.4 mM), phosphoenolpyruvate (PEP; 33 mM), coenzyme-A (0.27 mM), putrescine (1 mM), spermidine (1.5 mM), HEPES (57 mM), folinic acid (0.1 mM), *E. coli* tRNA mixture (0.26 mg/ml), oxalic acid (4 mM), potassium glutamate (130 mM), magnesium glutamate (10 mM), 20 amino acids (2 mM each), and cell extracts (10 µl). For each reaction, 16 ng/µl plasmid was added. The soluble proteins were collected after centrifugation at 10,000 rpm for 5 min.

## Characteristics of Cell-Free Synthesis of Glycosyltransferase

The abilities of the proteins produced *via* CFPS were analyzed using Reb A as the substrate. A 200-µl reaction system in a 2-ml centrifuge tube was incubated at 35°C and 250 rpm for 12 h. The reaction solution contained 50 mM PBS (pH 8.0), 2 mM Reb A, 2 mM UDP-glucose, and 50 µl of precipitated proteins collected from the CFPS reaction. After incubation, 200 µl of phosphoric acid (0.9 M) was added to suspend the reaction and 200 µl of sodium hydrate (2 M) was added after 5 min to neutralize the reaction system. The reactants were determined by high-performance liquid chromatography (HPLC) to confirm the types of SGs.

## Heterologous Expression and Purification of PgUGT in *E. coli*

The plasmid pET30a-PgUGT was transformed to *E. coli* BL21 (DE3). The positive clones of BL21 (DE3)/PgUGT were verified and precultured in the LB medium containing 50 µg/ml kanamycin at 37°C overnight. The precultured cells were then transferred into a 100-ml LB medium with 50 µg/ml kanamycin and 0.5 mM isopropyl-β-D-thiogalactopyranoside (IPTG) was added to induce protein expression after the OD<sub>600</sub> of the cells was in the range of 0.6–0.8. After 26 h of induction at 16°C, the cells were harvested by centrifugation at 7,000 rpm for 3 min at 4°C. The

cells were washed twice with PBS buffer (pH 7.5) and disrupted by ultrasonication. The supernatant was collected by centrifugation at 10,000 rpm for 30 min at 4°C to obtain the crude enzyme.

Mutations of PgUGT were generated by site-directed mutagenesis by PCR based on the plasmid pET30a-PgUGT, and the primers are listed in **Supplementary Table S1**. After confirming by DNA-sequencing, the mutated plasmids were transformed into *E. coli* BL21 (DE3) for fermentation and induction as mentioned previously.

Purification of the enzymes was performed by 5-ml nickel affinity chromatography using Ni-NTA agarose (Novagen, United States). The mobile phase A was 20 mM sodium phosphate buffer (pH 7.5) adding 500 mM NaCl, and the mobile phase B was 20 mM sodium phosphate buffer (pH 7.5) adding 500 mM NaCl and 250 mM imidazole. The non-target proteins were washed off with 80% phase A and 20% phase B. The target protein was eluted with 20% phase A and 80% phase B. The elution proteins were rebuffed to phase A with a 5-ml HiTrap Desalting column (Cytiva, United States). The purified protein was confirmed by sodium dodecyl sulfate-polyacrylamide gel electrophoresis (SDS-PAGE).

## Enzyme Activity Assay and Kinetic Parameters of PgUGT and Variants

The enzyme activities were carried out in a mixture (200 µl) of 5 mM Reb A and 2 mM UDP-glucose in 50 mM sodium phosphate buffer (pH 7.5) containing 0.02 mg/ml of the purified enzyme and incubated at 35°C for 10 min. After incubation, 200 µl phosphoric acid (0.9 M) was added to suspend the reaction and 200 µl of sodium hydrate (2 M) was added after 5 min to neutralize the reaction system. The reactants were determined by HPLC to confirm the concentrations of SGs. One unit (U) of glycosyltransferase activity was defined as the amount of enzyme that produced 1 µmol of Reb D from Reb A per minute under the described conditions.

The reactant containing 2 mM UDP-glucose, 0.1–1.8 mM Reb A, and 0.02 mg/ml purified enzyme in 50 mM sodium phosphate buffer (pH 7.5) was incubated at 35°C for 10 min. The suspending method of the reaction was the same as mentioned previously. The production of Reb D was determined by HPLC. The kinetic parameters ( $k_{cat}$ ,  $K_m$ , and  $k_{cat}/K_m$ ) were obtained by fitting data to the Michaelis–Menten equation by OriginPro 2018. Three replicate experiments were performed for each reaction.

## Temperature and pH Dependence of PgUGT and Mutants

The enzyme activity was measured at 25–50°C to reveal the optimal temperature of the enzymes with the pH of the reactant being 7.5. After incubation at different temperatures for 30 min, the residual enzyme activity was determined, indicating the thermostability of enzymes.

The optimal pH of PgUGT was determined at 35°C by measuring the activity in the range of 6.5–9.0. The pH stability was determined by measuring the residual enzyme activity at 35°C after incubation in the following buffers with different pH at 4°C for 24 h: 50 mM sodium phosphate buffer (6.5–8.0) and 50 mM Tris-HCl buffer (pH 8.0–9.5). Three replicate experiments were performed for each reaction.



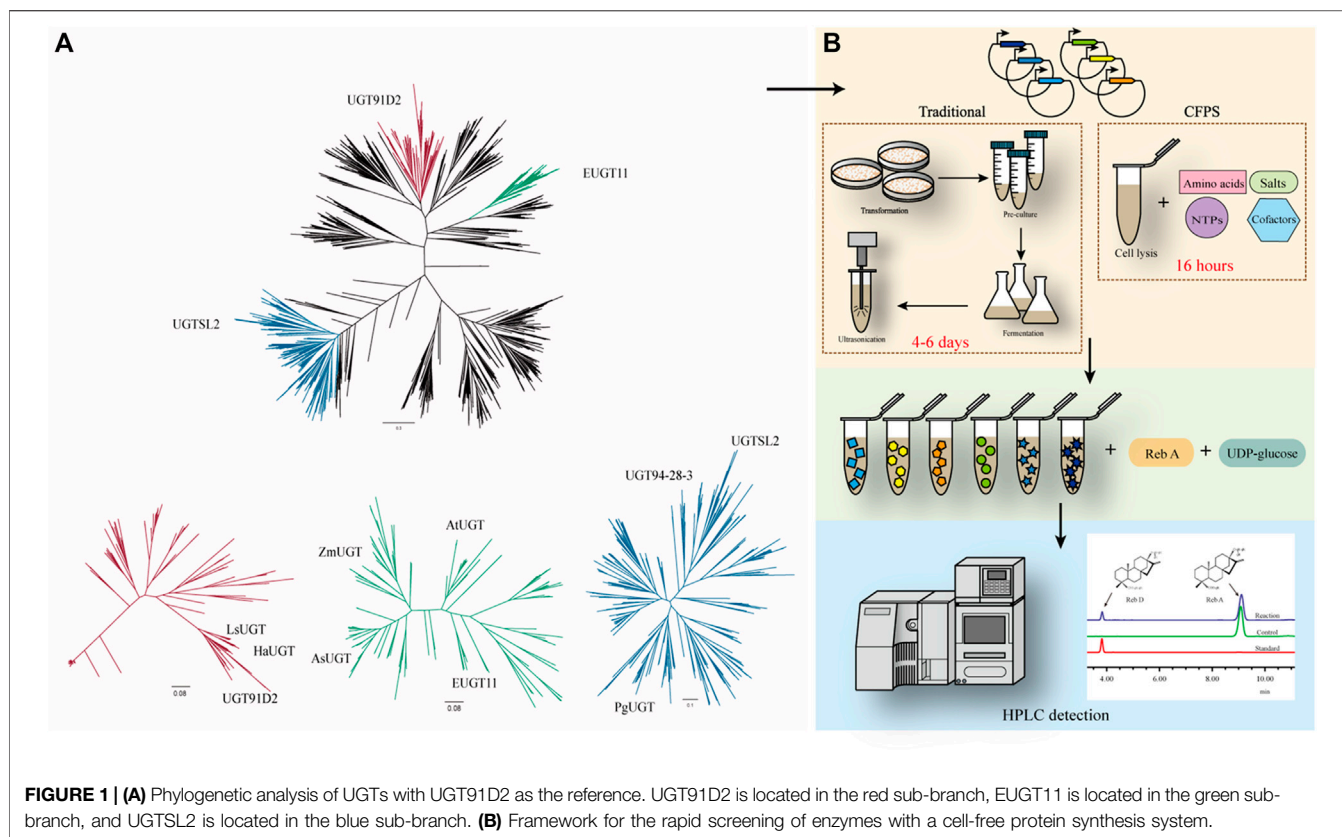


**TABLE 1 |** Information of the glycosyltransferases selected by phylogenetic analysis.

Enzyme	Identity with UGT91D2 (%)	Genebank number	Number of amino acids	Molecular weight (kDa)	Isoelectric point	Source of organism	Phylogenetic sites
AsUGT	36.07	AZQ26909.1	486	52.92	5.81	<i>Avena strigosa</i>	EUGT11-subbranch
AtUGT	39.44	XP_020148974.1	454	49.22	6.34	<i>Aegilops tauschii</i> subsp. <i>strangulata</i>	EUGT11-subbranch
ZmUGT	39.09	NP_001150595.1	470	51.29	7.26	<i>Zea mays</i>	EUGT11-subbranch
LsUGT	65.04	XP_023735445.1	474	53.31	5.29	<i>Lactuca sativa</i>	UGT91D2-subbranch
HaUGT	66.67	XP_022009959.1	493	55.36	5.34	<i>Helianthus annuus</i>	UGT91D2-subbranch
CsUGT	38.46	ALO19883.1	469	52.23	6.41	<i>Camellia sinensis</i>	Other sub-branch
PgUGT	34.40	A0A0A6ZF4.1	442	49.13	5.62	<i>Panax ginseng</i>	UGTSL2-subbranch
UGT94-28-3	34.00	Itkin et al. (2016)	473	52.83	5.78	<i>Siraitia grosvenorii</i>	UGTSL2-subbranch

## Structure Modeling and Semi-Rational Design

The three-dimensional structure of PgUGT was built in two ways. The homology model was obtained by Discovery Studio 2020 based on the crystal structure of PDB code 2vce, 5u6m, 5u6n, 5v2k, 6inf, 6ing, 6kvi, and 6o86. The other one was built by the online RoseTTAFold service (<https://rosetta.bakerlab.org/>) (Baek et al., 2021). The models retrieved

from different methods were evaluated with the scoring program SAVES v6.0 (<https://saves.mbi.ucla.edu>). The model with the highest scores was used as the input file for the FireProt online program (<https://loschmidt.chemi.muni.cz/fireprot/>) (Musil et al., 2017). Based on the predicted change in Gibbs free energy, FireProt provided two mutation lists after energy- and evolution-based calculation. Candidate mutants were selected from the given lists.



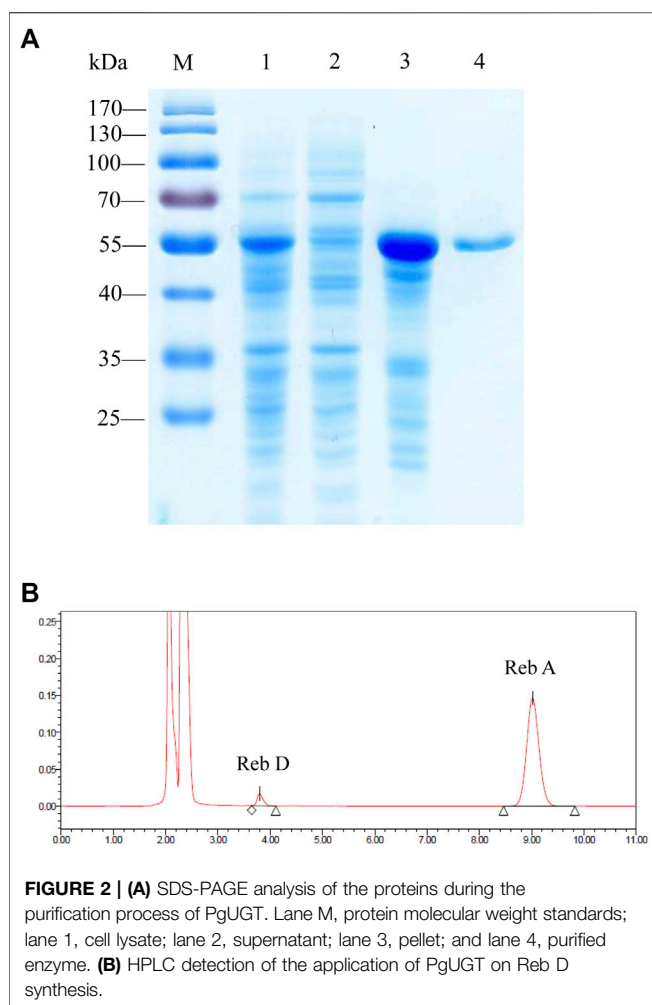


**FIGURE 2 | (A)** SDS-PAGE analysis of the proteins during the purification process of PgUGT. Lane M, protein molecular weight standards; lane 1, cell lysate; lane 2, supernatant; lane 3, pellet; and lane 4, purified enzyme. **(B)** HPLC detection of the application of PgUGT on Reb D synthesis.

## HPLC Analysis

The reactants were centrifuged and the supernatant was filtered through a cellulose nitrate membrane (0.22  $\mu$ m) for detection. The samples were analyzed by using a Waters 2,690–2489 HPLC system.

Steviol glycosides were detected by UV detection at 210 nm. An HPLC analysis was performed using a Sepax Sapphire-C18 5 column (250 mm  $\times$  4.6 mm) at 40°C. The flow rate was set to 1 ml/min with 68% mobile phase A (1.38 g/L sodium phosphate buffer, pH 2.6) and 32% mobile phase B (acetonitrile). The injection volume was 10  $\mu$ l. Standard curves for Reb A (99%) and Reb D (97%) were generated as the external standard method for quantification.

## RESULTS AND DISCUSSION

### Phylogeny Analysis and Rapid Screening of Glycosyltransferase for Rebaudioside D Synthesis

To discover a novel enzyme for Reb D synthesis, phylogenetic analysis of protein sequences was performed for mining functional enzymes, in which the protein sequence of

UGT91D2 from *S. Rebaudiana* was used as a template. There were 4,510 sequences with homology between 30 and 90% and the query covered greater than 40 sequences screened from the NCBI BLAST (<http://blast.ncbi.nlm.nih.gov/Blast.cgi>). Enzymes from *Siraitia grosvenorii* with similar glycosylation mechanisms were not recorded in the NCBI database, which was manually added for phylogenetic analysis (Itkin et al., 2016). In total, there were 4,520 sequences available for phylogenetic analysis. The glycosyltransferase sequences were aligned with MAFFT v7.475 (Katoh and Standley, 2014). The phylogenetic trees were constructed with approximately maximum-likelihood methods by FastTree (Price et al., 2009).

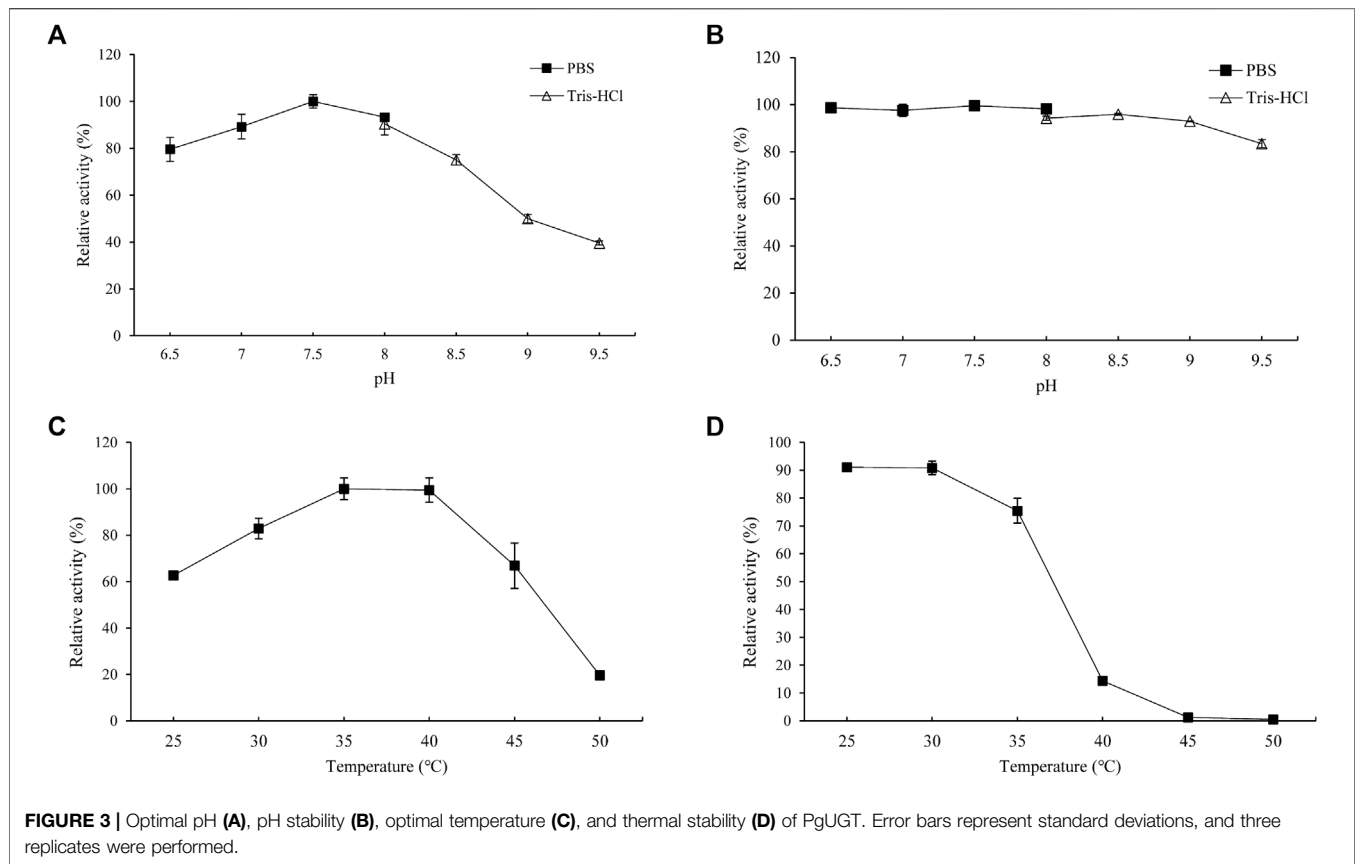
In previous studies, there were three enzymes, namely, UGT91D2, EUGT11, and UGTSL2 capable of catalyzing Reb A to Reb D. The similarity between EUGT11 and UGT91D2 was 41.99%, while UGTSL2 shared 32.73% of its identity with UGT91D2. Despite the fact that these enzymes had the same catalytic capacity, they were separated into three phylogenetic branches (Figure 1A). UGTs in these three main sub-branches potentially have the glycosylation capacity of Reb A. Eight UGTs were chosen for further examination to find new enzymes for Reb D production. Among these sequences, LsUGT and HaUGT were chosen from the sub-branch of UGT91D2, whereas AsUGT, AtUGT, and ZmUGT were selected from the sub-branch of EUGT11. In the sub-branch of UGTSL2, PgUGT and UGT94-28-3 were picked. In addition, CsUGT was chosen from the other sub-branches. The information of these eight GTs is summarized in Table 1.

To verify the catalytic properties of the enzymes chosen from the phylogeny tree, the DNA sequences of the enzymes were synthesized and inserted in the vectors for expression. The traditional approaches to determine the catalytic ability of the proteins take at least 4 days from the acquisition of the target DNA sequence to the determination of its properties if *E. coli* is used as the host generally. The cell-free protein synthesis system (CFPS) of *E. coli* has successfully synthesized a variety of proteins (Dudley et al., 2020; Karim et al., 2020). It takes only 16 h to obtain free proteins in an optimized CFPS after adding the vectors, significantly reducing the validation time (Figure 1B).

As a positive control for the feasibility of the CFPS, the gene of EUGT11 was inserted into the vector and added into the system and the other eight selected sequences. After 16 h of protein synthesis, the supernatant from the CFPS was added to the reaction system with Reb A and UDP-glucose as substrates. According to the HPLC results of SGs, the glycosylated product of Reb A catalyzed by EUGT11 had the same HPLC retention time as Reb D (Lin et al., 2020; Wang et al., 2020). In addition, PgUGT exhibited glycosylation ability on Reb A as EUGT11 among eight UGTs, which indicated that PgUGT would be a novel enzyme suitable for Reb D synthesis.

### Heterologous Expression and Purification of Glycosyltransferase From *P. ginseng*

After the rapid screening of eight enzymes with the CFPS, the plasmid containing PgUGT was expressed in *E. coli* BL21 (DE3) for further characterization. After induction with 0.5 mM IPTG at 16°C for 24 h, the fermented cells were collected and disrupted



by ultrasonication. The ginseng-derived UGT forms inclusion bodies when expressed in *E. coli*, and active enzymes were obtained by purifying soluble proteins (Figure 2A). The PgUGT protein carries a His-tag, and an enterokinase cleavage site at the N-terminus was purified *via* nickel column affinity chromatography. The purified enzyme showed a single band on the SDS-PAGE gel with a theoretical molecular mass of 54.9 kDa.

The catalytic ability of purified protein was verified by reactions using Reb A as the substrate. The HPLC results confirmed that PgUGT expressed in *E. coli* could synthesize Reb D from Reb A (Figure 2B).

### Biochemical Characterization of PgUGT

The effects of pH on the enzyme activity and stability of PgUGT were determined (Figures 3A,B). The optimum pH of PgUGT was 7.5. In a previous study, the optimal pH of EUGT11 expressed in *E. coli* was 8.5 (Wang et al., 2020). At pH 6.5–8.0, it exhibited more than 80% of total activity. The stability of PgUGT was high in this range of pH as well. However, the activity reduced greatly at a pH value of more than 8.5. The residual activity remained more than 92% when incubated in two buffers at pH 6.5–9.0 for 24 h. Therefore, the optimal reaction pH and pH stability revealed that PgUGT was a neutral enzyme.

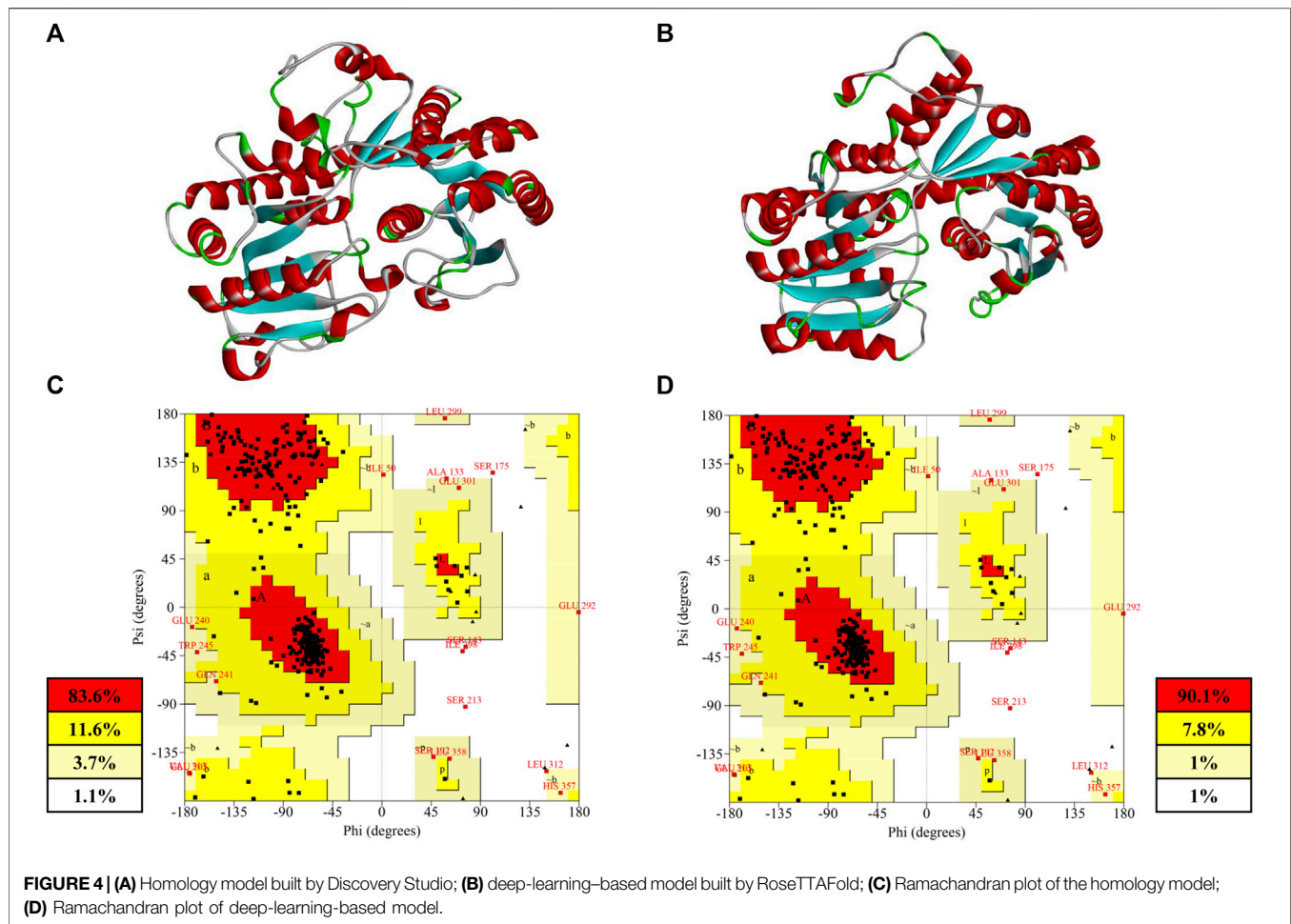
The effect of temperature on PgUGT activity was explored at various temperatures ranging from 30–50°C. PgUGT exhibited maximum enzyme activity at 35°C, but the relative activity was

similar at 40°C (Figure 3C). The activity showed a significant decrease over 40°C. The optimal temperature of EUGT11 expressed in *E. coli* was 35°C (Wang et al., 2020). A previous research study has shown that the optimum reaction temperature of plant-derived UGTs expressed in *E. coli* is usually between 30 and 35°C (Gachon et al., 2005; Louveau and Osbourn, 2019). As shown in Figure 2D, the thermostability of PgUGT remained 90% at 25–30°C after 30 min of incubation. When the temperature increased, the thermostability decreased. Only 14% of enzyme activity remained after 30 min of incubation at 40°C.

For industrial application, thermostability and enzyme activity play important roles in the feasibility of enzymes (Xu et al., 2020). A higher application temperature in biocatalyst production ensures reduction in microbial contamination, better solubility, and often a more favorable equilibrium position (Bommarius and Paye, 2013). In a previous study, the optimal temperature for Reb A synthesis by the whole-cell biocatalyst was 50°C, which was favorable for industrial application (Chen et al., 2021). Considering the possibility of combining PgUGT and UGT76G1 to utilize St as a substrate for Reb D synthesis, the thermostability of PgUGT should be improved.

### Structural Modeling of PgUGT

The crystal structure of mesophilic and thermophilic proteins revealed the relationship between protein configuration and thermostability (Haney et al., 1999). However, there was no



crystal structure for PgUGT. Therefore, two structures of PgUGT were predicted to improve the thermostability and activity of PgUGT by a semi-rational design (**Figures 4A,B**). One was modeled *via* homology modeling by Discovery Studio 2020 based on the structure of 2vce, 5u6m, 5u6n, 5v2k, 6inf, 6ing, 6kvi, and 6o86. The alignment among the sequences is shown in **Supplementary Figure S1**. Homology modeling based on crystal structures with high sequence similarity is the most common approach. The lower the sequence similarity, the less accurate the model will be, which is the bottleneck of homology modeling (Muhammed and Aki-Yalcin, 2019). Recently, machine learning-based modeling was favored by researchers, which complements the deficiency of homology modeling with high accuracy (Baek et al., 2021). Another 3D-structure of PgUGT was modeled through the deep learning modeling method RoseTTAFold (<https://robetta.bakerlab.org/>).

Both of the modeled structures of PgUGT consisted of two Rossmann-like domains at the N-terminal and C-terminal, which was a typical characteristic of GT-B fold glycosyltransferase (Lee et al., 2019; Zhang et al., 2021). The accuracy of the structure prediction of two structures was further confirmed by the Ramachandran analysis with SAVES

v6.0 (<https://saves.mbi.ucla.edu>) (**Figures 4C,D**). Generally, a good quality model would be expected to have more than 90% residues in the most favored regions, and a reliable model should have more than 80% (Laskowski et al., 1993). As shown in **Figures 4C,D**, 90.1% of the residues in the model predicted by RoseTTAFold were found in the most favored regions, while there were 83.6% residues in the homology model in the same regions. Both of the models were reliable for subsequent analysis and a better quality was shown in the model predicted by deep learning.

## Semi-Rational Design of Potential Thermostable Mutants

In previous studies, the semi-rational design by using computational tools in protein engineering was a common strategy. Improving thermostability may decrease the enzyme activity because it could change the flexibility of the structure (Xu et al., 2020). But, there are cases in which the thermostability was improved and the enzyme activity was increased by using FireProt (Cheng et al., 2020; Xia et al., 2021). Protein analysis tools such as Rate4Site, FoldX, and Rosetta design were assembled to offer a reliable design of stable multiple-point mutants in FireProt (Musil et al., 2017).

**TABLE 2** | Information of the mutations selected for characterization.

Mutation	Conserved	Homology model $\Delta\Delta G$ (kcal·mol <sup>-1</sup> )		RoseTTAFold model $\Delta\Delta G$ (kcal·mol <sup>-1</sup> )	
		FoldX	Rosetta	FoldX	Rosetta
A11L	Y <sup>[a]</sup>	-3.20	— <sup>[c]</sup>	-1.90	—
V38I	Y	-1.0	—	-0.23	—
F39Y	Y	-0.47	—	-0.66	—
D54L	N <sup>[b]</sup>	-0.04	—	-3.26	-3.61
S55P	N	-1.13	-2.43	-0.1	—
S58G	N	-2.12	—	-3.2	-2.77
N109K	N	-0.62	—	-2.98	-2.79
S120P	N	-0.3	—	-0.46	—
G147W	N	-1.17	-2.35	-1.9	-7.13
A250E	N	-0.58	—	-0.7	—
I279L	N	-0.9	—	-0.35	—
L290F	Y	-0.33	—	-0.95	—
V304L	N	-0.8	—	-1.11	-9.27
Q305E	N	-0.45	—	-0.64	—
T329I	Y	-1.78	—	-0.98	—
R356M	Y	-2.92	—	-0.55	—

<sup>a</sup>Residue on the given position is conserved through protein evolution.

<sup>b</sup>Residue on the given position is not conserved through protein evolution.

<sup>c</sup>Data are not provided by FireProt.

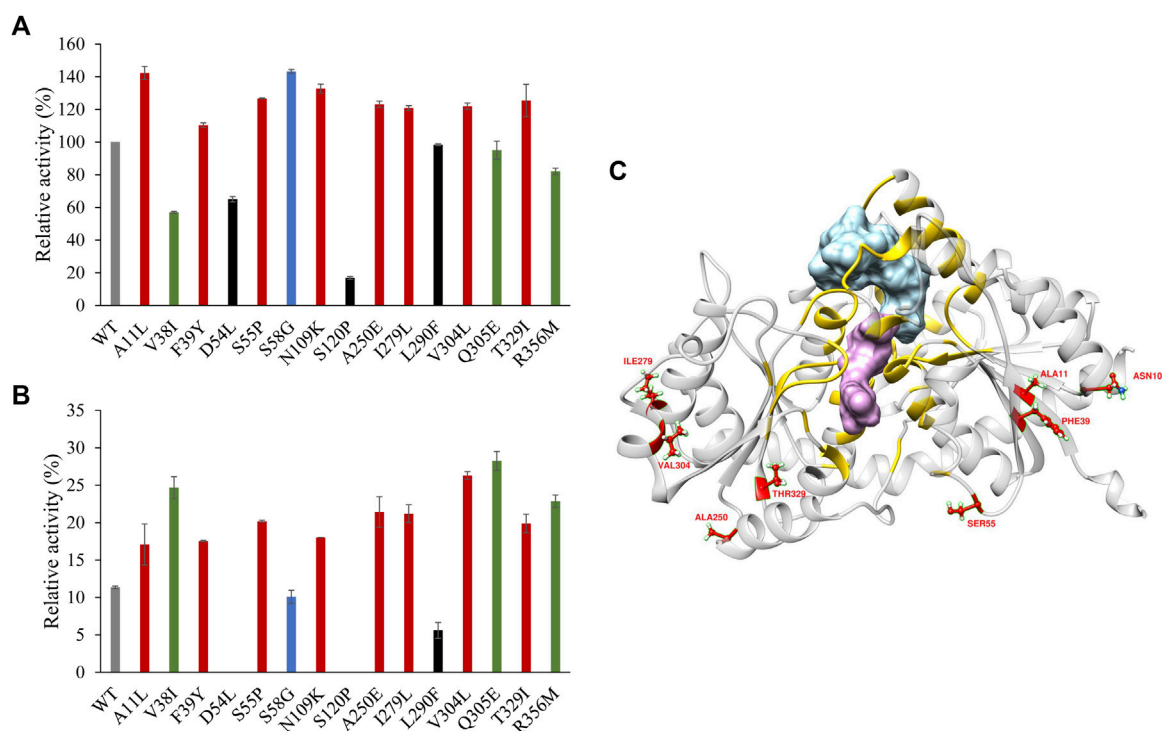


**FIGURE 5** | (A) Enzyme activity of PgUGT variants. (B) Thermostability of PgUGT variants. Red, variants with both higher enzyme activity and better thermostability; green, variants with only better thermostability; blue, variants with only higher enzyme activity; black, variants with both reduced enzyme activity and worse thermostability. (C) PgUGT model docked with Reb A and UDP-glucose. Blue, Reb A; purple, UDP-glucose; yellow, residues around Reb A and UDP-glucoside within 6 Å. Error bars represent standard deviations, and three replicates were performed.

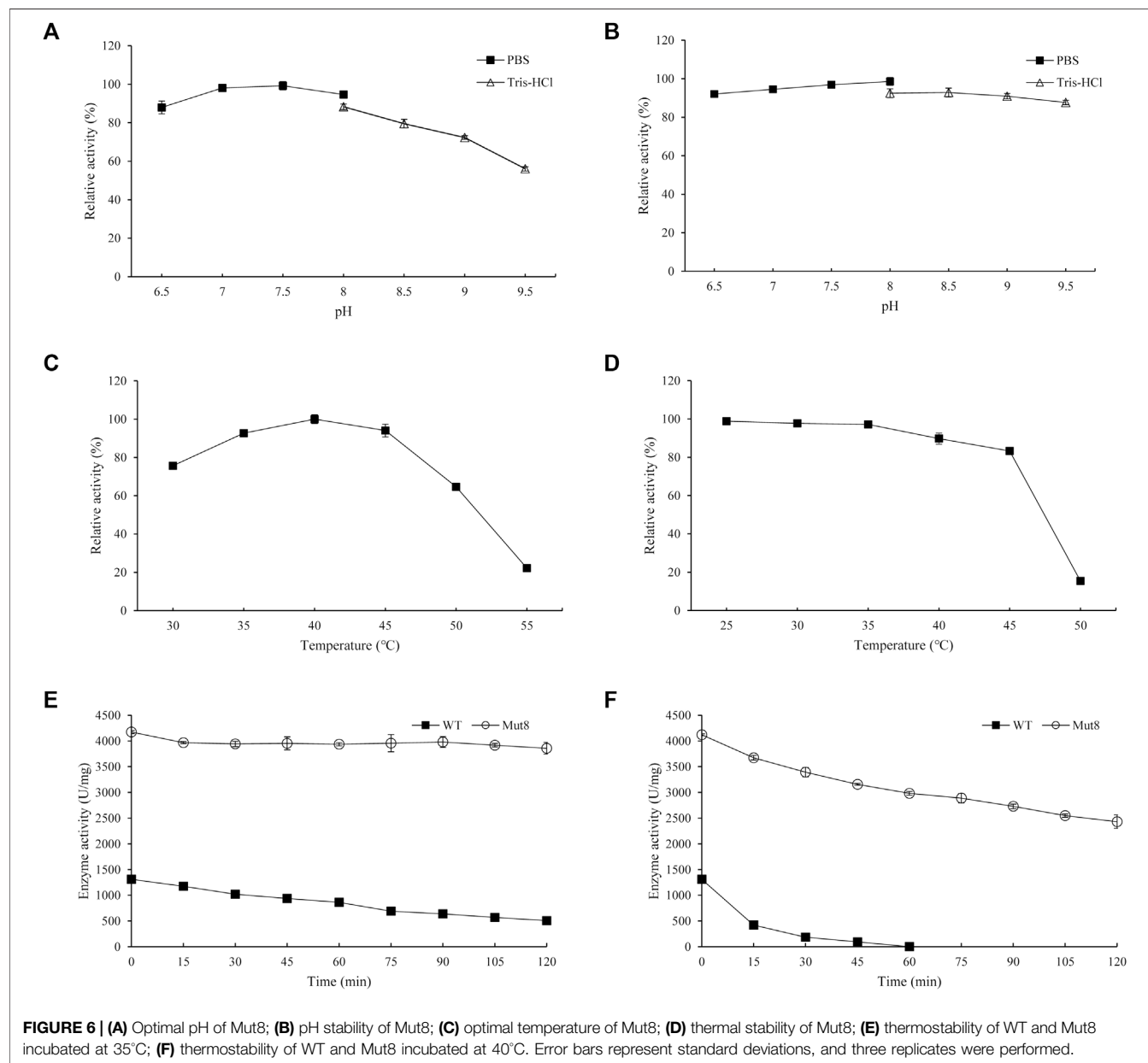
In this study, both of the predicted structures of PgUGT were analyzed by the FireProt server for calculation. As a result, 62 mutations were predicted based on the homology model and 45

mutations were shown based on the RoseTTAFold model. After cross matching the mutants, 16 site-directed mutants were selected. These mutants were shown in the results of both the



**TABLE 3 |** Specific activity and kinetic parameters of WT PgUGT and Mut8.

Enzyme	Specific activity (U mg <sup>-1</sup> )	$k_{cat}$ (min <sup>-1</sup> )	$K_m$ (mM)	$k_{cat}/K_m$ (min <sup>-1</sup> mM <sup>-1</sup> )
WT	1290.5 ± 52.0	22.1 ± 1.9	0.12 ± 0.0047	184.2
Mut8	4,122.5 ± 73.2	82.8 ± 4.7	0.21 ± 0.0046	394.3

**FIGURE 6 |** (A) Optimal pH of Mut8; (B) pH stability of Mut8; (C) optimal temperature of Mut8; (D) thermal stability of Mut8; (E) thermostability of WT and Mut8 incubated at 35°C; (F) thermostability of WT and Mut8 incubated at 40°C. Error bars represent standard deviations, and three replicates were performed.

models after excluding those with elevated energy (Table 2). Considering that all of the mutants were predicted based on modeled structures, to filter the mutants which would cause the inactivation of PgUGT, the single mutants were characterized.

Sixteen variants were constructed and expressed in *E. coli* BL21 (DE3). To determine the thermostability of the variants, all

the purified proteins were incubated at 40°C for 30 min. The activity of the enzymes without heat treatment and the residual activity after incubation were determined under optimal reaction conditions. Among the 16 site-directed mutants, G147W was devoid of enzyme activity. Nine of them showed more than 10% higher enzyme activity than the WT. At the same time, 11

mutants had better thermostability than the WT. Consequently, the variants A11L, F39Y, S55P, N109K, A250E, I279L, V304L, and T329I had both of the aforementioned enhancements, which could be combined for further improvement (**Figures 5A,B**).

With the RoseTTAFold Model predicted with the WT sequence, the structures of Reb A and UDP-glucose were docked into PgUGT by Ledock (Zhang and Zhao, 2016). The docking conformations were evaluated based on the positions of ligands and the scores provided by Ledock. As shown in **Figure 5C**, the residues located within the distance of 6 Å around Reb A and UDP-glucose were yellow, which might be the key residues of the active pocket. However, all of the eight mutations were out of that area, suggesting that these residues may influence the substrate channel gating functions (Chen J. et al., 2020).

## Characterization of Combination Mutation Mut8

Based on the characterization of site-directed mutants, a combination mutation containing the eight mutations (A11L/F39Y/S55P/N109K/A250E/I279L/V304L/T329I, Mut8) was constructed and analyzed. After fermentation and purification, the enzyme activity of Mut8 was determined after adjusting it to the same concentration of the WT at 35°C. The specific activity of WT PgUGT was 1,290.5 U·mg<sup>-1</sup>, whereas the activity of the Mut8 reached 4122.5 U·mg<sup>-1</sup>, showing approximately a 3.2-fold increase (**Table 3**). The kinetics of the WT and Mut8 was evaluated by the Michaelis–Menten equation (**Supplementary Figure S2**). Both of them were incubated with different concentrations of the substrates. When compared to EUGT11 and UGTSL2, the WT of PgUGT and Mut8 had a similar affinity for Reb D to EUGT11 and was higher than UGTSL2 (Chen L. et al., 2020; Lin et al., 2020). Although Mut8 showed lower affinity for Reb A than the WT, the  $k_{\text{cat}}$  value of Mut8 indicated a higher catalytic rate. Consequently, the kinetic parameters of WT and Mut8 showed that the catalytic efficiency of Mut8 ( $k_{\text{cat}}/K_m = 394.3 \text{ min}^{-1}\text{mM}^{-1}$ ) was 2.14-fold higher than that of the WT ( $k_{\text{cat}}/K_m = 184.2 \text{ min}^{-1}\text{mM}^{-1}$ ).

Furthermore, the biochemical characteristic of Mut8 was determined. The optimal pH of Mut8 was consistent with that of the WT for Reb D synthesis (**Figures 6A,B**). Similarly, the Mut8 maintained over 92% activity after 24 h of incubation in buffers, of which the pH ranged from 6.5 to 9.0. A significant improvement was found in the curves of optimum temperature and thermostability (**Figures 6C,D**). The optimal temperature of enzyme activity increased from 35 to 40°C. The residual activity of Mut8 remained 83.3 and 15.4% after incubation at 45 and 50°C for 30 min, respectively, while WT was almost completely inactivated. Compared with the activity without heat treatment, the enzyme activity of the WT was reduced to 38.5% after incubation at 35°C for 2 h, while the residual enzyme activity of Mut8 remained over 93% (**Figure 6E**). Meanwhile, 59.0% of Mut8 activity was retained after incubation at 40°C for 2 h even though the WT was inactive within 1 h (**Figure 6F**). These results indicated that Mut8 was a mutant with significant improvement in both

enzyme activity and thermostability compared to those in WT, which made it more suitable for industrial application.

## CONCLUSION

In this study, PgUGT from *P. ginseng* was characterized for Reb D synthesis. The optimal pH and temperature of the purified PgUGT were pH 7.5 and 35°C, respectively. Although the relative enzyme activity of PgUGT was stable in the pH range of 6.5–9.0, its thermostability decreased significantly over 35°C. Based on the two kinds of structure modeling and FireProt, 16 site-directed variants were constructed and validated. Eight of them showed improvement in both enzyme activity and thermostability. Furthermore, a combined mutant Mut8 containing eight mutations was characterized, which had a 3.2-fold increase in the enzyme activity and significant enhancement on thermostability.

To the best of our knowledge, this is the first report wherein UGT from *P. ginseng* was found to act as catalysts in the production of Reb D from Reb A. In addition, the mutant Mut8 could be a great potential enzyme for the industrial production of Reb D and other steviol glycosides.

## DATA AVAILABILITY STATEMENT

The original contributions presented in the study are included in the article/**Supplementary Material**, further inquiries can be directed to the corresponding authors.

## AUTHOR CONTRIBUTIONS

MC: Conceptualization, methodology, investigation, and writing—original draft. FS: Investigation and formal analysis. YQ: Data curation. SH: Resources. YR: Resources. SL: Supervision. YL: Supervision, funding acquisition, and project administration.

## FUNDING

This work was financially supported by the National Key R&D Program of China (2018YFA0901700), the National Natural Science Foundation of China (31871739), and Key-Area Research and Development Program of Guangdong Province (2020B020226007).

## SUPPLEMENTARY MATERIAL

The Supplementary Material for this article can be found online at: <https://www.frontiersin.org/articles/10.3389/fbioe.2022.884898/full#supplementary-material>

## REFERENCES

- Archer, E. (2018). In Defense of Sugar: A Critique of Diet-Centrism. *Prog. Cardiovasc. Dis.* 61 (1), 10–19. doi:10.1016/j.pcad.2018.04.007
- Baek, M., DiMaio, F., Anishchenko, I., Dauparas, J., Ovchinnikov, S., Lee, G. R., et al. (2021). Accurate Prediction of Protein Structures and Interactions Using a Three-Track Neural Network. *Science* 373 (6557), 871–876. doi:10.1126/science.abj8754
- Bommarius, A. S., and Paye, M. F. (2013). Stabilizing Biocatalysts. *Chem. Soc. Rev.* 42 (15), 6534–6565. doi:10.1039/c3cs60137d
- Bursać Kovačević, D., Maras, M., Barba, F. J., Granato, D., Roohinejad, S., Mallikarjunan, K., et al. (2018). Innovative Technologies for the Recovery of Phytochemicals from Stevia rebaudiana Bertoni Leaves: A Review. *Food Chem.* 268, 513–521. doi:10.1016/j.foodchem.2018.06.091
- Castro-Muñoz, R., Correa-Delgado, M., Córdova-Almeida, R., Lara-Nava, D., Chávez-Muñoz, M., Velásquez-Chávez, V. F., et al. (2022). Natural Sweeteners: Sources, Extraction and Current Uses in Foods and Food Industries. *Food Chem.* 370, 130991. doi:10.1016/j.foodchem.2021.130991
- Ceunen, S., and Geuns, J. M. C. (2013). Steviol Glycosides: Chemical Diversity, Metabolism, and Function. *J. Nat. Prod.* 76 (6), 1201–1228. doi:10.1021/np400203b
- Chen, J., Fan, F., Qu, G., Tang, J., Xi, Y., Bi, C., et al. (2020a). Identification of Absidia Orchidis Steroid 11 $\beta$ -Hydroxylation System and its Application in Engineering *Saccharomyces cerevisiae* for One-step Biotransformation to Produce Hydrocortisone. *Metab. Eng.* 57, 31–42. doi:10.1016/j.ymben.2019.10.006
- Chen, L., Cai, R., Weng, J., Li, Y., Jia, H., Chen, K., et al. (2020b). Production of Rebaudioside D from Stevioside Using a UGTSL2 Asn358Phe Mutant in a Multi-enzyme System. *Microb. Biotechnol.* 13 (4), 974–983. doi:10.1111/1751-7915.13539
- Chen, L., Sun, P., Zhou, F., Li, Y., Chen, K., Jia, H., et al. (2018). Synthesis of Rebaudioside D, Using Glycosyltransferase UGTSL2 and *In Situ* UDP-Glucose Regeneration. *Food Chem.* 259, 286–291. doi:10.1016/j.foodchem.2018.03.126
- Chen, M., Zeng, X., Zhu, Q., Wang, D., Han, S., Liang, S., et al. (2021). Effective Synthesis of Rebaudioside A by Whole-Cell Biocatalyst *Pichia pastoris*. *Biochem. Eng. J.* 175, 108117. doi:10.1016/j.bej.2021.108117
- Cheng, Z., Lan, Y., Guo, J., Ma, D., Jiang, S., Lai, Q., et al. (2020). Computational Design of Nitrile Hydratase from *Pseudonocardia thermophila* JCM3095 for Improved Thermostability. *Molecules* 25 (20), 4806. doi:10.3390/molecules25204806
- Chica, R. A., Doucet, N., and Pelletier, J. N. (2005). Semi-rational Approaches to Engineering Enzyme Activity: Combining the Benefits of Directed Evolution and Rational Design. *Curr. Opin. Biotechnol.* 16 (4), 378–384. doi:10.1016/j.copbio.2005.06.004
- Dudley, Q. M., Karim, A. S., Nash, C. J., and Jewett, M. C. (2020). *In Vitro* Prototyping of Limonene Biosynthesis Using Cell-free Protein Synthesis. *Metab. Eng.* 61, 251–260. doi:10.1016/j.ymben.2020.05.006
- Foo, J. L., Ching, C. B., Chang, M. W., and Leong, S. S. J. (2012). The Imminent Role of Protein Engineering in Synthetic Biology. *Biotechnol. Adv.* 30 (3), 541–549. doi:10.1016/j.biotechadv.2011.09.008
- Gachon, C. M. M., Langlois-Meurinne, M., and Saindrenan, P. (2005). Plant Secondary Metabolism Glycosyltransferases: the Emerging Functional Analysis. *Trends Plant Sci.* 10 (11), 542–549. doi:10.1016/j.tplants.2005.09.007
- Hagger, M. S., Trost, N., Keech, J. J., Chan, D. K. C., and Hamilton, K. (2017). Predicting Sugar Consumption: Application of an Integrated Dual-Process, Dual-phase Model. *Appetite* 116, 147–156. doi:10.1016/j.appet.2017.04.032
- Haney, P. J., Badger, J. H., Buldak, G. L., Reich, C. I., Woese, C. R., and Olsen, G. J. (1999). Thermal Adaptation Analyzed by Comparison of Protein Sequences from Mesophilic and Extremely Thermophilic Methanococcus Species. *Proc. Natl. Acad. Sci. U.S.A.* 96 (7), 3578–3583. doi:10.1073/pnas.96.7.3578
- Hanson, J. R. (2016). From Caá-Ehé to a Commercial Sweetener - the Diterpenoid Glycosides of Stevia rebaudiana. *Sci. Prog.* 99 (4), 413–419. doi:10.3184/003685016x14773090197508
- Itkin, M., Davidovich-Rikanati, R., Cohen, S., Portnoy, V., Doron-Faigenboim, A., Oren, E., et al. (2016). The Biosynthetic Pathway of the Nonsugar, High-Intensity Sweetener Mogroside V from *Siraitia grosvenorii*. *Proc. Natl. Acad. Sci. U.S.A.* 113 (47), E7619–E7628. doi:10.1073/pnas.1604828113
- Karim, A. S., Dudley, Q. M., Juminaga, A., Yuan, Y., Crowe, S. A., Heggstad, J. T., et al. (2020). *In Vitro* Prototyping and Rapid Optimization of Biosynthetic Enzymes for Cell Design. *Nat. Chem. Biol.* 16 (8), 912–919. doi:10.1038/s41589-020-0559-0
- Karim, A. S., and Jewett, M. C. (2016). A Cell-free Framework for Rapid Biosynthetic Pathway Prototyping and Enzyme Discovery. *Metab. Eng.* 36, 116–126. doi:10.1016/j.ymben.2016.03.002
- Katoh, K., and Standley, D. M. (2014). MAFFT: Iterative Refinement and Additional Methods. *Methods Mol. Biol.* 1079, 131–146. doi:10.1007/978-1-62703-646-7\_8
- Kirk, O., Borchert, T. V., and Fuglsang, C. C. (2002). Industrial Enzyme Applications. *Curr. Opin. Biotechnol.* 13 (4), 345–351. doi:10.1016/S0958-1669(02)00328-2
- Kroyer, G. (2010). Stevioside and Stevia-Sweetener in Food: Application, Stability and Interaction with Food Ingredients. *J. Verbr. Lebensm.* 5 (2), 225–229. doi:10.1007/s00003-010-0557-3
- Laskowski, R. A., MacArthur, M. W., Moss, D. S., and Thornton, J. M. (1993). PROCHECK: a Program to Check the Stereochemical Quality of Protein Structures. *J. Appl. Cryst.* 26 (2), 283–291. doi:10.1107/s0021889892009944
- Lee, S. G., Salomon, E., Yu, O., and Jez, J. M. (2019). Molecular Basis for Branched Steviol Glucoside Biosynthesis. *Proc. Natl. Acad. Sci. U.S.A.* 116 (26), 13131–13136. doi:10.1073/pnas.1902104116
- Lin, M., Wang, F., and Zhu, Y. (2020). Modeled Structure-Based Computational Redesign of a Glycosyltransferase for the Synthesis of Rebaudioside D from Rebaudioside A. *Biochem. Eng. J.* 159, 107626. doi:10.1016/j.bej.2020.107626
- Louveau, T., and Osbourn, A. (2019). The Sweet Side of Plant-Specialized Metabolism. *Cold Spring Harb Perspect. Biol.* 11 (12), a034744. doi:10.1101/cshperspect.a034744
- Mohamed, A. A., Ceunen, S., Geuns, J. M. C., Van den Ende, W., and De Ley, M. (2011). UDP-dependent Glycosyltransferases Involved in the Biosynthesis of Steviol Glycosides. *J. Plant Physiol.* 168 (10), 1136–1141. doi:10.1016/j.jplph.2011.01.030
- Mora, M. R., and Dando, R. (2021). The Sensory Properties and Metabolic Impact of Natural and Synthetic Sweeteners. *Compr. Rev. Food Sci. Food Saf.* 20 (2), 1554–1583. doi:10.1111/1541-4337.12703
- Muhammed, M. T., and Aki-Yalcin, E. (2019). Homology Modeling in Drug Discovery: Overview, Current Applications, and Future Perspectives. *Chem. Biol. Drug Des.* 93 (1), 12–20. doi:10.1111/cbdd.13388
- Musil, M., Stourac, J., Bendl, J., Brezovsky, J., Prokop, Z., Zendulka, J., et al. (2017). FireProt: Web Server for Automated Design of Thermostable Proteins. *Nucleic Acids Res.* 45 (W1), W393–W399. doi:10.1093/nar/gkx285
- Nakano, K., Sawada, S., Yamada, R., Mimitsuka, T., and Ogino, H. (2018). Enhancement of the Catalytic Activity of D-Lactate Dehydrogenase from *Sporolactobacillus laevolacticus* by Site-Directed Mutagenesis. *Biochem. Eng. J.* 133, 214–218. doi:10.1016/j.bej.2018.02.015
- Olsson, K., Carlsen, S., Semmler, A., Simón, E., Mikkelsen, M. D., and Møller, B. L. (2016). Microbial Production of Next-Generation Stevia Sweeteners. *Microb. Cel Fact* 15 (1), 207. doi:10.1186/s12934-016-0609-1
- Prakash, I., Bunders, C., Devkota, K., Charan, R., Ramirez, C., Priedemann, C., et al. (2014). Isolation and Characterization of a Novel Rebaudioside M Isomer from a Bioconversion Reaction of Rebaudioside A and NMR Comparison Studies of Rebaudioside M Isolated from Stevia rebaudiana Bertoni and Stevia rebaudiana Morita. *Biomolecules* 4 (2), 374–389. doi:10.3390/biom4020374
- Price, M. N., Dehal, P. S., and Arkin, A. P. (2009). FastTree: Computing Large Minimum Evolution Trees with Profiles Instead of a Distance Matrix. *Mol. Biol. Evol.* 26 (7), 1641–1650. doi:10.1093/molbev/msp077
- Sheldon, R. A., and Pereira, P. C. (2017). Biocatalysis Engineering: the Big Picture. *Chem. Soc. Rev.* 46 (10), 2678–2691. doi:10.1039/c6cs00854b
- Wang, Z., Hong, J., Ma, S., Huang, T., Ma, Y., Liu, W., et al. (2020). Heterologous Expression of EUGT11 from *Oryza sativa* in *Pichia pastoris* for Highly Efficient One-Pot Production of Rebaudioside D from Rebaudioside A. *Int. J. Biol. Macromolecules* 163, 1669–1676. doi:10.1016/j.jbiomac.2020.09.132
- Xia, Y., Li, X., Yang, L., Luo, X., Shen, W., Cao, Y., et al. (2021). Development of Thermostable Sucrose Phosphorylase by Semi-rational Design for Efficient Biosynthesis of Alpha-D-Glucosylglycerol. *Appl. Microbiol. Biotechnol.* 105 (19), 7309–7319. doi:10.1007/s00253-021-11551-0
- Xiong, W., Liu, B., Shen, Y., Jing, K., and Savage, T. R. (2021). Protein Engineering Design from Directed Evolution to De Novo Synthesis. *Biochem. Eng. J.* 174, 108096. doi:10.1016/j.bej.2021.108096

- Xu, Z., Cen, Y.-K., Zou, S.-P., Xue, Y.-P., and Zheng, Y.-G. (2020). Recent Advances in the Improvement of Enzyme Thermostability by Structure Modification. *Crit. Rev. Biotechnol.* 40 (1), 83–98. doi:10.1080/07388551.2019.1682963
- Zhang, J., Tang, M., Chen, Y., Ke, D., Zhou, J., Xu, X., et al. (2021). Catalytic Flexibility of rice Glycosyltransferase OsUGT91C1 for the Production of Palatable Steviol Glycosides. *Nat. Commun.* 12 (1), 7030. doi:10.1038/s41467-021-27144-4
- Zhang, N., and Zhao, H. (2016). Enriching Screening Libraries with Bioactive Fragment Space. *Bioorg. Med. Chem. Lett.* 26 (15), 3594–3597. doi:10.1016/j.bmcl.2016.06.013

**Conflict of Interest:** The authors declare that the research was conducted in the absence of any commercial or financial relationships that could be construed as a potential conflict of interest.

**Publisher's Note:** All claims expressed in this article are solely those of the authors and do not necessarily represent those of their affiliated organizations, or those of the publisher, the editors, and the reviewers. Any product that may be evaluated in this article, or claim that may be made by its manufacturer, is not guaranteed or endorsed by the publisher.

Copyright © 2022 Chen, Song, Qin, Han, Rao, Liang and Lin. This is an open-access article distributed under the terms of the Creative Commons Attribution License (CC BY). The use, distribution or reproduction in other forums is permitted, provided the original author(s) and the copyright owner(s) are credited and that the original publication in this journal is cited, in accordance with accepted academic practice. No use, distribution or reproduction is permitted which does not comply with these terms.





# Surface Functionalization of SBA-15 for Immobilization of Myoglobin

Hengmin Miao<sup>1,2</sup>, Maosheng Li<sup>1,3</sup>, Fang Wang<sup>1</sup>, Jiao Li<sup>2\*</sup>, Ying-Wu Lin<sup>4,5\*</sup> and Jiakun Xu<sup>1\*</sup>

<sup>1</sup>Key Laboratory of Sustainable Development of Polar Fisheries, Ministry of Agriculture and Rural Affairs, Yellow Sea Fisheries Research Institute, Chinese Academy of Fishery Sciences, Lab for Marine Drugs and Byproducts of Pilot National Lab for Marine Science and Technology, Qingdao, China, <sup>2</sup>School of Materials Science and Engineering, Shandong University of Technology, Zibo, China, <sup>3</sup>School of Food Science and Engineering, Qilu University of Technology (Shandong Academy of Sciences), Jinan, China, <sup>4</sup>School of Chemistry and Chemical Engineering, University of South China, Hengyang, China, <sup>5</sup>Key Laboratory of Protein Structure and Function of Universities in Hunan Province, University of South China, Hengyang, China

## OPEN ACCESS

### Edited by:

Hui-Min Qin,  
Tianjin University of Science and  
Technology, China

### Reviewed by:

Longhai Dai,  
Hubei University, China  
Lijun Guan,  
Heilongjiang Academy of Agricultural  
Sciences, China

### \*Correspondence:

Jiao Li  
haiyan9943@163.com  
Ying-Wu Lin  
linlinying@hotmail.com  
Jiakun Xu  
xujuk@ysfri.ac.cn

### Specialty section:

This article was submitted to  
Industrial Biotechnology,  
a section of the journal  
Frontiers in Bioengineering and  
Biotechnology

Received: 30 March 2022

Accepted: 13 April 2022

Published: 19 May 2022

### Citation:

Miao H, Li M, Wang F, Li J,  
Lin Y-W and Xu J (2022) Surface  
Functionalization of SBA-15 for  
Immobilization of Myoglobin.  
Front. Bioeng. Biotechnol. 10:907855.  
doi: 10.3389/fbioe.2022.907855

Mesoporous molecular sieve SBA-15 was successfully modified with 3-aminopropyltriethoxysilane (APTES) and 3-glycidyloxypropyltrimethoxysilane (GPTMS). The functionalized SBA-15 were characterized by small-angle X-ray (SAXRD), thermogravimetric analysis (TG), N<sub>2</sub> adsorption, and Fourier transformed infrared spectrum (FT-IR). APTES functionalized SBA-15 (named SBA-15-A) and GPTMS functionalized SBA-15 (named SBA-15-G) were used to immobilize myoglobin (Mb). The loading amounts of Mb by SBA-15-A and SBA-15-G were 511.2 and 547.8 mg/g, respectively, whereas only 359.6 mg/g was achieved by SBA-15. Mb/SBA-15-G and Mb/SBA-15-A demonstrated better reusability than SBA-15, retaining 84.6% and 82.7% of the initial activity after repeated use seven times. The Mb/SBA-15-A and Mb/SBA-15-G also exhibited improved thermal stability and storage stability.

**Keywords:** myoglobin, SBA-15, organic functionalization, protein immobilization, biocatalysis

## 1 INTRODUCTION

The enzyme, as a natural catalyst, has the characteristics and advantages of strong catalytic selectivity, fast reaction speed, mild reaction conditions, and being clean and pollution-free. It is widely used in medicine, food, chemical industry, energy, and environmental protection, among other fields (Yu et al., 2011; Alkan et al., 2009; Mislovicová et al., 2004; Katchalski-Katzir and Kraemer, 2000). At present, industrial biotechnology, which relies on biocatalysis as its core technology, has become an important engine driving the rapid development of the social economy. As a peroxidase, myoglobin can catalyze a variety of reactions, including the oxidation of guaiacol and indole (Xu et al., 2012) and the decolorization of industrial dyes (Zhang et al., 2019a). As a result, the efficient recovery and reuse of myoglobin is the foundation of the economic and industrial application of myoglobin to improve the reusability of myoglobin; immobilizing myoglobin on a solid support is a good solution (Jakub et al., 2018; Zhao et al., 2006), which has attracted extensive attention.

To date, a variety of new types of carriers and immobilization technologies have been developed to improve the reusability of enzymes and lower the cost of enzyme biocatalysts for industrial applications. These include acrylic resins molecular sieves (Katchalski-Katzir and Kraemer, 2000), aldehyde-agarose (Guisán, 1988), gelatin (Norouzzian et al., 2002), magnetic microparticles of polymers (Bozhinova et al., 2004), and layered double hydroxides (LDH) (Ren et al., 2002). Among these materials, inorganic materials have garnered increasing attention due to their unique advantages, such as easy regeneration, nontoxicity, low cost, and high stability. As inorganic support, the mesoporous molecular sieves not only have the common advantages of inorganic

materials but also have adjustable pores, changeable composition, and large pore volume. They are a promising immobilized enzyme carrier that is widely used in the research of enzyme immobilization. Mesoporous silica MCM-41 was first explored to immobilize enzymes by Díaz and Jr (1996). Following that, MCM-48, SBA-15, and other types of mesoporous molecular sieves were used for enzyme immobilization. SBA-15 is a form of mesoporous silica nanoparticle with uniform pore size, long-range ordered pore structure, and a more stable structure. It has received much attention in recent years.

The immobilization method can significantly influence the reuse performance of the enzyme. The physical adsorption method has the advantages of being simple, fast, and low cost, but the force between the carrier and the enzyme is too weak, and the enzyme adsorbed into the material channel is easy to leach from the material channel in the process of reuse. For example, Serra et al. found that 30% of the adsorbed lipase was leached from the support within 2 h (Serra et al., 2008). Li et al. used SBA-15 to physically adsorb lipase. Due to the weak force between the enzyme and the support, the enzyme is leached from the pore during reuse, and only 32% of the initial activity is retained after reusing it five times (Li et al., 2009). To overcome the problem of enzyme leaching, the covalent bonding between enzyme and support is a common method for reducing enzyme leaching and improving the reuse performance of the enzyme. In the previous study, many studies showed that there are rich Si-OH groups on the surface of channels of silica materials (Kawai and Tsutsumi, 1998; Kimura et al., 1998), which can serve as the sites for the anchor of organic groups. For example, Shah et al. immobilized the penicillin acylase from SBA-15 on APTES functionalized, and the results show that immobilized enzyme rarely leaked from the carrier and has good reusability.

3-Aminopropyltriethoxysilane (APTES) and 3-glycidyloxypropyltrimethoxysilane (GPTMS) have abundant surface functional groups for surface modification, which are widely used functional reagents, and their ethoxy groups can react with hydroxyl groups on the surface of mesoporous molecular sieves and graft the amino and epoxy functional groups onto the surface of mesoporous molecular sieves. In this study, we used APTES and GPTMS to functionalize SBA-15 with amino and epoxy organic groups, as shown in **Supplementary Figure S1**. Small-angle X-ray (SAXRD), nitrogen adsorption-desorption experiments, Fourier transform infrared spectroscopy (FT-IR), and thermogravimetry (TG) were used to characterize the materials, which were then used to immobilize myoglobin. The amino group on SBA-15-A cannot react with the amino group on myoglobin. Glutaraldehyde needs to be added as a bridge, and the aldehyde group reacts with the amino group to connect SBA-15-A with myoglobin to realize the immobilization of myoglobin. Under the condition of immobilization, the epoxy group on SBA-15-G can react directly with the amino group on myoglobin to realize the immobilization of myoglobin. The immobilization process is shown in **Supplementary Figure S2**. We compared the changes in immobilized myoglobin loading of SBA-15, SBA-15-A, and SBA-15-G and studied the reuse performance of the immobilized enzymes.

## 2 MATERIALS AND METHODS

### 2.1 Materials

3-Aminopropyltriethoxysilane (APTES), 3-glycidyloxypropyltrimethoxysilane (GPTMS), glutaraldehyde, and guaiacol were purchased from TCI. SBA-15 was synthesized in previous reports, and H64D/V68I Mb were expressed in *E. coli* BL21(DE3) cells, cultured, and purified using the procedure described previously.

### 2.2 Methods

#### 2.2.1 Preparation and Functionalization of SBA-15

The SBA-15 mesoporous materials were synthesized using a previously reported method (Zhao et al., 1998a; Zhao et al., 1998b), with P123 acting as a structure-directing agent and the TMB acting as a pore dilator agent. The functionalization of SBA-15 with 3-aminopropyltriethoxysilane (APTES) and 3-glycidyloxypropyltrimethoxysilane (GPTMS) was performed using the previously reported methods (Bourkaib et al., 2021; Lu et al., 2007). 1.0 ml of APTMS or GPTMS was added to 1.0 g of SBA-15 suspended in 50 ml of toluene and refluxed overnight under an N<sub>2</sub> atmosphere. Further, the resulting solid was filtered, washed, and dried to obtain the functionalized SBA-15-A and SBA-15-G.

#### 2.2.2 Characterization of SBA-15, SBA-15-A, and SBA-15-G

Nitrogen adsorption-desorption experiments were performed using an ASAP 2460 Micromeritics System. Samples were degassed in a vacuum at 200°C for 2 h before measurement. The pore diameter distributions were calculated from desorption branches using the Barrett-Joyner-Halenda (BJH) method, and the surface areas were calculated from desorption branches using the Brunauer-Emmett-Teller (BET) method. The small-angle X-ray diffraction patterns were obtained using Cu K $\alpha$  radiation on a Bruker D8 advance diffractometer (Bruker, Kontich, Belgium), and the data were collected from 0.5° to 10° in 0.5° steps. Fourier transformed infrared (FT-IR) spectra were recorded on a Shimadzu 8201 PC spectrophotometer, and the samples were prepared using the standard KBr disk method. Thermogravimetric (TG) calculations were carried out on a Perkin Elmer thermogravimetric analyzer in the air (50 ml min<sup>-1</sup>) at 10 K min<sup>-1</sup> from 30°C to 800°C.

#### 2.2.3 Adsorption of Myoglobin Onto SBA-15

The following is the procedure of Mb immobilization with SBA-15-A. A total of 5 mg SBA-15-A was mixed with 1 ml Mb solution (3 mg/ml) and stirred in 2 ml phosphate buffer (50 mM, pH6) for 15 h at 25°C. As a crosslinking agent, 2.0 wt% glutaraldehyde was added, and the mixture was stirred for 30 min at 25°C. The amount of glutaraldehyde involved in the immobilization process of SBA-15-A was optimized by varying the volumes of glutaraldehyde used in the protocol described for enzyme crosslinking. Furthermore, the reaction mixture was centrifuged, the supernatant was removed, and the precipitate was washed thrice for 1 h with 1 ml of phosphate buffer (50 mM, pH 6). The UV absorption value of the supernatant was measured

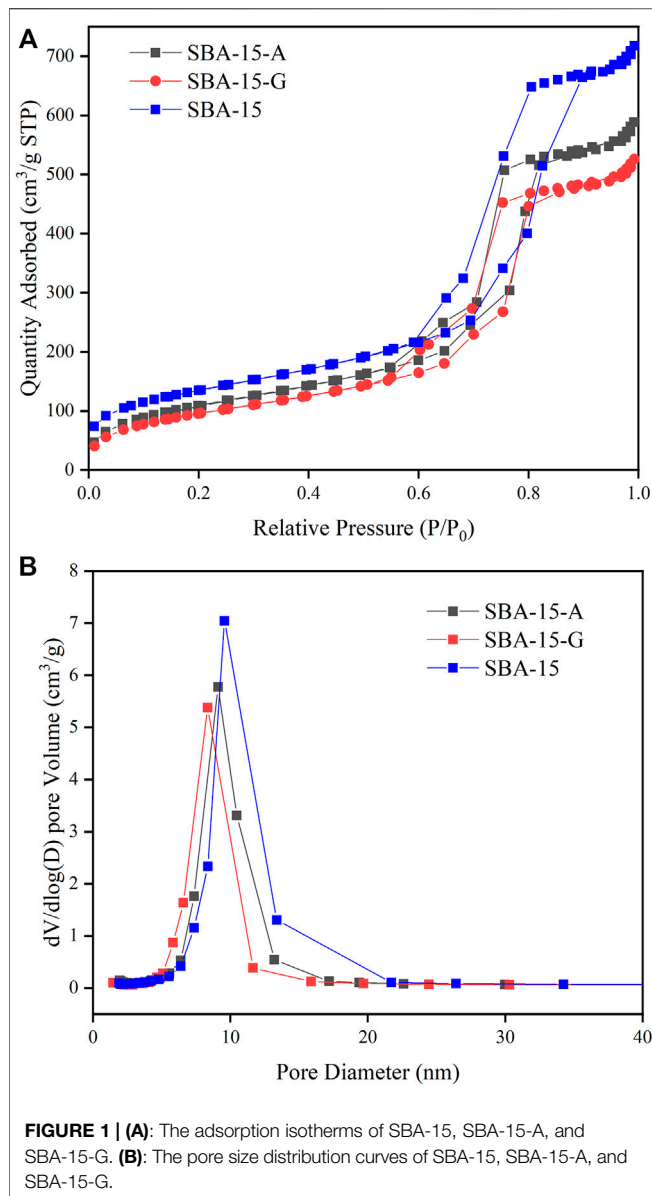


**FIGURE 1 | (A):** The adsorption isotherms of SBA-15, SBA-15-A, and SBA-15-G. **(B):** The pore size distribution curves of SBA-15, SBA-15-A, and SBA-15-G.

at 408 nm to determine the concentration of protein in the supernatant. The final products were identified as Mb/SBA-15-A. The procedures of Mb immobilization onto SBA-15-G and SBA-15 were carried out by a similar procedure as that for SBA-15-A without the glutaraldehyde treatment. The final products were identified as Mb/SBA-15-G and Mb/SBA-15, respectively.

## 2.2.4 Catalytic Activity of Free Mb and Immobilized Mb

The assays comparing the catalytic activity of free Mb, Mb/SBA-15, Mb/SBA-15-A, and Mb/SBA-15-G were performed using the oxidation of guaiacol, and the product was checked by monitoring the UV absorption at 470 nm (Zhang et al., 2019b). The reaction mixture (50 mM of phosphate buffer, 1  $\mu$ M of Mb, and 2.5 mM of guaiacol) was incubated for 15 min at 25°C, and the reaction was initiated by the addition of H<sub>2</sub>O<sub>2</sub> (final concentration, 10 mM). The relative activity of an

immobilized enzyme is the percentage of activity retained in the immobilized enzyme when compared to free enzyme activity.

## 2.2.5 Operational Stability Test for Mb/SBA-15, Mb/SBA-15-A, and Mb/SBA-15-G

The influence of metal ions (Ba<sup>2+</sup>, Ca<sup>2+</sup>, Mg<sup>2+</sup>, Mn<sup>2+</sup>, and Al<sup>3+</sup>), organic solvents (methanol, ethanol, isopropanol, glycol, and formic acid), storage time, and temperature on Mb activity were studied to assess the stability of the immobilized protein. The reactions were carried out in phosphate buffer at a concentration of 50 mM and pH 6.

The following experiment was carried out to investigate the effect of metal ions or organic solvents on Mb activity: Mb/SBA-15, Mb/SBA-15-A, and Mb/SBA-15-G were incubated for 1 h in a buffer solution (phosphate buffer, 50 mM, pH 6) containing various metal ions (10 mM) or organic solvents (10% v/v), with a control group containing only buffer solution. Then, the enzyme activity was tested. The effect of temperature on the activity was examined by incubation for 1 h in phosphate buffer (50 mM, pH6) in a temperature range between 10°C and 60°C. The effect of storage time on Mb activity was tested by determining the remaining activity after storing the Mb in phosphate buffer (50 mM, pH 6) for different time periods of 20 days at 25°C. The activity was assayed every 5 days.

## 2.2.6 Reusability Test for Mb/SBA-15, Mb/SBA-15-A, and Mb/SBA-15-G

After centrifugation of the reaction solution, the supernatant was tested using UV, and the precipitate was washed three times with phosphate buffer (50 mM, pH 6). The reusability of the immobilized Mb was tested for seven consecutive assays using the method described above. The remaining activity was calculated by comparing it with the first assay.

# 3 RESULTS AND DISCUSSION

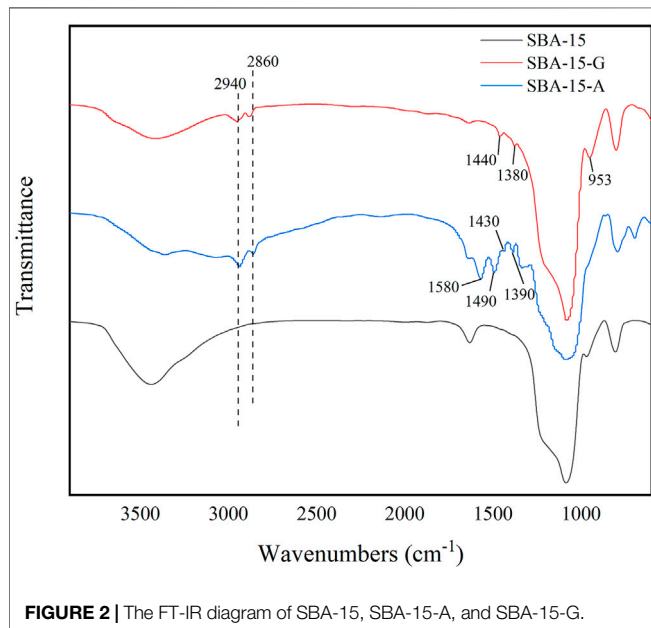
## 3.1 Structural Characteristics of the SBA-15

The general shape of the adsorption isotherms is not modified after functionalization (Figure 1A). The adsorption curves exhibit typical Langmuir IV adsorption-desorption isotherms (Shah et al., 2008) and H1 hysteresis under high relative pressure. It belongs to hexagonal column mesoporous material. The pore size distribution curves of SBA-15, SBA-15-A, and SBA-15-G are shown in Figure 1B. From the curves, it can be seen that the pore size distribution of the modified material is reduced due to the introduction of organic groups, proving that the organic groups are successfully grafted to the surface of the material. The specific structural parameters of SBA-15, SBA-15-A, and SBA-15-G are shown in Table 1. It can be seen that the pore diameter, pore volume, and specific surface area of SBA-15-A and SBA-15-G were smaller than SBA-15, and the pore diameters of SBA-15, SBA-15-A, and SBA-15-G were 9.8, 8.7, and 8.6 nm, respectively. The decrease in pore size is due to the addition of organic groups.

Supplementary Figure S3 shows the TG diagrams of SBA-15, SBA-15-A, and SBA-15-G. The result shows that SBA-15 has a

**TABLE 1** | Specific structural parameters of SBA-15, SBA-15-A, and SBA-15-G.

Samples	BJH pore diameter (nm)	BET surface area (m <sup>2</sup> /g)	BJH pore volume (cm <sup>3</sup> /g)
SBA-15	9.8	484.133	1.08
SBA-15-A	8.7	434.013	0.92
SBA-15-G	8.6	403.629	0.83

**FIGURE 2** | The FT-IR diagram of SBA-15, SBA-15-A, and SBA-15-G.

slight weight loss (3.2%) with an increase in temperature because of the evaporation of physically adsorbed water and dehydroxylation on the material surface. The functionalized samples SBA-15-A and SBA-15-G, on the contrary, have significant weight losses of 13.5% and 9.1%, respectively. The first weight loss at 25°C–100°C can be attributed to dehydration, and the latter weight loss is due to the combustion of amino groups and epoxy groups. The results of the thermogravimetric analysis in **Supplementary Figure S3** further showed that the amino and epoxy organic groups were successfully grafted onto the surface of SBA-15.

Small-angle XRD patterns of SBA-15, SBA-15-A, and SBA-15-G are depicted in **Supplementary Figure S4**. All of the samples revealed three peaks, denoted as (100), (110), and (200) reflections. These peaks are the characteristic of hexagonal mesoporous structures, associated with p6 mm hexagonal symmetry (Zhao et al., 1998a). This indicates that the long-range-order structure of the SBA-15 was not disrupted after functionalization.

**Figure 2** depicts the FT-IR spectra of SBA-15, SBA-15-A, and SBA-15-G. It can be seen that SBA-15 modified by amino and epoxy has a distinct absorption peak that SBA-15 does not have. In the SBA-15-A absorption spectrum, the absorption peaks near 2,940 and 2,860 cm<sup>-1</sup> correspond to the symmetrical vibration and asymmetric vibration absorption of -CH<sub>2</sub>- (Phan and Jones,

**TABLE 2** | The maximum adsorption amount and remained activity of Mb onto SBA-15, SBA-15-G, and SBA-15-A.

Samples	Adsorption proteins (mg/g)	Retained activity (%)
SBA-15-G	547.8 ± 9.87	91.16 ± 1.42
SBA-15-A	511.2 ± 11.21	90.48 ± 1.46
SBA-15	359.6 ± 10.73	93.24 ± 1.36

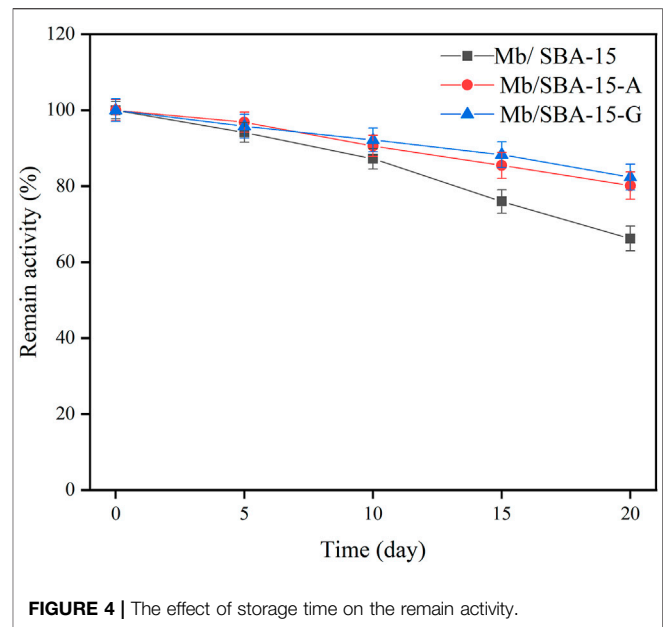
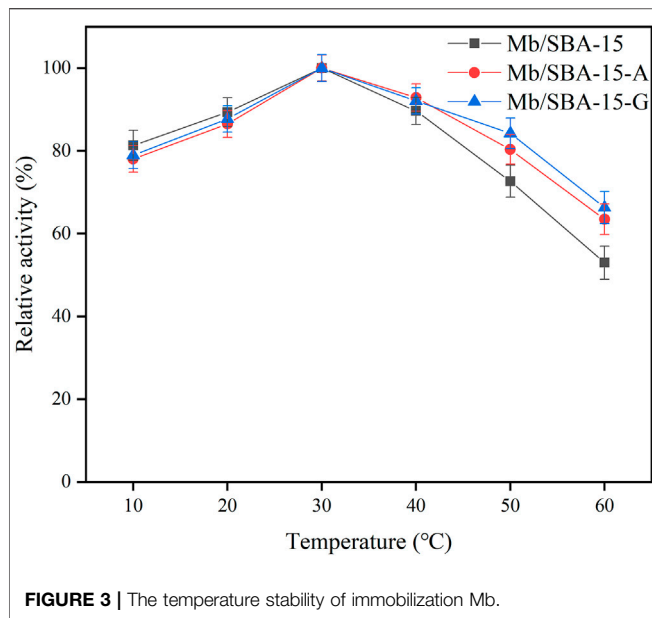
2006), the absorption peaks at 1,580 cm<sup>-1</sup> and 1,490 cm<sup>-1</sup> correspond to the symmetrical bending vibration and symmetrical vibration of N-H (Nguyen et al., 2008), and the absorption peaks at 1,430 and 1,390 cm<sup>-1</sup> correspond to the bending vibration absorption of C-H (Moller et al., 1999). The presence of these absorption peaks demonstrated that the amino groups were successfully grafted onto the surface of SBA-15. Similarly, in the infrared absorption spectrum of SBA-15-G, the absorption peaks near 2,940 and 2,860 cm<sup>-1</sup> are asymmetric vibrations and symmetric vibration absorption of -CH<sub>2</sub>-, respectively; the absorption peaks at 1,440 and 1,380 cm<sup>-1</sup> correspond to the bending vibration absorption of C-H; and 953 cm<sup>-1</sup> corresponds to the stretching vibration of the epoxy group. These absorption peaks indicate that the epoxy group is successfully grafted to the surface of SBA-15.

### 3.2 Activity and Protein Loading Test

**Table 2** compares the Mb load and retained activity of immobilized Mb in SBA-15-A and SBA-15-G mesoporous molecular sieves to SBA-15 mesoporous molecular sieves. It can be seen that SBA-15 modified by organic groups increases the load of Mb. The Mb load of SBA-15 is 359.6 mg/g, while SBA-15-G and SBA-15-A have enzyme loads of 547.8 and 511.2 mg/g, respectively, because of the protein interaction with the mesoporous material. Due to the physical adsorption of myoglobin by SBA-15, the adsorption force on the protein is small, and the protein adsorbed into the pore is easy to leak out from the pore, resulting in the low load of the material. The organic groups on the surface of the modified SBA-15 are covalently adsorbed with myoglobin adsorbed into the pore diameter. The covalent bond force is strong, making it difficult for the protein to leak out of the pore. As a result, the protein loading amount of SBA-15 was increased after modification.

Although the protein loading of the modified material is increased, the activity of the immobilized enzyme obtained from the modified mesoporous material is slightly reduced because the activity of the immobilized enzyme is directly related to the pore size of the mesoporous material. The addition of organic groups reduces the pore size of the carrier,



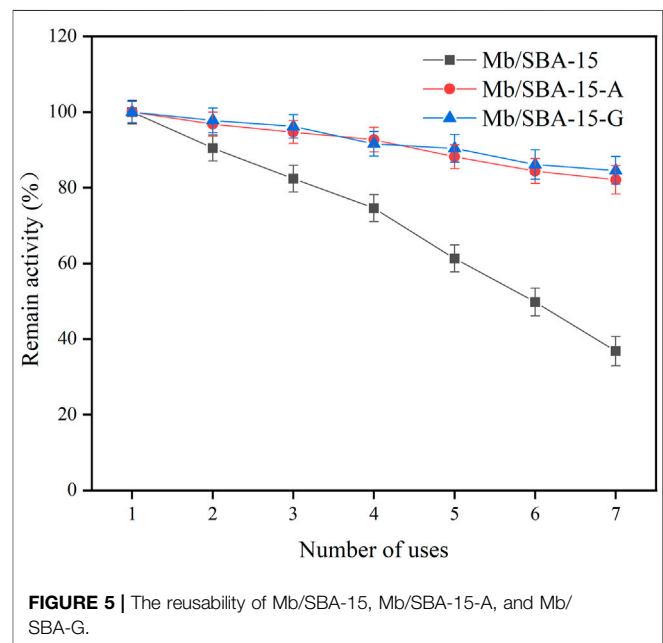


which was previously conducive to the enzyme catalytic reaction (Lü et al., 2008; Miao et al., 2022). The substrate and product can diffuse well in the pore channel during the reaction process, reducing the mass transfer resistance of the substrate and product. Meanwhile, the organic group reduces the pore size of the material, and the diffusion of the substrate and product in the pore channel is affected, resulting in the reduction in the immobilized enzyme activity.

**Supplementary Figure S5** shows the optimization of glutaraldehyde addition, showing the change of protein load with the additional volume of glutaraldehyde solution (2.0 wt %). It shows that the fixed load of protein is greatest when the volume of glutaraldehyde is 0.6 ml. At this time, the volume fraction of glutaraldehyde (volume ratio of protein solution to added glutaraldehyde solution) is 20%.

### 3.3 Stability of Mb/SBA-15, Mb/SBA-15-A, and Mb/SBA-15-G

The temperature stability of the immobilized enzyme is shown in **Figure 3**. It shows that the optimum reaction temperature of Mb/SBA-15, Mb/SBA-15-A, and Mb/SBA-15-G was 30°C, indicating that the modification of materials does not affect the optimum reaction temperature of immobilized enzyme. We can also see that the temperature stability of the immobilized enzyme prepared by the modified material is improved. At 60°C, Mb/SBA-15 retained 52.98% of the relative enzyme activity, while Mb/SBA-15-A and Mb/SBA-15-G retained 63.48% and 66.31% of the relative enzyme activity, which were 10.5% and 13.33% higher than Mb/SBA-15, respectively, because the modified carrier was covalently connected to the enzyme molecule. This strong interaction results in the enzyme molecule having high thermal stability (Eş et al., 2015). As a result, Mb/SBA-15-A and Mb/SBA-15-G have better thermal stability than Mb/SBA-15.



The effect of storage time on the remaining activity of the immobilized enzyme is shown in **Figure 4**. It shows that Mb/SBA-15-A and Mb/SBA-15-G retained 80.13% and 82.41% of the remaining activity, respectively, after 20 days, whereas Mb/SBA-15 retained only 66.21%. Consequently, the Mb/SBA-15-A and Mb/SBA-15-G exhibited better storage stability than Mb/SBA-15.

**Supplementary Figures S6A,B** show the effects of metal ions and organic solvents on the activity of Mb/SBA-15, Mb/SBA-15-A, and Mb/SBA-15-G, respectively. It can be seen that the stability of metal ions and organic solvents of Mb/SBA-15-A and Mb/SBA-15-G were slightly lower than that of Mb/SBA-15.

**TABLE 3 |** The cumulative enzyme activity loss rate of Mb/SBA-15.

Reuse times	1	2	3	4	5	6	7
Cumulative enzyme leaching rate (%)	9.21 ± 2.31	17.83 ± 2.12	25.37 ± 2.34	32.12 ± 2.11	37.55 ± 2.21	41.9 ± 2.03	45.12 ± 2.14

### 3.4 Reusability of Mb/SBA-15, Mb/SBA-15-A, and Mb/SBA-G

The ability of immobilized enzymes to be reused is critical for their practical application. The reusability of Mb/SBA-15, Mb/SBA-15-A, and Mb/SBA-G is shown in **Figure 5**. The reusability of Mb/SBA-15 was poor, with only 36.41% of the initial activity being retained after seven consecutive uses. In the reuse process, the leaching of protein can be detected in the supernatant because the force between the enzyme and the carrier in Mb/SBA-15 was primarily physical adsorption, and the force is weak (Dettori et al., 2018). The enzyme will fall off from the carrier during the reuse process, resulting in a decrease in the activity of the immobilized enzyme. During the reuse of Mb/SBA-15, the cumulative enzyme leaching rate was shown in **Table 3**. It can be seen that after seven repeated uses, 45.12% of myoglobin was leached, which was the main reason for the decrease in protein activity. However, Mb/SBA-15-A and Mb/SBA-15-G have high reusability. Mb/SBA-15-A retains 82.7% of the initial enzyme activity, and Mb/SBA-15-G retains 84.6% of the initial enzyme activity after seven consecutive uses. In the reuse process, no protein leaching is detected in the supernatant because glutaraldehyde is used as a bridge between the enzyme and the carrier in Mb/SBA-15-A and forms a covalent bond with the amino group on the myoglobin molecule. The force between Mb/SBA-15-A immobilized enzyme myoglobin and mesoporous material is strong. Similarly, the surface of Mb/SBA-G contains an epoxy group, which can directly react with the amino group on the myoglobin molecule to form a covalent bond. The Mb/SBA-15-G immobilized enzyme has a strong force between myoglobin and mesoporous molecule. Hence, the immobilized enzyme obtained by amino and epoxy modified SBA-15 has good reusability.

## 4 CONCLUSION

We successfully functionalized the surface of the SBA-15 mesoporous molecular sieve using APTES and GPTMS. The

functionalized SBA-15 mesoporous molecular sieve was successfully grafted with organic functional groups and retained its unique pore structure. The modified SBA-15 had higher protein loading ability, higher thermal stability, better storage stability, and reuse performance compared to that of SBA-15. The improvement of the reusability of immobilized protein is of great significance for the industrial application of myoglobin.

## DATA AVAILABILITY STATEMENT

The original contributions presented in the study are included in the article/**Supplementary Material**, Further inquiries can be directed to the corresponding authors.

## AUTHOR CONTRIBUTIONS

HM: data curation and writing-original draft. ML: data analysis. FW: data analysis. JL: supervision. Y-WL: writing-review and editing. JX: supervision, writing-review, and editing.

## FUNDING

This work was supported by the National Natural Science Foundation of China (32171263, 21977042), Central Public-Interest Scientific Institution Basal Research Fund, CAFS (no. 2020TD67), and Special Project of Major Scientific and Technological Innovation in Shandong Province (2018SDKJ0303-1-2223).

## SUPPLEMENTARY MATERIAL

The Supplementary Material for this article can be found online at: <https://www.frontiersin.org/articles/10.3389/fbioe.2022.907855/full#supplementary-material>

## REFERENCES

- Alkan, S., Gür, A., Ertan, M., Savran, A., and Genel, Y. (2009). Immobilization of Catalase via Adsorption into Natural and Modified Active Carbon Obtained from walnut in Various Methods. *Afr. J. Biotechnol.* 8 (11), 2089–2095. doi:10.1016/j.febslet.2005.10.057
- Bourkaib, M. C., Gaudin, P., Vibert, F., Guiavarc'h, Y., Delaunay, S., Framboisier, X., et al. (2021). APTES Modified SBA15 and Meso-Macro Silica Materials for the Immobilization of Aminoacylases from *Streptomyces Ambofaciens*. *Microporous Mesoporous Mater.* 323, 111226. doi:10.1016/j.micromeso.2021.111226
- Bozhinova, D., Galunsky, B., Yueping, G., Franzreb, M., Köster, R., and Kasche, V. (2004). Evaluation of Magnetic Polymer Micro-beads as Carriers of

- Immobilised Biocatalysts for Selective and Stereoselective Transformations. *Biotechnol. Lett.* 26 (4), 343–350. doi:10.1023/B:BILE.0000015471.18648.40
- Dettori, L., Vibert, F., Guiavarc'h, Y., Delaunay, S., Humeau, C., Blin, J. L., et al. (2018). N-α-acylation of Lysine Catalyzed by Immobilized Aminoacylases from *Streptomyces Ambofaciens* in Aqueous Medium. *Microporous Mesoporous Mater.* 267, 24–34. doi:10.1016/j.micromeso.2018.03.018
- Díaz, J., and Jr, K. (1996). Enzyme Immobilization in MCM-41 Molecular Sieve. *J. Mol. Catal. B Enzymatic* 2 (2–3), 115–126. doi:10.1016/S1381-1177(96)00017-3
- Eş, I., Vieira, J. D. G., and Amaral, A. C. (2015). Principles, Techniques, and Applications of Biocatalyst Immobilization for Industrial Application. *Appl. Microbiol. Biotechnol.* 99 (5), 2065–2082. doi:10.1007/s00253-015-6390-y

- Guisán, J. (1988). Aldehyde-agarose Gels as Activated Supports for Immobilization-Stabilization of Enzymes. *Enzyme Microb. Tech.* 10 (6), 375–382. doi:10.1016/0141-0229(88)90018-X
- Zdarta, J., Meyer, A., Jesionowski, T., and Pinelo, M. (2018). A General Overview of Support Materials for Enzyme Immobilization: Characteristics, Properties, Practical Utility. *Catalysts* 8 (2), 92. doi:10.3390/catal8020092
- Katchalski-Katzir, E., and Kraemer, D. M. (2000). Eupergit C, a Carrier for Immobilization of Enzymes of Industrial Potential. *J. Mol. Catal. B Enzymatic* 10 (1-3), 157–176. doi:10.1016/S1381-1177(00)00124-7
- Kawai, T., and Tsutsumi, K. (1998). Reactivity of Silanol Groups on Zeolite Surfaces. *Colloid Polym. Sci.* 276 (11), 992–998. doi:10.1007/s003960050338
- Kimura, T., Kuroda, K., Sugahara, Y., and Kuroda, K. (1998). Esterification of the Silanol Groups in the Mesoporous Silica Derived from Kanemite. *J. Porous Mater.* 5 (2), 127–132. doi:10.1023/A:1009641304742
- Li, Y., Zhou, G., Li, C., Qin, D., Qiao, W., and Chu, B. (2009). Adsorption and Catalytic Activity of Porcine Pancreatic Lipase on Rod-like SBA-15 Mesoporous Material. *Colloids Surf. A: Physicochemical Eng. Aspects* 341 (1-3), 79–85. doi:10.1016/j.colsurfa.2009.03.041
- Lü, Y., Lu, G., Wang, Y., Guo, Y., Guo, Y., Zhang, Z., et al. (2007). Functionalization of Cubic Ia3d Mesoporous Silica for Immobilization of Penicillin G Acylase. *Adv. Funct. Mater.* 17 (13), 2160–2166. doi:10.1002/adfm.200600505
- Lu, Y., Guo, Y., Wang, Y., Liu, X., Wang, Y., Guo, Y., et al. (2008). Immobilized Penicillin G Acylase on Mesoporous Silica: The Influence of Pore Size, Pore Volume and Mesophases. *Microporous Mesoporous Mater.* 114 (1-3), 507–510. doi:10.1016/j.micromeso.2007.12.027
- Miao, H., Li, M., Sun, X., Xia, J., Li, Y., Li, J., et al. (2022). Effects of Pore Size and Crosslinking Methods on the Immobilization of Myoglobin in SBA-15. *Front. Bioeng. Biotechnol.* 9, 827552. doi:10.3389/fbioe.2021.827552
- Mislovičová, D., Masárová, J., Vikartovská, A., Gemeiner, P., and Michalková, E. (2004). Biospecific Immobilization of Mannan-Penicillin G Acylase Neoglycoenzyme on Concanavalin A-Bead Cellulose. *J. Biotechnol.* 110 (1), 11–19. doi:10.1016/j.jbiotec.2004.01.006
- Moller, K., Bein, T., and Fischer, R. X. (1999). Synthesis of Ordered Mesoporous Methacrylate Hybrid Systems: Hosts for Molecular Polymer Composites. *Chem. Mater.* 11 (3), 665–673. doi:10.1021/cm9805368
- Nguyen, T. P. B., Lee, J.-W., Shim, W. G., and Moon, H. (2008). Synthesis of Functionalized SBA-15 with Ordered Large Pore Size and its Adsorption Properties of BSA. *Microporous Mesoporous Mater.* 110 (2-3), 560–569. doi:10.1016/j.micromeso.2007.06.054
- Norouzian, D., Javadpour, S., Moazami, N., and Akbarzadeh, A. (2002). Immobilization of Whole Cell Penicillin G Acylase in Open Pore Gelatin Matrix. *Enzyme Microb. Tech.* 30 (1), 26–29. doi:10.1016/S0141-0229(01)00445-8
- Phan, N. T. S., and Jones, C. W. (2006). Highly Accessible Catalytic Sites on Recyclable Organosilane-Functionalized Magnetic Nanoparticles: An Alternative to Functionalized Porous Silica Catalysts. *J. Mol. Catal. A: Chem.* 253 (1-2), 123–131. doi:10.1016/j.molcata.2006.03.019
- Ren, L., Jing, H., Zhang, S., Evans, D. G., and Xue, D. (2002). Immobilization of Penicillin G Acylase in Layered Double Hydroxides Pillared by Glutamate Ions. *J. Mol. Catal. B Enzymatic* 18 (1-3), 3–11. doi:10.1016/S1381-1177(02)00008-5
- Serra, E., Mayoral, Á., Sakamoto, Y., Blanco, R. M., and Díaz, I. (2008). Immobilization of Lipase in Ordered Mesoporous Materials: Effect of Textural and Structural Parameters. *Microporous Mesoporous Mater.* 114 (1-3), 201–213. doi:10.1016/j.micromeso.2008.01.005
- Shah, P., Sridevi, N., Prabhune, A., and Ramaswamy, V. (2008). Structural Features of Penicillin Acylase Adsorption on APTES Functionalized SBA-15. *Microporous Mesoporous Mater.* 116 (1-3), 157–165. doi:10.1016/j.micromeso.2008.03.030
- Xu, J., Shoji, O., Fujishiro, T., Ohki, T., Ueno, T., and Watanabe, Y. (2012). Construction of Biocatalysts Using the Myoglobin Scaffold for the Synthesis of Indigo from Indole. *Catal. Sci. Technol.* 2 (4), 739–744. doi:10.1039/C2CY00427E
- Yu, H., Guo, Y., Wu, D., Zhan, W., and Lu, G. (2011). Immobilization of Glucose Isomerase onto GAMM Support for Isomerization of Glucose to Fructose. *J. Mol. Catal. B: Enzymatic* 72 (1-2), 73–76. doi:10.1016/j.molcatb.2011.05.006
- Zhang, P., Xu, J., Wang, X.-J., He, B., Gao, S.-Q., and Lin, Y.-W. (2019a). The Third Generation of Artificial Dye-Decolorizing Peroxidase Rationally Designed in Myoglobin. *ACS Catal.* 9, 7888–7893. doi:10.1021/acscatal.9b02226
- Zhang, P., Yuan, H., Xu, J., Wang, X.-J., Gao, S.-Q., Tan, X., et al. (2019b). A Catalytic Binding Site Together with a Distal Tyr in Myoglobin Affords Catalytic Efficiencies Similar to Natural Peroxidases. *ACS Catal.* 10, 891–896. doi:10.1021/acscatal.9b05080
- Zhao, D., Huo, Q., Feng, J., Chmelka, B. F., and Stucky, G. D. (1998a). Nonionic Triblock and star Diblock Copolymer and Oligomeric Surfactant Syntheses of Highly Ordered, Hydrothermally Stable, Mesoporous Silica Structures. *J. Am. Chem. Soc.* 120 (24), 6024–6036. doi:10.1021/ja506344k10.1021/ja974025i
- Zhao, D., Feng, J., Huo, Q., Melosh, N., Fredrickson, G. H., Chmelka, B. F., et al. (1998b). Triblock Copolymer Syntheses of Mesoporous Silica with Periodic 50 to 300 Angstrom Pores. *Science* 279 (5350), 548–552. doi:10.1126/science.279.5350.548
- Zhao, X. S., Bao, X. Y., Guo, W., and Lee, F. Y. (2006). Immobilizing Catalysts on Porous Materials. *Mater. Today* 9 (3), 32–39. doi:10.1016/S1369-7021(06)71388-8

**Conflict of Interest:** The authors declare that the research was conducted in the absence of any commercial or financial relationships that could be construed as a potential conflict of interest.

**Publisher's Note:** All claims expressed in this article are solely those of the authors and do not necessarily represent those of their affiliated organizations or those of the publisher, the editors, and the reviewers. Any product that may be evaluated in this article, or claim that may be made by its manufacturer, is not guaranteed or endorsed by the publisher.

Copyright © 2022 Miao, Li, Wang, Li, Lin and Xu. This is an open-access article distributed under the terms of the Creative Commons Attribution License (CC BY). The use, distribution or reproduction in other forums is permitted, provided the original author(s) and the copyright owner(s) are credited and that the original publication in this journal is cited, in accordance with accepted academic practice. No use, distribution or reproduction is permitted which does not comply with these terms.



# Molecular and Biochemical Differences of the Tandem and Cold-Adapted PET Hydrolases Ple628 and Ple629, Isolated From a Marine Microbial Consortium

Ingrid E. Meyer Cifuentes<sup>1</sup>, Pan Wu<sup>2,3</sup>, Yipei Zhao<sup>2,3</sup>, Weidong Liu<sup>2</sup>, Meina Neumann-Schaal<sup>4</sup>, Lara Pfaff<sup>5</sup>, Justyna Barys<sup>1</sup>, Zhishuai Li<sup>2</sup>, Jian Gao<sup>2</sup>, Xu Han<sup>2</sup>, Uwe T. Bornscheuer<sup>6</sup>, Ren Wei<sup>5</sup> and Başak Öztürk<sup>1\*</sup>

<sup>1</sup>Junior Research Group Microbial Biotechnology, Leibniz Institute DSMZ—German Collection of Microorganisms and Cell Cultures, Braunschweig, Germany, <sup>2</sup>Tianjin Institute of Industrial Biotechnology, Chinese Academy of Sciences, Tianjin, China, <sup>3</sup>College of Biotechnology, Tianjin University of Science and Technology, Tianjin, China, <sup>4</sup>Research Group Metabolomics, Leibniz Institute DSMZ—German Collection of Microorganisms and Cell Cultures, Braunschweig, Germany, <sup>5</sup>Junior Research Group Plastic Biodegradation, Institute of Biochemistry, Department of Biotechnology and Enzyme Catalysis, University of Greifswald, Greifswald, Germany, <sup>6</sup>Department of Biotechnology and Enzyme Catalysis, Institute of Biochemistry, University of Greifswald, Greifswald, Germany

## OPEN ACCESS

### Edited by:

Bo Yu,

Institute of Microbiology (CAS), China

### Reviewed by:

Yu Ji,

RWTH Aachen University, Germany

Daochen Zhu,

Jiangsu University, China

### \*Correspondence:

Başak Öztürk

basak.oeztuerk@dsMZ.de

### Specialty section:

This article was submitted to Industrial Biotechnology, a section of the journal Frontiers in Bioengineering and Biotechnology

Received: 27 April 2022

Accepted: 23 May 2022

Published: 21 July 2022

### Citation:

Meyer Cifuentes IE, Wu P, Zhao Y, Liu W, Neumann-Schaal M, Pfaff L, Barys J, Li Z, Gao J, Han X, Bornscheuer UT, Wei R and Öztürk B (2022) Molecular and Biochemical Differences of the Tandem and Cold-Adapted PET Hydrolases Ple628 and Ple629, Isolated From a Marine Microbial Consortium. *Front. Bioeng. Biotechnol.* 10:930140. doi: 10.3389/fbioe.2022.930140

Polybutylene adipate terephthalate (PBAT) is a biodegradable alternative to polyethylene and can be broadly used in various applications. These polymers can be degraded by hydrolases of terrestrial and aquatic origin. In a previous study, we identified tandem PETase-like hydrolases (Ples) from the marine microbial consortium I1 that were highly expressed when a PBAT blend was supplied as the only carbon source. In this study, the tandem Ples, Ple628 and Ple629, were recombinantly expressed and characterized. Both enzymes are mesophilic and active on a wide range of oligomers. The activities of the Ples differed greatly when model substrates, PBAT-modified polymers or PET nanoparticles were supplied. Ple629 was always more active than Ple628. Crystal structures of Ple628 and Ple629 revealed a structural similarity to other PETases and can be classified as member of the PETases IIa subclass,  $\alpha/\beta$  hydrolase superfamily. Our results show that the predicted functions of Ple628 and Ple629 agree with the bioinformatic predictions, and these enzymes play a significant role in the plastic degradation by the consortium.

**Keywords:** biodegradable plastics, PETase-like enzymes, tandem PETases, marine biodegradation, PETase activity

## 1 INTRODUCTION

Biodegradable plastics have been introduced to the market as an ecologically-friendly alternative to recalcitrant plastics (Platt, 2006). These are especially used in applications where the desired product is intended to have a short life (e.g., single-use plastics), and recycling is not feasible or possible (Wei et al., 2020). Difficulties in recycling might appear when plastics contain other types of materials (e.g., paper and other organic matter) (Hopewell et al., 2009; Hahladakis and Iacovidou, 2019). One such biodegradable polymer is polybutylene adipate co-terephthalate (PBAT). PBAT is an aliphatic-aromatic co-polyester synthesized by polycondensation of terephthalic acid (T), adipic acid (A) and 1, 4-butanediol (B) (Jian et al., 2020). Due to its composability and similarity in mechanical



properties, it is marketed as a biodegradable alternative to polyethylene and is widely used to manufacture agricultural mulch films, plastic bags, and paper coatings (BASF, 2022). At the same time, PBAT can be used as a carbon source due to its bioavailability and its low crystallinity makes it accessible to enzymatic degradation (Tiso et al., 2022). The formed products T, A, and B can be further up-cycled to produce new materials (Tiso et al., 2022).

There are numerous known enzymes with PBAT hydrolytic activity. These are cutinase-like serine hydrolases (Kleeberg et al., 2005; Thumarat et al., 2012; Perz et al., 2016b) that originate from the terrestrial environment or the aquatic environment (Wallace et al., 2017). Poly (ethylene terephthalate) (PET) is an aromatic polyester, and PBAT is an aliphatic-aromatic polymer with a terephthalate-diol component. They both share some structural similarities in relation to the T-diol component. PETases can degrade PET (Yoshida et al., 2016) and are assumed to degrade PBAT polymers as well (Kawai et al., 2020). Some PBAT-degrading enzymes can also degrade PET, albeit with less efficiency (Gouda et al., 2002; Kleeberg et al., 2005), possibly due to the high proportion of aromatic moieties in PET (Marten et al., 2005) and higher crystallinity (Wei et al., 2022). Enzymatic PBAT degradation yields a mixture of the terephthalate-butanediol monoester (BT) intermediate and monomers (Perz et al., 2016b). Similarly, the degradation of PET yields a mixture of mono-(2-hydroxyethyl) terephthalic acid (MHET), bis (2-hydroxyethyl) terephthalate (BHET) and monomers (Yoshida et al., 2016). Not all PBAT-degrading enzymes can degrade the BT intermediate: Thc\_Cut1 cutinase from *Thermobifida cellulosilytica* can degrade PBAT efficiently to its monomers (Perz et al., 2016b), while PpEst from *Pseudomonas alcaligenes* cannot degrade the BT intermediate and is inhibited by it (Wallace et al., 2017). Although HiC, a cutinase from *Humicola insolens*, is not inhibited by BHET and MHET when incubated with PET (Eugenio et al., 2021), the release of BT after degradation of a PBAT-blend by HiC seems to inhibit the activity of the enzyme (Perz et al., 2016b). Among these enzymes, only PpEst (Wallace et al., 2017) originates from the aquatic environment. PE-H from the marine bacterium *Pseudomonas aestusnigri* was shown to degrade PET, but the activity of this enzyme was not tested on PBAT (Bollinger et al., 2020).

We have previously identified two putative PETase-like enzymes (Ples) from a marine microbial consortium, named “I1,” which grows on a commercial PBAT-blend film (ecovio® FT 2341) as the only carbon source (Meyer-Cifuentes et al., 2020). These enzymes were named Ple628 and Ple629. The genes encoding for these enzymes are in tandem, with a few hundred bases and no open reading frames in between. The enzymes were characterized as  $\alpha/\beta$  hydrolases, and had the lipase/esterase signature GX SXG (Ollis et al., 1992; Arpigny and Jaeger, 1999). They are closely related to each other (74% amino acid (aa) identity) and to known PETases such as the *Ideonella sakaiensis* PETase (IsPETase) (A0A0K8P6T7, GAP38373) (Yoshida et al., 2016), leaf compost cutinase LCC (AEV21261.1) (Sulaiman et al., 2012) and *Thermobifida fusca* cutinase Thf42\_Cut1 (ADV92528.1) (Herrero Acero et al., 2011) (45–50% aa identity). Metatranscriptomic and proteomic analyses showed

that the genes encoding these enzymes were highly upregulated during incubation with the commercial PBAT-blend, and the production of the proteins increased, especially in the biofilm growing on the plastic film (Meyer-Cifuentes et al., 2020). We postulated that these enzymes perform the depolymerization of ecovio® FT 2341, and in the process release BT (named previously as “Bte”) as well as aliphatic oligomers (Meyer-Cifuentes et al., 2020). The BT then gets degraded to B and T by a third enzyme, Mle046, whose function we have recently verified after recombinant expression and biochemical analysis (Meyer-Cifuentes and Öztürk, 2021). The functions of Ple628 and Ple629, their differences and biochemical properties, however, remained unverified.

In this study, we recombinantly expressed, purified and characterized Ple628 and Ple629 as marine PET hydrolases. In this framework, we comparatively analyze their kinetic properties, degradation products, and activity on smaller PBAT oligomers (supplied as powder), ecovio®FT, PBAT, and PBSeT (supplied as film), as well as PET nanoparticles. We also elucidate and analyze the structures of both proteins by crystallography.

## 2 RESULTS

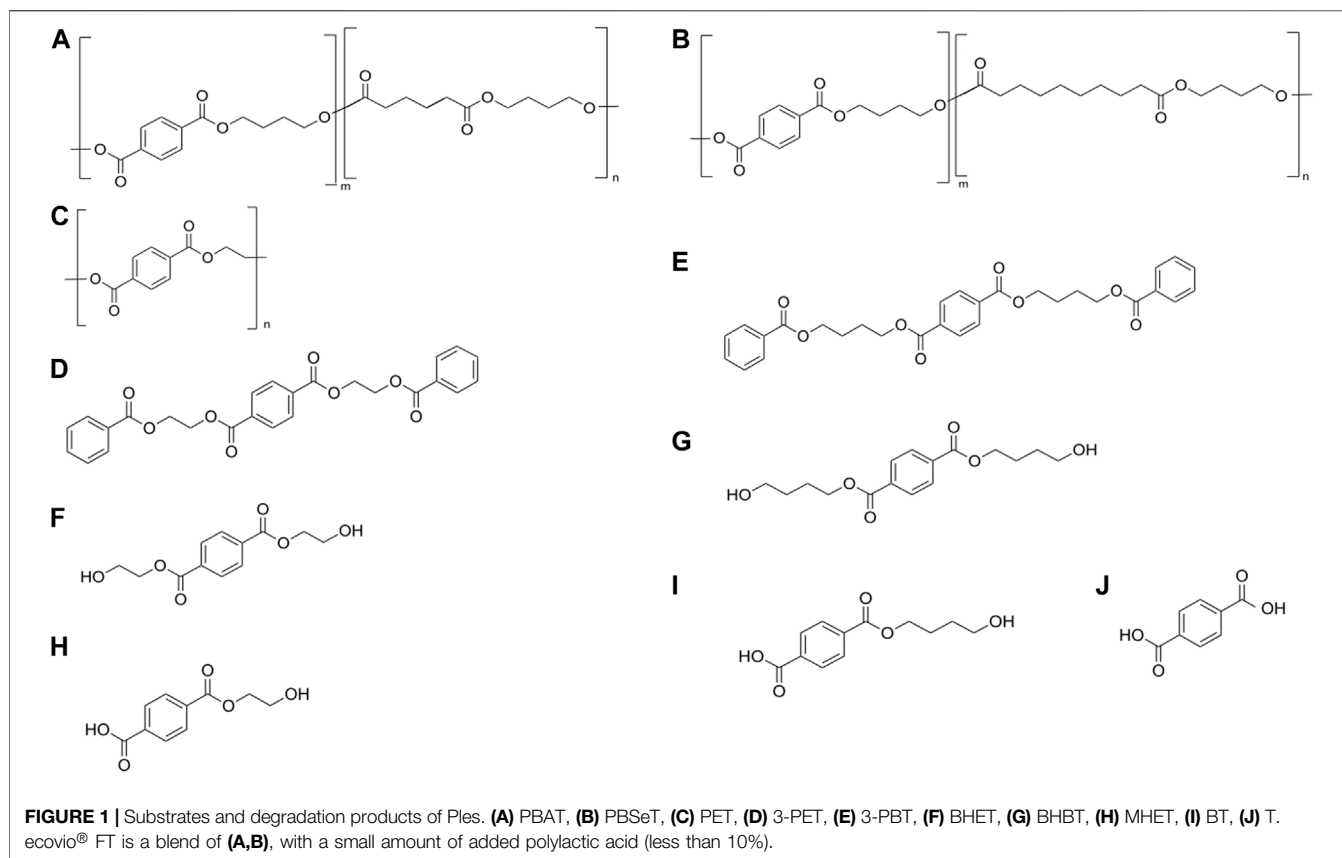
### 2.1 Ple628 and Ple629 Purification and Identification

The Ple628 and Ple629 sequences were retrieved from a previous study (Meyer-Cifuentes et al., 2020). Phylogenetic analysis of Ple628 and Ple629 and other PETase-like enzymes were described in more detail in the previously mentioned study (Meyer-Cifuentes et al., 2020). These two enzymes were phylogenetically classified as type IIa PETases (Supplementary Figure S1). Additionally, the *ple628* and *ple629* sequences used in this study were codon optimized for recombinant protein expression. We successfully produced and purified Ple628 and Ple629 from *E. coli* Origami (DE3). The sizes were similar to those predicted bioinformatically (32.6 and 31.7 kDa for Ple628 and Ple629, respectively) (Supplementary Figure S2). The purest fractions of each protein were pooled and used in this study. The substrates and degradation products that were tested and measured in this study are given in Figure 1.

### 2.2 Kinetic Parameters of Ple628 and Ple629

To further analyze the differences observed between Ple628 and Ple629, we determined their enzymatic kinetic parameters,  $K_m$  and  $k_{cat}$ . These parameters were obtained by measuring the hydrolysis of (4-nitrophenyl) acetate (pNPA). We observed that Ple628 had a higher affinity for the substrate pNPA compared to Ple629. Ple628 required 1.8 mM of the substrate to saturate half of the Ple628 present in the reaction, while Ple629 required 2.1 mM. However, the calculated turnover rate was higher for Ple629 ( $284.5 \text{ min}^{-1}$ ) than for Ple628 ( $269.9 \text{ min}^{-1}$ ). This observation indicates that Ple629 hydrolyses the small substrate pNPA somewhat faster than Ple628.

The kinetic parameters of Ple629 on ecovio®FT film were calculated by plotting different Ple629 concentrations against the



rates of ecovio® FT degradation [inverse Michaelis-Menten ( $^{inv}MM$ )]. This method allows the analysis of enzymatic activities and subsequent calculation of kinetic parameters of enzymes acting on insoluble substrates (Bååth et al., 2021; Vogel et al., 2021). For the analysis, we tested concentrations from 0.5 to 6.5  $\mu M$  of Ple629 and measured the formation of BT and T. The highest degradation rate was achieved with 4.5  $\mu M$  of Ple629. The  $^{inv}K_m$  is 1.86  $\mu M$  and the  $^{inv}k_{cat}$  is 0.017  $h^{-1}$ .

## 2.3 Activity of Ple629 and Ple628 on Small Terephthalate-Esters

We analyzed the range of action of both enzymes, Ple629 and Ple628, on oligomeric model substrates of PBAT and PET. The substrates tested were bis(2-(benzoyloxy)ethyl) terephthalate (3-PET), bis(4-(benzoyloxy)butyl) terephthalate (3-PBT), bis(hydroxyethyl) terephthalate (BHET) and bis(4-hydroxybutyl) terephthalate (BHBT). All these model substrates were supplied as powder. The formation of the degradation products, BT, MHET, and T, was monitored after 1, 2, and 24 h of incubation. For the degradation of BHET, an additional sampling point after 30 min was included.

We observed that Ple629 could degrade 3-PET and, to some extent, 3-PBT. Ple629 incubation with 1 mg of 3-PBT released a maximum amount of 35.9  $\pm$  4.1  $\mu M$  of BT after 24 h (Figure 2). In comparison, when 1 mg of 3-PET was used as the substrate, more than 2,000  $\mu M$  of MHET was formed. The catalysis of 3-PET by

Ple629 also yielded high amounts of T after 24 h of incubation (approximately 1,900  $\mu M$  of T). Formation of T after 3-PBT degradation by Ple629 was only detected after 24 h of incubation. Conversely, Ple629 incubation with 3-PET yielded T readily after 1 h of incubation. Ple628 could also degrade 3-PET but to a lesser extent than Ple629. Relative to MHET formation after 3-PET degradation by Ple629, we detected less than 30% of MHET formation (601.6  $\pm$  374.1  $\mu M$  of MHET) when Ple628 was incubated with 3-PET. Consequently, Ple628 produced low amounts of T (13.4  $\pm$  8.0  $\mu M$ ) which were only detected after 24 h of incubation. Similar to Ple629, Ple628 had poor activity on 3-PBT. With Ple628, a maximum of 4.7  $\pm$  0.8  $\mu M$  of BT was released after 24 h of incubation. Only 0.6  $\pm$  0.5  $\mu M$  of T was detected when Ple628 was incubated after 24 h with 3-PBT.

The intermediates of 3-PET and 3-PBT degradation, BHET and BHBT, respectively, were also degraded by Ple628 and Ple629. Ple629 achieved maximum MHET formation after 2 h of incubation with BHET (758.2  $\pm$  60.9  $\mu M$ ) (Figure 2). T was also formed after 30 min, and its production increased throughout the incubation. The maximum amount of T produced was 194.7  $\pm$  4.3  $\mu M$  after 24 h. Compared to BHET degradation, Ple629 showed lower activity with BHBT. With BHBT, the maximum amounts of BT and T formed after 24 h of incubation were 513.2  $\pm$  31.4 and 42.3  $\pm$  1.9  $\mu M$ , respectively. Conversely, the incubation of Ple628 with the substrate BHET produced less MHET than with Ple629. After 30 min and 24 h, only 8.4 and 112.9  $\pm$  2.0  $\mu M$  of MHET were formed, respectively.

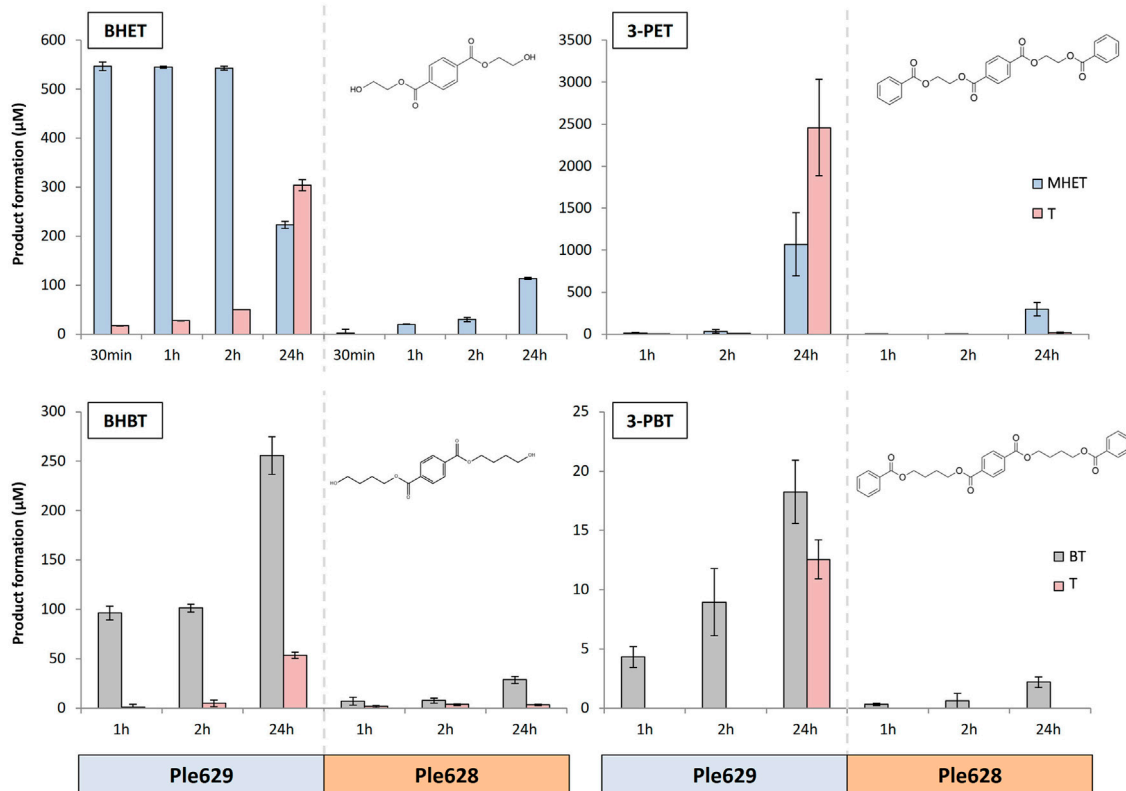


**FIGURE 2 |** Degradation of small terephthalate-esters by Ples. Formation of T (dark pink) and MHET (light blue) or BT (light gray) (in  $\mu\text{M}$ ) after degradation of BHET, BHBT, 3-PET, and 3-PBT by Ple628 and Ple629. The degradation of BHET and 3-PET leads to the formation of MHET and T and the degradation of BHBT and 3-PBT to the formation of BT and T. The molecular structure of each substrate is shown at the uppermost right corner of each bar plot. The sampling points are shown at 30 min, 1 h, 2 h, and 24 h. The error bars indicate the standard deviation ( $n = 3$ ).

We did not detect T production at any time point, which indicates that MHET was not further hydrolyzed to T and ethylene glycol. Compared to MHET formation after BHET degradation by Ple628, low amounts of BT were formed when BHBT was used as the substrate. After 24 h of incubation, Ple628 could form only  $56.93 \pm 5.9 \mu\text{M}$  of BT. Traces of T were detected at each time point ( $1.6 \pm 1.0$  to  $2.1 \pm 0.5 \mu\text{M}$  T).

## 2.4 Temperature Optima of Ple628 and Ple629

Ple628 and Ple629 were incubated at different temperatures for 72 h to find the temperature range that gave the highest activity. When using ecovio® FT as film, we found that Ple629 and Ple628 are mostly active at 30°C (Figure 3). Relative to the Ples enzymatic activity observed at 30°C, the Ples retained most of their activity when the incubation temperature was reduced to 20°C. At 20°C, the Ple629 and Ple628 produced (relative to 30°C) 68 and 58% of BT, respectively. On the contrary, temperatures above 30°C negatively affected the activity of both enzymes. When Ple628 or Ple629 were incubated at 40°C, the BT formation dropped to 31% and 18% compared to the product formation at 30°C, respectively. At 60°C, the highest temperature

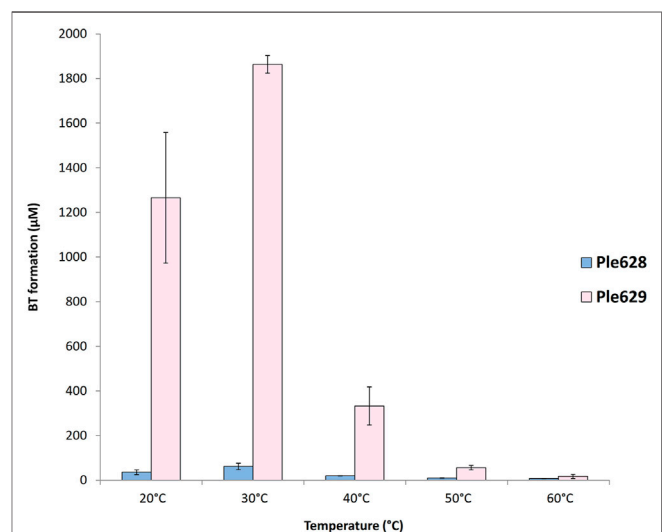


**FIGURE 3 |** Ples temperature optimum of incubation. Formation of BT (in  $\mu\text{M}$ ) after degradation of ecovio® FT by Ple628 and Ple629. Ple628 and Ple629 are shown in blue and pink, respectively. The tested temperatures were 20, 30, 40, 50, and 60°C. The error bars indicate the standard deviation ( $n = 3$ ).

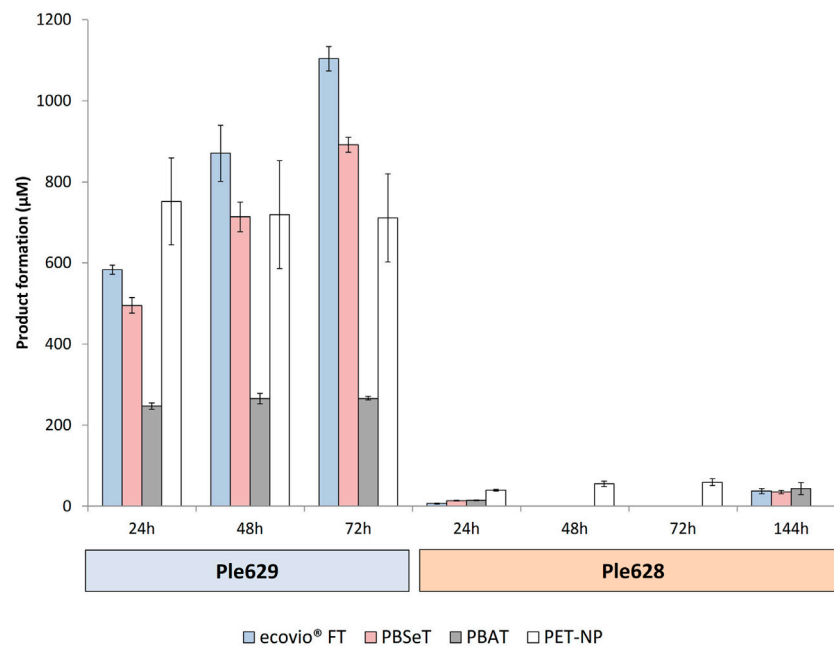


**FIGURE 4 |** Degradation of biodegradable plastics and PET-NP by Ples. Formation of BT or MHET (in  $\mu\text{M}$ ) after degradation of ecovio® FT (light blue), PBAT (light gray), PBSeT (dark pink) and PET-NP (white) by Ple629 and Ple628. The degradation of biodegradable plastics and PET-NP leads to the formation of BT and MHET, respectively. The sampling points are shown at 24, 48, 72, and 144 h. The error bars indicate the standard deviation ( $n = 3$ ).

tested, the BT formation dropped further to 12 and 0.9% for Ple628 and Ple629, respectively. T was also formed, but only in the presence of Ple629. Specifically, T was detected when Ple629 was incubated at 20, 30 and 40°C exclusively. At higher temperatures, T was undetectable. No products were released in the absence of an enzyme at temperatures  $\geq$  of 50°C. This indicates that the substrate ecovio® FT and the intermediate BT are not affected by auto-hydrolysis at 50°C.

The melting temperatures ( $T_m$ s) of Ple628 and Ple629 were determined to be 41.4°C and 38.1°C in PBS by nanoDSF, and 47.1°C and 43.2°C by DSC (Supplementary Table S1), respectively.

## 2.5 Activity of Ple629 and Ple628 on Biodegradable Plastic Films and PET Nanoparticles

The activity of the enzymes Ple629 and Ple628 was tested on PBAT, PBSeT, ecovio® FT films and on PET nanoparticles (PET-NP) at 30°C over time. We observed that both enzymes, Ple628 and Ple629, can hydrolyze all tested polymers. Compared to Ple629, however, Ple628 was less active on all tested polymer substrates. Ple628 produced low amounts of BT, the intermediate product of ecovio® FT degradation, in the presence of PBAT, PBSeT or ecovio® FT. Even after 144 h of incubation, Ple628 produced less than 50  $\mu\text{M}$  of BT with either of the tested polymers. Ple629 yielded  $1,103.6 \pm 29.8$ ,  $891.5 \pm 18.6$  and  $265.9 \pm 4.2 \mu\text{M}$  of BT after 72 h with ecovio® FT, PBSeT and PBAT (Figure 4). Comparable to the assays with the biodegradable plastics, Ple628 produced low amounts of

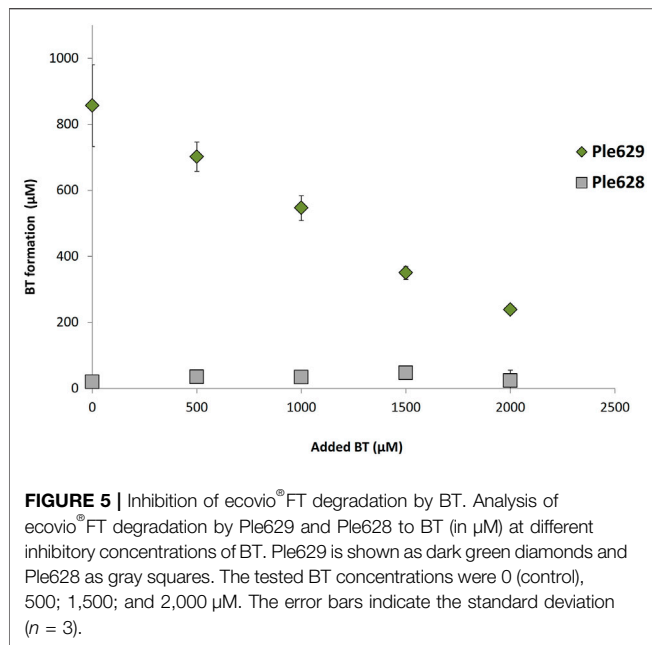
MHET after PET-NP degradation. After 72 h, Ple628 released only  $52.9 \pm 1.1 \mu\text{M}$  of MHET, compared to  $785.9 \pm 27.8 \mu\text{M}$  of MHET released by Ple629 (Figure 4). The product formation did not significantly increase between 48 and 72 h of incubation for any of the enzymes.

To some extent, Ple629 could degrade the biodegradable plastic films to T. After 72 h,  $35.1 \pm 2.5$ ,  $31.2 \pm 1.6$  and  $18.9 \pm 1.3 \mu\text{M}$  of T were detected after degradation of ecovio® FT, PBSeT, and PBAT, respectively (Supplementary Figure S3). Surprisingly, Ple629 released high amounts of T after PET-NP degradation, reaching a maximum of  $736.3 \pm 12.0 \mu\text{M}$  after 72 h of incubation. As expected, lower amounts ( $9.5 \pm 1.3 \mu\text{M}$ ) of T were released in the presence of Ple628. When the plastic polymers were supplied as the substrate, less than 1  $\mu\text{M}$  of T was formed.

Interestingly, with PBAT as the substrate, the production of BT by Ple629 ceased after 24 h and remained the same between 48 and 72 h ( $265 \pm 0.03 \mu\text{M}$ ). This observation might indicate that Ple629 has limited activity on PBAT compared to the other polymers tested (Figure 4). By comparing the amount of products (BT and T) released in the presence of Ple629, we could also observe that the enzyme degrades more efficiently ecovio® FT over PBSeT and PBAT. We detected insignificant degradation of untreated (without addition of Ple629 or Ple628) ecovio® FT and PBSeT to BT ( $3.5\text{--}11.0 \mu\text{M}$  BT released after 72 h).

We additionally semi-quantitatively analyzed the release of T and other products by LC-MS after degradation of PBAT and PBSeT by Ple629 or Ple628. A, T and sebacic acid (S), the building blocks of the tested PBAT-like films and mixtures of these





monomers were detected (Supplementary Figure S4). The amount of each monomer increased in each reaction after 72 h of incubation. When Ple628 was incubated with either PBAT or PBSeT, T was detected only after 72 h. Conversely, T was readily produced and detected after 24 h when PBAT or PBSeT were incubated with Ple629. The amount of T produced after 72 h was 75-times higher after degradation by Ple629 than Ple628 for both plastics. BT was the only compound detected consistently in all assays. The amount of BT increased 3 times between 24 and 72 h of degradation when PBAT or PBSeT was incubated with Ple629. Approximately 1.5 times more BT was detected when PBSeT was used as the substrate than when PBAT was used. For Ple628, no significant change in BT concentration was observed between these time points. The total amount of BT produced by Ple628 was 6 times less than Ple629 when PBAT was used as a substrate, and 10 times less when PBSeT was used. A mixture of adipate-butanediol (A + B) was only detected after degradation of PBAT with Ple628. Sebacic acid + butanediol (S + B) was not detected in any assay. S and A were both detected in experiments supplied with PBAT and PBSeT, even though PBAT does not contain S and PBSeT does not contain A. This is likely due to cross contamination during the successive extrusion of the films for the study.

## 2.6 Inhibition of ecovio® FT Degradation by BT

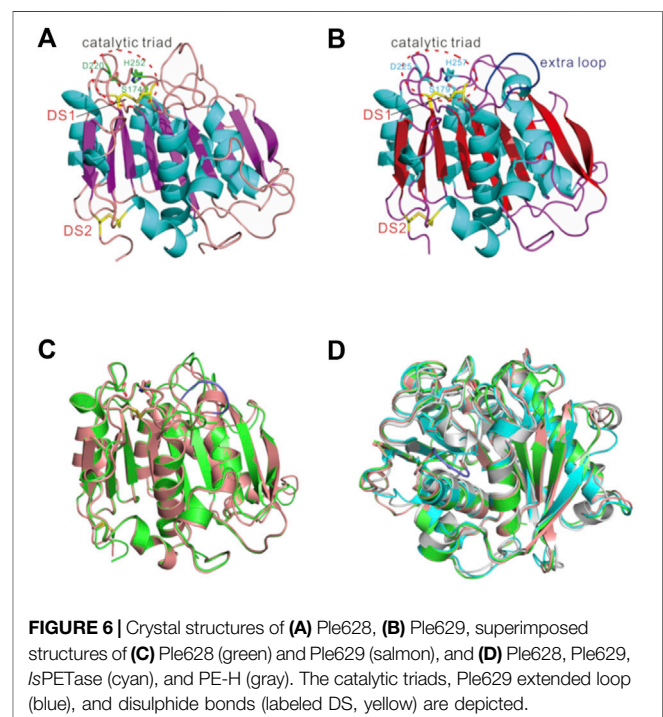
Films of ecovio® FT were incubated with Ple628 and Ple629 and with increasing concentrations of BT. Previously, homologous enzymes with PET hydrolyzing activities were found to be inhibited by the intermediates BHET and MHET (Barth et al., 2015, 2016). Therefore, we aimed to determine if the activities of Ple628 and Ple629 are also inhibited by intermediates of ecovio® FT degradation, specifically BT. Without the addition

of BT, the degradation of 5 mg of ecovio® FT yielded 204 mg/L of BT. Reactions supplied with more than 1,000 µM of additional BT released less than 50% (Figure 5) of the BT formed by subtracting the amount of supplementary BT. This observation indicates that Ple629 is inhibited by this degradation product. As shown before, Ple628 already had very low activity on ecovio® FT and released only small amounts of BT with or without the addition of external BT. Because of this, we could not assess product inhibition of Ple628 by BT.

## 2.7 Ple628 and Ple629 Sequences and Crystal Structures Reveal Similarity to Known PETases

For structural determination of Ple628 and Ple629, the signal peptide sequences (M1-A25 for Ple628, and M1-A27 for Ple629) were removed for the production of the core domain of the protein. As predicted from the sequence homology to the lipase and cutinase families, Ple628 and Ple629 both belong to the  $\alpha/\beta$  hydrolase superfamily, and the central twisted  $\beta$ -sheet is formed by nine mixed  $\beta$ -strands ( $\beta 1$ – $\beta 9$ ) and surrounded by eight  $\alpha$ -helices (Figures 6A,B). The catalytic triad S174/S179-D220/D225-H252/H257 was conserved among all PETase-like proteins (positions in Ple628/Ple629, respectively). Like previously described for IsPETase and PE-H (Joo et al., 2018; Bollinger et al., 2020; Wei et al., 2022), Ple628 and Ple629 form two disulfide bridges, DS1(C217-C254/C222-C259) and DS2(C288-C305/C297-C314) (positions in Ple628/Ple629, respectively). The data collection and refinement statistics are given in Supplementary Table S2.

The main structural difference between Ple628 and Ple629 was the presence of an extended loop in Ple629, which is longer than



the one present in Ple628, with the four extra residues S264, G265, F266, and G267 (**Figure 6C**). Ple628 has a shorter extended loop, similar to the *IsPETase* (Joo et al., 2018) and PE-H (Bollinger et al., 2020) (**Figure 6D**). The root-mean-square deviation (RMSD) of atomic positions of Ple628, Ple629, and previously characterized PETases and other hydrolases confirmed that Ple629 is more similar to mesophilic PETases such as PE-H and *IsPETase* than it is to LC-cutinase and Est119 (**Supplementary Table S3**). Interestingly, Ple629 is structurally more similar to the marine PETase PE-H than to Ple628.

### 3 DISCUSSION

In this study, we purified and biochemically characterized two tandem PETases from a marine microbial consortium that grows on the aliphatic-aromatic co-polyester ecovio®FT. These PETases degrade a broad range of aromatic and aromatic-aliphatic polyesters at moderate temperatures and perform the first step of ecovio®FT degradation by the marine consortium that they originate from (Meyer-Cifuentes et al., 2020).

To understand the mode of action and differences between Ple628 and Ple629, derivatives of PBAT and smaller oligomeric model substrates were used. The other PETases and PBAT hydrolases that are referenced in this section for comparison are summarized in the **Supplementary Table S4**. We observed that, in general, Ple628 has a lower activity with all the insoluble polyesters tested than Ple629. In different experiments, we detected the formation of BT, MHET, and T, with BT or MHET being the main degradation product. Similar studies have found that PET degradation by TfCut2, a cutinase isolated from *Thermobifida fusca* KW3, leads to the production of mainly MHET (the counterpart of BT in PET degradation) (60–70%), followed by BHET (14%) and T (8–32%) (Wei et al., 2016). Other studies also showed that some PETases, such as *IsPETase*, Mors1, PE-H and LCC, produce mainly MHET as the primary hydrolysis product rather than T after PET degradation (Yoshida et al., 2016; Bollinger et al., 2020; Blázquez-Sánchez et al., 2021; Erickson et al., 2022). However, other studies have observed T as the main hydrolysis product rather than MHET when *IsPETase* was incubated with amorphous PET films (Joo et al., 2018; Blázquez-Sánchez et al., 2021). In contrast to the assays performed by Yoshida et al. (Yoshida et al., 2016), Blázquez-Sánchez et al. (Blázquez-Sánchez et al., 2021) and Joo et al. (Joo et al., 2018), both used higher amounts of *IsPETase* (>100 nm) and longer incubation times (>24 h). This is an indication that the main source of T release was the hydrolysis of the secondary degradation from other oligomers, including MHET itself. *IsPETase* degrades MHET but at a very slow rate, and this was observed for other *IsPETase* variants as well (Brott et al., 2021).

During PET degradation, the formation of T is also possible to a lesser degree due to terminal digestions of the polymer containing T-terminal by PETase-like enzymes (Joo et al., 2018). In our study, T was produced to some extent, especially when BHET and PET-NP were supplied as the substrate. This observation suggests that BHET is a better substrate for Ple628

and Ple629 than its counterpart substrate, BHBT. During the degradation of ecovio®FT and its blend components, BT tended to accumulate as a degradation product. The further hydrolysis of this intermediate to T requires several hours in most cases. Similar to our study, low degradability of the hydrolysis products of PET degradation by single hydrolases has been observed before (Kleeberg et al., 2005). For instance low degradability of MHET by the cutinase HiC from *Humicola insolens* has been observed repeatedly (Carniel et al., 2017; de Castro et al., 2017). Likewise, another study performed on two cutinases, HiC and Thc-Cut1, the latter isolated from *T. cellulositica*, showed that HiC has poorer activity on the products released after the degradation of PBAT than Thc-Cut1, and Thc-Cut1 converted BHBT to T without the accumulation of BT (Perz et al., 2016b). In contrast to HiC, Ples have higher activity on T esterified with shorter alcohols (BHET over BHBT). Yet, HiC can degrade BHET quickly when supplied as a single substrate (Carniel et al., 2017). With PBAT, HiC cleaved butanediol-adipic acid ester bonds (B + A) better than BT (Perz et al., 2016b). It must be stressed, however, that in nature, ecovio®FT, PBAT, and PBSeT can be completely degraded by the action of other microbes in the consortium carrying downstream-pathway enzymes required for the complete mineralization of these biodegradable polymers (Meyer-Cifuentes et al., 2020).

The activity of Ples on ecovio®FT can be limited by product inhibition, e.g., BT. Similarly to our observations that BT inhibits ecovio®FT degradation, Barth et al. (Barth et al., 2015) found that the cutinase TfCut2 can be inhibited by the PET degradation products, MHET and BHET. Additionally, they observed that both products have a similar effect on the hydrolysis of PET by TfCut2. The same was observed for another cutinase, the LCC (Barth et al., 2016). In natural environments, the inhibition of Ples by BT can be relieved by the presence of another type of enzyme, namely Mles, as described before (Meyer-Cifuentes et al., 2020; Meyer-Cifuentes and Öztürk, 2021).

The  $^{inv}MM$  kinetics on ecovio®FT showed that the maximal turnover rates were achieved at 4.5  $\mu M$  Ple629, after which a saturation point was reached, and the turnover rates dropped. A similar phenomenon was observed during the degradation of PET by HiC, TfC, and *IsPETase* (Bååth et al., 2021), as well as the LCC (Abhijit et al., 2018), and it is explained by the overcrowding of the enzyme surface (Mukai et al., 1993; Hiraishi et al., 2010; Bååth et al., 2021) and the rapid depletion of suitable attack sites on the enzyme surface (Scandola et al., 1998). The  $^{inv}K_m$  value of Ple629 on ecovio®FT of 1.86  $\mu M$  is higher than that of *IsPETase* on PET at 40°C (0.039) and TfC and HiC on PET at 50°C (0.026 and 0.043, respectively) by approximately 50-times (Bååth et al., 2021). Although the results are difficult to compare as the substrates used are different, ecovio®FT required more enzyme to reach saturation than PET.

Bååth et al., observed that 3-PET (denoted as BETEB in the publication) gave much higher turnover rates than amorphous PET (Bååth et al., 2021) with *IsPETase*. PBAT hydrolases Ppest (Wallace et al., 2017) and Cbotu\_EstA (Perz et al., 2016a) released more products when 3-PBT (denoted as BABuTABuBA in these publications) was used than when PBAT was used. In our study,

Ple629 released more products per mol enzyme when the model substrate 3-PET was used compared to nano-PET particles, but much less when 3-PBT was used compared to ecovio® FT and its blend components. Perz et al., also observed that the degradation rates for 3-PBT were much lower than for PBAT (Perz et al., 2016b). It has been previously demonstrated that molecules that contain more aliphatic domains are more readily degraded than those that contain a high proportion of B + T bonds, which are very rigid (Gan et al., 2004; Marten et al., 2005; Kasuya et al., 2009; Perz et al., 2016b). PBAT also has a low crystallinity (around 10%), while 3-PBT is highly crystalline, which may account for its low degradability (Perz et al., 2016b). Similar to 3-PET and 3-PBT, far more degradation products were released when BHET was used compared to BHBT, suggesting that this substrate possibly fits the enzyme active site better.

The degradation of PET-NP has been analyzed similarly with IsPETase and variants of IsPETase at different temperatures in a previous study (Brott et al., 2021). By comparing the total amount of products formed after 24 h of incubation at 30°C we observed that Ple629 presents better activity than the IsPETase wild type (WT) and than each variant tested in that study (Brott et al., 2021). Between 30 and 60°C, IsPETase WT and the different IsPETase variants produced less than 400 µM of MHET, T and BHET together, while Ple629 produced more than 1,200 µM of MHET and T together. The activity was comparable to the activity of an engineered high-thermal stability variant of IsPETase, namely DuraPETase, and its variants incubated at 60°C, which indicates that Ple629 has enhanced degradation capabilities towards PET-NP. Similarly, DuraPETase has increased degradation activity against highly crystalline PET films compared to IsPETase (Cui et al., 2021). Unlike IsPETase and DuraPETase, however, Ple629 did not degrade PET film.

The crystal structures of Ple628 and Ple629 are highly similar to those of previously characterized PETases. Both enzymes are classified as IIa PETases (**Supplementary Figure S1**), like the other characterized marine PETase, PE-H (Bollinger et al., 2020). Both enzymes possessed two disulfide bonds. The second disulfide bond, which is in the proximity of the active site, was shown to improve the activity of IsPETase (Fecker et al., 2018; Joo et al., 2018), and is also present in the other type IIa and IIb enzymes such as PE-H (Bollinger et al., 2020) and Mors1 (Blázquez-Sánchez et al., 2021) (**Supplementary Figure S1**).

Other activities of other tandem cutinases with high amino acid identity have previously been shown to be different, both on small substrates and plastic polymers (Herrero Acero et al., 2011; Thumarat et al., 2015; Perz et al., 2016a; Arnling Bååth et al., 2022). The tandem cutinases in these studies had even higher amino acid identity to each other than Ple628 and Ple629, demonstrating that even a few amino acid differences can lead to differences in activity in closely related enzymes. For Ple628 and Ple629, some factors that could contribute to the difference in activity are: 1) the differences in the amino acids next to the catalytic H (H252 in Ple628 and H257 in Ple629), which have been shown to influence the activity of IsPETase (Joo et al., 2018) and PE-H (Bollinger et al., 2020); 2) the presence of a longer

extended loop in Ple629, which was previously proposed to be an extra substrate binding site for IsPETase (Chen et al., 2018) (**Figure 6B**). Likely, a combination of these factors is necessary to explain the difference in activity.

The findings of this study confirm the proposed functions of Ple628 and Ple629 as PET hydrolases with an activity on PBAT and its derivatives. These enzymes depolymerize PBAT and its derivatives, as well as PET nanoparticles to their monomers, with the aromatic terephthalate-diol monoester as the intermediate degradation product. In nature, the formed monomers and oligomers are further degraded by the action of other hydrolases, as well as oxidoreductases, lyases, etc. released by different bacteria (Sasoh et al., 2006; Yoshida et al., 2016; Li et al., 2020; Meyer-Cifuentes et al., 2020; Meyer-Cifuentes and Öztürk, 2021). In this study, Ple629 had higher catalytic activity than Ple628 both on polymeric and oligomeric substrates. In our previous study, the fold upregulation for *ple628* gene expression was higher than for *ple629* during ecovio FT degradation (Meyer-Cifuentes et al., 2020). The Ple629 protein was only detected when the biofilm proteome was examined separately, and not in the whole community proteome. These findings led to the hypothesis that Ple628 played a bigger role in ecovio FT degradation than Ple629. The underlying mechanism of gene expression regulation of these tandem cutinases is not known, and why the less active enzyme is produced at higher levels is unclear. Due to its much higher activity, however, we now postulate that Ple629 could also play a significant role in ecovio FT degradation, although its expression levels are low, and should be included in the overall ecovio FT degradation mechanism by the marine microbial consortium II.

## 4 MATERIALS AND METHODS

### 4.1 Chemicals and Substrates

Ecovio® FT 2341, and its blend components PBAT and PBSeT were supplied by BASF SE as plastic films. All other model substrates were in-house synthesized. The structures and synthesis protocols of the substrates BHET, BHBT, 3-PET, 3-PBT, and PET-NP are given in the **Supplementary Material**.

### 4.2 Recombinant Expression and Purification of Ple628 and Ple629

The signal peptides for both proteins were predicted with SignalP 5.0 (Almagro Armenteros et al., 2019). These were excluded from the final protein construct. Codon-optimized *ple628* and *ple629* were synthetically produced and cloned into the pCold II plasmid with an N-terminal His-Tag by BioCat GmbH (Germany). The plasmids were chemically transformed into *E. coli* Origami (DE3) (Merck, Germany) cells. Pre-cultures of 4-5 transformants were grown at 30°C overnight. The cultures were inoculated 1:500 into 500 ml of TB supplemented with ampicillin to an end concentration of 100 mg/L. The cultures were grown to an OD<sub>600</sub> of 0.8–1 at 37°C, 140 rpm on a MaxQ™ 4,000 orbital shaker (Fischer Scientific, Germany). After induction with 0.5 mM IPTG, the cultures were grown further to an OD<sub>600</sub> of



2, and then overnight at 16°C, 140 rpm. The cell pellets were collected by centrifugation at 4°C, 6,000 × g for 10 min in an Avanti J-26 XPI centrifuge with a JA-14 rotor (Beckman Coulter, United States). The pellets were frozen at −20°C for 20 min, and resuspended in His-Tag binding buffer (20 mM sodium phosphate and 0.5 M NaCl, pH 7.4) at a ratio of 1:10 of the culture volume. Cells were disrupted by sonication with a Sonopuls HD2070 sonicator (Bandelin, Germany). Cell lysates were cleared by centrifugation at 4°C 15,000 × g for 30 min in an Avanti J-26 XPI centrifuge with a JA-14 rotor (Beckman Coulter, United States) and filtrated through a 0.2 µm filter.

The proteins were purified in the same manner as described previously (Meyer-Cifuentes and Öztürk, 2021). Briefly, the cleared lysates were purified on a 5 ml His-Trap<sup>TM</sup> HP affinity Ni-Sepharose column (Cytiva, Germany) connected to an ÄKTA<sup>TM</sup> Start Purification System (Cytiva, Germany). Proteins were bound and eluted from the column by using the predefined affinity purification protocol included in the UNICORN<sup>®</sup> start 1.1 software (Cytiva, Germany). The purity of the fractions presenting a peak was determined by SDS-PAGE. These fractions were further concentrated and desalted on a Pierce<sup>TM</sup> Protein Concentrator PES 10K MWCO (Thermo Fischer Scientific, United States). The fractions were further polished by size exclusion chromatography on a HiPrep<sup>TM</sup> 16/60 Sephacryl<sup>TM</sup> S-200 HR column (Cytiva, Germany) connected to an ÄKTA<sup>TM</sup> Start Purification System (Cytiva, Germany) in a buffer consisting of 25 mM Tris-HCl and 200 mM NaCl, pH 7.5. Fractions containing the pure protein were determined by SDS-PAGE, pooled and concentrated on a Pierce<sup>TM</sup> Protein Concentrator PES 10K MWCO (Thermo Fischer Scientific, United States). The concentration of the purified protein was determined with the Qubit Protein Assay kit and measured on a Qubit 3.0 Fluorometer (Invitrogen, United States).

### 4.3 Km and Kcat Determination

In a 96-well-plate, the purified Ple628 or Ple629 (end concentration 0.005 µg/µl) was combined with pNPA with concentrations ranging from 0.1–2.5 mM in 60 µl PBS, pH 7.0. The formation of 4-nitrophenolate was measured continuously at 405 nm at 20°C in a TECAN Infinite<sup>®</sup> M200 plate reader (TECAN, Switzerland) and retrieved using the TECAN i-control v. 1.5.14.0 software (TECAN, Switzerland). The concentration of 4-nitrophenolate was calculated using a standard series in the reaction buffer and measured under the same conditions. Each assay was performed in triplicate. Km, Vmax and kcat were determined by non-linear least squares regression (<http://biomodel.uah.es/en/metab/enzymas/MM-regresion.htm>, last accessed 19.10.2021).

### 4.4 Activity Assay on Small Terephthalate-Esters

Activity assays with BHET and BHBT were performed in 20% DMSO in PBS, pH 7.0, to keep the substrates soluble at a final concentration of 0.5 mM. As the substrates 3-PET and 3-PBT were not soluble in this reaction buffer, they were treated as

insoluble substrates, and the reactions were performed in PBS, pH 7.0. One mg of 3-PET or 3-PBT was used per assay. The final reaction volume for each experiment was 200 µl, and the final concentration of Ple628 or 629 was 0.156 µM. 50 µl of sample was taken after 1, 2, and 24 h. An additional 50 µl samples were taken for the BHET assays after 30 min. The reactions were stopped by the addition of 50 µl of cold methanol. The inactivated reactions were centrifuged for 10 min at 12,000 × g at 20°C to remove the debris, and the filtrates were transferred to HPLC vials. The degradation products BT and T were detected with a 1260 Infinity II LC System (Agilent Technologies, United States) equipped with an Agilent Poroshell 120 HPH-C18 column (Agilent Technologies, United States). The measurement protocol was modified from Palm et al., (Palm et al., 2019). A gradient of acetonitrile 99.9% HPLC grade (Fischer Scientific, United States) and 0.1% (v/v) formic acid (98–100% Suprapur<sup>®</sup>, Sigma-Aldrich, United States) in Milli-Q water was used. The flow rate was set at 0.2 ml/min. 10 µl of the sample was injected. Acetonitrile was increased from 5 to 44% until minute 12 and then to 70% at minute 15, remaining constant for 3 min. Both products were detected at 240 nm and the quantification was realized using calibration curves. Reactions without the enzyme were used as negative controls. Trace amounts of product formed in the negative controls were subtracted from the enzyme assay results during the calculation. Each assay was performed in triplicate.

### 4.5 Determination of Melting Points

The melting points of Ple628 and Ple629 were determined by nano differential scanning fluorimetry using the Prometheus NT.48 (NanoTemper Technologies, Germany). The measurement was conducted in ddH<sub>2</sub>O and PBS buffer (pH 7.4) using a protein concentration of 1 mg/ml and a temperature profile from 20 to 95°C at 1°C/min. The instrument has a fixed excitation wavelength of 285 nm in combination with emission wavelengths of 330 and 350 nm.

### 4.6 Activity Assay on Biodegradable Plastic Films and PET-NP

To determine the optimum temperature for ecovio<sup>®</sup>FT degradation, 0.156 µM of Ple628 or Ple629 were incubated with 5 mg of ecovio<sup>®</sup>FT, supplied as film, in 500 µl of PBS at temperatures between 20–60°C, with 10°C increments. After 72 h, the concentrations of BT and T were measured as described above. Each assay was performed in triplicate.

To quantify the degradation of ecovio<sup>®</sup>FT, PBAT and PBSeT, 5 mg of each plastic substrate was immersed in 500 µl of PBS, pH 7.0. Ple628 or Ple629 was added to each assay tube to a final concentration of 0.156 µM. The reactions were incubated at 30 °C. 50 µl samples were taken after 24, 48, and 72 h for incubations with Ple629 and after 24 and 144 h of incubation with Ple628. The concentrations of BT and T were measured as described above. Reactions without the enzyme were used as negative controls. Each assay was performed in triplicate. Additionally, the full spectrum of degradation



products was determined by LC-MS. Samples were analyzed using a 6545 Q-TOF mass spectrometer coupled to a 1290 series HPLC (Agilent, Germany) using an Acquity BEH C18 column (particle size 1.7  $\mu\text{M}$ ,  $2.1 \times 150$  mm, Waters, United States). The samples were run with a 1  $\mu\text{l}$  injection volume at 35°C. The eluents were A (water + 0.1% formic acid) and B (acetonitrile + 0.1% formic acid) using the following gradient: 5–44% B in 12 min, 44–70% B in 3 min, and 70% B for an additional 3 min. Compounds were detected by recording a DAD spectrum (230–640 nm) and by mass spectrometry in negative mode in a mass range of 100–1000  $m/z$  with the following ESI settings: gas temperature 300°C, drying gas 8 L/min, nebulizer 18 psig, sheath gas 350°C and 12 L/min, capillary voltage 3 kV and fragmentor 180 V. MassHunter version B.08.00 software was used for data evaluation.

Heterogenous kinetics of ecovio® FT degradation by Ple629 were determined as described before using inverse Michaelis-Menten kinetics (enzyme concentration vs rate,  $^{inv}\text{MM}$ ) (Scandola et al., 1998; Ronkvist et al., 2009; Wei et al., 2016; Bååth et al., 2021). To determine the  $^{inv}\text{MM}$  kinetics of Ple629, 5 mg of ecovio® FT film was incubated with Ple629, concentrations ranging from 0.5–6.5  $\mu\text{M}$  in 500 ml of PBS, pH 7.0. 50  $\mu\text{l}$  samples were taken after 6 and 24 h, and the concentrations of T and BT were measured as described above. Assays without the enzyme were used as negative controls. Each assay was performed in triplicate. The inverse  $K_m$  ( $_{inv}K_m$ ) and  $k_{cat}$  ( $_{inv}k_{cat}$ ) values were calculated with the linearized form of the kinetic function  $1/V$  against  $1/E_0$ . The following formula was used:

$$v_0 = \frac{k_{cat} \cdot S_0 \cdot E_0}{K_m + E_0}, \quad (1)$$

where  $V$  is the substrate degradation rate measured as ( $\mu\text{M}$  BT produced/h) + ( $\mu\text{M}$  T produced/h),  $S_0$  is the substrate amount in mg, and  $E_0$  is the enzyme concentration in  $\mu\text{M}$ .

PET-NP was produced as previously described (Brott et al., 2021; Pfaff et al., 2021; Vogel et al., 2021). One hundred  $\mu\text{g}$  (0.2 mg/ml) PET-NP were hydrolyzed by 10  $\mu\text{g}$  of Ple628 or Ple629 in a reaction volume of 500  $\mu\text{L}$ . The degradation was performed in triplicates in PBS buffer (pH 7.4) at 30°C and 1,000 rpm for 24, 48, and 72 h in a ThermoMixer C (Eppendorf AG, Germany). The hydrolysis products were analyzed via reverse-phase HPLC on a VWR Hitachi LaChrom Elite system (VWR International, United States) equipped with a Kinetex® column (5  $\mu\text{M}$  EVO C18 100 Å,  $150 \times 4.6$  mm; Phenomenex®, Germany). Ten  $\mu\text{l}$  injected sample were separated at 30°C with a gradient of acetonitrile and 0.1% (v/v) formic acid in water. Acetonitrile was increased from 5 to 44% over 12 min and then to 70% over 3 min, after which the ratio remained constant for a further 3 min, using a flow rate of 0.8 ml/min. The amounts of T, MHET, and BHET were detected via UV at 240 nm and the quantification was realized using calibration curves.

## 4.7 Crystallization, Data Collection, Structure Determination

The genes encoding Ple628 and Ple629 were chemically synthesized by GENE ray Biotech Co. (China) and ligated

into the pET32a vector. The plasmids were transformed into *E. coli* BL21 (DE3) cells which were grown in LB medium at 37°C to an  $\text{OD}_{600}$  of 0.8 and then induced by 0.4 mM IPTG at 16°C for 24 h. Cells were harvested by centrifugation at  $5,000 \times g$  for 15 min, then re-suspended in lysis buffer containing 25 mM Tris-HCl, pH 7.5, 150 mM NaCl, and 20 mM imidazole, followed by disruption with a French Press (Thermo Electron, United States). Cell debris was removed by centrifugation at  $17,000 \times g$  for 1 h. The supernatant was then applied to a Ni-NTA column FPLC system (GE Healthcare, United States). The target proteins eluted at 100 mM imidazole when using a 20–250 mM imidazole gradient. Proteins were dialyzed against buffer containing 25 mM Tris-HCl, pH 7.5, and 150 mM NaCl, and subjected to TEV protease digestion, overnight, to remove the 6x His tag. The mixtures were then passed through another Ni-NTA column. Untagged proteins were eluted with 25 mM Tris-HCl, pH 7.5, 150 mM NaCl. After washing unbound proteins, the target protein was purified by using a DEAE Sepharose Fast Flow (Cytivia, Germany) and then a HiLoad 16/600 Superdex 200 GF column (Cytivia, Germany). The purity of proteins (>95%) was checked by SDS-PAGE analysis. The purified proteins were concentrated to 25 mg/ml for crystallization screening.

All crystallization experiments were conducted at 25°C using the sitting-drop vapor-diffusion method. In general, 1  $\mu\text{L}$  Ple628 containing solution (25 mM Tris-HCl, pH 7.5, 150 mM NaCl; 25 mg/ml) was mixed with 1  $\mu\text{L}$  of reservoir solution in 48-well Cryschem Plates (Hampton Research, United States), and equilibrated against 100  $\mu\text{L}$  of the reservoir solution. The optimized crystallization condition of Ple628 was 20% PEG 8000, 0.2 M calcium acetate, 0.1 M sodium cacodylate, pH 6.5. The optimized crystallization condition of Ple629 (25 mM Tris-HCl, pH 7.5, 150 mM NaCl; 23 mg/ml) was 30% PEG 8000, 0.2 M ammonium acetate, 0.1 M tri-sodium citrate dihydrate, pH 5.6. Within 5–6 days, the crystals reached dimensions suitable for X-ray diffraction.

The X-ray diffraction data sets were collected at beam line BL02U1 of SSRF and BL17B, BL18U1, and BL19U1 beamline of National Facility for Protein Science in Shanghai (NFPS) at the Shanghai Synchrotron Radiation Facility (Zhang et al., 2019). The Ple628 crystals were mounted in a cryoloop and soaked with cryoprotectant solution (21% PEG 8000, 0.4 M calcium acetate, 0.1 M sodium cacodylate, pH 6.5, 20% glycerol) prior to data collection at 100 K. The cryoprotectant solution for Ple629 is 30% PEG 8000, 0.2 M ammonium acetate, 0.1 M tri-sodium citrate dihydrate, pH 5.6, and 10% glycerol. The diffraction images were processed by using the HKL2000 software (Otwinowski and Minor, 1997). The crystal structures of Ple628 and Ple629 were both solved by the molecular replacement method with Phaser (McCoy et al., 2007) using the structure of polyester hydrolase from *Pseudomonas aestusnigri* (PDB code 6SCD) (Bollinger et al., 2020) as a search model. Further refinement was carried out using the programs Phenix v 1.19.2 (Afonine et al., 2012; Liebschner et al., 2019) and Coot (v 0.9.6) (Emsley and Cowtan, 2004). Prior to structural refinements, 5% of

randomly selected reflections were set aside for calculating R<sub>free</sub> (Brünger et al., 1998) as a monitor. Data collection and refinement statistics are summarized in the **Supplementary Table S2**. All figures were prepared by using the PyMOL program (<https://pymol.org/2/>, last accessed on 26.10.2021). The RMSD values were calculated with Coot v 0.9.6.

## 4.8 Sequence Analysis of the PETases

The sequences used in the alignment were retrieved from the UniProt database, and aligned with the Clustal Omega 1.2.2 software built in Geneious Prime 2021.2.2.

## DATA AVAILABILITY STATEMENT

The nucleotide sequences of ple628 and ple629 were deposited in the GenBank database with the accession numbers OK558824 and OK558825, respectively.

## AUTHOR CONTRIBUTIONS

MN-S performed the LC/MS analysis of the degradation products. PW and JG performed the expression, purification, crystallization and optimization of Ple628 protein crystals. YZ and XH performed the expression, purification, crystallization and optimization of Ple629 protein crystals. WL and ZL performed the X-ray data collection, structure determination and refinement of both structures. UB supervised a part of the project and acquired funding. BÖ supervised the project and acquired funding. IM and BÖ wrote the paper, BÖ, IM, MN-S, RW, and WL revised and edited the paper. All authors have read and agreed with the final version of the MS.

## REFERENCES

- Abhijit, N. S., White, C., Englaender, J. A., Zwarycz, A., Butterfoss, G. L., Linhardt, R. L., et al. (2018). Stabilizing Leaf and Branch Compost Cutinase (LCC) with Glycosylation: Mechanism and Effect on PET Hydrolysis. *Gross Biochem.* 57 (7), 1190–1200. doi:10.1021/acs.biochem.7b01189
- Afonine, P. V., Grosse-Kunstleve, R. W., Echols, N., Headd, J. J., Moriarty, N. W., Mustyakimov, M., et al. (2012). Towards Automated Crystallographic Structure Refinement with phenix.refine. *Acta Crystallogr. D. Biol. Cryst.* 68, 352–367. doi:10.1107/s0907444912001308
- Almagro Armenteros, J. J., Tsirigos, K. D., Sønderby, C. K., Petersen, T. N., Winther, O., Brunak, S., et al. (2019). SignalP 5.0 Improves Signal Peptide Predictions Using Deep Neural Networks. *Nat. Biotechnol.* 37, 420–423. doi:10.1038/s41587-019-0036-z
- Arnling Bååth, J., Novy, V., Carneiro, L. V., Guebitz, G. M., Olsson, L., Westh, P., et al. (2022). Structure-function Analysis of Two Closely Related Cutinases from *Thermobifida Cellulosilytica*. *Biotechnol. Bioeng.* 119, 470–481. doi:10.1002/bit.27984
- Argpigny, J. L., and Jaeger, K.-E. (1999). Bacterial Lipolytic Enzymes: Classification and Properties. *Biochem. J.* 343, 177–183. doi:10.1042/bj3430177
- Bååth, J. A., Borch, K., Jensen, K., Brask, J., and Westh, P. (2021). Comparative Biochemistry of Four Polyester (PET) Hydrolases\*. *ChemBioChem* 22, 1627–1637. doi:10.1002/cbic.202000793
- Barth, M., Honak, A., Oeser, T., Wei, R., Belisário-Ferrari, M. R., Then, J., et al. (2016). A Dual Enzyme System Composed of a Polyester Hydrolase and a Carboxylesterase Enhances the Biocatalytic Degradation of Polyethylene Terephthalate Films. *Biotechnol. J.* 11, 1082–1087. doi:10.1002/biot.201600008

## FUNDING

The authors LP and RW gratefully acknowledge the financial support received from the European Union's Horizon 2020 research and innovation program (MIX-UP, grant number 870294; upPE-T, grant number 953214). The authors, IM and BÖ thank BASF SE for financial support. The authors PW, YZ, WL, ZL, JG, and HX acknowledge the financial support provided by the National Key Research and Development Program of China (2021YFC2103600, 2021YFA0910200), and from Tianjin Synthetic Biotechnology Innovation Capacity Improvement Project (TSBICIP-PTJJ-008, TSBICIP-IJCP-003, TSBICIP-KJGG-009-01, TSBICIP-KJGG-002-06), Youth Innovation Promotion Association CAS and China Scholarship Council.

## ACKNOWLEDGMENTS

The authors thank Anja Gatzemeier, Dominik Werner, and Pia Bauer (Microbial Biotechnology group, DSMZ) and Gesa Martens (Research Group Metabolomics, DSMZ) for technical assistance. Furthermore, we thank the staff from BL10U2 (BL17U)/BL17B/BL18U1/BL19U1 beamlines of the National Facility for Protein Science in Shanghai (NFPS) at Shanghai Synchrotron Radiation Facility (SSRF) for assistance during data collection.

## SUPPLEMENTARY MATERIAL

The Supplementary Material for this article can be found online at: <https://www.frontiersin.org/articles/10.3389/fbioe.2022.930140/full#supplementary-material>

- Barth, M., Oeser, T., Wei, R., Then, J., Schmidt, J., and Zimmermann, W. (2015). Effect of Hydrolysis Products on the Enzymatic Degradation of Polyethylene Terephthalate Nanoparticles by a Polyester Hydrolase from *Thermobifida Fusca*. *Biochem. Eng. J.* 93, 222–228. doi:10.1016/j.bej.2014.10.012
- [Dataset] BASF (2022). *ecovio® – Certified Compostable Polymer with Bio-Based Content*. Ludwigshafen, Germany: BASF. Available at: [https://plastics-rubber.basf.com/global/en/performance\\_polymers/products/ecovio.html](https://plastics-rubber.basf.com/global/en/performance_polymers/products/ecovio.html) (Accessed June 10, 2022).
- Blázquez-Sánchez, P., Engelberger, F., Cifuentes-Anticevic, J., Sonnendecker, C., Griñén, A., Reyes, J., et al. (2022). Antarctic Polyester Hydrolases Degrade Aliphatic and Aromatic Polyesters at Moderate Temperatures. *Appl. Environ. Microbiol.* 88, e0184221. doi:10.1128/AEM.01842-21
- Bollinger, A., Thies, S., Knieps-Grünhagen, E., Gertzen, C., Kobus, S., Höppner, A., et al. (2020). A Novel Polyester Hydrolase from the Marine Bacterium *Pseudomonas Aestusnigri* - Structural and Functional Insights. *Front. Microbiol.* 11, 114. doi:10.3389/fmicb.2020.00114
- Brott, S., Pfaff, L., Schuricht, J., Schwarz, J. N., Böttcher, D., Badenhorst, C. P. S., et al. (2021). Engineering and Evaluation of Thermostable IsPETase Variants for PET Degradation. *Eng. Life Sci.* 22, 192–203. doi:10.1002/elsc.202100105
- Brünger, A. T., Adams, P. D., Clore, G. M., DeLano, W. L., Gros, P., Grosse-Kunstleve, R. W., et al. (1998). *Crystallography & NMR System: A New Software Suite for Macromolecular Structure Determination*. *Acta Cryst. D.* 54, 905–921. doi:10.1107/s0907444998003254
- Carniel, A., Valoni, É., Nicomedes, J., Gomes, A. d. C., and Castro, A. M. d. (2017). Lipase from *Candida antarctica* (CALB) and Cutinase from *Humicola Insolens*

- Act Synergistically for PET Hydrolysis to Terephthalic Acid. *Process Biochem.* 59, 84–90. doi:10.1016/j.procbio.2016.07.023
- Chen, C. C., Han, X., Ko, T. P., Liu, W., and Guo, R. T. (2018). Structural Studies Reveal the Molecular Mechanism of PET Ase. *Febs J.* 285, 3717–3723. doi:10.1111/febs.14612
- Cui, Y., Chen, Y., Liu, X., Dong, S., Tian, Y. e., Qiao, Y., et al. (2021). Computational Redesign of a PETase for Plastic Biodegradation under Ambient Condition by the GRAPE Strategy. *ACS Catal.* 11, 1340–1350. doi:10.1021/acscatal.0c05126
- de Castro, A. M., Carniel, A., Nicomedes Junior, J., da Conceição Gomes, A., and Valoni, É. (2017). Screening of Commercial Enzymes for Poly(ethylene Terephthalate) (PET) Hydrolysis and Synergy Studies on Different Substrate Sources. *J. Ind. Microbiol. Biotechnol.* 44, 835–844. doi:10.1007/s10295-017-1942-z
- Emsley, P., and Cowtan, K. (2004). Coot: Model-Building Tools for Molecular Graphics. *Acta Crystallogr. D. Biol. Cryst.* 60, 2126–2132. doi:10.1107/S0907444904019158
- Erickson, E., Shakespeare, T. J., Bratti, F., Buss, B. L., Graham, R., Hawkins, M. A., et al. (2022). Comparative Performance of PETase as a Function of Reaction Conditions, Substrate Properties, and Product Accumulation. *ChemSusChem* 15, e202101932. doi:10.1002/cssc.202101932
- Eugenio, E. d. Q., Campisano, I. S. P., de Castro, A. M., Coelho, M. A. Z., and Langone, M. A. P. (2021). Kinetic Modeling of the Post-consumer Poly(ethylene Terephthalate) Hydrolysis Catalyzed by Cutinase from *Humicola Insolens*. *J. Polym. Environ.* 30, 1627–1637. doi:10.1007/s10924-021-02301-4
- Fecker, T., Galaz-Davison, P., Engelberger, F., Narui, Y., Sotomayor, M., Parra, L. P., et al. (2018). Active Site Flexibility as a Hallmark for Efficient PET Degradation by *I. Sakaiensis* PETase. *Biophysical J.* 114, 1302–1312. doi:10.1016/j.bpj.2018.02.005
- Furukawa, M., Kawakami, N., Tomizawa, A., and Miyamoto, K. (2019). Efficient Degradation of Poly(ethylene Terephthalate) with *Thermobifida Fusca* Cutinase Exhibiting Improved Catalytic Activity Generated Using Mutagenesis and Additive-Based Approaches. *Sci. Rep.* 9, 16038. doi:10.1038/s41598-019-52379-z
- Gan, Z., Kuwabara, K., Yamamoto, M., Abe, H., and Doi, Y. (2004). Solid-state Structures and Thermal Properties of Aliphatic-Aromatic Poly(butylene Adipate-Co-Butylene Terephthalate) Copolyesters. *Polym. Degrad. Stab.* 83, 289–300. doi:10.1016/S0141-3910(03)00274-X
- Gouda, M. K., Kleeberg, I., Vanden Heuvel, J., Muller, R.-J., and Deckwer, W.-D. (2002). Production of a Polyester Degrading Extracellular Hydrolase from *Thermomonospora Fusca*. *Biotechnol. Prog.* 18, 927–934. doi:10.1021/bp020048b
- Hahladakis, J. N., and Iacovidou, E. (2019). An Overview of the Challenges and Trade-Offs in Closing the Loop of Post-consumer Plastic Waste (PCPW): Focus on Recycling. *J. Hazard. Mater.* 380, 120887. doi:10.1016/j.jhazmat.2019.120887
- Herrero Acero, E., Ribitsch, D., Steinkellner, G., Gruber, K., Greimel, K., Eiteljoerg, I., et al. (2011). Enzymatic Surface Hydrolysis of PET: Effect of Structural Diversity on Kinetic Properties of Cutinases from *Thermobifida*. *Macromolecules* 44, 4632–4640. doi:10.1021/ma200949p
- Hiraishi, T., Komiya, N., Matsumoto, N., Abe, H., Fujita, M., and Maeda, M. (2010). Degradation and Adsorption Characteristics of PHB Depolymerase as Revealed by Kinetics of Mutant Enzymes with Amino Acid Substitution in Substrate-Binding Domain. *Biomacromolecules* 11, 113–119. doi:10.1021/bm900967a
- Hopewell, J., Dvorak, R., and Kosior, E. (2009). Plastics Recycling: Challenges and Opportunities. *Phil. Trans. R. Soc. B* 364, 2115–2126. doi:10.1098/rstb.2008.0311
- Jian, J., Xiangbin, Z., and Xianbo, H. (2020). An Overview on Synthesis, Properties and Applications of Poly(butylene-Adipate-Co-Terephthalate)-PBAT. *Adv. Industrial Eng. Polym. Res.* 3, 19–26. doi:10.1016/j.aiepr.2020.01.001
- Joo, S., Cho, I. J., Seo, H., Son, H. F., Sagong, H.-Y., Shin, T. J., et al. (2018). Structural Insight into Molecular Mechanism of Poly(ethylene Terephthalate) Degradation. *Nat. Commun.* 9, 382. doi:10.1038/s41467-018-02881-1
- Kasuya, K.-I., Ishii, N., Inoue, Y., Yazawa, K., Tagaya, T., Yotsumoto, T., et al. (2009). Characterization of a Mesophilic Aliphatic-Aromatic Copolyester-Degrading Fungus. *Polym. Degrad. Stab.* 94, 1190–1196. doi:10.1016/j.polydegststab.2009.04.013
- Kawai, F., Kawabata, T., and Oda, M. (2020). Current State and Perspectives Related to the Polyethylene Terephthalate Hydrolases Available for Biorecycling. *ACS Sustain. Chem. Eng.* 8, 8894–8908. doi:10.1021/acssuschemeng.0c01638
- Kleeberg, I., Welzel, K., Vandenheuevel, J., Müller, R.-J., and Deckwer, W.-D. (2005). Characterization of a New Extracellular Hydrolase from *Thermobifida Fusca* Degrading Aliphatic–Aromatic Copolyesters. *Biomacromolecules* 6, 262–270. doi:10.1021/bm049582t
- Li, W.-J., Narancic, T., Kenny, S. T., Niehoff, P.-J., O'Connor, K., Blank, L. M., et al. (2020). Unraveling 1,4-butanediol Metabolism in *Pseudomonas Putida* KT2440. *Front. Microbiol.* 11, 382. doi:10.3389/fmicb.2020.00382
- Liebschner, D., Afonine, P. V., Baker, M. L., Bunkóczi, G., Chen, V. B., Croll, T. I., et al. (2019). Macromolecular Structure Determination Using X-Rays, Neutrons and Electrons: Recent Developments in *Phenix*. *Acta Cryst. Sect. D. Struct. Biol.* 75, 861–877. doi:10.1107/S2059798319011471
- Marten, E., Müller, R.-J., and Deckwer, W.-D. (2005). Studies on the Enzymatic Hydrolysis of Polyesters. II. Aliphatic-Aromatic Copolyesters. *Polym. Degrad. Stab.* 88, 371–381. doi:10.1016/j.polydegststab.2004.12.001
- McCoy, A. J., Grosse-Kunstleve, R. W., Adams, P. D., Winn, M. D., Storoni, L. C., and Read, R. J. (2007). Phasercrystallographic Software. *J. Appl. Cryst.* 40, 658–674. doi:10.1107/S0021889807021206
- Meyer-Cifuentes, I. E., and Öztürk, B. (2021). Mle046 Is a Marine Mesophilic MHETase-like Enzyme. *Front. Microbiol.* 12, 2031. doi:10.3389/fmicb.2021.693985
- Meyer-Cifuentes, I. E., Werner, J., Jehmlich, N., Will, S. E., Neumann-Schaal, M., and Öztürk, B. (2020). Synergistic Biodegradation of Aromatic-Aliphatic Copolyester Plastic by a Marine Microbial Consortium. *Nat. Commun.* 11, 5790. doi:10.1038/s41467-020-19583-2
- Mukai, K., Yamada, K., and Doi, Y. (1993). Kinetics and Mechanism of Heterogeneous Hydrolysis of poly[(R)-3-hydroxybutyrate] Film by PHA Depolymerases. *Int. J. Biol. Macromol.* 15, 361–366. doi:10.1016/0141-8130(93)90054-p
- Ollis, D. L., Cheah, E., Cygler, M., Dijkstra, B., Frolow, F., Franken, S. M., et al. (1992). The  $\alpha/\beta$  Hydrolase Fold. *Protein Eng. Des. Sel.* 5, 197–211. doi:10.1093/protein/5.3.197
- Otwinowski, Z., and Minor, W. (1997). “[20] Processing of X-Ray Diffraction Data Collected in Oscillation Mode,” in *Methods in Enzymology. Vol. 276 of Macromolecular Crystallography Part A* (Cambridge, MA, USA: Academic Press), 307–326. doi:10.1016/s0076-6879(97)70606-x
- Palm, G. J., Reisky, L., Böttcher, D., Müller, H., Michels, E. A. P., Walczak, M. C., et al. (2019). Structure of the Plastic-Degrading *Ideonella Sakaiensis* MHETase Bound to a Substrate. *Nat. Commun.* 10, 1717. doi:10.1038/s41467-019-09326-3
- Perz, V., Baumschlager, A., Bleymaier, K., Zitzenbacher, S., Hromic, A., Steinkellner, G., et al. (2016a). Hydrolysis of Synthetic Polyesters by Clostridium Botulinum Esterases. *Biotechnol. Bioeng.* 113, 1024–1034. doi:10.1002/bit.25874
- Perz, V., Bleymaier, K., Sinkel, C., Kueper, U., Bonnekessel, M., Ribitsch, D., et al. (2016b). Substrate Specificities of Cutinases on Aliphatic-Aromatic Polyesters and on Their Model Substrates. *New Biotechnol.* 33, 295–304. doi:10.1016/j.nbt.2015.11.004
- Pfaff, L., Breite, D., Badenhorst, C. P. S., Bornscheuer, U. T., and Wei, R. (2021). “Fluorimetric High-Throughput Screening Method for Polyester Hydrolase Activity Using Polyethylene Terephthalate Nanoparticles,” in *Methods in Enzymology. Vol. 648 of Enzymatic Plastic Degradation* (Cambridge, MA, USA: Academic Press), 253–270. chap. 12. doi:10.1016/bs.mie.2020.11.003
- Platt, D. K. (2006). *Biodegradable Polymers: Market Report*. Shrewsbury, UK: Smithers rapra limited.
- Ronkvist, Å. M., Xie, W., Lu, W., and Gross, R. A. (2009). Cutinase-catalyzed Hydrolysis of Poly(ethylene Terephthalate). *Macromolecules* 42, 5128–5138. doi:10.1021/ma9005318
- Sasoh, M., Masai, E., Ishibashi, S., Hara, H., Kamimura, N., Miyauchi, K., et al. (2006). Characterization of the Terephthalate Degradation Genes of *Comamonas* Sp. Strain E6. *Appl. Environ. Microbiol.* 72, 1825–1832. doi:10.1128/aem.72.3.1825-1832.2006

- Scandola, M., Focarete, M. L., and Frisoni, G. (1998). Simple Kinetic Model for the Heterogeneous Enzymatic Hydrolysis of Natural Poly(3-Hydroxybutyrate). *Macromolecules* 31, 3846–3851. doi:10.1021/ma980137y
- Sulaiman, S., Yamato, S., Kanaya, E., Kim, J.-J., Koga, Y., Takano, K., et al. (2012). Isolation of a Novel Cutinase Homolog with Polyethylene Terephthalate-Degrading Activity from Leaf-Branch Compost by Using a Metagenomic Approach. *Appl. Environ. Microbiol.* 78, 1556–1562. doi:10.1128/AEM.06725-11
- Thumarat, U., Kawabata, T., Nakajima, M., Nakajima, H., Sugiyama, A., Yazaki, K., et al. (2015). Comparison of Genetic Structures and Biochemical Properties of Tandem Cutinase-type Polyesters from *Thermobifida Alba* AHK119. *J. Biosci. Bioeng.* 120, 491–497. doi:10.1016/j.jbiosc.2015.03.006
- Thumarat, U., Nakamura, R., Kawabata, T., Suzuki, H., and Kawai, F. (2012). Biochemical and Genetic Analysis of a Cutinase-type Polyestrase from a Thermophilic *Thermobifida Alba* AHK119. *Appl. Microbiol. Biotechnol.* 95, 419–430. doi:10.1007/s00253-011-3781-6
- Tiso, T., Winter, B., Wei, R., Hee, J., de Witt, J., Wierckx, N., et al. (2022). The Metabolic Potential of Plastics as Biotechnological Carbon Sources - Review and Targets for the Future. *Metab. Eng.* 71, 77–98. doi:10.1016/j.ymben.2021.12.006
- Tournier, V., Topham, C. M., Gilles, A., David, B., Folgoas, C., Moya-Leclair, E., et al. (2020). An Engineered PET Depolymerase to Break Down and Recycle Plastic Bottles. *Nature* 580, 216–219. doi:10.1038/s41586-020-2149-4
- Vogel, K., Wei, R., Pfaff, L., Breite, D., Al-Fathi, H., Ortmann, C., et al. (2021). Enzymatic Degradation of Polyethylene Terephthalate Nanoplastics Analyzed in Real Time by Isothermal Titration Calorimetry. *Sci. Total Environ.* 773, 145111. doi:10.1016/j.scitotenv.2021.145111
- Wallace, P. W., Haernvall, K., Ribitsch, D., Zitzenbacher, S., Schittmayer, M., Steinkellner, G., et al. (2017). PpEst Is a Novel PBAT Degrading Polyestrase Identified by Proteomic Screening of *Pseudomonas pseudoalcaligenes*. *Appl. Microbiol. Biotechnol.* 101, 2291–2303. doi:10.1007/s00253-016-7992-8
- Wei, R., Oeser, T., Schmidt, J., Meier, R., Barth, M., Then, J., et al. (2016). Engineered Bacterial Polyester Hydrolases Efficiently Degrade Polyethylene Terephthalate Due to Relieved Product Inhibition. *Biotechnol. Bioeng.* 113, 1658–1665. doi:10.1002/bit.25941
- Wei, R., Tiso, T., Bertling, J., O'Connor, K., Blank, L. M., and Bornscheuer, U. T. (2020). Possibilities and Limitations of Biotechnological Plastic Degradation and Recycling. *Nat. Catal.* 3, 867–871. doi:10.1038/s41929-020-00521-w
- Wei, R., von Haugwitz, G., Pfaff, L., Mican, J., Badenhurst, C. P. S., Liu, W., et al. (2022). Mechanism-based Design of Efficient PET Hydrolases. *ACS Catal.* 12, 3382–3396. doi:10.1021/acscatal.1c05856
- Yoshida, S., Hiraga, K., Takehana, T., Taniguchi, I., Yamaji, H., Maeda, Y., et al. (2016). A Bacterium that Degrades and Assimilates Poly(ethylene Terephthalate). *Science* 351, 1196–1199. doi:10.1126/science.aad6359
- Zhang, W.-Z., Tang, J.-C., Wang, S.-S., Wang, Z.-J., Qin, W.-M., and He, J.-H. (2019). The Protein Complex Crystallography Beamline (BL19U1) at the Shanghai Synchrotron Radiation Facility. *Nucl. Sci. Tech.* 30, 170. doi:10.1007/s41365-019-0683-2

**Conflict of Interest:** The authors declare that the research was conducted in the absence of any commercial or financial relationships that could be construed as a potential conflict of interest.

**Publisher's Note:** All claims expressed in this article are solely those of the authors and do not necessarily represent those of their affiliated organizations, or those of the publisher, the editors, and the reviewers. Any product that may be evaluated in this article, or claim that may be made by its manufacturer, is not guaranteed or endorsed by the publisher.

Copyright © 2022 Meyer Cifuentes, Wu, Zhao, Liu, Neumann-Schaal, Pfaff, Barys, Li, Gao, Han, Bornscheuer, Wei and Öztürk. This is an open-access article distributed under the terms of the Creative Commons Attribution License (CC BY). The use, distribution or reproduction in other forums is permitted, provided the original author(s) and the copyright owner(s) are credited and that the original publication in this journal is cited, in accordance with accepted academic practice. No use, distribution or reproduction is permitted which does not comply with these terms.





# Feasible Cluster Model Method for Simulating the Redox Potentials of Laccase CueO and Its Variant

Qixuan Jiang<sup>1</sup>, Ziheng Cui<sup>1</sup>, Ren Wei<sup>2</sup>, Kaili Nie<sup>1</sup>, Haijun Xu<sup>1\*</sup> and Luo Liu<sup>1\*</sup>

<sup>1</sup>Beijing Bioprocess Key Laboratory, Beijing University of Chemical Technology, Beijing, China, <sup>2</sup>Junior Research Group Plastic Biodegradation at Institute of Biochemistry, University of Greifswald, Greifswald, Germany

## OPEN ACCESS

### Edited by:

Hui-Min Qin,  
Tianjin University of Science and  
Technology, China

### Reviewed by:

Changzhu Wu,  
University of Southern Denmark,  
Denmark  
Hui Luo,  
University of Science and Technology  
Beijing, China

### \*Correspondence:

Haijun Xu  
hixu@mail.buct.edu.cn  
Luo Liu  
liuluo@mail.buct.edu.cn

### Specialty section:

This article was submitted to  
Industrial Biotechnology,  
a section of the journal  
Frontiers in Bioengineering and  
Biotechnology

**Received:** 31 May 2022

**Accepted:** 20 June 2022

**Published:** 22 July 2022

### Citation:

Jiang Q, Cui Z, Wei R, Nie K, Xu H and  
Liu L (2022) Feasible Cluster Model  
Method for Simulating the Redox  
Potentials of Laccase CueO and  
Its Variant.  
Front. Bioeng. Biotechnol. 10:957694.  
doi: 10.3389/fbioe.2022.957694

Laccases are regarded as versatile green biocatalysts, and recent scientific research has focused on improving their redox potential for broader industrial and environmental applications. The density functional theory (DFT) quantum mechanics approach, sufficiently rigorous and efficient for the calculation of electronic structures, is conducted to better comprehend the connection between the redox potential and the atomic structural feature of laccases. According to the crystal structure of wild type laccase CueO and its variant, a truncated miniature cluster model method was established in this research. On the basis of thermodynamic cycle, the overall Gibbs free energy variations before and after the one-electron reduction were calculated. It turned out that the trends of redox potentials to increase after variant predicted by the theoretical calculations correlated well with those obtained by experiments, thereby validating the feasibility of this cluster model method for simulating the redox potentials of laccases.

**Keywords:** cluster model, redox potential, quantum mechanics, laccase, molecular simulation

## INTRODUCTION

Laccases (EC 1.10.3.2) are oxidoreductases with cupredoxin-like domains that can catalyze various substrates oxidized and simultaneously reduce oxygen to water (Madhavi and Lele, 2009; Janusz et al., 2020; Shiroya, 2021). Laccases contain at least four copper atoms comprising one type 1 copper (T1 Cu) serving as the electron entry position to the protein, and one type 2 copper (T2 Cu) and two type 3 coppers (T3 Cu) that compose a trinuclear cluster (TNC) (Sakurai and Kataoka, 2007; Solomon et al., 2008; Liu et al., 2014; Giacobelli, 2017). Given the apparent stability and eco-friendliness of laccases, scientific efforts have been diverted these days to exploit such enzymes in emerging fields such as enzymatic biofuel cells and the degradation of noxious contaminants (Bilal et al., 2019; Li et al., 2020; Moreno et al., 2020). The redox potentials of laccases generally range from 0.43 to 0.79 V versus the normal hydrogen electrode (NHE) (Mateljak et al., 2019). Through directed evolution of laccases, the redox potential value is expected to be improved to fulfill the requirement for many biotechnological and environmental applications.

The copper efflux oxidase (CueO) has conspicuously superior stability in high temperature or alkaline environment when compared to other bacterial laccases. Nevertheless, its relatively low redox potential is detrimental to catalytic activity from a thermodynamic perspective (Santhanam et al., 2011; Martins et al., 2015; Chauhan et al., 2017). Two beneficial substitutions D439T and L502K were found to improve the onset potential up to 0.42 and 0.44 V, respectively (Zhang et al., 2019). The crystal structure of CueO revealed that D439 and L502 form hydrogen bonds with coordinated residues of T1 Cu, H443 and C500, respectively. The redox potential of CueO is mostly

governed by the T1 Cu site (Hong et al., 2011; Vázquez-Lima et al., 2012). Computational simulation of the redox potential variation influenced by single-site variants adjoining the T1 Cu site is one interesting avenue of investigation.

Selecting appropriate methods and developing a computational scheme for catalytic processes associated with redox-active metalloenzymes is a challenging task. With the rapid development of computing science, numerous multiscale modeling approaches for enzymes have been adopted, including molecular dynamics (MD), free energy perturbation (FEP), empirical valence bond (EVB), hybrid quantum mechanics/molecular mechanics (QM/MM), and the quantum mechanics (QM) cluster approach (Ahmadi et al., 2018; Sheng et al., 2020). Supposing that the selected QM region is reasonable, the same consequences will be given by QM cluster and QM/MM approaches essentially (Siegbahn, 2006; Liao and Thiel, 2012). The cluster approach is the simple and efficient method for elucidating mechanisms of redox-active metalloenzymes, dealing with the crucial active site region of the metalloenzymes in a QM manner, proved fruitful in reproducing high-precision energy calculations. Lately, Mina Ghiasi et al. (2021) carried out a DFT research on the activation mechanism of the human carbonic anhydrase VII cluster model and demonstrated that the activator molecule participates in proton transfer reactions, enhancing the formation of the active zinc hydroxide species.

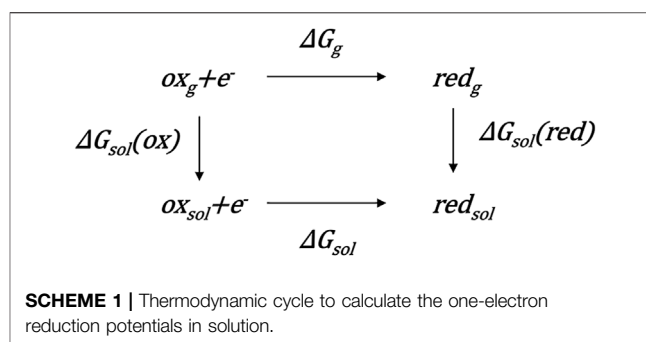
In this work, we developed a T1 Cu site active center cluster model protocol for calculating the redox potentials of WT CueO and its variant L502K. The dynamics simulations were carried out, and according to the obtained equilibrium structures, the target cluster model structures were designed, whose oxidized and reduced states were geometrically optimized separately in the solvated environment at the B3LYP-D3(BJ)/6-311G\* level. Their vapor phase and solvation Gibbs free energies were calculated at the M062X/def2TZVP and M06X/6-311G\* level, respectively, to achieve the redox potentials. Several different DFT and solvation approaches were attempted during the simulation to achieve more accurate results.

## METHODS

### Quantum Mechanics Cluster Model Approach

The QM cluster model approach, which uses finite models to investigate the active sites of metalloenzymes, is an important tool to elucidate enzymatic reaction mechanisms. Many aspects of the metalloenzyme mechanisms have been understood, employing a relatively small model (Blomberg et al., 2014).

Density functional theory (DFT), a currently used QM atomistic simulation method, can be utilized to describe the electronic structure of the enzyme cluster model system (Himo, 2017). The hybrid functional B3LYP has dominated in the geometric optimization applications, accounting for its simple form, low dependence on the integration lattice point, fast calculation speed, and moderate accuracy. Nonetheless, the B3LYP functional is not suitable for describing weak interactions caused by dispersion (Grimme et al., 2016). In this respect, the recent developed technique, adding an empirical dispersion correction, known as DFT-D, has been shown to dramatically improve the energies in the field of homogeneous



catalysis (Witte et al., 2015). When it comes to energy calculations, the M06 functional appears to offer better performance in predicting the overall trends of relative energies than the B3LYP functional (Walker et al., 2013).

Since the cluster approach contains only an enzyme fraction, namely, the active site and its surroundings, when the structures are designed, environment influences need to be taken into account. This environment impact is usually simulated by two simple approximations: steric hindrance and static electricity. To prevent the overall structure of the model from unraveling during optimization, some atoms at the model boundary are fixed. The electrostatic effect of solvent contribution is approximated by the implicit solvation model. The implicit solvation model treats the solvent as a dielectric continuum, in which different solvation environment can be represented by regulating permittivity  $\epsilon$ . Furthermore, it should be noted that as the model size increases, the approximation improves. With these two approximations, a cluster model suitable for the T1 Cu site active center of WT CueO and its variant can be constructed.

### Theoretical Methods for Calculating Redox Potentials

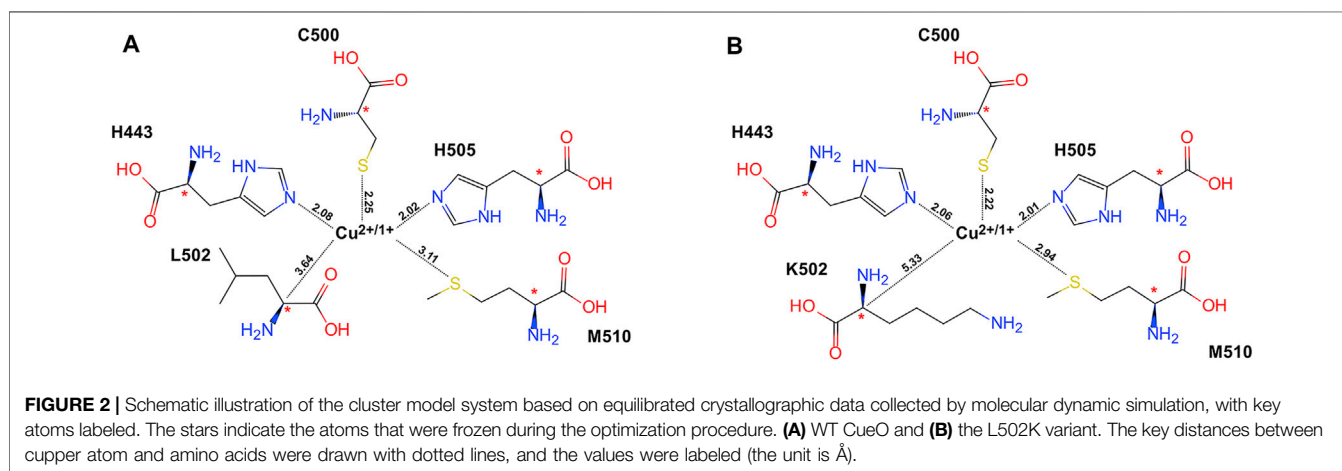
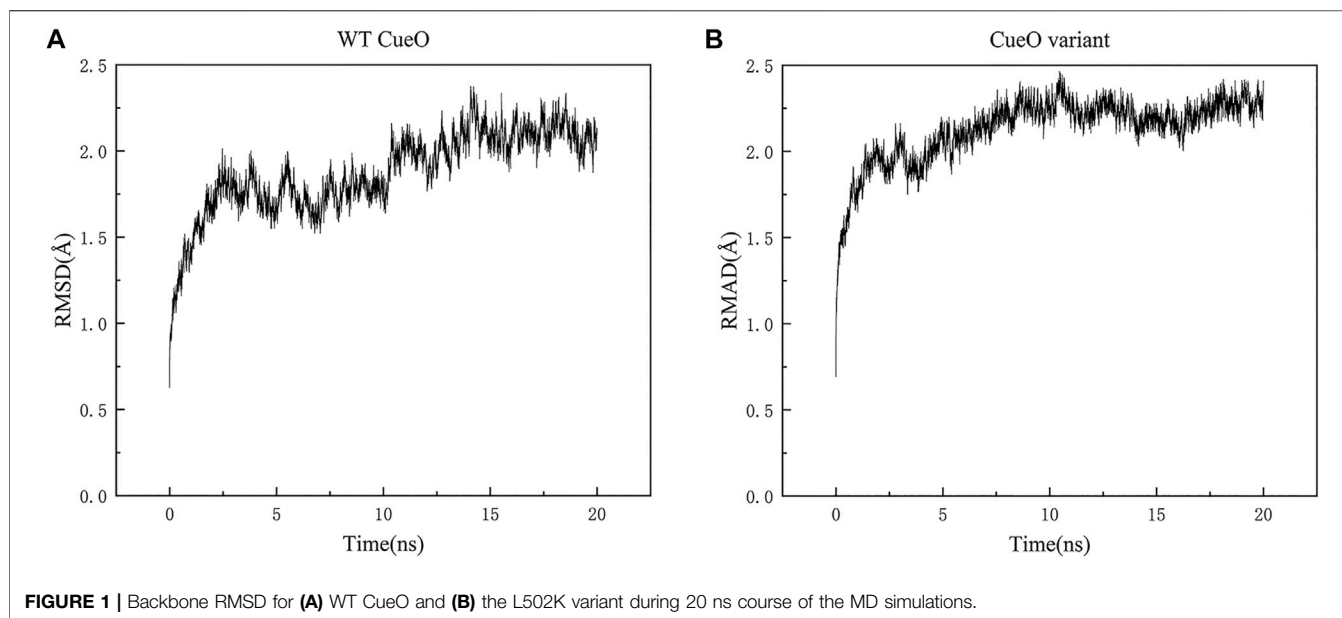
The theoretical estimate for the concerned potential of the redox reaction ( $ox + e^- \rightarrow red$ ) is

$$-\Delta E = -\frac{\Delta G}{nF}, \quad (1)$$

where  $\Delta E$  is the redox potential,  $\Delta G$  is the variation of Gibbs free energy,  $n$  is the number of electrons, and  $F$  is the Faraday constant (Bruschi et al., 2016). The main problem associated with the calculation is that the reactions always take place in solution, whereas directly calculating the solvated Gibbs free energy is low in accuracy (Yan et al., 2016). It is well known that the accuracy of gas phase energy is higher than that of liquid phase energy in QM calculations; consequently, the thermodynamic cycle in **Scheme 1** and the following formula are proposed to exactly calculate the  $\Delta G$  value,

$$\Delta G = \Delta G_g + \Delta \Delta G_{sol} \quad (2)$$

where  $\Delta G_g = G_g(red) - G_g(ox)$  is the gas phase Gibbs free energy difference and  $\Delta \Delta G_{sol} = \Delta G_{sol}(red) - \Delta G_{sol}(ox)$  is the differential free energy of solvation (Uudsemaa and Tamm, 2003). The Gibbs free energy for oxidized and reduced states in the gas phase are



calculated respectively to hence the  $\Delta G_g$  value. An implicit solvent model is used for both states yielding the differential solvation energy  $\Delta\Delta G_{sol}$  (Holland et al., 2006). The redox potential can eventually be obtained by Eqs 1 and 2.

## Molecular Dynamic Simulations

The crystal structure of CueO resolved at an atomic resolution of 1.1 Å (PDB code: 3OD3) was used as a starting point of MD simulations (Singh et al., 2011). The structure of the L502K variant was generated using the WT CueO structure as a template by YASARA software version 17.8.15 (Krieger and Vriend, 2014). Molecular dynamics (MD) simulation and analysis were performed with NAMD software version 2.14 (Phillips et al., 2020). Protonation statuses of residues were determined by the H++ online program and checked manually (Anandakrishnan et al., 2012). A cubic box with a protein-to-border distance of 10 Å was established and filled with TIP3P water molecules. The systems were minimized and equilibrated for 20 ns with the T1 Cu site kept fixed. Root mean

square deviation (RMSD) was calculated by VMD package tools (Phillips et al., 2020).

## Quantum Chemical Calculations

The quantum chemical calculations for optimization and vibration analysis of the system were performed at the B3LYP-D3(BJ)/6-311G\* level of theory combined with the SMD solvent model. The total charge of oxidized and reduced was 1 and 0, respectively, because the amino acid ligands are neutral, while the SG atom in C500 is coordinated with copper ions, leading to the HG atom originally attached to the SG atom deprotonated. The spin multiplicity of oxidized and reduced was 2 and 1, respectively. More precise electron energies in vacuum were calculated at the M062X/def2TZVP level dependent on the optimized structures. Simultaneously, the M062X/6-311G\* level was selected for calculating the solvation free energy difference. All quantum mechanical calculations were carried out using the Gaussian 16 program package (Frisch et al., 2016).

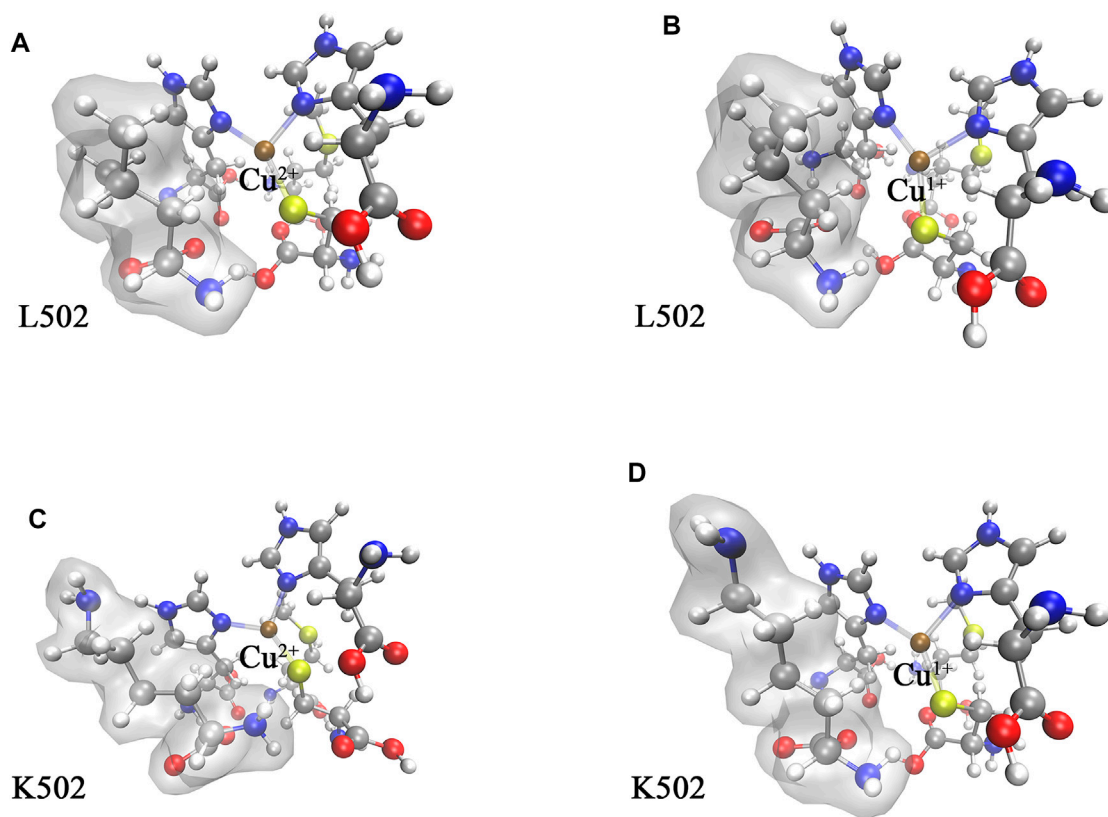


**FIGURE 3** | The optimized structure of CueO T1 Cu active site cluster models in the water phase: **(A)** WT in the oxidation state, **(B)** WT in the reduction state, **(C)** L502K variant in the oxidation state, and **(D)** L502K in the reduction state. The colors correspond to atoms: brown for copper, yellow for sulfur, red for oxygen, blue for nitrogen, dark gray for carbon, and light gray for hydrogen. The amino acid residue 502 was highlighted by adding a transparent molecular surface.

## RESULTS AND DISCUSSION

### Molecular Dynamic Simulations

Molecular dynamic simulations testing on both structures (WT CueO L502K variant) showed good results in **Figure 1**. The backbone RMSD of the equilibrated structures relative to the original structures range from 0.63 to 2.38 Å and 0.69 to 2.46 Å for WT CueO and the L502K variant, respectively.

### Energetics of the Catalytic Site

The cluster models for QM research studies were constructed with the residues involved in the biocatalysis active site. The copper ion ( $\text{Cu}^{2+}$  or  $\text{Cu}^{1+}$ ) in the core and its ligands (H443, C500, and H505) and L502 for the WT or K502 for the variant, as well as the hydrophobic residues M510, were considered in the enzyme cluster model as shown in **Figure 2**. After a consolidating procedure in the cluster model, the  $\alpha$  carbon atoms of all residues were fixed in their positions at molecular dynamic equilibrium dependent on the crystal structure during the geometry optimization for the sake of avoiding cluster model discretization inconsistent with actuality.

The optimized structures of the WT CueO and its variant cluster models are displayed in **Figure 3**. Owing to the conserved

**TABLE 1** | DFT-calculated energetics for the WT CueO and L502K active sites and for the redox reactions (the unit is kcal/mol).

	WT	Variant (L502K)
$G_g(\text{ox})$	-2949799.37	-2984537.94
$G_g(\text{red})$	-2949931.72	-2984656.64
$\Delta G_g$	-132.35	-118.69
$\Delta G_{\text{sol}}(\text{ox})$	-122.04	-88.45
$\Delta G_{\text{sol}}(\text{red})$	-82.05	-85.04
$\Delta \Delta G_{\text{sol}}$	40.00	3.42
$\Delta G$	-92.35	-115.27

**TABLE 2** | Redox potentials of the active site (the unit is V).

	WT	Variant (L502K)
$E_{\text{exp}}$	0.35	0.44
$\Delta E$	4.00	5.00
$E_{\text{calc}}$	-0.44	0.56

cupredoxin-like domain, the changes of bond distances between copper ion and coordination atom were small (less than 0.1 Å), and it was speculated that the changes of electron density around



the T1 Cu site stemmed from capturing an electron majorly affected redox potentials.

**Table 1** summarizes the crucial energies involved calculating the redox potential. The gas phase Gibbs free energy changes of the redox processes were calculated using the Shermo software (Lu and Chen, 2021). The gas phase free energy difference of WT and variant is  $-132.35$  and  $-118.69$  kcal/mol, respectively. In solution, according to the electric field intensity near the copper complexes, the copper complexes were solvated, thus exhibiting different solvation free energies. The final results showed that the Gibbs free energy variation of variant gaining one electronic is  $22.92$  kcal/mol higher than WT.

## Redox Potentials of the Active Site

To obtain theoretical values that could be compared with experimental values, the computed  $E_{dac}$  value is written as  $E_{dac} = \Delta E - \Delta E_H$ , where  $\Delta E_H$  is the standard hydrogen electrode potential.  $\Delta E_H$  is commonly used as a primary reference electrode to know the relative potentials of other redox reactions. Unfortunately, there is no universal agreement on the assigned  $\Delta E_H$  value, which proposed the range from  $4.28$  to  $4.74$  V (Isse and Gennaro, 2010; Marenich et al., 2014). In order to avoid this uncertainty, we used the value  $4.44$  V for water, provided by the IUPAC24. The theoretical values  $E_{dac}$  at the active sites relative versus  $\Delta E_H$  accessed by subtracting  $4.44$  eV from  $\Delta E$  are summarized in **Table 2**, as well as the experimental values obtained by Zhang et al. (2019).

When compared to earlier results, this DFT research estimated redox potentials qualitatively match with the experiment. It has previously been presented that the redox potential values of copper-containing oxidases depend on the T1 Cu pocket (Kojima et al., 1990). Depending on the structure of the native high potential laccase (*T. versicolor*), Klaus Piontek et al. (2002) proposed a mechanism that assumes a decrease in electron density contribution at the metal cation through a stretching of the bond between the metal and the ligating amino acid. This mechanism could possibly explain why redox potential increased after the L502K variant. Furthermore, variant-induced structural perturbations on the electron transfer pathway were interpreted as an additional structural determinant (Xu et al., 1998).

## CONCLUSION

In the present work, we investigated the feasibility of cluster models to calculate the redox potential of WT laccase CueO and its variant L502K based on the Gibbs free energy. The redox

potential of WT CueO was  $0.79$  V lower than the experimental values, while the redox potential of L502K was  $0.12$  V higher than the experimental values. Although the cluster method is not sufficiently accurate for determining absolute redox potentials, the trend of variant-induced redox potential changes is consistent with experimental data. Gibbs free energy variation is a function of state; from the perspective of the structures, the structural changes caused by the variant eventually led to a change in the Gibbs free energy, which led to changes in the redox potential.

Due to the atomic range limitation of the quantitative calculation, the variant sites slightly far from the active site cannot be predicted using the cluster model. With the development of computational methods, the cluster model or the QM/MM method will be able to investigate a broader range of simulations in the future, yielding more accurate results.

## DATA AVAILABILITY STATEMENT

The datasets presented in this study can be found in online repositories. The names of the repository/repositories and accession number(s) can be found below: <http://www.wwpdb.org/>, 3OD3.

## AUTHOR CONTRIBUTIONS

Conceptualization, LL and HX; methodology, QJ; formal analysis, ZC; writing—original draft preparation, LL and QJ; writing—review and editing, RW and KN; supervision, LL and HX; and funding acquisition, LL and HX. All authors have read and agreed to the published version of the manuscript.

## FUNDING

This study was funded by the National Key Research and Development Program of China (grant number 22021YFC2101004). This study was funded by the National Natural Science Foundation of China (grant numbers 31961133017, 52073022, and 21978017). These grants are part of the MIX-UP project that received funding within the framework of a joint NSFC and EU H2020 collaboration. In Europe, MIX-UP has received funding from the European Union's Horizon 2020 research and innovation program under grant agreement No. 870294.

## REFERENCES

- Ahmadi, S., Barrios Herrera, L., Chehelamirani, M., Hostaš, J., Jalife, S., and Salahub, D. R. (2018). Multiscale Modeling of Enzymes: QM-Cluster, QM/MM, and QM/MM/MD: A Tutorial Review. *Int. J. Quantum Chem.* 118 (9), e25558. doi:10.1002/qua.25558
- Anandakrishnan, R., Aguilar, B., and Onufriev, A. V. (2012). H++ 3.0: Automating pK Prediction and the Preparation of Biomolecular Structures for Atomistic Molecular Modeling and Simulations. *Nucleic Acids Res.* 40 (W1), W537–W541. doi:10.1093/nar/gks375
- Bilal, M., Rasheed, T., Nabeel, F., Iqbal, H. M. N., and Zhao, Y. (2019). Hazardous Contaminants in the Environment and Their Laccase-Assisted Degradation - A Review. *J. Environ. Manag.* 234, 253–264. doi:10.1016/j.jenvman.2019.01.001
- Blomberg, M. R. A., Borowski, T., Himo, F., Liao, R.-Z., and Siegbahn, P. E. M. (2014). Quantum Chemical Studies of Mechanisms for Metalloenzymes. *Chem. Rev.* 114 (7), 3601–3658. doi:10.1021/cr400388t
- Bruschi, M., Breglia, R., Arrigoni, F., Fantucci, P., and De Gioia, L. (2016). Computational Approaches to the Prediction of the Redox Potentials of Iron and Copper Bioinorganic Systems. *Int. J. Quantum Chem.* 116 (22), 1695–1705. doi:10.1002/qua.25228

- Chauhan, P. S., Goradia, B., and Saxena, A. (2017). Bacterial Laccase: Recent Update on Production, Properties and Industrial Applications. *3 Biotech* 7 (5), 323–420. doi:10.1007/s13205-017-0955-7
- Frisch, M. J., Trucks, G. W., Schlegel, H. B., Scuseria, G. E., Robb, M. A., Cheeseman, J. R., et al. (2016). *Gaussian 16 Rev. C.01*. Wallingford, CT: Gaussian, Inc.
- Ghiasi, M., Shahabi, P., and Supuran, C. T. (2021). Quantum Mechanical Study on the Activation Mechanism of Human Carbonic Anhydrase VII Cluster Model with Bis-Histamine Schiff Bases and Bis-Spinacemine Derivatives. *Bioorg. Med. Chem.* 44, 116276. doi:10.1016/j.bmc.2021.116276
- Giacobelli, V. G. (2017). *Wild-Type and Mutated Laccases for a Green Industry*. Campania: Fedoa.unina.it.
- Grimme, S., Hansen, A., Brandenburg, J. G., and Bannwarth, C. (2016). Dispersion-corrected Mean-Field Electronic Structure Methods. *Chem. Rev.* 116 (9), 5105–5154. doi:10.1021/acs.chemrev.5b00533
- Himo, F. (2017). Recent Trends in Quantum Chemical Modeling of Enzymatic Reactions. *J. Am. Chem. Soc.* 139 (20), 6780–6786. doi:10.1021/jacs.7b02671
- Holland, J. P., Green, J. C., and Dilworth, J. R. (2006). Probing the Mechanism of Hypoxia Selectivity of Copper Bis(thiosemicarbazono) Complexes: DFT Calculation of Redox Potentials and Absolute Acidities in Solution. *Dalton Trans.* 4 (6), 783–794. doi:10.1039/b512656h
- Hong, G., Ivnitski, D. M., Johnson, G. R., Atanassov, P., and Pachter, R. (2011). Design Parameters for Tuning the Type I Cu Multicopper Oxidase Redox Potential: Insight from a Combination of First Principles and Empirical Molecular Dynamics Simulations. *J. Am. Chem. Soc.* 133 (13), 4802–4809. doi:10.1021/ja105586q
- Isse, A. A., and Gennaro, A. (2010). Absolute Potential of the Standard Hydrogen Electrode and the Problem of Interconversion of Potentials in Different Solvents. *J. Phys. Chem. B* 114 (23), 7894–7899. doi:10.1021/jp100402x
- Janusz, G., Pawlik, A., Świdarska-Burek, U., Polak, J., Sulej, J., Jarosz-Wilkolazka, A., et al. (2020). Laccase Properties, Physiological Functions, and Evolution. *Int. J. Mol. Sci.* 21 (3), 966. doi:10.3390/ijms21030966
- Kojima, Y., Tsukuda, Y., Kawai, Y., Tsukamoto, A., Sugiura, J., Sakaino, M., et al. (1990). Cloning, Sequence Analysis, and Expression of Ligninolytic Phenoloxidase Genes of the White-Rot Basidiomycete *Coriolus Hirsutus*. *J. Biol. Chem.* 265 (25), 15224–15230. doi:10.1016/s0021-9258(18)77245-1
- Krieger, E., and Vriend, G. (2014). YASARA View-Molecular Graphics for All Devices-From Smartphones to Workstations. *Bioinformatics* 30 (20), 2981–2982. doi:10.1093/bioinformatics/btu426
- Li, Z., Wei, R., Gao, M., Ren, Y., Yu, B., Nie, K., et al. (2020). Biodegradation of Low-Density Polyethylene by *Microbulbifer Hydrolyticus* IRE-31. *J. Environ. Manag.* 263, 110402. doi:10.1016/j.jenvman.2020.110402
- Liao, R.-Z., and Thiel, W. (2012). Comparison of QM-Only and QM/MM Models for the Mechanism of Tungsten-dependent Acetylene Hydratase. *J. Chem. Theory Comput.* 8 (10), 3793–3803. doi:10.1021/ct3000684
- Liu, J., Chakraborty, S., Hosseinzadeh, P., Yu, Y., Tian, S., Petrik, I., et al. (2014). Metalloproteins Containing Cytochrome, Iron-Sulfur, or Copper Redox Centers. *Chem. Rev.* 114 (8), 4366–4469. doi:10.1021/cr400479b
- Lu, T., and Chen, Q. (2021). Shermo: A General Code for Calculating Molecular Thermochemistry Properties. *Comput. Theor. Chem.* 1200, 113249. doi:10.1016/j.comptc.2021.113249
- Madhavi, V., and Lele, S. (2009). Laccase: Properties and Applications. *BioResources* 4 (4), 1694–1717. doi:10.1016/B978-0-12-805419-2.00007-1
- Marenich, A. V., Ho, J., Coote, M. L., Cramer, C. J., and Truhlar, D. G. (2014). Computational Electrochemistry: Prediction of Liquid-phase Reduction Potentials. *Phys. Chem. Chem. Phys.* 16 (29), 15068–15106. doi:10.1039/c4cp01572j
- Martins, L. O., Durão, P., Brissos, V., and Lindley, P. F. (2015). Laccases of Prokaryotic Origin: Enzymes at the Interface of Protein Science and Protein Technology. *Cell Mol. Life Sci.* 72 (5), 911–922. doi:10.1007/s00018-014-1822-x
- Mateljak, I., Monza, E., Lucas, M. F., Guallar, V., Aleksejeva, O., Ludwig, R., et al. (2019). Increasing Redox Potential, Redox Mediator Activity, and Stability in a Fungal Laccase by Computer-Guided Mutagenesis and Directed Evolution. *ACS Catal.* 9 (5), 4561–4572. doi:10.1021/acscatal.9b00531
- Moreno, A. D., Ibarra, D., Eugenio, M. E., and Tomás-Pejó, E. (2020). Laccases as Versatile Enzymes: from Industrial Uses to Novel Applications. *J. Chem. Technol. Biotechnol.* 95 (3), 481–494. doi:10.1002/jctb.6224
- Phillips, J. C., Hardy, D. J., Maia, J. D. C., Stone, J. E., Ribeiro, J. V., Bernardi, R. C., et al. (2020). Scalable Molecular Dynamics on CPU and GPU Architectures with NAMD. *J. Chem. Phys.* 153 (4), 044130. doi:10.1063/5.0014475
- Piontek, K., Antorini, M., and Choinowski, T. (2002). Crystal Structure of a Laccase from the Fungus *Trametes Versicolor* at 1.90-Å Resolution Containing a Full Complement of Coppers. *J. Biol. Chem.* 277 (40), 37663–37669. doi:10.1074/jbc.m204571200
- Sakurai, T., and Kataoka, K. (2007). Basic and Applied Features of Multicopper Oxidases, CueO, Bilirubin Oxidase, and Laccase. *Chem. Rev.* 7 (4), 220–229. doi:10.1002/tcr.20125
- Santhanam, N., Vivanco, J. M., Decker, S. R., and Reardon, K. F. (2011). Expression of Industrially Relevant Laccases: Prokaryotic Style. *Trends Biotechnol.* 29 (10), 480–489. doi:10.1016/j.tibtech.2011.04.005
- Sheng, X., Kazemi, M., Planas, F., and Himo, F. (2020). Modeling Enzymatic Enantioselectivity Using Quantum Chemical Methodology. *ACS Catal.* 10 (11), 6430–6449. doi:10.1021/acscatal.0c00983
- Shiroya, A. J. (2021). *Recent Advances of Laccase Enzyme in Industrial Biotechnology: A Review*. Surat: Pharma News.
- Siegbahn, P. E. M. (2006). The Performance of Hybrid DFT for Mechanisms Involving Transition Metal Complexes in Enzymes. *J. Biol. Inorg. Chem.* 11 (6), 695–701. doi:10.1007/s00775-006-0137-2
- Singh, S. K., Roberts, S. A., McDevitt, S. F., Weichsel, A., Wildner, G. F., Grass, G. B., et al. (2011). Crystal Structures of Multicopper Oxidase CueO Bound to Copper (I) and Silver (I): Functional Role of a Methionine-Rich Sequence. *J. Biol. Chem.* 286 (43), 37849–37857. doi:10.1074/jbc.m111.293589
- Solomon, E. I., Augustine, A. J., and Yoon, J. (2008). O<sub>2</sub> Reduction to H<sub>2</sub>O by the Multicopper Oxidases. *Dalton Trans.* 6 (30), 3921–3932. doi:10.1039/b800799c
- Uudsemaa, M., and Tamm, T. (2003). Density-functional Theory Calculations of Aqueous Redox Potentials of Fourth-Period Transition Metals. *J. Phys. Chem. A* 107 (46), 9997–10003. doi:10.1021/jp0362741
- Vázquez-Lima, H., Guadarrama, P., and Martínez-Anaya, C. (2012). Geometric Distortions on a Three-Coordinated T1 Cu Site Model as a Potential Strategy to Modulate Redox Potential. A Theoretical Study. *J. Mol. Model* 18 (2), 455–466. doi:10.1007/s00894-011-1063-y
- Walker, M., Harvey, A. J. A., Sen, A., and Dessent, C. E. H. (2013). Performance of M06, M06-2X, and M06-HF Density Functionals for Conformationally Flexible Anionic Clusters: M06 Functionals Perform Better than B3LYP for a Model System with Dispersion and Ionic Hydrogen-Bonding Interactions. *J. Phys. Chem. A* 117 (47), 12590–12600. doi:10.1021/jp408166m
- Witte, J., Goldey, M., Neaton, J. B., and Head-Gordon, M. (2015). Beyond Energies: Geometries of Nonbonded Molecular Complexes as Metrics for Assessing Electronic Structure Approaches. *J. Chem. Theory Comput.* 11 (4), 1481–1492. doi:10.1021/ct501050s
- Xu, F., Berka, R. M., Wahleithner, J. A., Nelson, B. A., Shuster, J. R., Brown, S. H., et al. (1998). Site-Directed Mutations in Fungal Laccase: Effect on Redox Potential, Activity And pH Profile. *Biochem. J.* 334 (1), 63–70. doi:10.1042/bj3340063
- Yan, L., Lu, Y., and Li, X. (2016). A Density Functional Theory Protocol for the Calculation of Redox Potentials of Copper Complexes. *Phys. Chem. Chem. Phys.* 18 (7), 5529–5536. doi:10.1039/c5cp06638g
- Zhang, L., Cui, H., Zou, Z., Garakani, T. M., Novoa-Henriquez, C., Jooyeh, B., et al. (2019). Directed Evolution of a Bacterial Laccase (CueO) for Enzymatic Biofuel Cells. *Angew. Chem. Int. Ed.* 58 (14), 4562–4565. doi:10.1002/anie.201814069

**Conflict of Interest:** The authors declare that the research was conducted in the absence of any commercial or financial relationships that could be construed as a potential conflict of interest.

**Publisher's Note:** All claims expressed in this article are solely those of the authors and do not necessarily represent those of their affiliated organizations, or those of the publisher, the editors, and the reviewers. Any product that may be evaluated in this article, or claim that may be made by its manufacturer, is not guaranteed or endorsed by the publisher.

Copyright © 2022 Jiang, Cui, Wei, Nie, Xu and Liu. This is an open-access article distributed under the terms of the Creative Commons Attribution License (CC BY). The use, distribution or reproduction in other forums is permitted, provided the original author(s) and the copyright owner(s) are credited and that the original publication in this journal is cited, in accordance with accepted academic practice. No use, distribution or reproduction is permitted which does not comply with these terms.



## OPEN ACCESS

## EDITED BY

Hui-Min Qin,  
Tianjin University of Science and  
Technology, China

## REVIEWED BY

Lijun Guan,  
Heilongjiang Academy of Agricultural  
Sciences, China  
Shuhong Mao,  
Tianjin University of Science and  
Technology, China

## \*CORRESPONDENCE

Fengguang Zhao,  
fgzhao@scut.edu.cn  
Shuangyan Han,  
syhan@scut.edu.cn

## SPECIALTY SECTION

This article was submitted to Bioprocess  
Engineering,  
a section of the journal  
Frontiers in Bioengineering and  
Biotechnology

RECEIVED 13 August 2022

ACCEPTED 26 August 2022

PUBLISHED 13 September 2022

## CITATION

Zhang Y, Liu C, Yang M, Ou Z, Lin Y,  
Zhao F and Han S (2022),  
Characterization and application of a  
novel xylanase from *Halolactibacillus*  
*miurensis* in wholewheat bread making.  
*Front. Bioeng. Biotechnol.* 10:1018476.  
doi: 10.3389/fbioe.2022.1018476

## COPYRIGHT

© 2022 Zhang, Liu, Yang, Ou, Lin, Zhao  
and Han. This is an open-access article  
distributed under the terms of the  
[Creative Commons Attribution License](#)  
(CC BY). The use, distribution or  
reproduction in other forums is  
permitted, provided the original  
author(s) and the copyright owner(s) are  
credited and that the original  
publication in this journal is cited, in  
accordance with accepted academic  
practice. No use, distribution or  
reproduction is permitted which does  
not comply with these terms.

# Characterization and application of a novel xylanase from *Halolactibacillus miurensis* in wholewheat bread making

Yaping Zhang<sup>1</sup>, Chun Liu<sup>1</sup>, Manli Yang<sup>1</sup>, Zuyun Ou<sup>2</sup>, Ying Lin<sup>1</sup>,  
Fengguang Zhao<sup>3\*</sup> and Shuangyan Han<sup>1\*</sup>

<sup>1</sup>Guangdong Key Laboratory of Fermentation and Enzyme Engineering, School of Biology and Biological Engineering, South China University of Technology, Guangzhou, China, <sup>2</sup>Dongguan Huamei Food Co. Ltd., Dongguan, China, <sup>3</sup>School of Light Industry and Engineering, South China University of Technology, Guangzhou, China

The presence of arabinoxylan in wholewheat flour affects its quality significantly. Here, an efficient arabinoxylan hydrolytic enzyme, Hmxyn, from *Halolactibacillus miurensis* was identified and heterologously expressed in *pichia pastoris*. Moreover, its relevant properties, including potential application in the wholewheat bread were evaluated. Recombinant Hmxyn exhibited maximal activity at 45°C and pH 6.5, and was stable at mid-range temperature (<55°C) and pH (5.5–8.0) conditions. Hmxyn had a clear hydrolysis effect on wheat arabinoxylan in dough and caused the degradation of the water-unextractable arabinoxylan, which increased the content of wheat soluble arabinoxylan of dough. The fermentation characteristics results and microstructure analysis revealed that Hmxyn improved the organizational structure and air holding capacity of fermented dough, thus promoting the dough expansion. Baking experiments further showed that Hmxyn significantly increased specific volume- and texture-linked properties of wholewheat breads. This study indicates the application potential of Hmxyn in the preparation of wholewheat bread.

## KEYWORDS

xylanase, wheat arabinoxylan, enzyme activity, dough fermentation, bread quality

## Introduction

The “2022 Dietary Guidelines for Chinese residents” suggested that their daily diet should consist of grains, including 50–150 g of whole grains and miscellaneous beans ([Chinese-Nutrition-Society, 2022](#)). Regular intake of whole grains is contributed to maintain a healthy weight and reduce the risk of diabetes, cardiovascular disease, and some cancers ([Giacco et al., 2011](#)). Wholewheat bread is a wholegrain food that contains much more fibers, vitamins, minerals, phytochemicals, and non-starch polysaccharides, than refined white bread ([Hirawan et al., 2010](#); [Jonnalagadda et al., 2011](#)). However, the quality of most bread made of whole wheat is unacceptable due to poor processing and reduced organoleptic characteristics, which was resulted from high dietary fiber content

and rough texture (Hemdane et al., 2016). With a view towards improving the quality of wholewheat bread, processing aids, such as enzymes, are added to the flour to modify the processability of dough to solve these issues (Penella et al., 2008; Bae et al., 2014).

Xylanases are hydrolytic enzymes that catalyze the cleavage of  $\beta$ -1,4 linkages in the xylan backbone and have attracted considerable research interest in breadmaking (Mantyla et al., 2007). Xylanase modifies the structure and function of arabinoxylan by attacking the arabinoxylan backbone and reducing the degree of polymerization, thereby improves bread quality (Courtin and Delcour, 2002). Previous studies have shown that some xylanases could increase the softness and specific volume of wheat bread, and retarded its staling during storage (Jiang et al., 2005; Carvalho et al., 2016; Ghoshal et al., 2017).

Different xylanase families have specific effects on arabinoxylans in terms of their breaking points and reaction products, which, in turn, exert distinct effects on bread making (Driss et al., 2013). It is generally believed that water-unextractable arabinoxylan exerts a negative effect on dough properties and bread quality, whereas the opposite is shown by water-extractable arabinoxylan (Wang et al., 2003). The type and source of xylanase determine its effects on arabinoxylans, especially in regard to the preference for soluble or insoluble arabinoxylans, which has been consistently neglected in the past (Driss et al., 2013). In addition, xylanase induces the release of xylo-oligosaccharides from flour, following which these oligomers exert pre-biotic effects and stimulate the growth of intestinal bifidobacterial, thereby promoting intestinal health (Chapla et al., 2012).

Bread preparation process may be divided into three stages: mixing, fermentation, and baking (Dahiya et al., 2020). During the mixing and fermentation stages when xylanase is known to work, the temperature is maintained at 30°C–40°C (Collins et al., 2005). When switching to the baking stage with temperature up to 150°C–210°C, the enzyme often deactivated due to high temperature. Simultaneously, the pH of the dough should also be considered, due to the carbonic acid produced by the dissolution of carbon dioxide in water and the organic acids produced by bacteria in the dough, which urge working environments to be weakly acidic (Verjans et al., 2010; Balestra et al., 2015). Optimal xylanase activity at medium temperatures and weak acidity is more advantageous for the baking industry from economic perspective, due to less enzymes being needed. Therefore, the focus of current research is geared towards seeking specific xylanases that best suit the processing environment of whole wheat bread.

This study first reported a novel xylanase Hmxyn derived from *H. miurensis* and expressed it in *pichia pastoris*. Hmxyn showed maximum efficacy under conditions involving mid-range temperatures and a weakly acidic environment, which

was ideal for dough fermentation, and promoted solubilization of arabinoxylan in wholewheat dough. Furthermore, Hmxyn appeared potential for improving the fermentation performance and quality of wholewheat bread. Thus, the findings of the current study indicate that Hmxyn may be a promising candidate for bread improver in wholewheat bread baking.

## Materials and methods

### Materials

*Escherichia coli* DH5 $\alpha$ , *P. pastoris* X-33 were used as host for plasmid propagation and heterologous gene expression. Wheat arabinoxylan was purchased from Megazyme International (Irish, Ireland). Beechwood xylan was purchased from Sigma-Aldrich (St. Louis, MO, United States). Oat pelt xylan, pectin, and sodium carboxymethyl cellulose were purchased from Solarbio (Beijing, China). The restriction endonucleases were purchased from Thermo Fisher Scientific (Shanghai, China). Wholewheat flour with 57% water absorption, 11.00% protein, and 12.10% moisture was purchased from Saixin Flour Industry Co. Ltd. (Bayannur, China). The buffered methanol-complex and glycerol-complex medium (BMMY/BMGY), yeast extract peptone dextrose agar medium (YPD), and low salt Luria Bertani media (LBL) were prepared according to the yeast fermentation processing guidelines (Invitrogen). Unless otherwise stated, other reagents were analytical pure reagents, purchased from China.

### Gene mining for putative xylanase and sequence analysis for target gene

BLASTP was performed in NCBI database (<https://blast.ncbi.nlm.nih.gov/Blast>) using *Thermomyces lanuginosus* xylanase as a probe sequence for potential bread-making xylanase enzymes. MEGA-X software was used to construct phylogenetic tree according to the neighbor-joining statistical method. Conserved domains were predicted by CD-search tool (<https://www.ncbi.nlm.nih.gov/Structure/cdd/wrpsb.cgi>) in NCBI database. The signal peptide of enzyme was predicted using the SignalP 5.0 (<https://services.healthtech.dtu.dk/service.php?SignalP-5.0>). The molecular mass of the deduced protein was predicted using ExPASy (<http://web.expasy.org/protparam/>) and sequence alignments were performed by DNAMAN 6.0 software. Three-dimensional structure of the enzyme was obtained via homology modeling, using the SWISS-MODEL online server (<https://swissmodel.expasy.org/>).



## Construction of recombinant expression *P. pastoris* strain expressing *H. miurensis* xylanase

The gene sequence of *H. miurensis* xylanase (abbreviated as Hmxyn) was optimized based on the codon preference of *P. pastoris*. Then it was outsourced to Generay Biotech Co. Ltd. (Shanghai, China) for full gene synthesis. The *hmxyn* gene fragment was further inserted into the pPICZαA vector at *EcoR* I and *Not* I sites with a poly histidine tag (6×His tag) located in the C-terminus. The ligation product was transformed into the *E. coli* DH5α cells and identified via PCR, *EcoR* I/*Not* I double enzyme digestion, and DNA sequencing. The resulting plasmid containing *hmxyn* was named pPICZα-*hmxyn*. Then, the pPICZα-*hmxyn* plasmid was linearized by restriction endonuclease *Sac* I and transformed into *P. pastoris* X-33 using the electroporation method. Yeast colony PCR was used to further screen positive clones. The upstream primer was 5'-GCTGTTACTTCCAACGAAAC-3', and the downstream primer was 5'-TTGAATTTCGAAGTAATC-3'.

## Expression and purification of *H. miurensis* xylanase

Positive colonies were cultured in 5 mL BMGY medium at 30°C overnight. Then, the yeast cells were transferred into 25 mL BMMY medium with initial OD<sub>600</sub> at 0.5–1.0 and cultured at 30°C for 192 h. During cultivation process, 1.0% (v/v) methanol was supplemented to BMMY culture every 24 h to induce the protein expression. And samples were collected to measure the protein concentration, OD<sub>600</sub> and xylanase activity every 24 h.

For purification of 6×His-tagged recombinant Hmxyn, the *P. pastoris* culture supernatant was firstly collected after centrifugation for 10 min (10,000×g, 4°C). The supernatant was then passed through a 0.22 μm ultrafiltration membrane to prevent clogging of the Ni-NTA column. After pre-equilibrated with buffer A (100 mmol/L phosphate buffer, 500 mmol/L NaCl, pH 7.0), the supernatant was loaded onto a Ni-NTA column in 2 mL/min. The column was eluted with the buffer B (100 mmol/L phosphate buffer, 500 mmol/L imidazole, and 500 mmol/L NaCl, pH 7.0) containing a step gradient at a flow rate of 2 mL/min, and the fractions with enzymatic activity were collected. Further, high concentrations of imidazole and NaCl were removed from the enzyme components by dialysis to avoid their interference with subsequent experiments. Dialysate contained 100 mmol/L phosphate buffer (pH 6.0) and 50 mmol/L NaCl. The purified Hmxyn were estimated using sodium dodecyl sulfate-polyacrylamide gel electrophoresis (SDS-PAGE). And the protein concentration of purified Hmxyn was measured using the Bradford method, with bovine serum albumin (BSA) as the standard.

## Enzymatic properties of Hmxyn

Xylanase activity of Hmxyn was determined using wheat arabinoxylan as the substrate by monitoring reducing sugars production (Jwa et al., 2022). Briefly, 0.1 mL diluted Hmxyn and 0.1 mL of 1.0% (w/v) wheat arabinoxylan was incubated in 100 mmol/L phosphate buffer (pH 6.5) at 45°C for 10 min. Next, 0.3 mL of 3,5-dinitro salicylic acid (DNS) reagent was immediately added to reaction mixture and boiled for 5 min to terminate the reaction. After cooled to room temperature, the amount of reducing sugars released was estimated by measuring absorbance at 540 nm using a microplate reader (Gene Com. Ltd., Hong Kong, China). One unit (U) of enzyme activity was defined as the amount of Hmxyn that liberate 1 μmol of reducing sugars per minute under the described conditions.

The optimal pH value of Hmxyn was measured by determining the activity between pH 5.0–9.0 in 45°C. To determine pH stability of Hmxyn, purified enzymes were firstly incubated between pH 3.0–9.0 at 4°C for 12 h. Next, residual activity of Hmxyn was further measured using above method. Buffers used were 100 mmol/L citrate buffer (pH 3.0–6.0), 100 mmol/L phosphate buffer (pH 6.0–8.0), and 100 mmol/L Tris-HCl buffer (pH 7.0–9.0). Optimal temperature of Hmxyn was investigated by measuring the activity in a range of 25°C–55°C in pH 7.0. To determine the thermostability of Hmxyn, enzymes were pre-incubated at 30°C–80°C for 60 min in pH 6.5 and then the residual enzyme activities were assayed.

## Substrate specificity and hydrolysis property of Hmxyn

Several substrates of xylan (wheat arabinoxylan, beechwood xylan, and oat spelt xylan) were used to estimate the substrate specificity of Hmxyn, for which purpose purified Hmxyn was incubated with 1.0% (w/v) of each substrate in 100 mmol/L phosphate buffer (pH 6.5) at 45°C for 10 min. And the amount of reducing sugars produced was calculated as described in 2.5 with xylose as the standard. For conducting kinetic experiments ( $K_m$  and  $V_{max}$ ) of Hmxyn, seven various concentrations (1–20 g/L) of each tested substrates were incubated with the purified Hmxyn at 45°C for 5 min. The generation speed of reducing sugar was calculated using the DNS method and the data were analyzed using the nonlinear regression option in Origin 9.0 software.

Hydrolysis property of Hmxyn were studied by analyzing the hydrolysis products of different substrates. 0.1 mL 1% (w/v) of standard xylooligosaccharides (X2–X6) were incubated with 10 U Hmxyn at 45°C in pH 6.5 for 24 h separately. The hydrolysis products were spotted onto a thin-layer chromatography (TLC) plate (Qingdao Ocean Chemical Co., Ltd., Qingdao, China) for

TLC analysis with a mixture of butanol-acetic acid-water (2:1:1, v/v/v) as developing agent. The results were visualized by spraying the mixture of methanol-sulfuric acid (95:5, v/v) and followed by heating at 150°C for 3–5 min. Mixtures of xylose (X1) and xylooligosaccharides (X2–X5) were used as standard in this study.

## Extraction and determination of wheat arabinoxylan

The wheat arabinoxylan contents in dough was determined by the phloroglucinol-acetic acid method with proper modification (Douglas, 1981). Freeze-dried dough powder (25 mg) was suspended in 5 mL water and a 0.5 mL suspension was added to a stoppered glass tube for the determination of total arabinoxylan. Next, the remaining suspension was stirred at 25°C for 30 min. Subsequently, following centrifugation at 2500×g for 10 min, the supernatant (0.5 mL) was transferred into a stoppered glass tube to determine the water-extractable arabinoxylan content. Next, 5 mL of the freshly prepared extracting solution (110 mL glacial acetic acid, 1 mL 1.75% w/v glucose aqueous, 5 mL 20% w/v phloroglucinol-ethanol solution, and 2 mL concentrated hydrochloric) was added into the reaction glass tube. The tubes were placed in a boiling water bath for 25 min and then rapidly cooled in cold water. Absorbance at 552 nm and 510 nm was measured using a microplate reader (Gene Com. Ltd., Hong Kong, China). The standard curve was drawn using the absorbance value of 552 nm subtracting the absorbance value of 510 nm as the ordinate and standard concentration as the abscissa. Total arabinoxylan and water-extractable arabinoxylan contents in flour were calculated using a standard curve, and the water-unextractable arabinoxylan content of dough was calculated by subtracting the water-extractable arabinoxylan content from total arabinoxylan content.

## Determination of dough fermentability

Dough was prepared according to a previously described method with proper modifications (Liu et al., 2017). The recipe for dough was follows: whole-wheat flour (100 g), oil (3 g), salt (1.6 g), sugar (6 g), dehydrated yeast (1 g), water (38 g), milk powder (2.4 g), egg liquid (6 g) and appropriate amounts of Hmxyn (1,021.65 U/mg). These ingredients were mixed for 18 min at 180 r/min to form dough. Next, the dough was divided into 25 g pieces each and was placed in a graduated tube. Following fermentation at 38°C and 80% relative humidity (RH) for 0–80 min. The fermented dough was freeze-dried for scanning electron microscopy (SEM) observation.

## Scanning electron microscopy of dough

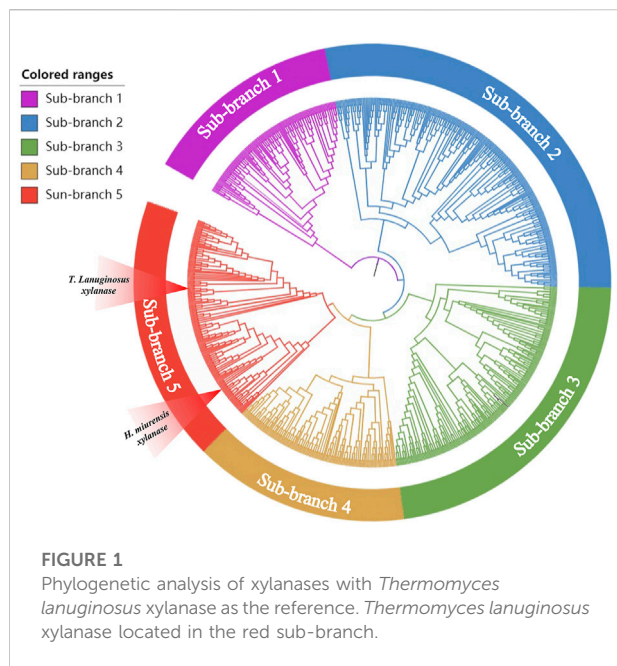
The microstructure of dough was observed using a previously described method (Zhang et al., 2019). Firstly, the freeze-dried dough was manually separated to obtain natural fracture dough. Next, the dough samples were pasted onto the sample table with conductive tape, and sprayed with gold using ion sputtering instrument (EMS 150TES, United States). Subsequently, the dough samples were visualized under a Merlin microscope (Carl Zeiss AG, Germany) at ×40 and ×500 magnification.

## Bread making process and quality assessment

Dough was prepared according to the method of 2.9. Wheat flour (100 g), oil (3 g), salt (1.6 g), sugar (6 g), dehydrated yeast (1 g), water (38 g), milk powder (2.4 g), egg liquid (6 g) and appropriate amounts of Hmxyn (1,021.65 U/mg) were put into the kneading bowl to form dough after mixed. Subsequently, the pH of unfermented dough was measured using a pH meter (PB-10, Sartorius, Germany) (Balestra et al., 2015), followed by divided and shaped the dough (50 g pieces each). After fermentation at 38°C and 80% relative humidity (RH) for 60 min, the pH of fermented dough was determined and the fermented dough was baked in an oven (KX32-V2171, Jiu Yang, China) for 10 min at 180°C. When the breads were cooled to room temperature, the weight, loaf volume and crumb texture of wholewheat breads were evaluated. The specific volume was calculated by volume-to-weight (mL/g). As for crumb texture analysis, a Texture Analyzer (TA-XT Plus, Stable Microsystem, Surrey, United Kingdom) which equipped with a 25 mm cylindrical aluminum probe was used. The test parameters were performed as follows: 50% compression ratio, 10 s gap between two compressions, 5 g trigger force, 1 mm/s pre-test speed, 1 mm/s test speed, and 5 mm/s post-test speed. Finally, bread slices with a thickness of 2 cm were placed on the test bench and the chewiness, gumminess, and hardness of the bread slices were recorded by Texture Analyzer.

## Statistical analysis

All experiments were performed at least in triplicate ( $n = 3$ ), and the results were shown as means  $\pm$  standard deviation (SD). Differences between treatments were analyzed using analysis of variance (ANOVA) and significance was set at  $p < 0.05$ .



## Results and discussion

### Gene mining and sequence analysis of Hmxyn

With an increasing number of microorganisms being sequenced, gene mining is gradually turning into a powerful tool that be used to detect novel genes encoding enzymes, such as glycosyltransferase,  $\alpha$ -amylase, and pectinase (Xiao et al., 2008; Xiao et al., 2014; Chen et al., 2022). Xylanase from *Thermomyces lanuginosus* (GenBank: spO43097.1) has been developed as a stellar bread improver by Danish enzyme maker Novozymes and has been listed in the China National Food Safety Standard Food Additive Usage Standard (GB2760). To explore a novel breadmaking xylanase, *T. lanuginosus* Xylanase was chosen as the probe for BLASTP in the NCBI database and 40%–60% amino acid similarity with probe sequences were used to construct a phylogenetic tree via the neighbor-joining statistical method (Chen et al., 2022). The results showed that the protein sequences obtained using BLASTP were divisible into different phylogenetic branches (Figure 1). Five new sequences (GenBank: XP031898167, EWZ46984.1, WP062323915.1, WP091499835.1, QPC67585.1) not yet been studied, but located at the same branch of the probe sequence, were selected as candidates. However, only the candidate xylanase derived from *H. miurensis* (GenBank: WP062323915.1) possessed a considerable expression of heterologous proteins in *P. pastoris* and showed wheat arabinoxylan hydrolysis activity in pre-experiments (Supplementary Figure S1). Therefore, the *H. miurensis* xylanase was selected for further studies.

*H. miurensis* xylanase contains 331 amino acids and a signal peptide consisting of 27 amino acids. Structural analyses of *H. miurensis* xylanase revealed the presence of a family 11 of glycoside hydrolases domain (11–191 amino acids), and a carbohydrate-binding module of family 36 (213–331 amino acids) which increase the affinity of the enzyme to its substrate (xylan) (Figure 2A). Homology modeling of Hmxyn using a previously characterized xylanase (XynJ, PDB: 6kka.1.A) from *Bacillus* sp. revealed that a typical  $\beta$ -jelly roll structure acted as the xylanase domain, while a  $\beta$ -sandwich structure acted as the CBM36 domain (Figure 2B). Sequence alignment of Hmxyn with XynJ xylanase was used to identify conserved residues, including two catalytic glutamic acids, Glu125 and Glu216, which were involved in substrate binding and catalysis (Supplementary Figure S2).

### Expression, purification, and biochemical characterization of Hmxyn

Hmxyn was cloned into the expression vector pPICZaA, and then transformed into *P. pastoris* X-33 competent cells by electroporation. The recombinant strains were cultivated and induced in BMMY medium with a methanol concentration of 1% (v/v). As induced expression time increased, the enzyme activity with wheat arabinoxylan as substrate and protein concentration also increased gradually, reaching 550.68 U/mL and 0.51 mg/ml after 168 h (Figure 2C). Ni-NTA affinity chromatography was used to purify recombinant Hmxyn with 6 $\times$  His-tag from fermentation broth, and wheat arabinoxylan was used as the substrate to determine the specific activity of the purified enzyme, which was 1,021.65 U/mg. The purified enzyme generated a single band with a molecular mass of approximately 45 kDa on SDS-PAGE, which was higher than the predicted molecular weight (39.1 kDa) basis of the amino acid sequence (Figure 2D). This may be attributed to the presence of protein translational modifications (PTMs) in *P. pastoris*, as three predicted O-linked glycosylation sites and five predicted N-glycosylation sites were found in Hmxyn.

The effects of pH and temperature on the activity and stability of purified Hmxyn were further investigated. As can be seen from Figure 3A, the optimum pH of Hmxyn was 6.5, while maintaining more than 80% of its activity in the range of pH 5.5 to pH 7.0. However, the enzyme activity was greatly reduced when the pH was higher than 7.0 or below 5.5. Recombinant Hmxyn exhibited good stability while maintaining a degree of activity that exceeded 80% within the pH range of 5.5–8.0 (Figure 3B). This indicated that Hmxyn can retain its activity and stability over a wide pH range. Recombinant Hmxyn exhibited maximum enzyme activity at 45°C, while retaining more than 60% of its total activity between 30–50°C (Figure 3C). In addition, Hmxyn was thermostable to temperatures below 50°C, considering it retained more than 60%

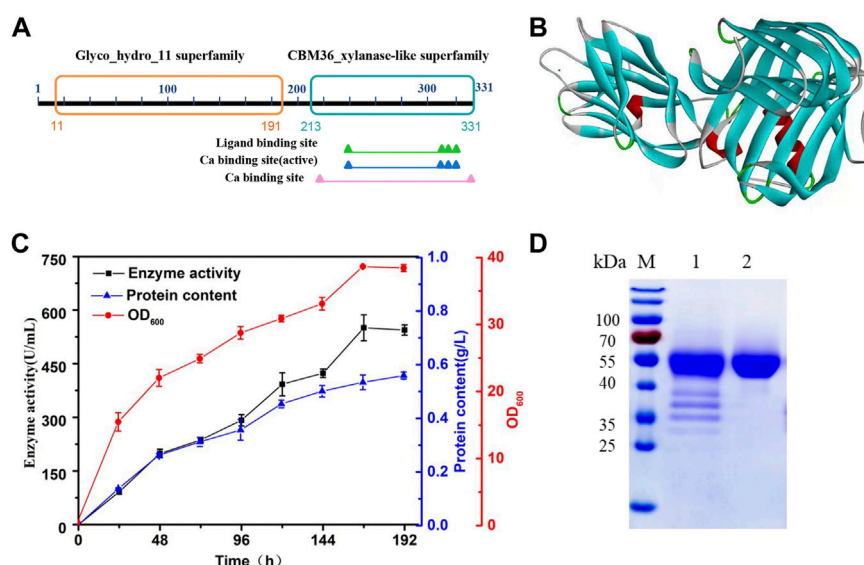


FIGURE 2

Protein sequence, three-dimensional structure, expression, and purification analysis of Hmxyn. (A) Conserved domains analysis of the amino acid sequence of Hmxyn. (B) The predicted structure of Hmxyn. Red represents  $\alpha$ -helix, blue represents  $\beta$ -sheet, green represents  $\beta$ -turn, and gray represents random coil structure. (C) Heterologous expression of Hmxyn in *Pichia pastoris*. (D) SDS-PAGE analysis of purified recombinant Hmxyn. Lane M, molecular markers. lane 1, crude enzyme; lane 2, purified fractions after Ni-NTA affinity chromatography.

of the enzymatic activity after incubation below 50°C for 60 min (Figure 3D).

Although many xylanases from different sources have been identified, few considered the adaptability of enzymes in specific breeding making environment. The various steps involved in dough preparation are usually performed at medium and low temperatures (Collins et al., 2005). Hmxyn showed good enzymatic activity over a wide temperature range extending from 30 to 55°C, consistent with the temperature of dough preparation. The pH activity of xylanase is also vital for baking, and a dough pH between 5.5 and 6.5 was tested in later experiments (Supplementary Table S1). A pH of 6.5 was optimum for Hmxyn xylanase and the enzyme showed approximately 80% of its original activity between pH 5.5 and 6.5 consistent with the pH of bread dough. Hmxyn is the first reported xylanase with good wheat arabinoxylan hydrolysis activity from *H. miurensis*, and its fine biochemical characteristics indicate its potential in wholewheat bread industrial applications.

## Substrate specificity and hydrolysis property of Hmxyn

Substrate specificity of Hmxyn was evaluated using wheat arabinoxylan, beechwood xylan, oat spelt xylan, sodium carboxymethyl cellulose (CMC-Na), and pectin as substrates. Enzyme activity was strong on wheat

arabinoxylan (1,021.65 U/mg), beechwood xylan (1,291.35 U/mg), and oat spelt xylan (1,146.97 U/mg), but negligible for CMC-Na and pectin (Figure 3E). Under optimal conditions, the values of kinetic constants,  $K_m$  and  $V_{max}$ , of recombinant Hmxyn were 16.59 g/L and 2,275.89  $\mu\text{mol}/\text{min}/\text{mg}$  for wheat arabinoxylan; 5.64 g/L and 1,640.49  $\mu\text{mol}/\text{min}/\text{mg}$  for beechwood xylan; and 5.82 g/L and 1,607.73  $\mu\text{mol}/\text{min}/\text{mg}$  for oat spelt xylan (Supplementary Figure S3). The  $K_m$  value of Hmxyn on beechwood xylan revealed a higher substrate affinity in comparison with xylanases from *Pseudopedobacter* (Sharma et al., 2018) and *Thermoascus aurantiacus* (Varnai et al., 2014) which showed values of 6.2 g/L and 11.14 g/L, respectively.

Hydrolysis properties of Hmxyn were investigated using standard xylooligosaccharides (X2-X6) series as substrates. Collectively, Hmxyn hydrolyzed xylopentose (X5), xylotetraose (X4), and xylotriose (X3) into xylobiose (X2) as the major end products, but did not hydrolyze xylobiose (Figure 3F). Xylobiose is a high valuable biomolecule with great prebiotic effects, such as promoting the production of probiotics, reducing cholesterol levels and enhancing biological calcium absorption, etc. (Zheng et al., 2020). This characteristic makes Hmxyn useful in the production of xylobiose. In addition, the hydrolysis pattern of Hmxyn was similar to that of other reported xylanases, such as those from *Paenibacillus* sp. (An et al., 2015) and *Trichoderma* sp. (Zhou et al., 2011), where the enzymes were active against xylooligosaccharides with at least three xylose chains (X3), predominantly generating xylobiose.



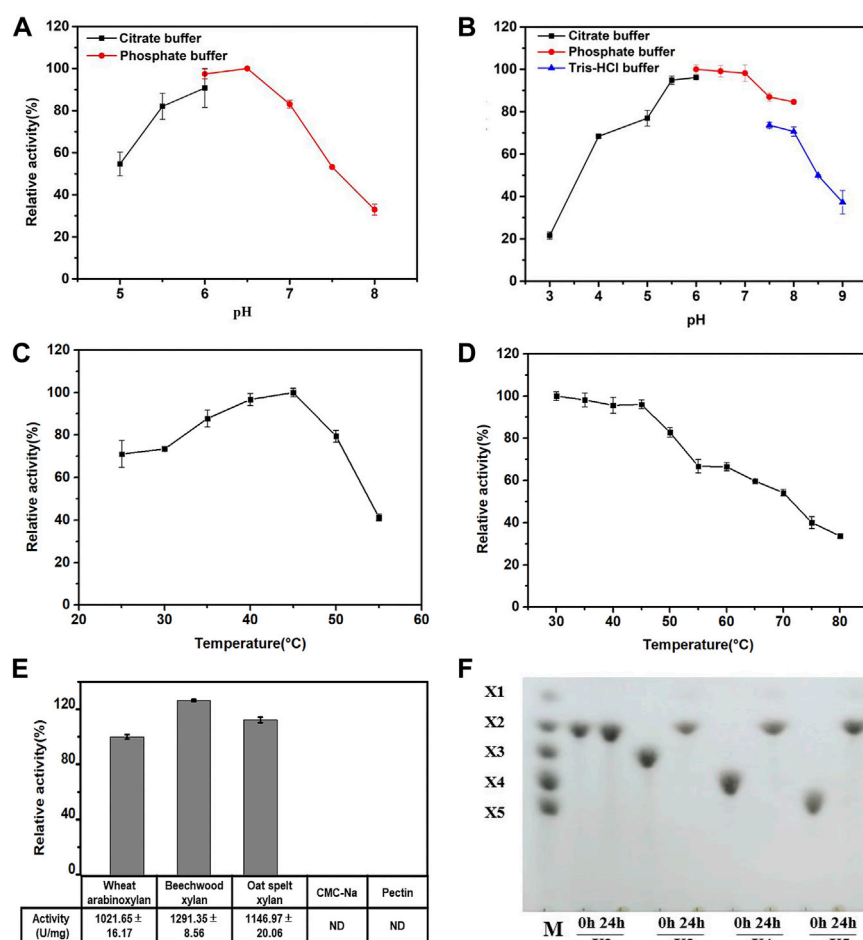


FIGURE 3

Biochemical characteristics of recombinant Hmxyn. (A) Effect of pH on Hmxyn activity. (B) Effect of pH on the stability of Hmxyn. Purified Hmxyn was incubated at 4°C for 12 h in 100 mmol/L citrate buffers (pH 3.0–6.0), 100 mmol/L phosphate buffer (pH 6.0–8.0) and 100 mmol/L Tris-HCl buffer (pH 7.0–9.0). (C) Effect of temperature on Hmxyn activity. (D) Effect of temperature on the stability of Hmxyn. The Hmxyn was incubated in 100 mmol/L phosphate buffer (pH 7.0) at different temperatures (25–55°C) for 60 min. (E) Substrate specificity of Hmxyn. (F) Hydrolysis products from linear xylooligosaccharides by Hmxyn. Lane M, size markers, xylose (X1), xylobiose (X2), xylotriose (X3), xylotetraose (X4) and xylopentaose (X5).

## Solubilization of arabinoxylan in wholewheat dough by Hmxyn

The presence of non-starch polysaccharides in bran and germ cell walls of whole wheat flour reportedly affect the quality of wholewheat flour (Autio, 2006). Xylanase improves bread quality by acting on the arabinoxylan backbone and reducing the degree of polymerization. Different xylanase preparations exert specific effects on arabinoxylan which, in turn, exert distinct effects on bread making. Although the biochemical characteristics of Hmxyn showed that it could hydrolyze commercial wheat arabinoxylan, its effect on wheat arabinoxylans in real dough is not clear. The results of Figure 4 showed that addition of Hmxyn degraded the content of water-unextractable arabinoxylan thereby improved the content of

wheat- extractable arabinoxylan of dough. The content of water-extractable arabinoxylan in the Hmxyn-treated dough significantly increased from 1.51% (control) to 1.99%, with an increase of 31.7% (Figure 4A), whereas the water-unextractable arabinoxylan content decreased from 2.69% (control) to 2.21% (Figure 4B).

Previous studies have suggested that water-extractable arabinoxylan has a low water affinity, thereby inducing water redistribution in the gluten network, which improves dough and bread quality (Li et al., 2012). By contrast, water-unextractable arabinoxylan exerts an opposite impact on water solubility, viscosity, and hydration properties, including dough consistency, bread volume, and bread texture (Wang et al., 2003). Therefore, increasing the content of water-extractable arabinoxylan in dough may enhance the quality of both

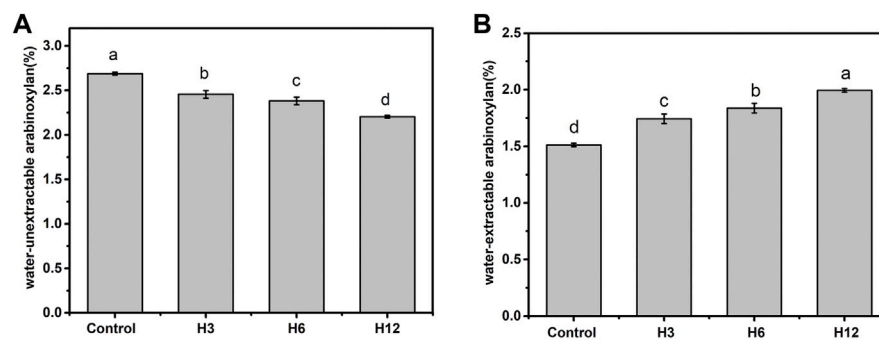


**FIGURE 4**

The content of wheat arabinoxylan in dough with the Hmxyn treatment. (A) Content of water-unextractable arabinoxylan. (B) Content of water-extractable arabinoxylan. Different letters in the same column represent significant differences ( $p < 0.05$ ). Control: control sample; H3-H12: dough prepared with the addition of 3, 6, and 12 mg Hmxyn per 1 kg wholewheat flour.

dough and bread. Solubilization of arabinoxylan by Hmxyn suggests its potential for application in wholewheat bread.

## Effect of Hmxyn addition on dough fermentation

It has been reported that water-extractable arabinoxylan may increase the elasticity and strength of gluten-starch films around the gas cells, and slow down the diffusion of  $\text{CO}_2$  from the dough due to its high viscosity (Marta et al., 1995; Koegelenberg and Chimphango, 2017). Furthermore, the addition of water-extractable arabinoxylan was beneficial to increase the water viscosity between gas cells and gluten, thereby exerting a positive effect on the structure of dough (Goesaert et al., 2005; Koegelenberg and Chimphango, 2017). Thus, degradation of water-unextractable arabinoxylan and solubilization of water-extractable arabinoxylan by Hmxyn, may contribute to the enhancement of dough fermentation quality.

Fermentability is an important index to measure the performance of yeast and the air holding capacity of bread. The stronger the fermentation power of dough, the larger the volume of bread. To evaluate the potential application of Hmxyn, the effects of Hmxyn on dough fermentation were assessed. The dough volume increased in all groups with increasing fermentation time (Figures 5A,B). In the early stage of dough fermentation (0–20 min), the volume of dough increased slowly, owing to the low release of carbon dioxide caused by the adaptive growth of yeast. In the middle stage of fermentation (20–60 min), there were a rapid increase in the dough volume due to a large amount of carbon dioxide was released, and the gluten network structure in the dough can prevent its escape. At the later stage of fermentation (>60 min), the increase of volume slowed down or even decrease, considering the gluten network structure was partially destroyed, resulting in the release of carbon dioxide.

Therefore, the dough fermented for 60 min was used in subsequent bread making. In addition, the volume of fermented dough treated with Hmxyn was larger than that of the control group (Figures 5A,B), especially in the middle and late stages of dough fermentation. When the addition dosage was 6 mg Hmxyn per 1 kg flour, the dough volume increased 3.5 and 3.9 times at 60 and 80 min, ~23.8% and ~16.3% higher than the control group, respectively. And the positive effects were better than those at 60 mg Pentopon Mono BG per 1 kg flour dosage. The above results showed that the addition of Hmxyn was beneficial to increase the fermentation ability of dough.

To further determine the effect of Hmxyn on fermented dough quality, the interior microstructure of fermented dough was observed by the scanning electron microscopy (SEM). Compared to those of the control group (untreated dough), a larger number of pores as well as bigger sized pores were observed in Hmxyn treated dough (Figures 6A1–A5), consistent with the result of dough fermentability. SEM ( $\times 500$  magnification) revealed that less starch exposure and more continuous network structures in the gluten matrix was observed in the Hmxyn treated dough compared with untreated dough (Figures 6A1–A5). As can be seen, the addition of Hmxyn improved the organizational structure and the air holding capacity of fermented dough, and then improved the fermentation capacity of dough. In addition, low-dose Hmxyn in flour can achieve effective enhancement effects on fermented dough compared with commercial enzymes.

## Effect of Hmxyn addition on wholewheat bread quality

Considering the application potential of Hmxyn in improving wholewheat bread, the effects of Hmxyn on end-

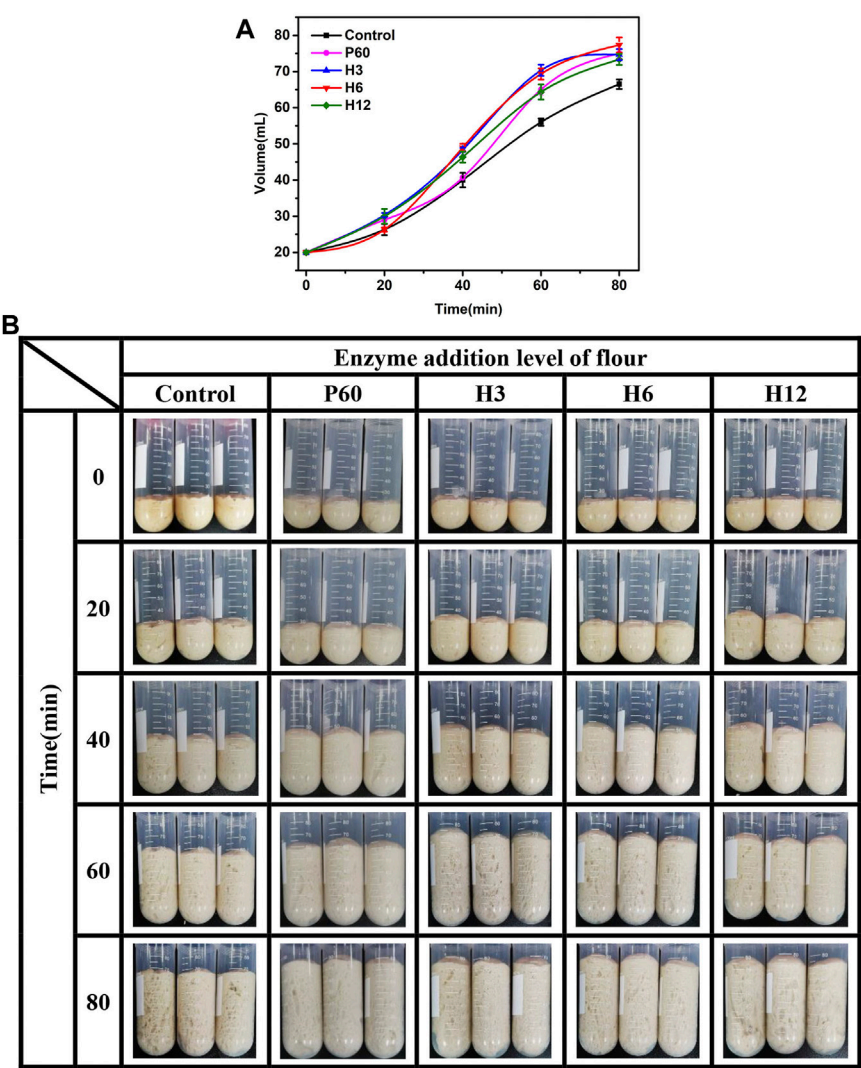


**FIGURE 5** Effect of Hmxyn addition on dough fermentation. **(A)** Curve of volume of fermented dough with time-variation. **(B)** Photos of fermented dough with time-variation. Control: control sample; H3-H12: dough prepared with the addition of 3, 6, and 12 mg Hmxyn per 1 kg wholewheat flour. P60: dough prepared with the addition of 60 mg Pentopan Mono BG per 1 kg wholewheat flour.

products bread were further studied and a commercial xylanase Pentopan Mono BG was used as positive control. Bread pores and volume are important indicators that may be used to evaluate bread, where the larger the specific volume of bread, the easier it is to accept. Moreover, bread slices treated with Hmxyn and Pentopan Mono BG had larger stoma compared with control group (Figure 6B), which was consistent with the results previously observed in the SEM of fermented dough (Figures 6A1–A5). In addition, the specific volumes of wholewheat bread samples supplemented with different concentrations of Hmxyn increased significantly, compared with those of the control group (Table 1). However, when the xylanase dose was

increased from 6 to 12 mg Hmxyn per 1 kg flour, bread volume decreased slightly (Table 1). Meanwhile, the addition Hmxyn at 3–6 mg per 1 kg flour improved the specific volume of wholewheat bread have a similar effect with Pentopan Mono BG-treated bread (60 mg Pentopan Mono BG per 1 kg flour).

Textural profiles of bakery products are associated with consumer perception. Softer, smoother, and superior flavor are the most important characteristics of breads. In this study, the effects of the addition of different xylanases on the textural properties of bread samples were evaluated via TPA and the results are shown (Table 1). The hardness, gumminess, and chewiness of all bread samples treated with

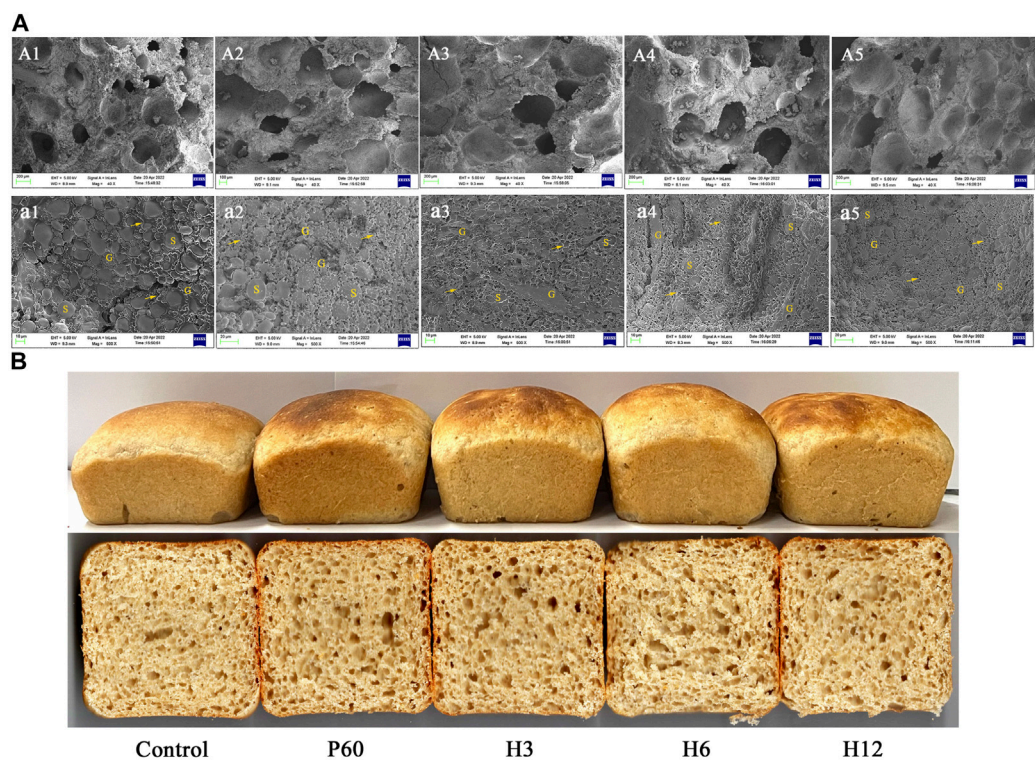


**FIGURE 6** (A): Scanning electron micrographs of fermented dough treated with different enzymes. A1, a1: control samples; A2, a2: dough prepared with 60 mg Pentopan Mono BG per 1 kg wholewheat flour; A3–A5, a3–a5: dough prepared with 3, 6, and 12 mg Hmxyn per 1 kg wholewheat flour; A1–A5:  $\times 40$  magnification; a1–a5:  $\times 500$  magnification. S, G and arrows represent starch granules, gluten matrix, and gluten network, respectively. (B) Images of bread with different enzyme treated. Control: control sample; H3–H12: dough prepared with the addition of 3, 6, and 12 mg Hmxyn per 1 kg wholewheat flour. P60: dough prepared with the addition of 60 mg Pentopan Mono BG per 1 kg wholewheat flour.

**TABLE 1** The effects of Hmxyn on quality of wholewheat bread.

Addition level	Specific volume (cm <sup>3</sup> /g)	Hardness (g)	Gumminess (g)	Chewiness (g)
Control	2.68 $\pm$ 0.10 <sup>c</sup>	1269.98 $\pm$ 81.09 <sup>a</sup>	795.26 $\pm$ 36.81 <sup>a</sup>	620.50 $\pm$ 37.58 <sup>a</sup>
P60	3.02 $\pm$ 0.01 <sup>ab</sup>	896.70 $\pm$ 30.53 <sup>b</sup>	550.83 $\pm$ 20.68 <sup>b</sup>	417.47 $\pm$ 20.75 <sup>c</sup>
H3	3.02 $\pm$ 0.05 <sup>ab</sup>	869.21 $\pm$ 31.32 <sup>bc</sup>	544.96 $\pm$ 22.51 <sup>b</sup>	426.48 $\pm$ 18.19 <sup>c</sup>
H6	3.09 $\pm$ 0.09 <sup>a</sup>	828.88 $\pm$ 73.62 <sup>c</sup>	516.2 $\pm$ 41.92 <sup>bc</sup>	423.57 $\pm$ 29.57 <sup>c</sup>
H12	2.91 $\pm$ 0.06 <sup>b</sup>	941.44 $\pm$ 100.27 <sup>b</sup>	577.44 $\pm$ 54.10 <sup>b</sup>	452.25 $\pm$ 48.58 <sup>b</sup>

Different letters in the same column indicate a significant difference at  $p < 0.05$ . Control: control sample; H3–H12: dough prepared with the addition of 3, 6, and 12 mg Hmxyn per 1 kg wholewheat flour. P60: dough prepared with the addition of 60 mg Pentopan Mono BG per 1 kg wholewheat flour.

different enzymes decreased significantly compared with that of the control group. The addition of Hmxyn at 6 mg per 1 kg flour reduced ( $p < 0.05$ ) the bread crumb hardness, gumminess, and chewiness by 34.73%, 35.09%, and 31.74%, respectively. Notably, the positive effects on bread hardness and gumminess were better than the Pentopan Mono BG treatment. However, when the Hmxyn dose was increased from 6 to 12 mg per 1 kg flour, wholewheat bread

hardness, gumminess and chewiness increased slightly, which was also consistent with the change seen in wholewheat bread volume. These results showed that the level of xylanase had to be optimized to be effective and that 6 mg Hmxyn per 1 kg flour was most effective in reducing the hardness and chewiness of bread. Similar trends in the association between bread hardness and the addition of various xylanases, such as *Aspergillus foetidus* xylanase



(Shah et al., 2006), *Thermoascus aurantiacus* xylanase (Oliveira et al., 2014), and *Plectosphaerella cucumerina* (Zhan et al., 2014), have been reported in other studies.

## Conclusion

In this study, a novel xylanase from *H. miurensis* showing wheat arabinoxylan hydrolysis activity was identified and expressed in *P. pastoris*. Application of recombinant Hmxyn significantly degraded the water-unextractable arabinoxylan and thereby improved the organizational structure, air holding capacity and the expansion rate of dough. Baking tests showed that Hmxyn played a positive role in the specific volume, texture, and crumb structure. However, an appropriate dosage is required to avoid certain negative effects that the inappropriate use of Hmxyn may exert on bread volume, texture, appearance, and firmness. As it should be, other properties of the recombinant Hmxyn, such as synergy with other enzymes and bread additives, need to be further studied in future.

## Data availability statement

The datasets presented in this study can be found in online repositories. The names of the repository/repositories and accession number(s) can be found in the article/Supplementary Material.

## Author contributions

All authors contributed to the background research and writing of the article, as well as the editing. In addition, all authors have read and approved the final version of this manuscript. Specific contributions are as follows: YZ: Formal analysis, Data curation, Writing-original draft. CL: Methodology, Visualization. MY: Methodology, Visualization. ZO: Conceptualization, Methodology. YL:

Conceptualization, Methodology. FZ: Conceived and designed the analysis, Writing-review and editing. SH: Conceptualization, Supervision, Writing-review and editing, Funding acquisition.

## Funding

This work was supported by the Key-Area Research and Development Program of Guangdong Province (2020B020226007), National Key Research and Development Program of China (2021YFC2100400), and Tianjin Synthetic Biotechnology Innovation Capacity Improvement Project (TSBICIP-KJGG-005).

## Conflict of interest

Author ZO is employed by Dongguan Huamei Food Co., Ltd.

The remaining authors declare that the research was conducted in the absence of any commercial or financial relationships that could be construed as a potential conflict of interest.

## Publisher's note

All claims expressed in this article are solely those of the authors and do not necessarily represent those of their affiliated organizations, or those of the publisher, the editors and the reviewers. Any product that may be evaluated in this article, or claim that may be made by its manufacturer, is not guaranteed or endorsed by the publisher.

## Supplementary material

The Supplementary Material for this article can be found online at: <https://www.frontiersin.org/articles/10.3389/fbioe.2022.1018476/full#supplementary-material>

## References

- An, J., Xie, Y., Zhang, Y., Tian, D. S., Wang, S. H., Yang, G. Y., et al. (2015). Characterization of a thermostable, specific GH10 xylanase from *Caldicellulosiruptor bescii* with high catalytic activity. *J. Mol. Catal. B Enzym.* 117, 13–20. doi:10.1016/j.molcatb.2015.04.003
- Autio, K. (2006). Effects of cell wall components on the functionality of wheat gluten. *Biotechnol. Adv.* 24 (6), 633–635. doi:10.1016/j.biotechadv.2006.07.002
- Bae, W., Lee, S. H., Yoo, S. H., and Lee, S. (2014). Utilization of a maltotetraose-producing amylase as a whole wheat bread improver: Dough rheology and baking performance. *J. Food Sci.* 79 (8), 1535–1540. doi:10.1111/1750-3841.12538
- Balestra, F., Pinnavaia, G. G., and Romani, S. (2015). Evaluation of the effects of different fermentation methods on dough characteristics. *J. Texture Stud.* 46 (4), 262–271. doi:10.1111/jtxs.12124
- Carvalho, E. A., Goes, L. M. D. S., Uetanabaro, A., Da Silva, E. G. P., Rodrigues, L. B., Pirovani, C. P., et al. (2016). Thermoresistant xylanases from *Trichoderma stromaticum*: Application in bread making and manufacturing xylo-oligosaccharides. *Food Chem.* 221 (PT.2), 1499–1506. doi:10.1016/j.foodchem.2016.10.144
- Chapla, D., Pandit, P., and Shah, A. (2012). Production of xylooligosaccharides from corn cob xylan by fungal xylanase and their utilization by probiotics. *Bioresour. Technol.* 115, 215–221. doi:10.1016/j.biortech.2011.10.083

- Chen, M., Song, F., Qin, Y., Han, S., Rao, Y., Liang, S., et al. (2022). Improving thermostability and catalytic activity of glycosyltransferase from panax ginseng by semi-rational design for rebaudioside D synthesis. *Front. Bioeng. Biotechnol.* 10, 884898. doi:10.3389/fbioe.2022.884898
- Chinese-Nutrition-Society (2022). *Dietary guidelines for Chinese residents*(2022). Beijing: People's Medical Publishing House.
- Collins, T., Gerday, C., and Feller, G. (2005). Xylanases, xylanase families and extremophilic xylanases. *FEMS Microbiol. Rev.* 29 (1), 3–23. doi:10.1016/j.femsre.2004.06.005
- Courtin, C. M., and Delcour, J. A. (2002). Arabinoxylans and endoxylanases in wheat flour bread-making. *J. Cereal Sci.* 35 (3), 225–243. doi:10.1006/jcrs.2001.0433
- Dahiya, S., Bajaj, B. K., Kumar, A., Tiwari, S. K., and Singh, B. (2020). A review on biotechnological potential of multifarious enzymes in bread making. *Process Biochem.* 99, 290–306. doi:10.1016/j.procbio.2020.09.002
- Douglas, S. G. (1981). A rapid method for the determination of pentosans in wheat flour. *Food Chem.* 7 (2), 139–145. doi:10.1016/0308-8146(81)90059-5
- Driss, D., Bhiri, F., Siela, M., Bessess, S., Chaabouni, S., and Ghorbel, R. (2013). Retracted: Improvement of Breadmaking Quality by Xylanase GH11 from *Penicillium occitanis* Pol6. *J. Texture Stud.* 44 (1), 75–84. doi:10.1111/j.1745-4603.2012.00367.x
- Ghoshal, G., Shivhare, U. S., and Banerjee, U. C. (2017). Rheological properties and microstructure of xylanase containing whole wheat bread dough. *J. Food Sci. Technol.* 54 (7), 1928–1937. doi:10.1007/s13197-017-2627-3
- Giacco, R., Della Pepa, G., Luongo, D., and Riccardi, G. (2011). Whole grain intake in relation to body weight: From epidemiological evidence to clinical trials. *Nutr. Metabolism Cardiovasc. Dis.* 21 (12), 901–908. doi:10.1016/j.numecd.2011.07.003
- Goesaert, H., Brijs, K., Veraverbeke, W. S., Courtin, C. M., Gebruers, K., and Delcour, J. A. (2005). Wheat flour constituents: How they impact bread quality, and how to impact their functionality. *Trends Food Sci. Technol.* 16 (1–3), 12–30. doi:10.1016/j.tifs.2004.02.011
- Hemdane, S., Jacobs, P. J., Dornez, E., Verspreet, J., Delcour, J. A., and Courtin, C. M. (2016). Wheat (*Triticum aestivum* L.) bran in bread making: A critical review. *Compr. Rev. Food Sci. Food Saf.* 15 (1), 28–42. doi:10.1111/1541-4337.12176
- Hirawan, R., Ser, W. Y., Arntfield, S. D., and Beta, T. (2010). Antioxidant properties of commercial, regular- and whole-wheat spaghetti. *Food Chem.* 119 (1), 258–264. doi:10.1016/j.foodchem.2009.06.022
- Jiang, Z., Li, X., Yang, S., Li, L., and Tan, S. (2005). Improvement of the breadmaking quality of wheat flour by the hyperthermophilic xylanase B from *Thermotoga maritima*. *Food Res. Int.* 38 (1), 37–43. doi:10.1016/j.foodres.2004.07.007
- Jonnalagadda, S. S., Harnack, L., Liu, R. H., McKeown, N., Seal, C., Liu, S. M., et al. (2011). Putting the whole grain puzzle together: Health benefits associated with whole grains summary of American society for nutrition 2010 satellite symposium. *J. Nutr.* 141 (5), 1011s–1022s. doi:10.3945/jn.110.132944
- Jwa, B., Sz, C., Cl, D., Xia, B., Zxa, B., and Twa, B. (2022). Efficient secretion of xylanase in *Escherichia coli* for production of prebiotic xylooligosaccharides. *LWT* 162, 113481. doi:10.1016/j.lwt.2022.113481
- Koegelenberg, D., and Chimphango, A. F. A. (2017). Effects of wheat-bran arabinoxylan as partial flour replacer on bread properties. *Food Chem.* 221, 1606–1613. doi:10.1016/j.foodchem.2016.10.130
- Li, J., Kang, J., Wang, L., Li, Z., Wang, R., Chen, Z. X., et al. (2012). Effect of water migration between arabinoxylans and gluten on baking quality of whole wheat bread detected by magnetic resonance imaging (MRI). *J. Agric. Food Chem.* 60 (26), 6507–6514. doi:10.1021/jf301195k
- Liu, G., Wang, J. J., Hou, Y., Huang, Y. B., Zhang, Y. P., Li, C. Z., et al. (2017). Recombinant wheat endoplasmic reticulum oxidoreductin 1 improved wheat dough properties and bread quality. *J. Agric. Food Chem.* 65 (10), 2162–2171. doi:10.1021/acs.jafc.6b05192
- Mantyla, A., Paloheimo, M., Hakola, S., Lindberg, E., Leskinen, S., Kallio, J., et al. (2007). Production in *Trichoderma reesei* of three xylanases from *Chaetomium thermophilum*: A recombinant thermoxylanase for biobleaching of kraft pulp. *Appl. Microbiol. Biotechnol.* 76 (2), 377–386. doi:10.1007/s00253-007-1020-y
- Marta, S., Izydorczyk, R., Costas, G., and Biliaderis (1995). Cereal arabinoxylans: Advances in structure and physicochemical properties. *Carbohydr. Polym.* 28 (1), 33–48. doi:10.1016/0144-8617(95)00077-1
- Oliveira, D. S., Telis-Romero, J., Da-Silva, R., and Franco, C. M. L. (2014). Effect of a *Thermoascus aurantiacus* thermostable enzyme cocktail on wheat bread quality. *Food Chem.* 143, 139–146. doi:10.1016/j.foodchem.2013.07.103
- Penella, J. M. S., Collar, C., and Haros, M. (2008). Effect of wheat bran and enzyme addition on dough functional performance and phytic acid levels in bread. *J. Cereal Sci.* 48 (3), 715–721. doi:10.1016/j.jcs.2008.03.006
- Shah, A. R., Shah, R. K., and Madamwar, D. (2006). Improvement of the quality of whole wheat bread by supplementation of xylanase from *Aspergillus foetidus*. *Bioresour. Technol.* 97 (16), 2047–2053. doi:10.1016/j.biortech.2005.10.006
- Sharma, K., Antunes, I. L., Rajulapati, V., and Goyal, A. (2018). Molecular characterization of a first endo-acting  $\beta$ -1, 4-xylanase of family 10 glycoside hydrolase (Ps GH10A) from *Pseudopedobacter saltans* comb. nov. *Process Biochem.* 70, 79–89. doi:10.1016/j.procbio.2018.03.025
- Varnai, A., Tang, C., Bengtsson, O., Atterton, A., Mathiesen, G., and Eijssink, V. G. H. (2014). Expression of endoglucanases in *Pichia pastoris* under control of the GAP promoter. *Microb. Cell Fact.* 13 (1), 57–10. doi:10.1186/1475-2859-13-57
- Verjans, P., Ornez, E. D., Delcour, J. A., and Courtin, C. M. (2010). Selectivity for water-unextractable arabinoxylan and inhibition sensitivity govern the strong bread improving potential of an acidophilic GH11 *Aureobasidium pullulans* xylanase. *Food Chem.* 123 (2), 331–337. doi:10.1016/j.foodchem.2010.04.039
- Wang, M., Hamer, R. J., van Vliet, T., Gruppen, H., Marseille, H., and Weegels, P. L. (2003). Effect of water unextractable solids on gluten formation and properties: Mechanistic considerations. *J. Cereal Sci.* 37 (1), 55–64. doi:10.1006/jcrs.2002.0478
- Xiao, Z., Boyd, J., Grosse, S., Beauchemin, M., Coupe, E., and Lau, P. (2008). Mining Xanthomonas and Streptomyces genomes for new pectinase-encoding sequences and their heterologous expression in *Escherichia coli*. *Appl. Microbiol. Biotechnol.* 78 (6), 973–981. doi:10.1007/s00253-008-1389-2
- Xiao, Z., Wu, M., Grosse, S., Beauchemin, M., Lévesque, M., and Lau, P. (2014). Genome mining for new  $\alpha$ -amylase and glucoamylase encoding sequences and high level expression of a glucoamylase from *Talaromyces stipitatus* for potential raw starch hydrolysis. *Appl. Biochem. Biotechnol.* 172 (1), 73–86. doi:10.1007/s12010-013-0460-3
- Zhan, F. X., Wang, Q. H., Jiang, S. J., Zhou, Y. L., Zhang, G. M., and Ma, Y. H. (2014). Developing a xylanase XYNZG from *Plectosphaerella cucumerina* for baking by heterologously expressed in *Kluyveromyces lactis*. *BMC Biotechnol.* 14 (107), 107–109. doi:10.1186/s12896-014-0107-7
- Zhang, Y. P., Chen, M. R., Chen, Y., Hou, Y., and Hu, S. Q. (2019). Characterization and exploration of recombinant wheat catalase for improvement of wheat-flour-processing quality. *J. Agric. Food Chem.* 67 (9), 2660–2669. doi:10.1021/acs.jafc.8b06646
- Zheng, F. Z., Song, L. N., Basit, A., Liu, J. Q., Miao, T., Wen, J. Q., et al. (2020). An endoxylanase rapidly hydrolyzes xylan into major product xylobiose via transglycosylation of xylose to xylotriose or xylotetraose. *Carbohydr. Polym.* 237, 116121. doi:10.1016/j.carbpol.2020.116121
- Zhou, P., Zhu, H. F., Yan, Q. J., Katrolia, P., and Jiang, Z. Q. (2011). Purification and properties of a psychrotrophic *Trichoderma* sp. xylanase and its gene sequence. *Appl. Biochem. Biotechnol.* 164 (6), 944–956. doi:10.1007/s12010-011-9186-2



## OPEN ACCESS

## EDITED BY

Hui-Min Qin,  
Tianjin University of Science and  
Technology, China

## REVIEWED BY

Evangelia Chronopoulou,  
Agricultural University of Athens,  
Greece  
Yunjie Xiao,  
Tianjin University, China

## \*CORRESPONDENCE

Ling Liu,  
ll772x@sxmu.edu.cn  
Benjin Xu,  
bj0726@sxmu.edu.cn

<sup>†</sup>These authors have contributed equally  
to this work and share first authorship

## SPECIALTY SECTION

This article was submitted to Industrial  
Biotechnology, a section of the journal  
Frontiers in Bioengineering and  
Biotechnology

RECEIVED 26 August 2022

ACCEPTED 15 November 2022

PUBLISHED 06 December 2022

## CITATION

Du M, Hou Z, Liu L, Xuan Y, Chen X,  
Fan L, Li Z and Xu B (2022), <sup>1</sup>Progress,  
applications, challenges and prospects  
of protein purification technology.  
*Front. Bioeng. Biotechnol.* 10:1028691.  
doi: 10.3389/fbioe.2022.1028691

## COPYRIGHT

© 2022 Du, Hou, Liu, Xuan, Chen, Fan, Li  
and Xu. This is an open-access article  
distributed under the terms of the  
[Creative Commons Attribution License  
\(CC BY\)](https://creativecommons.org/licenses/by/4.0/). The use, distribution or  
reproduction in other forums is  
permitted, provided the original  
author(s) and the copyright owner(s) are  
credited and that the original  
publication in this journal is cited, in  
accordance with accepted academic  
practice. No use, distribution or  
reproduction is permitted which does  
not comply with these terms.

# <sup>1</sup>Progress, applications, challenges and prospects of protein purification technology

Miao Du<sup>1†</sup>, Zhuru Hou<sup>2†</sup>, Ling Liu<sup>1,3†\*</sup>, Yan Xuan<sup>1</sup>,  
Xiaocong Chen<sup>4</sup>, Lei Fan<sup>4</sup>, Zhuoxi Li<sup>4</sup> and Benjin Xu<sup>1,3\*</sup>

<sup>1</sup>Department of Medical Laboratory Science, Fenyang College, Shanxi Medical University, Fenyang, China, <sup>2</sup>Science and Technology Centre, Fenyang College of Shanxi Medical University, Fenyang, China, <sup>3</sup>Key Laboratory of Lvliang for Clinical Molecular Diagnostics, Fenyang, China, <sup>4</sup>Department of Basic Medicine, Fenyang College of Shanxi Medical University, Fenyang, China

Protein is one of the most important biological macromolecules in life, which plays a vital role in cell growth, development, movement, heredity, reproduction and other life activities. High quality isolation and purification is an essential step in the study of the structure and function of target proteins. Therefore, the development of protein purification technologies has great theoretical and practical significance in exploring the laws of life activities and guiding production practice. Up to now, there is no forthcoming method to extract any proteins from a complex system, and the field of protein purification still faces significant opportunities and challenges. Conventional protein purification generally includes three steps: pretreatment, rough fractionation, and fine fractionation. Each of the steps will significantly affect the purity, yield and the activity of target proteins. The present review focuses on the principle and process of protein purification, recent advances, and the applications of these technologies in the life and health industry as well as their far-reaching impact, so as to promote the research of protein structure and function, drug development and precision medicine, and bring new insights to researchers in related fields.

## KEYWORDS

protein purification, challenges and prospects, life and health industry, affinity chromatography, ultracentrifugation

## 1 Introduction

Protein plays a key role in cell life activities and is the most abundant macromolecule in living organisms. It participates in a series of biological events, such as maintaining the structures and properties of organisms, catalyzing certain chemical reactions, transporting nutrients and metabolic wastes, providing a material basis for the body's

**Abbreviations:** PEG, Polyethylene glycol; AFC, Affinity chromatography; PEGMA, Polyethylene glycol methacrylate; IPTG, Isopropyl-beta-D-thiogalactopyranoside; BTS, Benzylthio-Sephacrose; DTT, DL-Dithiothreitol; DDM, n-dodecyl-beta-D-maltopyranoside.

TABLE 1 Characteristics and applications of different expressed hosts.

Expression system	Advantages	Disadvantages	Applications
<i>E. coli</i>	<i>E. coli</i> is small and grows rapidly. It is comparatively easier genetic manipulation and fermentation process (Tripathi and Shrivastava, 2019), well genetically characterized (McElwain et al., 2022), simple cultivation conditions (Rosano and Ceccarelli, 2014), and a clear genetic background (Nagai et al., 2018). It has the potential of highly expressed proteins (Kesidis et al., 2020)	Target proteins are easy to form inclusion body and codon bias, which lacks the post-translational modification system (Liu et al., 2019) and endotoxin issues (Mamat et al., 2015), interfering with the expression of target proteins	The most commonly used prokaryotic expression system, widely used in the development of the vaccine (Shirley and Taha, 2018), the production of the hormone (Zielinski et al., 2019; Keshavarz et al., 2021), the synthesis of the important enzyme (Lu et al., 2018). The expressed protein is used for structural insights (Muller et al., 2022)
<i>Saccharomyces cerevisiae</i>	It has high expression level, rapid growth, easy culture, high tolerance to the environment (Tesfaw and Assefa, 2014), low culture costs (Duman-Scheel, 2019), and has a post-translational modification system (Baghban et al., 2019)	Recombinant proteins may accumulate excessively in cells, resulting in reducing the subsequent yield (Tomás-Gamisans, 2020). Intracellular post-translational modifications can lead to the production of hyperglycosylated proteins, which are immunogenic to the human body (Rasala and Mayfield, 2015; Xu et al., 2016). The replication plasmid YRp of <i>Saccharomyces cerevisiae</i> is unstable (Xie et al., 2018)	It can be used as an expression system for the inhibition of human dipeptidyl peptidase IV/CD26 (hDPPIV) (Zhang et al., 2016). It can produce hormones (Chigira et al., 2008), functional foods (Lahue et al., 2020), and biofuels (Boonchuay et al., 2021; Hong and Nielsen, 2012), and itself can also be used as probiotics
<i>Pichia pastoris</i>	As methanol is used as the sole carbon source and energy source, there are a methanol-regulated alcohol oxidase promoter (PAOX1) and a post-translational modification system, which has an efficient secretion mechanism (Juturu and Wu, 2018). It is highly similar to the mammalian cell expression system, but has lower culture costs and rapid expression than the mammalian cell expression system, more advantageous than <i>S. cerevisiae</i> (Karbalaei et al., 2020), and less endogenous secreted protein production to facilitate subsequent isolation and purification (Tachioka et al., 2016)	Glucose, glycerol, and ethanol severely inhibited promoter PAOX1 activity and affected exogenous protein expression (Turkanoglu Ozcelik et al., 2019). Methanol is flammable and toxic, which is detrimental to cell growth (Santoso et al., 2012)	It can express membrane proteins very well (Bill and Hedfalk, 2021). The production of anticancer drug (Liu et al., 2015), viral surface antigens (Gupta et al., 2020), antiviral proteins, important enzymes as well as viral subunit recombinant protein vaccines (Zhang et al., 2015; Chen et al., 2017), synthetic food-grade proteins and food additives (Bhataya et al., 2009; Zhang et al., 2021a)
Mammalian cell expression system	It can be naturally folded (Nigi et al., 2017) and has a highly similar post-translational modification system to human cells (Liu et al., 2022)	High culture costs, susceptible to animal viruses (Tripathi and Shrivastava, 2019), high growth conditions, long culture cycle (Tripathi and Shrivastava, 2019), low intracellular protein production	Expressing large and structurally complex recombinant proteins, such as secreted proteins and membrane proteins (Yeliseev et al., 2020). Produce drugs (Walsh, 2018), prepare monoclonal antibodies, produce important recombinant glycoproteins such as immunoglobulin G (IgG), growth factor, clotting factor VII, erythropoietin, and $\alpha$ -1 anti-trypsin (Nishida et al., 2017; Goh and Ng, 2018)
Insect baculovirus expression vector system	It is easy to cultivate and can express a large number of proteins. It has protein folding ability, and a better post-translational modification system (Kesidis et al., 2020)	Insect cells grew to a certain cell density and were infected with recombinant baculoviruses (Owczarek et al., 2019), thus the culture time is long, a large number of viruses are required. The costs of consumables and equipment required in the cultivation process is high (Kesidis et al., 2020), and the glycosylation modification system is not identical to the mammalian cells (Tripathi and Shrivastava, 2019)	It can express intracellular proteins, membrane proteins (Hardy et al., 2019), and secreted proteins very well. Prepare influenza vaccine (Trombetta et al., 2022) and virus-like particle (Chen et al., 2022), produce large protein complex (Zhai et al., 2019), produce highly efficient avian recombinant adeno-associated virus (Wang et al., 2017; Mi et al., 2021), produce cytoplasmic protein and secreted protein (Lemaitre et al., 2019), and use purified protein to develop detection reagents
Transgenic plants	It has low costs, relatively safe, low risk of contamination with animal pathogens, easy amplification and good stability. It is insensitive to metabolites, and has the ability to modify N-glycosylation (Dirisala et al., 2017; Lomonosoff and D'Aoust, 2016; Lojewska et al., 2016; Park and Wi, 2016; Buyel et al., 2017; Owczarek et al., 2019)	It is vulnerable to pesticides, herbicides and other pollution (Tripathi and Shrivastava, 2019)	Produce tumor immunotherapy agents (Chen et al., 2016; Hefferon, 2017). Develop the influenza vaccine (Loh et al., 2017; Owczarek et al., 2019). Synthesis of recombinases for disease therapy (Tekoah et al., 2015; Hefferon, 2017)
Transgenic animals			

(Continued on following page)



TABLE 1 (Continued) Characteristics and applications of different expressed hosts.

Expression system	Advantages	Disadvantages	Applications
	With a post-translational modification system and correct post-translational modification, the expressed target proteins have high yields and high product quality (Tripathi and Shrivastava, 2019)	Culture and subsequent purification costs are very high, long culture cycle, low scale-up capacity, vulnerable to virus, carcinogenic DNA and other contamination, and also vulnerable to ethical factors (Tripathi and Shrivastava, 2019)	Recombinant proteins are based on therapeutics, such as growth factors, monoclonal antibodies, vaccines and enzymes (Tripathi and Shrivastava, 2019)

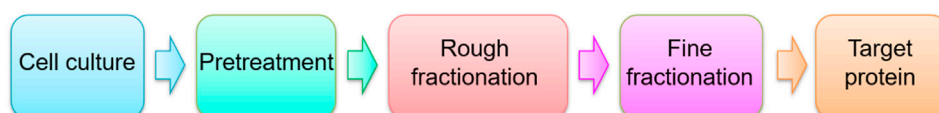


FIGURE 1  
Basic steps of protein purification.

immune defense, participating in intracellular redox reaction, electron transfer, learning and memory.

The first person engaged in the purification of proteins was Edwin Joseph Cohn, an American biochemist, who purified serum protein (Labrou, 2021). In recent years, with the completion of genome sequencing of many species (Shendure and Lieberman Aiden, 2012; Beigh, 2016; Park and Kim, 2016; Ing-Simmons and Vaquerizas, 2019), researches in protein related fields have gradually become the focus of the biotechnology industry (Labrou, 2021), and many purification technologies have been gradually applied from protein and enzyme separation to drug synthesis, vaccine research and development, clinical detection, environmental analysis and biophysical measurement (Pfaunmiller et al., 2013). Therefore, high-quality protein samples are of great significance for the subsequent structure and function research and related products development (Tang et al., 2021). However, proteins have the characteristics of complex structure, easy to be affected by internal and external factors, easy to be degraded, etc. It is difficult and challenging to purify them without being contaminated by the host, maintaining structural integrity and biological activity.

As a downstream technology of the biological industry, the key to protein purification is to define the purification strategy and finally establish an optimal scheme through continuous optimization of purification conditions, that is, using the least steps to achieve the purity, concentration, the activity and the yield we need, which is crucial for subsequent researches (Lojewski et al., 2016; Owczarek et al., 2019; Schiermeyer, 2020). The purification strategy is mainly based on the unique physical and chemical properties and the three-dimensional structures of the target proteins, including the sequence and number of amino acids, the charge, polarity, and hydrophilicity/hydrophobicity of the polypeptide chains, the shape of the proteins, and the

distribution of amino acid residues on the protein surface. The target proteins can be natural proteins from animals, plants and microorganisms, or recombinant proteins expressed by *E. coli*, yeast, mammalian cells and insect cells. Currently, recombinant proteins have become the main object of isolation and purification. Since different expression systems have their own advantages and disadvantages (Table 1), they should be selected according to the actual situation.

The complete protein isolation and purification steps generally include three steps: pretreatment, rough fractionation, and fine fractionation (Figure 1). In this review, the principles of common purification technologies and the recent advances made in this field are summarized, the applications of these technologies in life health industry and their far-reaching impact are discussed, and finally, the difficulties and challenges in the field of protein purification are prospected, in order to provide a variety of feasible solutions for the in-depth study of protein structure and function, and to bring new insights to readers in related fields.

## 2 Guidelines and strategies for protein purification

### 2.1 Identify the target of isolation and purification

Prior to purification, some basic properties of the target protein can be obtained through bioinformatics analysis softwares, such as the molecular weight (MW), isoelectric point (PI), solubility, molar extinction coefficient, stability, cysteine content, sensitivity to high concentration of salt ions or pH, secondary structure, hydrophilicity/hydrophobicity, sequence similarity to known proteins,

susceptibility to oxidation, and potential post-translational modification sites, etc. Should we choose prokaryotic expression, eukaryotic cell expression, or insect expression system to express the target proteins? Can the correct post-translational modification of the target protein be ensured after expression? Which tag should be selected to facilitate overexpression and purification when constructing the vector? Which method should be used for cell disruption after expression, and whether the disruption process will

TABLE 2 Separation basis and resolution of several purification methods (Labrou, 2021).

Separation mode	Separation basis	Resolving power
<b>Precipitate</b>		
Salting out	Solubility	Low
Organic solvent precipitation	Solubility	Low
Isoelectric point precipitation	Solubility, Charge properties	Low
Nonionic polymer precipitation	Solubility	Low
<b>Centrifugation</b>		
Differential centrifugation	Shape, Size	Low, Medium
Density gradient centrifugation	Size	Low, Medium
<b>Membrane separation</b>		
Dialysis	Size	Low, Medium
Ultrafiltration	Size/Shape	High
<b>Chromatography</b>		
Gel filtration chromatography	Size/Shape	High
Ion exchange chromatography	Charge	High
Hydrophobic interaction chromatography	Hydrophobicity	High
Affinity chromatography	Molecular recognition	High

cause the denaturation and structural change of the target protein? The purity, concentration, activity and yield of the final product should be determined to avoid over purification or failure to achieve the desired purity due to insufficient purification steps or resolution. All the above issues need to be considered comprehensively.

## 2.2 Reasonable selection of purification method

Select suitable purification methods according to the characteristics of the target protein and impurities, for example, choose to salt out, organic solvent precipitation, or choose centrifugation, electrophoresis, chromatography and other methods (Table 2). The purification scale should be determined according to the purpose of the target proteins, and the simple purification scheme should be used as far as

possible to achieve the best effect. In addition, the size of the chromatographic column, the concentration of the protein obtained, whether it is necessary to maintain its activity and avoid unnecessary contaminants should also be considered. The additives should be used as little as possible, the impurities that damage the sample should be removed as early as possible, and the additional purification steps should be reduced.

## 2.3 Identify detection and analysis techniques

For protein solutions containing different components, the detection methods for target proteins are usually different. Different detection methods should be selected in different purification steps according to their sensitivity, precision, accuracy, etc., so as to evaluate the activity, purity and recovery of samples quickly and accurately.

## 2.4 Determine protein storage conditions

In order to improve the stability of the target protein, prevent microbial growth and maintain the protein activity, various surfactants, metal chelators, protease inhibitors, preservatives and reducing agents (sh-mercaptoethanol or DTT) can usually be added to the buffer solution. In addition, under the premise of ensuring the activity of the target protein, it should be stored at  $-70^{\circ}\text{C}$ , and repeated freezing and thawing should be avoided.

## 3 Cell culture

Recombinant protein synthesis is the process of producing proteins in prokaryotic microorganisms or eukaryotic cells using recombinant DNA technology, and it is an important branch of the emerging synthetic biology. It is because of the development of recombinant DNA technology that people can produce a large number of protein products for research or treatment. Historical experience has continuously proved that the manufacture of a key protein molecule can quickly promote the rapid development of related fields, such as recombinant human insulin and recombinant human growth factors.

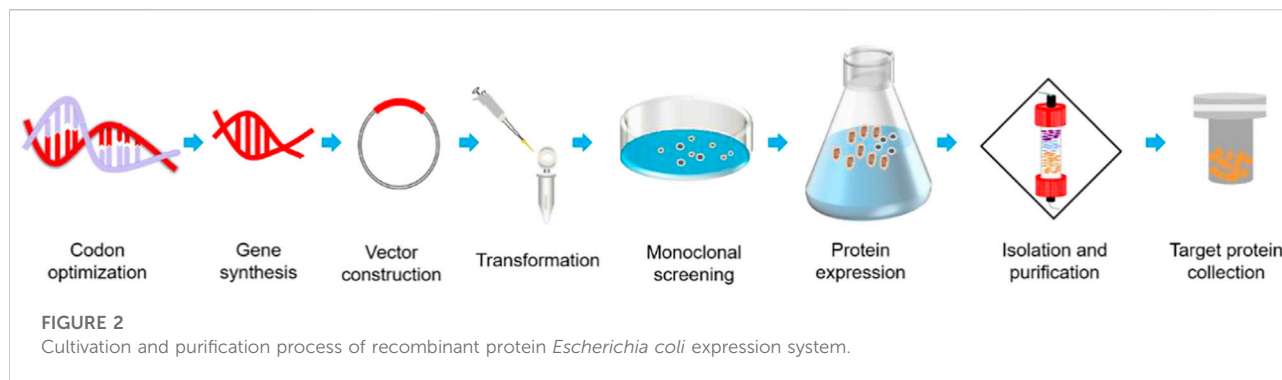
At present, the biggest bottleneck of recombinant protein manufacturing technology lies in “manufacturing”. The first difficulty is whether the target proteins can be expressed in large quantities by microorganisms or cells, and the second is how to obtain high-quality and active proteins through a series of processes and purification. Nowadays, expression systems such as *E. coli*, yeast, mammalian cells, insect cells, transgenic plants and transgenic animals are often used to obtain recombinant proteins. Here we take *E. coli* as an example to introduce the expression process of the target proteins. Firstly, the target

TABLE 3 Commonly used plasmids and characteristics of the *E. coli* expression system (Kesidis et al., 2020).

Plasmid series	Promoter	Derivant	Condition of culture (°C)	Repressible system	Prokaryotic resistance	Replicon	Cloned strain
pET	T7	IPTG	37	LacI	Amp, Kan,Str	pBR322	DH5α
pGEX	Tac	IPTG	37	LacI	Amp	pBR322	DH5α
pQE	T5	IPTG	37	LacI	Amp, Kan	pBR322	DH5α
pBAD	araBAD/ BAD	Arabinose	37	araC	Amp,Chl, Spe,Apr	pBR322, p15A, and pSC101	DH5α
pMAL	Tac	IPTG	37	LacI	Amp	pBR322	DH5α
pASK-IBA	Tet	Anhydrotetracycline	37	Tet-repressor	Chl, Amp	pBR322	DH5α
pRSET	T7	IPTG	37	LacI	Amp	pBR322	DH5α

gene was determined and suitable vectors (Table 3) and competent cells (Table 4) were selected, then the target gene was linked to an empty vector to construct a recombinant expression vector, and then the recombinant vector was transformed into host cells for culture. When OD<sub>600</sub> reaches 0.4–0.6, an appropriate proportion of inducer was added to induce protein expression at a certain temperature, and finally the thalli were collected for purification (Figure 2). As an expression host, *E. coli* has become one of the best hosts for the production of recombinant proteins due to its rapid reproduction, low costs, and rapid expression of a large amount of target proteins (Rosano and Ceccarelli, 2014). In order to avoid the influence of lack of post-translational modification systems, inclusion body formation, frameshift mutations and endotoxin production on subsequent purification, several means such as changing host, vector and target gene sequence constantly, optimizing culture conditions, and co-expressing target proteins with molecular chaperones are adopted by researchers to increase protein solubility and expression (Gopal and Kumar, 2013). For the problems encountered in the expression process, a series of effective solutions have been developed. For example, T7RNAP expression activity (Li Z. J. et al., 2022; Chee et al., 2022) or growth decoupling system (Li et al., 2016; Darlington et al., 2018) can be specifically regulated when expressing toxic proteins, but this method is not universally applicable. Zhang et al. (2022) developed a dynamic equilibrium system that can achieve the overexpression of basic growth-related genes (rRNA, RNAP core enzyme, sigma factor), accurately predict and express key proteins using an ec\_iECBD\_1354 enzyme constraint model, and dynamically regulate the expression intensity of key growth-related proteins based on a load-driven promoter. This system alleviates the host burden effect, improves the production of recombinant proteins, and is helpful to efficiently develop expression hosts based on the properties of target proteins. However, the *E. coli* expression system lacks post-

translational modifications, which is not conducive to the expression of eukaryotic proteins and many enzymes (Gupta et al., 2019), and increases the subsequent purification processes. Currently, the modified *E. coli* expression system can achieve the simple glycosylation modification of proteins (Gupta and Shukla, 2016), but it still needs to be further optimized. Some rare codons exist in protein-coding genes of higher animals, but these rare codons are not common in *E. coli*. Therefore, the expression of these proteins by *E. coli* expression system may lead to the reduction of target protein expression or premature termination of protein translation (Owczarek et al., 2019). In view of this, several online analysis softwares have been developed to detect the presence of rare codons in the gene sequence, and the expression of the target proteins can be improved through codon optimization (Gupta et al., 2019; Rosano et al., 2019). In addition, introducing short-term heat shock before induction (Oganesyan et al., 2007), adding D-sorbitol, glycerol, ethanol, NaCl (Diamant et al., 2001; Bowden et al., 1991; Oganesyan et al., 2007) and other chemical additives and/or target protein cofactors (Bushmarina et al., 2006; Rosano and Ceccarelli, 2014), glucose, lactose (Tahara et al., 2021) to the medium to change the culture conditions, and reduce the culture temperature (Carere et al., 2018; Wang et al., 2019) and IPTG concentration (Jhamb and Sahoo, 2012; Sina et al., 2015) are also effective ways to induce the high expression of the target proteins. Lactose operon *lac* is an inducible gene expression element, and 0.5–1 M IPTG is generally used to prevent LacI (repressor) from binding to the operator gene (Donovan et al., 1996) to achieve the expression of the target gene. In addition, to reduce the formation of inclusion bodies, coexpression of target proteins with molecular chaperones (de Marco et al., 2007; Jhamb and Sahoo, 2012; Rosano and Ceccarelli, 2014), use of weak promoters and low-copy plasmids (Kaur et al., 2018), adding fusion tags to the N-and/or C-terminus of expression vectors (Liu et al., 2019; Ruan et al., 2020), and adding signal peptides to



import the target proteins into the periplasmic region (Dow et al., 2015; Vargas-Cortez et al., 2017) are usually adopted.

## 4 Pretreatment

Before purification, the sample should be pretreated to release the total proteins from the tissue cells while maintaining the activity of the target proteins. Since different tissues and cells have different structures, different materials need to be pretreated by different methods. Commonly used pretreatment methods include mechanical method and non-mechanical method, the former includes high-speed bead milling, high-pressure homogenization and ultrasonic crushing, etc., while the latter includes osmotic pressure impact, freeze-thaw crushing, enzymatic hydrolysis and chemical crushing, etc. For example, connective tissue and adipose tissue should be removed by grinding, ultrasonic crushing (Tang et al., 2015) and centrifugation before the purification of animal materials. The seed materials should be shelled or even peeled to avoid the pollution of tannins and other substances, especially the oil seeds should be degreased with low boiling organic solvents such as ether. Plant tissues contain a wide variety of compounds, such as phenols, lipids, pigments, organic acids, carbohydrates, etc., which greatly interfere with protein extraction and proteomic analysis (Wang et al., 2008). In the purification of natural plant proteins, appropriate parts should be selected first for sampling, and then the cell wall and other components should be broken by mechanical or non-mechanical methods (Kielkopf et al., 2021) to obtain more cell lysates (Hunt, 2005), so as to ensure the smooth progress of the subsequent purification process. The purification of recombinant proteins produced by genetic engineering technology also requires pretreatment. The *E. coli* expression hosts are often collected by centrifugation at low temperature and broken by ultrasound. In addition, due to the mild and highly efficient action conditions of the enzyme, selecting a suitable enzyme can effectively decompose the plant or bacterial cell wall to achieve a better purification effect. Therefore, enzymatic hydrolysis has also been widely used in the process of sample pretreatment in recent years. When extracting oil crop proteins, the use of Viscozyme can fully degrade the cell wall

structure and promote the release of oil and protein in peanut cells (Liu et al., 2020a). Penha et al. (2020) using Viscozyme L under the condition of 50°C can improve the recovery rate of soybean protein from 42% to 83%, the recovery rate of isoflavones from 59% to 93%, and also reduce the residue of soybean dregs by 85%, so the utilization rate of raw materials was better improved. Enzymatic hydrolysis can also reduce the sensitization of food. Liang et al. (2021) found that Alcalase, Protamex and Flavourzyme could decompose the sensitizing proteins such as casein,  $\beta$ -lactoglobulin and  $\alpha$ -lactoferrin in milk, which not only reduced the sensitization of milk but also improved the content of free amino acids and nutritional quality. Therefore, the enzymatic hydrolysis can also be used to produce hypoallergenic dairy products to avoid allergic events. The above pretreatment methods can also be used as auxiliary means in the subsequent rough fractionation and fine fractionation, which can not only improve the extraction efficiency of the target proteins, but also reduce the use of some solvents (Li et al., 2021).

## 5 Rough fractionation

Protein extracts after pretreatment usually contains impurities such as cell debris, aggregates, nucleic acids, lipids and polysaccharides (Royce et al., 2018), it is necessary to select a set of appropriate methods to separate the target proteins from the impurities, while avoiding the degeneration and degradation of the target proteins.

### 5.1 Precipitation method

Precipitation method is based on the difference of solubility between proteins. By adding an appropriate precipitant to the protein extracts, the solubility of the target proteins can be changed to make it precipitate or aggregate, so as to achieve the effect of separation. Precipitation method can obtain a large amount of target proteins from cell extracts quickly and in batches (Matulis,



2016), which is a suitable choice for rough fractionation. The commonly used precipitation methods include salting out, isoelectric point precipitation and organic solvent fractionation.

### 5.1.1 Salting out precipitation

The solubility of protein is susceptible to the influence of ionic strength in solution. At low salt concentrations, the solubility of proteins will increase with the increase of salt concentrations in the solvent. This phenomenon is called salting in, and the proteins at this time still maintains the folded conformation and stability. If the salt concentration continues to increase, the hydration force of the solution will be enhanced, leading to the destruction of the hydration film on the surface of the proteins, resulting in the reduction of protein solubility, and then aggregation or precipitation. This phenomenon that the solubility of proteins decreases with the increase of salt concentrations is called salting out (Duong-Ly and Gabelli, 2014). The salting out method has the advantages of safety, mild action conditions, maintaining the biological activity of the target protein, low cost and simple operation. However, a large amount of salting-out agent is often left in the sediment, and some contaminants will also precipitate along with the target proteins. Therefore, desalination treatment is also an important part of the salting out precipitation method. Commonly used neutral inorganic salts are ammonium sulfate, sodium sulfate, magnesium sulfate and potassium phosphate. Ammonium sulfate has the advantages of good solubility, low price, easy preparation of high purity products, stability of protein structure and so on. It is the most commonly used neutral inorganic salt in salting out, especially for the purification of acidic proteins. In addition, ammonium sulfate can also be used with other precipitants to achieve better precipitation effect. Ovotransferrin has the functions of anti-oxidation, antibacterial and promoting iron absorption (Rathnapala et al., 2021). Abeyrathne et al. (2013) separated ovotransferrin from egg white by combining ammonium sulfate precipitation with citric acid. This process does not introduce highly polluting chemical reagents, so the ovotransferrin isolated by this method can be used in food and drug production after ultrafiltration desalination. In practical research, the optimal salt concentration of protein precipitation is usually determined by gradually increasing the salt concentration to separate the target proteins one by one under certain temperature and pH conditions. Hazim Abdul Hameed and Hussein Ali (2021) reported that 60% ammonium sulfate was the optimal ratio for rough fractionation when purifying the extracellular L-glutamate oxidase of *Streptomyces*, and the specific activity of the target protein could reach 8.25 U/mg. In addition, the ammonium sulfate salting out precipitation method can also be used for the isolation and purification of special

DNA structures, such as the purification of DNA origami nanostructures reported by Hanke et al. (2022).

### 5.1.2 Organic solvent precipitation

Organic solvent precipitation is another commonly used method for rough fractionation of proteins, the principle of organic solvent precipitation is that multifold organic solvent is added to the extract of biological macromolecules such as proteins to reduce the dielectric constant of the solution and increase the interaction between protein molecules, so that the solubility of proteins is significantly reduced and eventually aggregation or precipitation occurs. This method is conducive to the precipitation of high molecular weight proteins, while low molecular weight proteins or peptides are not easy to aggregate in organic solvents and remain in the supernatant (Baghalabadi and Doucette, 2020). Different organic solvents usually differ in their abilities to precipitate proteins, and common organic precipitants include acetone, isopropanol, ethanol, and methanol.

Organic solvents are usually volatile, so the residual organic solvents in the target proteins can be easily and quickly removed, and some organic solvents themselves can also be used as protein bactericides. As a commonly used organic solvent, acetone can greatly reduce protein degradation, have little impact on protein activity, and avoid contamination of impurities such as salt and polyphenol (Shaw and Riederer, 2003). When using the organic solvent precipitation to purify proteins on a large scale, it is necessary to first determine the optimal solvent concentration of the target proteins and the optimal volume ratio of protein extract to precipitant. The organic solvent selected as the precipitant should not have the ability to dissolve the target proteins, so the precipitant can be used to dissolve the soluble substances first, and then select an appropriate way to further extract the target proteins and other insoluble substances remaining in the precipitates (Wang et al., 2008; Wu et al., 2014). However, some organic solvents can destroy the hydrogen bonds in proteins and change the spatial structure of target proteins. For example, organic solvents such as ethanol release heat when mixed with water, which is easy to cause protein denaturation and inactivation. Furthermore, the precipitation process needs to consume a large amount of organic solvents and most of them are toxic and flammable, the operation is complex and the costs are high, the process needs to be carried out at low temperature, and the recovery rate is also lower than that of the salting-out method, all these make this method has certain limitations. However, in proteomic analysis, organic solvent precipitation can selectively deplete high molecular weight proteins or enrich low molecular weight proteins in soluble components, increase the detection coverage of small molecular weight proteins, and help improve the accuracy

of proteomic analysis (Periasamy et al., 2021; Nickerson et al., 2022).

### 5.1.3 Isoelectric point precipitation

The principle of isoelectric point precipitation is based on the fact that different proteins have different isoelectric points. When the pH value of proteins extract reaches the isoelectric point of the target protein, the net charge of the target protein is zero, the solubility is minimum, and the conformation is in the most compact state (Matulis, 2016), and no swimming occurs in the electric field, so as to achieve the purpose of separation. The isoelectric point precipitation is easy to operate and has various pH adjustment methods. However, this method also has defects. For example, when the pH reaches the isoelectric point of the target protein, it still has a certain solubility, resulting in incomplete precipitation. In addition, the inorganic acid/base (hydrochloric acid and sodium hydroxide) introduced in the adjustment of pH is easy to cause irreversible denaturation of the target proteins, and the isoelectric points of many proteins are relatively close, so the effect of isoelectric point precipitation alone is not ideal, with poor resolution and low purity, and generally only used for the preliminary purification of proteins. In order to solve the above problems, isoelectric point precipitation is often used together with other methods. For example, Watanabe et al. (2015) used isoelectric point precipitation combined with electrolytic water treatment technology to purify proteins from rice bran, which can not only significantly improve the purity and extraction efficiency of proteins, but also recover phosphorus containing compounds. Li et al. (2021) used ultrasonic assisted alkaline electrolyzed water to extract proteins from *Euphausia superba*, which can not only reduce the consumption of NaOH, but also maintain the activity of proteins and improve the yield of krill proteins.

### 5.1.4 Other precipitation methods

Nonionic polymer precipitation was first used to extract immunoglobulin. In recent years, it has been widely used in the isolation and purification of proteins, polypeptides, nucleic acids and enzymes (Wang et al., 2008). The polymers include dextran, NPEP, and polyethylene glycol (PEG) with different molecular weights.

The commonly used polymer PEG is an inert substance with high stability to proteins and can be stored at  $-20^{\circ}\text{C}$  for a long time. PEG is generally harmless to the human body and is widely used in cosmetics and medical products (Geng et al., 2019), but some people may develop systemic allergic reactions when using these products (Sellaturay et al., 2021). PEG combined with other forms of precipitant can improve the purification efficiency and reduce the consumption of some substances. Aqueous two-phase systems (ATPS), for example, have emerged as an alternative technology for protein recovery and concentration. Menegotto et al. (2021) established the maximum recovery condition of *A. platensis* protein using 16% sodium citrate and 18% PEG

(1500 Da), and achieved a purification factor of 1.02 and a protein recovery rate of 75%. Geng et al. (2019) used 15% PEG to separate ovalbumin, ovomucin and ovotransferrin at  $10^{\circ}\text{C}$ , pH6.5 and 100 mM NaCl, then obtained a purity of 95.1% ovalbumin by isoelectric precipitation (pH4.5,  $4^{\circ}\text{C}$ ) combined with HPLC purification, and the recovery rate was 46.4%. Ovalbumin can be extracted from several kilograms of egg white within 2–3 h. Furthermore, PEG is easier to extract LDL from egg yolk than ammonium sulfate (Wang et al., 2018).

## 5.2 Centrifugation method

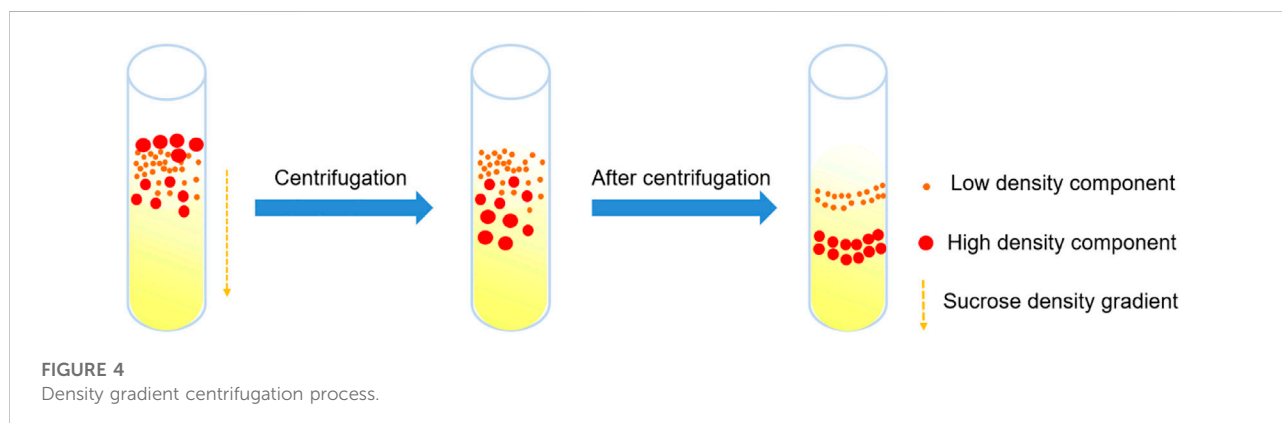
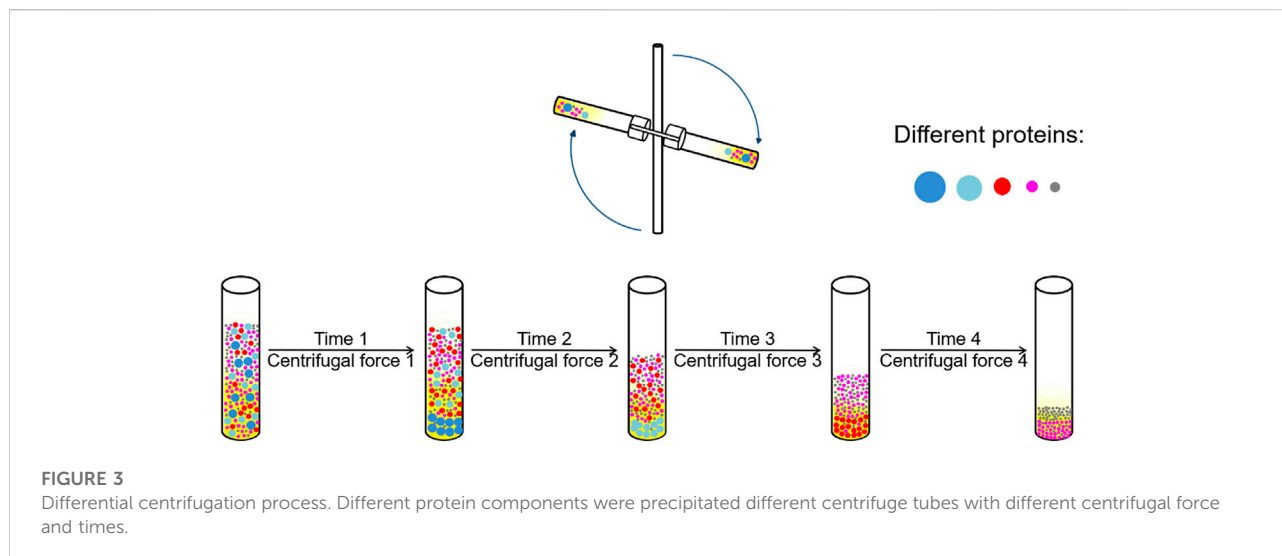
The principle of centrifugation is that when an object moves in a circle around a central axis, the moving object is subjected to centrifugal force, under the action of centrifugal force to achieve the purpose of protein separation. Centrifugation is also a suitable choice for rough fractionation, which can be used as a rough fractionation scheme alone or as a key step in multi-step purification. For example, after precipitation or mechanical crushing, more precipitates can be gathered together by centrifugation to achieve a better separation effect. The commonly used centrifugation methods in protein purification are differential centrifugation and density gradient centrifugation.

### 5.2.1 Differential centrifugation

Differential centrifugation is based on the difference in sedimentation velocity of proteins with different sizes. The method achieves the effect of separation by continuously increasing the relative centrifugal force, controlling the centrifugation time, and conducting multiple centrifugations (Figure 3). Muthunayake et al. (2020) used differential centrifugation to enrich Bacterial Ribonucleoprotein Bodies (BR bodies) from *Caulobacter crescentus*. Ma et al. (2020) isolated the apoptotic bodies by differential centrifugation after inducing the apoptosis of osteoclasts. Differential centrifugation can obtain different cells more quickly than the conventional washing method during the isolation of mouse bone marrow cells, and it does not affect the cell viability and the distribution of hematopoietic cell populations (Heib et al., 2021). The advantage of differential centrifugation is that it is relatively convenient to separate multiple samples simultaneously. However, this method requires repeated centrifugation, which is more complex. In addition, the precipitate needs to be washed, dissolved and re precipitated for many times during the purification process, which is easy to cause sample loss and yield reduction.

### 5.2.2 Density gradient centrifugation

Density gradient centrifugation is also called zonal centrifugation. The protein samples to be separated were placed on the surface of density gradient formed by the medium (sucrose,



cesium chloride, etc.) with gradually increasing density and high solubility, and the proteins of different shapes and sizes were separated by centrifugal force to form different settling zones at different settling speeds (Figure 4). This method can separate multiple components in mixed samples with high resolution and low cost. At present, it has been widely used for the isolation and purification of cells, organelles, viruses, bacteria, nucleic acids, proteins, etc. For example, the inner and outer membrane of liver tissue can be separated by sucrose density gradient centrifugation (Lin et al., 2010), and mitochondria after differential centrifugation can also be further refined purified (Clayton and Shadel, 2014). Szelechowski et al. (2013) purified adenoviruses and bacteriophages by cesium chloride density gradient centrifugation. Nasukawa et al. (2017) reduced the centrifugal force from 100,000g to 40,000 g and increased the centrifugation time from 1 to 2 h under the condition of 4°C, and completed the phage purification by non ultracentrifugation, realizing the virus purification without ultracentrifuge. In the final

step of bacterial ribosome purification, polysomes were purified for *in vitro* cell-free translation systems by centrifugation of samples containing 70S monomers, ribosomal subunits, and polysomes through a linear sucrose gradient of 7%–30% (w/w) (Rivera et al., 2015). Wichmann et al. (2021) used OptiPrep density gradient centrifugation to isolate a higher proportion of bacteria from the complex matrix with low microbial load, confirming the compatibility of this method with Raman spectroscopy, and the combination of the two methods can improve the accuracy of bacterial infection diagnosis.

### 5.3 Dialysis method

Dialysis is a method to separate colloidal substances such as proteins from other small molecular substances including inorganic salt ions and reducing agents based on the principle that protein and other macromolecular particles are large, have

TABLE 4 *E. coli* BL21 and its derived host for recombinant protein expression.

Strain name	Important features	Application
BL21	<i>E. coli</i> polymerase but no T7 RNA polymerase	It is mainly suitable for the expression of non-toxic proteins, and it can be used for the protein expression of plasmids (such as pGEX and pMAL)
BL21 (DE3)	The $\lambda$ phage DE3 region containing T7 phage RNA polymerase is integrated on chromosome BL21 allowed the simultaneous expression of both T7 RNA polymerase and <i>E. coli</i> RNA polymerase. (Ivanov et al., 1993)	For the efficient expression of the genes cloned in the expression vectors containing the phage T7 promoter (such as the pET series), and for the protein expression of the plasmids (such as pGEX and pMAL)
BL21 (DE3) pLysS	Carrying the pLysS plasmid, having chloramphenicol resistance, and containing genes expressing T7 lysozyme. T7 lysozyme can reduce the background expression level of the target gene, but does not interfere with IPTG induced expression	Suitable for the expression of toxic proteins and non-toxic proteins
BL21 (AI)	It has tetracycline resistance (Bhawsinghka et al., 2020), lacks Lon protease and OmpT extramembrane protease. It can effectively prevent the degradation of heterologous proteins in <i>E. coli in vivo</i>	Suitable for any T7 promoter-based expression vectors. Widely used for the high-level expression of toxic recombinant proteins (Bhawsinghka et al., 2020)
BL21 Star (DE3)	It contains <i>E. coli</i> RNA polymerase, has chloramphenicol resistance, and contains the rne131 mutation, which reduces the accumulation of endogenous RNase and enhances mRNA stability of intracellular mRNA in the strain (Jiang et al., 2021), thereby it increases the expression level of heterologous proteins	Suitable for the high-level protein expression of the T7 promoter expression vector (such as the pET series) and the non-T7 promoter expression vector (such as pGEX and pMAL), it is not suitable for the expression of toxic proteins (Jiang et al., 2021)
BL21 Star (DE3) pLysS	Containing the <i>E. coli</i> RNA polymerase, carrying the pLysS plasmid, having chloramphenicol resistance, and containing the rne131 mutation, enhances the cellular stability of the mRNA within the strain, thus increasing the expression level of the heterologous protein. Lower the background expression level of the target gene, but did not interfere with the IPTG-induced expression	It is suitable for high-level expression of protein expression in T7 promoter expression vectors (such as the pET series) and non-T7 promoter expression vectors (such as pGEX and pMAL)
BL21-CodonPlus (DE3)-RIPL	It is absent of the Lon protease and the OmpT protease, thus reducing the degradation of the recombinant proteins and enhancing the expression levels of foreign genes. In particular, the expression levels of AT-or GC-rich eukaryotic genes in the prokaryotic system. It can simultaneously express T7 RNA polymerase and <i>E. coli</i> RNA polymerase, and has resistance to tetracycline, chloramphenicol, streptomycin, and spectacular mycin	It can be used for the protein expression of plasmids (such as the pET series, pGEX, and pMAL)

colloidal properties, and cannot freely pass through the semi-permeable membrane (Echave et al., 2021). The activity of purified protease can be improved by attaching specific substances targeting the target protease to the semi permeable membrane (Labus et al., 2020). In order to improve the recovery rate of the target proteins during dialysis, factors such as buffer exchange time, the design of dialysis system, and the chemical and morphological characteristics of dialysis membrane should be considered. In terms of buffer exchange time, the increasing temperature can accelerate the molecular movement and increase the intrinsic diffusion of proteins across the semi-permeable membrane to reduce dialysis time, but increasing temperature may also have adverse effects on protein activity. Therefore, the maximum temperature at which protein activity can be maintained should be determined in advance when using dialysis for protein purification (Burgess, 2016). Dialysis is also commonly used for desalting treatment after the end of salting out. When the protein solution is in a high concentration and high salinity state, dialysis is usually the best method to remove ammonium sulfate from the sample (Duong-Ly and Gabelli, 2014). Phycocyanin has antioxidant, anticancer, liver and kidney protection effects (Piovan et al., 2022), and has been widely used in the production of drugs and nutritional products in recent

years. Khazi et al. (2020) pretreated *Cyanobacteria* to obtain the crude extract of phycocyanin. Ammonium sulfate was added into the crude extract in sections, and the supernatant was removed by centrifugation after full stirring, then the phycocyanin was resuspended and dialyzed overnight to achieve further purification effect.

## 5.4 Ultrafiltration method

Ultrafiltration is also a method based on membrane separation, which can achieve the effect of concentration and is also a common way of desalination (Thammasena et al., 2020). The performance of ultrafiltration membrane is the key to the success of protein separation. Most ultrafiltration membranes consist of a sturdy scaffold structure with a very thin polymer layer attached to it. Cellulose acetate can be used for filtration, gas separation, adsorption and ion exchange (Vatanpour et al., 2022) due to its advantages of film-forming, good chemical activity (Ma et al., 2022), high stability (Muhmed et al., 2019) and hydrophilicity, environmental protection, and appropriate costs (Sharma et al., 2020; Syamani, 2020). Although the production technology of membranes used for ultrafiltration



has not changed in the past few decades, the control technology of thin layer pore size distribution, membrane morphology and membrane modification has been significantly improved. It is this thin layer that provides the properties required for a selective permeability membrane and determines the flow resistance (Burgess, 2016). The new dopamine modified cellulose acetate ultrafiltration membrane is a relatively advanced filter membrane. The use of Dopamine-modified cellulose acetate overcome the trade-off between permeability and selectivity of conventional cellulose acetate membranes to some extent, possess good antifouling capability and long-term stability, and intercept effectively the target protein as well as improve the water permeability (Ma et al., 2022). In order to avoid the accumulation of intercepted proteins on the membrane surface, tangential flow filtration can be used (Busatto et al., 2018). The principle is that the protein solution is driven by the pump to flow along the direction tangent to the membrane surface. The pressure difference formed on the membrane makes part of the liquid pass through the membrane, while the other part of the liquid flows tangentially through the membrane surface to wash away the intercepted protein molecules. The currently developed one-way tangential flow ultrafiltration technique enables the continuous ultrafiltration of mAb by increasing the surface area and the residence time (Thakur et al., 2022). Ultrafiltration is also applied to the treatment of diseases such as acute heart failure (Costanzo, 2019), the removal of pathogens from seawater (Cordier et al., 2020), the purification of the vaccine product (Emami et al., 2019) and recombinant ferritin (Palombarini et al., 2019), and the treatment of galvanized wastewater (Oztel et al., 2020).

To sum up, the rough fractionation methods are relatively simple and have a large processing flux. They can not only remove a large number of impurities, but also concentrate the protein solution to achieve partial purification, while maintaining a high recovery rate (Mazi et al., 2016). Among the above rough fractionation techniques, PEG precipitation, ultrafiltration, differential centrifugation and other methods can achieve the concentration of viruses in wastewater (Dumke et al., 2021). During the SARS-CoV-2 pandemic, many countries used these methods to enrich and detect viruses in wastewater, thereby boosting epidemiological surveillance and playing an early warning effect (Ahmed et al., 2020; Medema et al., 2020; Ai et al., 2021; Hillary et al., 2021). However, the effect of rough fractionation is poor, so in some important structural and functional analysis studies, it is necessary to combine more refined fractionation methods to obtain the target proteins with higher purity.

## 6 Fine fractionation

After a series of pretreatment and rough fractionation, the volume of the sample was reduced and most of the impurity

proteins were removed. The purpose of fine fractionation is to separate the target proteins from some proteins of similar size and physical and chemical properties to obtain higher purity, so as to meet the needs of different research fields. At the same time, higher resolution and stronger specificity are required in the process of fine fractionation.

### 6.1 Chromatography

Chromatography is based on the difference in physical and chemical properties of different substances (Scopes, 2001). It has been used to extract plant pigments as early as the beginning of the 20th century. At present, chromatography has been widely used in the separation of proteins, nucleic acids, polysaccharides, peptides and other biological macromolecules. Chromatography can be divided into adsorption chromatography and non-adsorption chromatography according to whether the sample is bound to the filler. The former mainly includes ion exchange chromatography, hydrophobic chromatography, affinity chromatography and reverse phase chromatography, while the latter mainly includes gel filtration chromatography. Several commonly used chromatographic techniques are introduced as follows. (Table 5).

#### 6.1.1 Gel filtration chromatography

Gel filtration chromatography, also known as molecular sieve chromatography, is one of the most effective methods developed in the 1960s to separate and purify different proteins based on molecular size, and is also the gold standard for separating protein polymers from their monomers (London et al., 2014). In the elution process, proteins with high molecular weight first flow out along the gap between the gel particles, while proteins with low molecular weight can enter the gel mesh, resulting in flow obstruction and slow outflow.

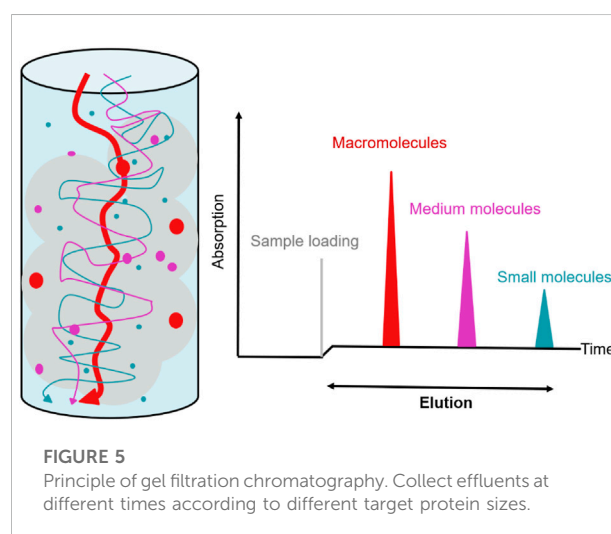
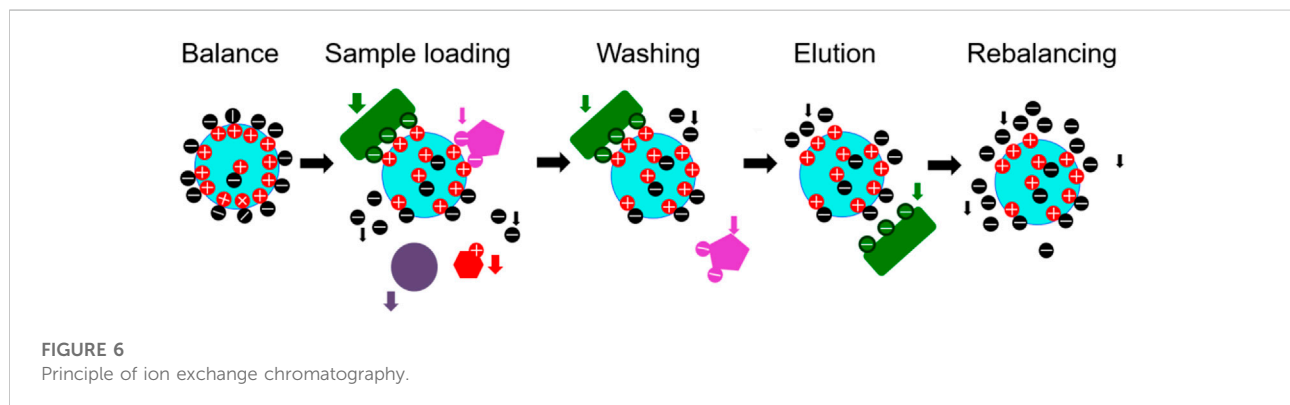


TABLE 5 Comparison of common chromatographic separation methods.

Types	Gel filtration chromatography	Ion exchange chromatography	Hydrophobic chromatography	Affinity chromatography
Characteristic				
Separation mechanism	Size	Charge	Hydrophobicity	Specific affinity
Selectivity	Secondary	High	Medium/high	Very high
Load	Low	High	High	High
Purification rate	Medium/low	High	High	High
Biocompatibility	Very nice	Good	Medium/good	Good
Purified protein yield	High	High	Medium/high	High
Capture concentration phase	+	+++	+++	+++
Intermediate purification stage	+	+++	+++	+++
Refining and purification stage	+++	+++	+	++



The required proteins can be collected according to the time sequence of elution (Figure 5). The matrix for gel filtration can be composed of a variety of materials, including simple substances such as dextran (Sephadex™ Series), agarose (Sepharose™ Series) and polyacrylamide (bio-Gel Series) or mixtures composed of dextran polyacrylamide (Sephacryl™ Series) or dextran-agarose (Superdex™ Series). Gel filtration chromatography, which has the advantages of simple operation, rapid separation without affecting biological activity, has been widely used for the isolation and purification of proteins or peptides (Gao et al., 2016). At the same time, the dextran gel can also be used for desalination after salting out. However, the gel filtration chromatography also has certain defects. The chromatography column is longer than other separation columns, so the flow rate is slower, the elution time is longer, and higher column pressure and more fillers are required. Gel filtration chromatography is often used in combination with other chromatography methods (Li Z. et al., 2022). To further investigate the effect of D614G substitution on the structure of SARS-CoV-2 spike protein, Zhang et al. (2021) purified

the SARS-CoV-2 spike protein carrying D614 or G614 with detergent DDM, further purified it through gel filtration chromatography and used it for structural analysis, providing a structural basis for the development of new coronavirus vaccine. Ye et al. (2022) used 70% methanol as elution buffer, and obtained high concentrations of isoorientin and four flavone C-glycosides from bamboo leaf flavonoid by gel filtration chromatography. Gel filtration chromatography can also be used in the last step of purification of low molecular weight hyaluronic acid (Karami et al., 2021). Cao et al. (2022) used TALON IMAC metal chelation chromatography and gel filtration chromatography to obtain pure serotonin 2A receptor (5-HT2AR) for research on the treatment of depression. Zhang Y. et al. (2021) obtained high-purity NMDA receptors by combined use of Strep-Tactin affinity chromatography and gel filtration chromatography (Superose six Increase), and the analysis of its three-dimensional structure by cryo-EM provided new insights for the development of antidepressants. Moreover, gel filtration chromatography also plays an important role in medical

examination and is the gold standard for the detection of macroprolactin (Vilar et al., 2019). When the recovery rate of thyroid stimulating hormone (TSH) does not decrease, the gel filtration chromatography can be used to detect the presence of macro-TSH as the evaluation index of normal thyroid function (Fukushita et al., 2021).

Gel filtration chromatography is suitable for the separation of proteins with larger or smaller molecular weight. When the molecular weight of proteins in the sample is moderate, the purity of the target proteins obtained is relatively low. When the molecular weight of proteins is 25% different from each other, they can be completely separated by a single gel column. In addition, the viscosity of the sample should not be too high, otherwise the mass transfer resistance will increase, and the gel particles will sometimes have non-specific adsorption, which is easy to block the column.

### 6.1.2 Ion exchange chromatography

Ion exchange chromatography uses ion exchanger as stationary phase to separate and purify according to the difference in reversible binding strength between component ions in the mobile phase and equilibrium ions on the exchanger. Ion exchangers are made by introducing several dissociable groups (active groups) into an insoluble polymer substance (the parent body). It is the many covalently bound charged groups and convertible ions fixed to the parent body that play a key role in the chromatography process. The interaction strength between the proteins and ion exchangers changes with the buffer salt concentration or pH, and the protein is eluted according to the binding strength, so as to achieve the purpose of separation and purification. According to the properties of active groups, ion exchangers can be divided into cation exchangers and anion exchangers. According to the difference of parent, ion exchangers can be divided into ion exchange resin, ion exchange cellulose, and ion exchange gel. The basic steps of ion exchange chromatography include: balance, loading, washing, elution and rebalance (Figure 6). Generally, the sample loading is completed under the condition of low salt ion concentration, and elution is carried out with high concentration salt ion buffer solution. Factors affecting the interaction between ion exchanger and protein include the charge of protein and ion exchanger, dielectric constant of medium, competition of other ions for ion exchanger and charged group of protein, charge distribution on protein surface, properties, temperature, additives of special ions in solvent, and non-electrostatic interaction and hydrogen bond between protein and ion exchanger (Evert and Irwin, 2011).

Ion exchange chromatography has the advantages of moderate costs, high resolution, easy expansion, and large-scale purification. Low concentration protein and polynucleotide solution can be rapidly concentrated to achieve the purification effect (Evert and Irwin, 2011). At present, it has been automated and has become the most functional and widely

used one among all chromatography technologies. However, even under the most accurate conditions, pure target protein cannot be obtained by ion exchange alone, so it is necessary to combine centrifugation, salting out and other steps to achieve fine purification. Antibacterial proteins produced by plant tissues are effectively effective against microbial invasion (Gonzalez-Lamothe et al., 2009). Radhakrishnan et al. (2022) isolated a leucine-rich lumen binding protein of 24 kDa from *Solanum trilobatum* leaves by ammonium sulfate precipitation and ion exchange chromatography, which was found to have antibacterial activity and edible properties, and can be used for the clinical treatment of *S. aureus* and *V. cholerae* infections to alleviate the bacterial drug resistance. Ion exchange chromatography can also remove various impurities such as target protein variants, host cell residual proteins, DNA, culture medium components, endotoxin, and viruses (Saraswat et al., 2013; Tripathi, 2016; Kimia et al., 2019; Masuda et al., 2019). In recent years, some improved ion exchange chromatography methods have been proposed. For example, Santry et al. (2020) added NatriFlo® HD-Q membrane and interfering agent to the anion exchange chromatography and developed the interference chromatography technology, which can purify high titer, and clinical grade oncolytic virus by using the difference of molecular bonding interaction, resulting in realizing the large-scale production of oncolytic virus and promoting the application of oncolytic virus in tumor immunotherapy. Jing et al. (2021) adopted a new double column continuous flow chromatography (called the new N-rich mode), that is, strong cation chromatography column (SCX) and weak cation chromatography column (WCX) were used respectively, and the buffer solution system, flow rate and elution gradient were optimized at the same time. After 22 cycles, enrich acidic variants of an IgG1 mAb with a purity of nearly 100% was obtained, significantly improving the purity of the target proteins.

### 6.1.3 Affinity chromatography

Affinity chromatography (AFC), also known as liquid chromatography, is the most selective technology developed in the 1960s. The principle of affinity chromatography is that one or a group of proteins can selectively and reversibly combine with specific ligands, and the separation of target proteins can be realized according to the different binding abilities of different proteins to specific ligands. Affinity ligands with special structures are usually fixed in the column as stationary phase carriers, forming the basis for affinity column separation or purification of complementary targets (Block et al., 2009). When the protein mixture passes through the chromatographic column, some proteins with affinity are adsorbed on the stationary phase carriers (Arora et al., 2017). Conversely, proteins without affinity will flow out directly (Figure 7). The adsorbed protein can be eluted by selecting an appropriate elution buffer and changing the

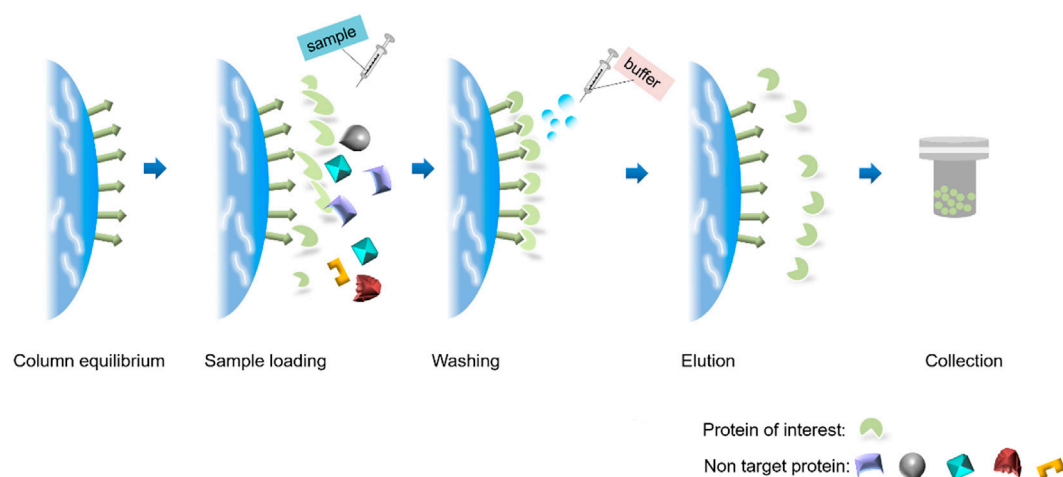


**FIGURE 7**  
Affinity chromatography process.

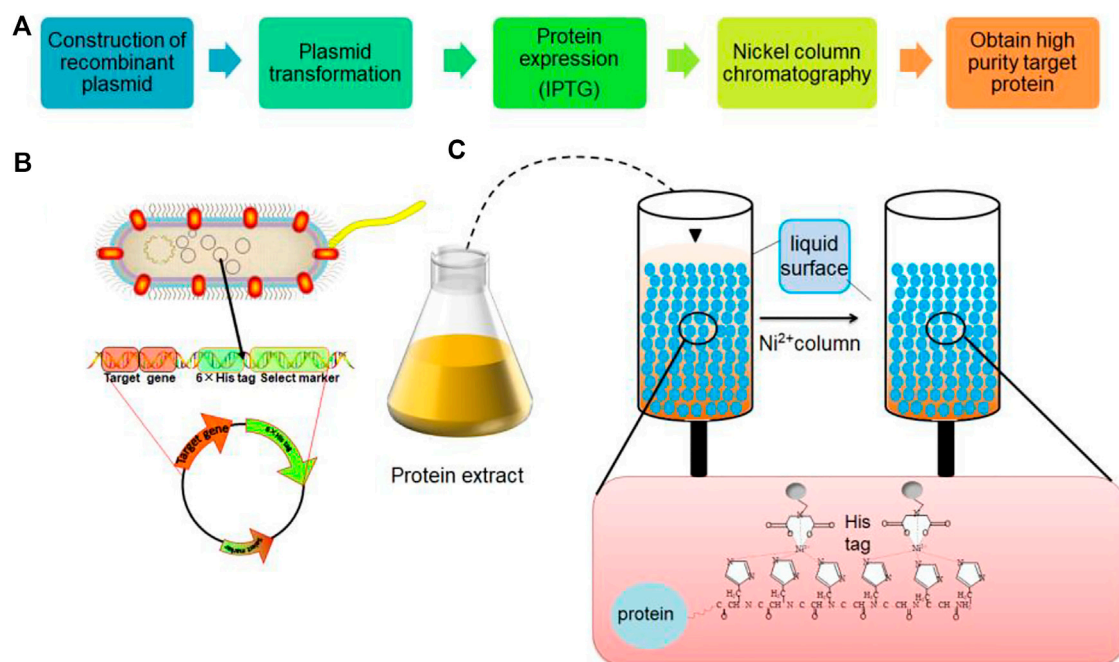


**FIGURE 8**  
Overall flow chart of nickel column chromatography. (A) Overall flow chart. (B) Plasmid construction transformation. (C) Nickel column chromatography process and his tag structure.

binding conditions. Affinity chromatography is fast, simple, and highly efficient (Lacki and Riske, 2020), which is often used to isolate compounds with specific tags or to study interactions between biological macromolecules. The

interactions between proteins and ligands are based on non-covalent interactions such as electrostatic gravity, molecular hydrophobicity, van der Waals forces and hydrogen bonding forces.



TABLE 6 Characteristics and applications of the common affinity tags.

Tags	Sequence/Size	Features	Application
Epitope Tags			
His	6–10 His/0.84 kDa (Mishra, 2020)	It has a small molecular weight, and no impact on the function and downstream application of the target proteins. It has low immunogenicity so that purified proteins were directly immunized to animals and antibodies were prepared (Freitas et al., 2022)	Bromberg et al. (2022) found that His tag can be used as a decoy modulating preferred orientation in cryo-EM, providing a new scheme for improving cryo-EM sample processing Williams et al. (2021) used the optimized His tag the integrate with recombinant proteins, which is not only convenient for affinity chromatography, but also provides an effective binding site for the radiolabeling of the recombinant protein. Therefore, the optimized His tag are used in the process of cancer molecular imaging and radionuclide therapy with more economic advantages
FLAG	DYKDDDDK/1.01 kDa (Mishra, 2020)	It has a small molecular weight, high hydrophilicity (Schmidt et al., 2012), The tag has high sensitivity and are easy to remove after use	Han et al. (2017) purified functional reprogramming factors from HEK293 cells using FLAG tag. Imagawa et al. (2021) purified virus-like particles with FLAG-tagged envelope protein through one-step affinity purification with FLAG tag, which could be used as a tetravalent dengue vaccine candidate
HA	YPYDVPDYA/1.1 kDa	The tag is derived from the influenza virus hemagglutinin (Zhou et al., 2012). The tag has little influence on the spatial structure of the target protein, and it is easy to be constructed into tag proteins fused to the N or C terminus	Vyas et al. (2020) CRISPR-Cas9 gene editing technology was used to connect HA tag as locators to the C-terminus of mouse nicotinic acetylcholine proteins (nAChRs) $\alpha 9$ or $\alpha 10$ . The expression of $\alpha 9$ and $\alpha 10$ proteins can be detected
Strep	Including Strep-tag II (WSHPQFEK) (Tremante et al., 2021), Twin-Strep-tag (WSHPQFEK-GGGSGGGSG-SA-WSHPQFEK) (Schmidt et al., 2013)	Strep-tag II is small, which does not affect the folding ability of protein, and has strong specific binding ability with affinity resin, which effectively avoids non-specific binding. Therefore, the purity of the target proteins obtained is high. The target proteins can be purified under mild conditions to maintain its activity (Johar et al., 2017)	Kawaguchi et al. (2019) purified highly purified recombinant human pancreatic lipase (recHPL) in the <i>E. coli</i> expression system using Strep-tag II. Twin Strep tag retains many advantages of Strep tag II, but for Strep tag II, it further improves the link strength between the target protein and Strep Tactin, and improves the purification efficiency (Schmidt et al., 2013). Xiong et al. (2019) used the high affinity between Twin-Strep-tag and streptavidin variants to establish a rapid separation method for lysosomes, mitochondria and peroxisome organelles, and studied the functions of these organelles after the purification. Yang et al. (2022) used Twin-Strep-tag to construct the TST-EGFP-GPI <sub>BY55</sub> affinity cell sorting system, which was able to efficiently separate gene transfer positive cells in a simple, convenient and rapid manner to facilitate gene research
V5	GKIPNPLLGLDST (Mishra, 2020)	The tag is derived from amino acids at positions 95–108 of the $\alpha$ subunit of RNA polymerase of simian parainfluenza virus type 5. (Huang et al., 2011)	Traore et al. (2021) used V5 tag and His <sub>6</sub> tag to isolate HupZ-V5-His <sub>6</sub> protein from group <i>A streptococcus</i> , and the analysis found that the binding of heme to HupZ was an O <sub>2</sub> -dependent process
Avi	GLNDIFEAQKIEW (Verma et al., 2018)	Almost all proteins can be easily and efficiently biotinylated at a unique Avi Tag site, either <i>in vitro</i> or <i>in vivo</i> . Biotinylation is achieved by the reaction of the enzyme and the substrate, with mild reaction conditions and highly marked specificity. The effect on the protein space structure is very small	Kim et al. (2021) fused the modified ubiquitin into Avi-tag, and using <i>in vitro</i> reconstituted E1-E2-E3 reactions that recapitulate the endogenous mono-ubiquitination reactions, we were able to isolate the monoubiquitin protein through biotin affinity purification and elution by proteolytic cleavage of Avi tag

(Continued on following page)

TABLE 6 (Continued) Characteristics and applications of the common affinity tags.

Tags	Sequence/Size	Features	Application
Myc	EQKLISEEDL/1.2 kDa (Mishra, 2020)	The tag is derived from peptide 410–419 of human c-Myc protein, which can be fused to the N-terminal or C-terminal of the target protein	Myc tag can be used as epitope tag, widely used in the detection of anti-c-Myc hybridoma E10 antibody Myc1-9E10 (Schuchner et al., 2020)
Protein/domain tags			
Glutathione S-transferase (GST)	26 kDa (Williams et al., 2020)	The tag was derived from <i>Schistosoma japonicum</i> , which could be expressed in different hosts and was widely applicable. It can be expressed in different hosts, and has a wide range of applications. Different proteases can be easily removed (Kim et al., 2021). It can increase the solubility and improve the expression and stability of foreign proteins. It has good specificity and helps to maintain the antigenicity and the activity of the proteins after eluting under mild and non-denaturing conditions. It has a large molecular weight and may affect protein functions and downstream experiments	Zhou et al. (2020) fused melittin (MET) with the GST tag and expressed melittin using the <i>E. coli</i> expression system. After affinity chromatography, digested with prescission protease, gel filtration chromatography, melittin with a purity of >90% was purified, which also showed strong antibacterial activity. Such a scheme could be used for large-scale industrial production of melittin
MBP	40 kDa (Greenfield et al., 2020)	It is one of the most commonly used crystallization chaperones for the target proteins (Fox et al., 2001), and can increase the solubility of the fusion proteins, especially the eukaryotic proteins. MBP tags can be easily detected by immunoassay	Nosaki et al. (2021) have successfully revealed the crystal structure of AtBIL1/BZR1 DBD and target DNA complex by the combination of MBP-mediated crystallization and MD simulation. This is shown to be capable of deciphering the protein-DNA recognition code of interest Li et al. (2019) found that MBP tag can assist in the crystallization of the CAMP factor of <i>Streptococcus agalaciae</i> , facilitating the subsequent study of the structure of the CAMP factor Guo et al. (2018) used MBP tag to prepare high purity and high activity MBP-MLIF in the <i>E. coli</i> expression system. On the whole, this method has advantages such as simplicity and application, which promotes the scientific research of stem cells
SUMO	11.2 kDa (Heinrich et al., 2019)	It can increase the expression amount of the fusion proteins (Mohammadi et al., 2022), and has the functions such as anti-protease hydrolysis, promoting the correct folding of the target protein, enhancing the solubility, and shielding the toxic proteins	Kim et al. (2019) used SUMO tag and His tag to construct a new vector pKSEC1 for the production of antimicrobial peptide-Abaecin, providing a new scheme for the treatment of bacterial infection Mohammadi et al. (2022) used SUMO tag to express a large number of recombinant human angiotensin-converting enzyme 2 (rhACE2) in <i>E. coli</i> , and the solubility of recombinant human angiotensin-converting enzyme 2 (rhACE2) could be improved in combination with freeze-thaw method, providing a reasonable choice for subsequent large-scale purification
Halo	33 kDa (Freidel et al., 2016)	Halo Tag monomeric proteins can be fused to either the N or C terminus of the recombinant proteins and express in prokaryotic and eukaryotic systems. Halo Tag can rapidly bind to ligands with high specificity and affinity to form stable covalent compounds	Deo et al. (2021) used the self-labeling Halo tag protein as a fluorescent indicator sensor scaffold to detect a single action potential in cultured neurons. Liu et al. (2018) connected the Halo tag and tobacco Etching virus (TEV) protease cleavage site at the n-terminal in the <i>E. coli</i> expression system. After chromatography and enzyme digestion, high purity Halo-FGF7 and rhFGF7 were respectively determined by <i>in vitro</i> and <i>in vivo</i> activity, MTT, the

(Continued on following page)

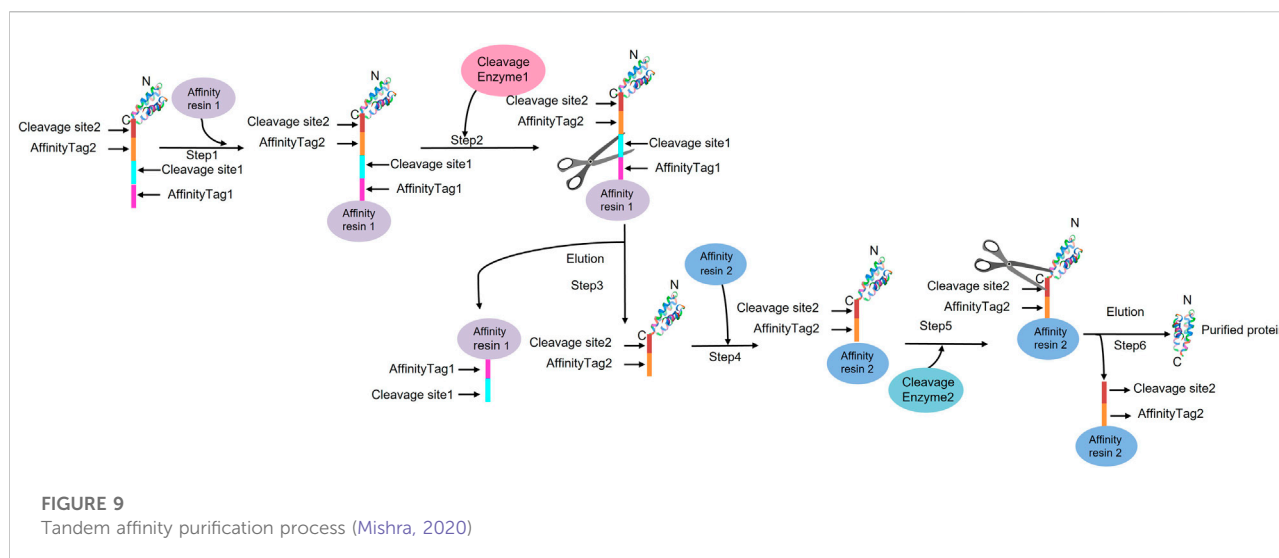
TABLE 6 (Continued) Characteristics and applications of the common affinity tags.

Tags	Sequence/Size	Features	Application
SNAP	19.4 kDa (Freidel et al., 2016)	The tag is derived from human O6-alkylguanine-DNA-alkyltransferase (Padayachee et al., 2019). It can covalently bind with the substrate to tag proteins with biotin or fluorescent groups; highly specialized, stable and suitable for protein detection and purification in various environments	protective effects of rhFGF7 and Halo-FGF7 on acute liver injury were further investigated by Western blot. Akin et al. (2021) used Halo tag to mark Nav1.7 channels in nerve cells to study the effect of paclitaxel (PTX) increase axonal localization and vesicular trafficking of Nav1.7 Fu et al. (2021) used SNAP as the tag to construct Snap-tagged EGFR/CMC in combination with HPLC-IT-TOF-MS to screen EGFR-targeted active compounds in traditional Chinese medicine, efficiently isolate and accurately identify them, and screen out important candidates for disease treatment. Moinpour et al. (2022) used the SNAP-tag biocoupling strategy to form stable covalent bonds between benzyl guanine (BG) -modified phospholipids and SNAP-tag fusion proteins, thus realizing programmable control of protein capture. It is also proved that the SNAP-tag biological coupling strategy can directly isolate proteins in the presence of complex biochemical mechanisms, which will facilitate the development of advanced lipid-based artificial organelles
Calmodulin-binding peptide (CBP)	RWKKNFIAVSAANRFKKIS (Mukherjee et al., 2015)	The tag is derived from the 26 amino acid sequences of myosin light streptokinase of skeletal muscle (Wyborski et al., 1999), with a small molecular weight. After purification of the target protein, the tag can not be removed (Zhao et al., 2013). It has the ability to improve the antigen solubility (Mukherjee et al., 2015)	Viala et al. (2017) studied the interaction between proteins by using tandem affinity purification technology consisting of CBP and two immunoglobulin G (IgG) binding domains of <i>Staphylococcus aureus</i> protein a (ProtA) isolated by the cleavage site of tobacco corrosion virus (TEV) protease
NusA	54.9 kDa (Dudenhoeffer et al., 2020)	Tag can increase the solubility of the target proteins	Hara et al. (2021) used NusA tag to dissolve and concentrate carotenoids
New type of tag XXA	192aa	The synthetic <i>Chlorella sorokiniana</i> antifreeze protein (Accession number: PRW45461) has excellent water solubility and can improve the solubility of the target proteins (Xie et al., 2022)	Xie et al. (2022) used XXA tag as a soluble tag to express Chrono, Notch2NL, nClu, bdNEDP1, NbALFA and other proteins in the prokaryotic expression system
Affinity Bioorthogonal Chemistry (ABC) Tags		The tag is a derivative of 3-methyl-6-(2-pyridinyl) tetrazine	ABC tag has dual functions, which can not only promote protein purification, but also serve as the follow-up arm of rapid and quantitative biological orthogonal labeling (Scinto et al., 2022)

The carrier of affinity chromatography should have the following characteristics (Chen et al., 2003): 1) Insoluble in water, but highly hydrophilic; 2) Inert substance with good specificity; 3) There are enough chemical groups for activation; 4) Stable physical and chemical properties; 5) Good mechanical properties, with a certain particle shape to maintain a certain flow rate; 6) Good permeability, with porous network structure for free passage of macromolecular substances; 7) It can resist the damage to microorganisms and alcohols. The commonly used stationary phase carriers include alumina,

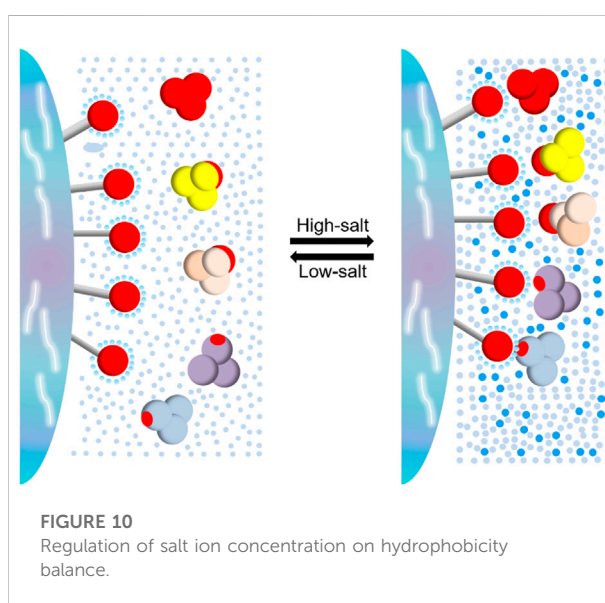
polyacrylamide gel, dextran gel, cellulose, agarose, metal chelate and so on.

Affinity tags are important recognition structures for affinity chromatography, located inside the N terminus of the target protein, whose essence is a protein or a peptide. Some affinity tags also help the protein fold (Kou et al., 2007), increase solubility (Hammarstrom et al., 2002; Chen et al., 2005; Nallamsetty and Waugh, 2006), and in turn increase the yield of the target proteins (Sun et al., 2005). Currently, multiple types of affinity tags have been developed. The most commonly used His tag



(Kinrade et al., 2020) is composed of six or more tandem histidine residues, and it is small, cheap, and has little impact on the structure and function of the target proteins (Figure 8) (Lichty et al., 2005). Abis et al. (2019) purified human soluble cyclooxygenase by nickel ion chelation chromatography combined with and BTS (Benzylthio-Sepharose) affinity chromatography, and the target proteins showed a high purity, as determined by SDS-PAGE analysis. Ge et al. (2022) purified the recombinant SARS-CoV-2 S1 protein by immobilized metal affinity chromatography and used it as an antigen for immunizing hens. Öztürk and Demir (2021) proposed to use CTS-p (HEMA) -Cu<sup>2+</sup> as an IMAC adsorbent, which can quickly, efficiently and repeatedly detect the amount of residues of melamine in different complex substrates. Wang et al. (2022) used titanium (IV) ion-fixed metal affinity chromatography (Ti<sup>4+</sup> -IMAC) to jointly extract DNA binding proteins (DBPs) and RNA binding proteins (RBPs), which contributes to the efficient analysis of nucleic acid-binding proteins in cells. Affinity tags can be divided into epitope tags and protein/domain tags, where His, Strep, HA, etc., are often used as epitope tags, GST, MBP, CBP, etc., are often used as protein/domain tags. At the same time, we also screened some new tags found in recent years (Table 6). The tandem use of affinity tags can successfully purify single proteins or protein complexes (Figure 9) (Mishra, 2020). For example, connecting His<sub>10</sub> at the C end and twin Strep tag at the N end can purify the complete membrane protein receptor CB2 from *E. coli* (Yeliseev et al., 2017). When the affinity tag interferes with the structure or function of the target proteins, the tag is often removed by enterokinase, factor Xa, thrombin, tobacco etch virus (TEV) or human rhinovirus 3C protease or by introducing an inclusion peptide (Zhao et al., 2013). It was found that the natural protein A in the cell wall of *S. aureus* has a strong specific affinity with the Fc fragment of IgG, and the protein A as

an affinity ligand can effectively reduce process impurities, and has become the gold standard for monoclonal antibody purification (Das et al., 2020). Protein A was genetically engineered to produce the alkali resistant recombinant protein A product MabSelect SuRe, and further purified to obtain a bispecific antibody m3s193 BsAb with a purity of more than 95%, which can be used for the treatment of gastric cancer (Chen et al., 2021). Therefore, using MabSelect SuRe or developing more potential recombinant protein A products and producing more antibodies against different cancers will effectively improve cancer cure rates and help the biomedical and health industries.





### 6.1.4 Hydrophobic chromatography

There are some amino acids with hydrophobic side chains on the surface of most proteins, such as phenylalanine, tryptophan, methionine, etc. The number, size and distribution of these amino acids determine the properties of proteins (O'Connor and Cummins, 2017). Hydrophobic chromatography is a purification technology developed based on the hydrophobicity difference of proteins. The balance of hydrophobicity is mainly controlled by salt (Figure 10). Generally, controlling the concentration of salt ions can effectively remove the self-aggregation or self-interaction caused by hydrophobic interaction within the sample. Hydrophobic chromatography can also be used to remove impurities and monitor the purity of the target proteins. Weigel et al. (2019) used hydrophobic chromatography to reversibly combine virus particles to remove residual contaminated DNA and proteins when purifying influenza A and B viruses.

## 7 Challenges and future perspectives

Protein is the material basis of life activities. With the continuous development of molecular biology, structural biology, genomics and bioinformatics, people gradually realize that it is far from enough to clarify the phenomenon and the nature of life activities only by genome sequence analysis. It is also necessary to study life activities from the perspective of proteomics. Only by integrating multi omics can we better understand the phenomena and laws of life, and then reveal the nature of life. Protein isolation and purification is an important technology in the field of biochemistry. At present, it has made unprecedented progress in food, medicine, agriculture, fermentation, textile and other fields. Since proteins are often exist in complex mixtures in tissues or cells, host contamination, sample solubility, structure integrity, purity and biological activity of proteins make purification a delicate and complex task. Therefore, efficient protein purification technology is the basis and key of protein related research.

Protein production has been facing great challenges. Firstly, the establishment of the protein purification scheme requires repeated trials, constant exploration, tedious steps and long cycle, which increases the risk of loss of protein activity. Secondly, the acquisition of high-purity target proteins requires the cooperation of multiple devices, which increases the research cost. Thirdly, other biological macromolecules other than target proteins are often treated as impurities. In fact, the recycling of these substances is of great significance in the field of life and health. Finally, the isolation and purification of membrane

proteins has always been a difficult problem in the field, and how to efficiently separate and purify various membrane proteins is still a valuable topic. Therefore, shortening the production process, reducing the production cost, and building a recycling system to recycle valuable substances without destroying the activity and yield of the target proteins are the directions for further development in the future.

At present, the bio health industry has become the focus of global attention, and is bound to be the next explosion point of economic development. With the continuous improvement of people's living standards, people's desire for a healthy life has become increasingly urgent. The most promising branches of the life health industry mainly include: second-generation sequencing, *in vitro* diagnosis, immunotherapy, stem cell therapy, biopharmaceutical, etc. The most critical steps in the second-generation sequencing process of library building, capture, and sequencing require the participation of a wide variety of enzymes or proteins. Moreover, the most important factor determining the detection accuracy of various biochemical detection reagents used by major hospitals and third-party detection institutions is the quality of antibodies, antigens or enzymes in these kits.

In recent years, immune and stem cell therapies have been developing rapidly. It is the wide variety of protein-like cytokines that play a key role in the process of cell culture, proliferation and activation, and these factors are key to the success of this therapeutic technique. Most biopharmaceutical molecules are proteins themselves, so the manufacturing cost and the successful development of dosage forms of these drug molecules are usually directly related to the success of this new drug research and development project. In the process of research, development and production of leading biopharmaceutical molecules, it is also inevitable to require the participation of some enzymes and protein molecules. Sometimes the activity or cost of a key enzyme can determine the life and death of this biopharmaceutical research and development project. Insulin, for example, requires two enzymes in its production process. Therefore, successful control of the production of these key raw materials enzymes will better benefit mankind.

In summary, although protein-related products are in the upstream of the life and health industry, it is this upstream that firmly affects the trend and direction of the entire industry. It can be seen that the core competitiveness of the above fields lies in a variety of core protein products upstream. Therefore, how to better accelerate the development of life and health in the post epidemic era is what people expect, and how to better apply the progress made in the protein field to protect people's life and health still requires our continuous efforts.

## Author contributions

All authors listed have made a substantial, direct and intellectual contribution to this work, and approved it for publication. Conception: LL and BX; Writing—original draft: MD, ZH, LL, and BX; Methodology, investigation and revising: ZH, YX, XC, LF, and ZL; Writing—Reviewing and Editing: MD, ZH, LL, and BX.

## Funding

This study was supported by Fundamental Research Program of Shanxi Province (Grant no. 202103021223397), Science and Technology Innovation Project of Colleges and Universities in Shanxi Province (Grant no. 2020L0749), Key R&D Projects of Introducing High-Level Scientific and Technological Talents in Lvliang City (Grant no. 2021RC-1-4), the Project of Luliang City Science and Technology Program (Grant no. 2020SHFZ29), the National College Students' Innovation and Entrepreneurship Training Program (Grant no. 202117114001), the Key Projects of Innovation and Entrepreneurship Training for College

Students in Shanxi Province (Grant no. S202117114008; Grant no. 20221577), and Projects of Innovation and entrepreneurship training program for college students of Fenyang College of Shanxi Medical University (Grant no. FDC202111).

## Conflict of interest

The authors declare that the research was conducted in the absence of any commercial or financial relationships that could be construed as a potential conflict of interest.

## Publisher's note

All claims expressed in this article are solely those of the authors and do not necessarily represent those of their affiliated organizations, or those of the publisher, the editors and the reviewers. Any product that may be evaluated in this article, or claim that may be made by its manufacturer, is not guaranteed or endorsed by the publisher.

## References

- Abeyrathne, E. D. N. S., Lee, H. Y., Ham, J. S., and Ahn, D. U. (2013). Separation of ovotransferrin from chicken egg white without using organic solvents. *Poult. Sci.* 92 (4), 1091–1097. doi:10.3382/ps.2012-02654
- Abis, G., Charles, R. L., Eaton, P., and Conte, M. R. (2019). Expression, purification, and characterisation of human soluble Epoxide Hydrolase (hsEH) and of its functional C-terminal domain. *Protein Expr. Purif.* 153, 105–113. doi:10.1016/j.pep.2018.09.001
- Ahmed, W., Angel, N., Edson, J., Bibby, K., Bivins, A., O'Brien, J. W., et al. (2020). First confirmed detection of SARS-CoV-2 in untreated wastewater in Australia: A proof of concept for the wastewater surveillance of COVID-19 in the community. *Sci. Total Environ.* 728, 138764. doi:10.1016/j.scitotenv.2020.138764
- Ai, Y. H., Davis, A., Jones, D., Lemeshow, S., Tu, H. L., He, F., et al. (2021). Wastewater SARS-CoV-2 monitoring as a community-level COVID-19 trend tracker and variants in Ohio, United States. *Sci. Total Environ.* 801, 149757. doi:10.1016/j.scitotenv.2021.149757
- Akin, E. J., Alsalam, M., Higerd, G. P., Liu, S. J., Zhao, P., Dib-Hajj, F. B., et al. (2021). Paclitaxel increases axonal localization and vesicular trafficking of Nav1.7. *Brain* 144 (6), 1727–1737. doi:10.1093/brain/awab113
- Arora, S., Saxena, V., and Ayyar, B. V. (2017). Affinity chromatography: A versatile technique for antibody purification. *Methods* 116, 84–94. doi:10.1016/j.ymeth.2016.12.010
- Baghalabadi, V., and Doucette, A. A. (2020). Mass spectrometry profiling of low molecular weight proteins and peptides isolated by acetone precipitation. *Anal. Chim. Acta X* 1138, 38–48. doi:10.1016/j.aca.2020.08.057
- Baghban, R., Farajnia, S., Rajabibazl, M., Ghasemi, Y., Mafi, A., Hoseinpoor, R., et al. (2019). Yeast expression systems: Overview and recent advances. *Mol. Biotechnol.* 61 (5), 365–384. doi:10.1007/s12033-019-00164-8
- Beigh, M. M. (2016). Next-generation sequencing: The translational medicine approach from "bench to bedside to population. *Med. (Basel)* 3 (2), 14. doi:10.3390/medicines3020014
- Bhataya, A., Schmidt-Dannert, C., and Lee, P. C. (2009). Metabolic engineering of *Pichia pastoris* X-33 for lycopene production. *Process Biochem.* 44 (10), 1095–1102. doi:10.1016/j.procbio.2009.05.012
- Bhawshingha, N., Glenn, K. F., and Schaaper, R. M. (2020). Complete genome sequence of *Escherichia coli* BL21-AI. *Microbiol. Resour. Announc.* 9 (10), e00009-20–e00020. doi:10.1128/MRA.00009-20
- Bill, R. M., and Hedfalk, K. (2021). Aquaporins - expression, purification and characterization. *Biochimica Biophysica Acta - Biomembr.* 1863 (9), 183650. doi:10.1016/j.bbamem.2021.183650
- Block, H., Maertens, B., Spriestersbach, A., Brinker, N., Kubicek, J., Fabis, R., et al. (2009). Immobilized-metal affinity chromatography (IMAC): A review. *Methods Enzymol.* 463, 439–473. doi:10.1016/s0076-6879(09)63027-5
- Boonchay, P., Techapun, C., Leksawasdi, N., Seesuriyachan, P., Hanmoungjai, P., Watanabe, M., et al. (2021). Bioethanol production from cellulose-rich corncob residue by the thermotolerant *Saccharomyces cerevisiae* TC-5. *J. Fungi (Basel)* 7 (7), 547. doi:10.3390/jof7070547
- Bowden, G. A., A. M. P., and Georgiou, G. (1991). Structure and morphology of protein inclusion bodies in *Escherichia coli*. *Nat. Biotechnol.* 9 (8), 725–730. doi:10.1038/nbt0891-725
- Bromberg, R., Cai, K., Guo, Y., Plymire, D., Emde, T., Puzio, M., et al. (2022). The His-tag as a decoy modulating preferred orientation in cryo-EM. *Front. Mol. Biosci.* 9, 912072. doi:10.3389/fmolb.2022.912072
- Burgess, R. R. (2016). *Guidelines to protein purification*. 2nd Edition. Amsterdam, Netherlands: Elsevier.
- Busatto, S., Vilanilam, G., Ticer, T., Lin, W. L., Dickson, D. W., Shapiro, S., et al. (2018). Tangential flow filtration for highly efficient concentration of extracellular vesicles from large volumes of fluid. *Cells* 7 (12), 273. doi:10.3390/cells7120273
- Bushmarina, N. A., Blanchet, C. E., Vernier, G., and Forge, V. (2006). Cofactor effects on the protein folding reaction: Acceleration of alpha-lactalbumin refolding by metal ions. *Protein Sci.* 15 (4), 659–671. doi:10.1110/ps.051904206
- Buyel, J. F., Twyman, R. M., and Fischer, R. (2017). Very-large-scale production of antibodies in plants: The biologization of manufacturing. *Biotechnol. Adv.* 35 (4), 458–465. doi:10.1016/j.biotechadv.2017.03.011
- Carere, J., Hassan, Y. I., Lepp, D., and Zhou, T. (2018). The enzymatic detoxification of the mycotoxin deoxynivalenol: Identification of DepA from the DON epimerization pathway. *Microb. Biotechnol.* 11 (6), 1106–1111. doi:10.1111/1751-7915.12874
- Cao, D. M., Yu, J., Wang, H., Luo, Z. P., Liu, X., He, L., et al. (2022). Structure-based discovery of nonhallucinogenic psychedelic analogs. *Science* 375 (6579), 403–411. doi:10.1126/science.abb8615
- Chee, W. K. D., Yeoh, J. W., Dao, V. L., and Poh, C. L. (2022). Highly reversible tunable thermal-repressible split-T7 RNA polymerases (Thermal-T7RNAPs) for

dynamic gene regulation. *ACS Synth. Biol.* 11 (2), 921–937. doi:10.1021/acssynbio.1c00545

Chen, H. Q., Xu, Z. N., Xu, N. Z., and Cen, P. L. (2005). Efficient production of a soluble fusion protein containing human  $\beta$ -defensin-2 in *E. coli* cell-free system. *J. Biotechnol.* 115 (3), 307–315. doi:10.1016/j.jbiotec.2004.08.012

Chen, J., Pan, Z. D., Han, L., Zhou, Y. X., Zong, H. F., Wang, L., et al. (2021). A novel bispecific antibody targeting CD3 and Lewis Y with potent therapeutic efficacy against gastric cancer. *Biomedicine* 9 (15), 1059. doi:10.3390/biomedicine9081059

Chen, J., Xu, W., Li, L. T., Yi, L. C., Jiang, Y. H., Hao, P. F., et al. (2022). Immunogenicity and protective potential of chimeric virus-like particles containing SARS-CoV-2 spike and H5N1 matrix 1 proteins. *Front. Cell. Infect. Microbiol.* 12, 967493. doi:10.3389/fcimb.2022.967493

Chen, L., Yang, X. Y., Luo, D., and Yu, W. C. (2016). Efficient production of a bioactive bevacizumab monoclonal antibody using the 2A self-cleavage peptide in transgenic rice callus. *Front. Plant Sci.* 7, 1156. doi:10.3389/fpls.2016.01156

Chen, T., Liu, Y., and Pan, J. Q. (2003). A new technology of isolation and purification: Affinity chromatography. *Mod. Food Technol.* 19 (2), 98–101. doi:10.3969/j.issn.1673-9078.2003.02.038

Chen, W. H., Chag, S. M., Poongavanam, M. V., Biter, A. B., Ewera, E. A., Rezende, W., et al. (2017). Optimization of the production process and characterization of the yeast-expressed SARS-CoV recombinant receptor-binding domain (RBD219-N1), a SARS vaccine candidate. *J. Pharm. Sci.* 106 (8), 1961–1970. doi:10.1016/j.xphs.2017.04.037

Chigira, Y., Oka, T., Okajima, T., and Jigami, Y. (2008). Engineering of a mammalian O-glycosylation pathway in the yeast *Saccharomyces cerevisiae*: Production of O-fucosylated epidermal growth factor domains. *Glycobiology* 18 (4), 303–314. doi:10.1093/glycob/cwn008

Clayton, D. A., and Shadel, G. S. (2014). Purification of mitochondria by sucrose step density gradient centrifugation. *Cold Spring Harb. Protoc.* 2014 (10), prot080028. doi:10.1101/pdb.prot080028, pdb

Cordier, C., Stavrakakis, C., Morga, B., Degremont, L., Voulgaris, A., Bacchi, A., et al. (2020). Removal of pathogens by ultrafiltration from sea water. *Environ. Int.* 142, 105809. doi:10.1016/j.envint.2020.105809

Costanzo, M. R. (2019). Ultrafiltration in acute heart failure. *Card. Fail. Rev.* 5 (1), 9–18. doi:10.15420/cfr.2018.29.2

Darlington, A. P. S., Kim, J., Jimenez, J. I., and Bates, D. G. (2018). Dynamic allocation of orthogonal ribosomes facilitates uncoupling of co-expressed genes. *Nat. Commun.* 9 (1), 695. doi:10.1038/s41467-018-02898-6

Das, T. K., Narhi, L. O., Sreedhara, A., Menzen, T., Grapentin, C., Chou, D. K., et al. (2020). Stress factors in mAb drug substance production processes: Critical assessment of impact on product quality and control strategy. *J. Pharm. Sci.* 109 (1), 116–133. doi:10.1016/j.xphs.2019.09.023

de Marco, A., Deuerling, E., Mogk, A., Tomoyasu, T., and Bukau, B. (2007). Chaperone-based procedure to increase yields of soluble recombinant proteins produced in *E. coli* *BMC Biotechnol.* 7, 32. doi:10.1186/1472-6750-7-32

Deo, C., Abdelfattah, A. S., Bhargava, H. K., Berro, A. J., Falco, N., Farrants, H., et al. (2021). The HaloTag as a general scaffold for far-red tunable chemigenetic indicators. *Nat. Chem. Biol.* 17 (6), 718–723. doi:10.1038/s41589-021-00775-w

Diamant, S., Eliahu, N., Rosenthal, D., and Goloubinoff, P. (2001). Chemical chaperones regulate molecular chaperones *in vitro* and in cells under combined salt and heat stresses. *J. Biol. Chem.* 276 (43), 39586–39591. doi:10.1074/jbc.M103081200

Dirisala, V. R., Nair, R. R., Srirama, K., Reddy, P. N., Rao, K. R. S. S., Satya Sampath Kumar, N., et al. (2017). Recombinant pharmaceutical protein production in plants: Unraveling the therapeutic potential of molecular pharming. *Acta Physiol. Plant.* 39 (1), 1–9. doi:10.1007/s11738-016-2315-3

Donovan, R. S., Robinson, C. W., and Glick, B. R. (1996). Review: Optimizing inducer and culture conditions for expression of foreign proteins under the control of the lac promoter. *J. Ind. Microbiol.* 16 (3), 145–154. doi:10.1007/BF01569997

Dow, B. A., Tatulian, S. A., and Davidson, V. L. (2015). Use of the amicyanin signal sequence for efficient periplasmic expression in *E. coli* of a human antibody light chain variable domain *Protein Expr. Purif.* 108, 9–12. doi:10.1016/j.pep.2014.12.017

Dudenhoeffer, B. R., Borggraefe, J., Schweimer, K., and Knauer, S. H. (2020). NusA directly interacts with antitermination factor Q from phage  $\lambda$ . *Sci. Rep.* 10 (1), 6607. doi:10.1038/s41598-020-63523-5

Duman-Scheel, M. (2019). *Saccharomyces cerevisiae* (Baker's Yeast) as an interfering RNA expression and delivery system. *Curr. Drug Targets* 20 (9), 942–952. doi:10.2174/1389450120666181126123538

Dumke, R., de la Cruz Barron, M., Oertel, R., Helm, B., Kallies, R., Berendonk, T. U., et al. (2021). Evaluation of two methods to concentrate SARS-CoV-2 from untreated wastewater. *Pathogens* 10 (2), 195. doi:10.3390/pathogens10020195

Duong-Ly, K. C., and Gabelli, S. B. (2014). Salting out of proteins using ammonium sulfate precipitation. *Methods Enzymol.* 541, 85–94. doi:10.1016/B978-0-12-420119-4.00007-0

Echave, J., Fraga-Corral, M., Garcia-Perez, P., Popovic-Djordjevic, J., H Avdovic, E., Radulovic, M., et al. (2021). Seaweed protein hydrolysates and bioactive peptides: Extraction, purification, and applications. *Mar. Drugs* 19 (9), 500. doi:10.3390/md19090500

Emami, P., Motevalian, S. P., Pepin, E., and Zydney, A. L. (2019). Purification of a conjugated polysaccharide vaccine using tangential flow diafiltration. *Biotechnol. Bioeng.* 116 (3), 591–597. doi:10.1002/bit.26867

Evert, K., and Irwin, H. (2011). Ion exchange chromatography. *Methods Biochem. Anal.* 54, 93–133. doi:10.1002/9780470939932.ch4

Fox, J. D., Kapust, R. B., and Waugh, D. S. (2001). Single amino acid substitutions on the surface of *Escherichia coli* maltose-binding protein can have a profound impact on the solubility of fusion proteins. *Protein Sci.* 10 (3), 622–630. doi:10.1111/ps.45201

Freidel, C., Kaloyanova, S., and Peneva, K. (2016). Chemical tags for site-specific fluorescent labeling of biomolecules. *Amino Acids* 48 (6), 1357–1372. doi:10.1007/s00726-016-2204-5

Freitas, A. I., Domingues, L., and Aguiar, T. Q. (2022). Tag-mediated single-step purification and immobilization of recombinant proteins toward protein-engineered advanced materials. *J. Adv. Res.* 36, 249–264. doi:10.1016/j.jare.2021.06.010

Fu, J., Jia, Q. Q., Liang, P. D., Wang, S. S., Zhou, H. X., Zhang, L. Y., et al. (2021). Targeting and covalently immobilizing the EGFR through SNAP-tag technology for screening drug leads. *Anal. Chem.* 93 (34), 11719–11728. doi:10.1021/acs.analchem.1c01664

Fukushima, M., Watanabe, N., Noh, J. Y., Yoshihara, A., Matsumoto, M., Suzuki, N., et al. (2021). A case of macro-TSH consisting of IgA-bound TSH. *Endocr. J.* 68 (10), 1241–1246. doi:10.1507/endocrj.EJ21-0021

Gao, P., Li, J., Li, Z., Hao, J., and Zan, L. (2016). Establishment and application of milk fingerprint by gel filtration chromatography. *J. Dairy Sci.* 99 (12), 9493–9501. doi:10.3168/jds.2015-10655

Ge, S. K., Wu, R., Zhou, T. T., Liu, X., Zhu, J., and Zhang, X. Y. (2022). Specific anti-SARS-CoV-2 S1 IgY-scFv is a promising tool for recognition of the virus. *AMB Expr.* 12 (1), 18. doi:10.1186/s13568-022-01355-4

Geng, F., Xie, Y. X., Wang, J. Q., Li, S. G., Jin, Y. G., and Ma, M. H. (2019). Large-scale purification of ovalbumin using polyethylene glycol precipitation and isoelectric precipitation. *Poult. Sci.* 98 (3), 1545–1550. doi:10.3382/ps/pey402

Goh, J. B., and Ng, S. K. (2018). Impact of host cell line choice on glycan profile. *Crit. Rev. Biotechnol.* 38 (6), 851–867. doi:10.1080/07388551.2017.1416577

Gonzalez-Lamothe, R., Mitchell, G., Gattuso, M., Diarra, M. S., Malouin, F., and Bouarab, K. (2009). Plant antimicrobial agents and their effects on plant and human pathogens. *Int. J. Mol. Sci.* 10 (8), 3400–3419. doi:10.3390/ijms10083400

Gopal, G. J., and Kumar, A. (2013). Strategies for the production of recombinant protein in *Escherichia coli*. *Protein J.* 32 (6), 419–425. doi:10.1007/s10930-013-9502-5

Greenfield, E. A., DeCaprio, J., and Brahmandam, M. (2020). Preparing GST-His or MBP-fusion proteins from bacteria. *Cold Spring Harb. Protoc.* 2020 (9), 100024. doi:10.1101/pdb.prot100024

Guo, Y., Yu, M., Jing, N., and Zhang, S. (2018). Production of soluble bioactive mouse leukemia inhibitory factor from *Escherichia coli* using MBP tag. *Protein Expr. Purif.* 150, 86–91. doi:10.1016/j.pep.2018.05.006

Gupta, J., Paul, S., Srivastava, A., Kaushik, N., Ghosh, S., Sharma, C., et al. (2020). Expression, purification and characterization of the hepatitis E virus like-particles in the *Pichia pastoris*. *Front. Microbiol.* 11, 141. doi:10.3389/fmicb.2020.00141

Gupta, S. K., Dangi, A. K., Smita, M., Dwivedi, S., and Shukla, P. (2019). Chapter 11-Effectual bioprocess development for protein production. *Appl. Microbiol. Bioeng.*, 203–227. doi:10.1016/b978-0-12-815407-6.00011-3

Gupta, S. K., and Shukla, P. (2016). Advanced technologies for improved expression of recombinant proteins in bacteria: perspectives and applications. *Crit. Rev. Biotechnol.* 36 (6), 1089–1098. doi:10.3109/07388551.2015.1084264

Hammarstrom, M., Hellgren, N., van Den Berg, S., Berglund, H., and Hard, T. (2002). Rapid screening for improved solubility of small human proteins produced as fusion proteins in *Escherichia coli*. *Protein Sci.* 11 (2), 313–321. doi:10.1111/ps.22102

Han, M.-J., Kim, H. R., O'Reilly, C., and Kim, C.-H. (2017). Purification of functional reprogramming factors in mammalian cell using FLAG-Tag. *Biochem. Biophysical Res. Commun.* 492 (2), 154–160. doi:10.1016/j.bbrc.2017.08.028

- Hanke, M., Hansen, N., Chen, R. P., Grundmeier, G., Fahmy, K., and Keller, A. (2022). Salting-out of DNA origami nanostructures by ammonium sulfate. *Int. J. Mol. Sci.* 23 (5), 2817. doi:10.3390/ijms23052817
- Hara, K. Y., Yagi, S., Hirono-Hara, Y., and Kikukawa, H. (2021). A method of solubilizing and concentrating astaxanthin and other carotenoids. *Mar. Drugs* 19 (8), 462. doi:10.3390/md19080462
- Hardy, D., Bill, R. M., Jawhari, A., and Rothnie, A. J. (2019). Functional expression of multidrug resistance protein 4 MRP4/ABCC4. *SLAS Discov.* 24 (10), 1000–1008. doi:10.1177/2472555219867070
- Hazim Abdul Hameed, D., and Hussein Ali, E. (2021). Extraction and purification of extracellular L-glutamate oxidase from streptomyces. *Arch. Razi Inst.* 76 (4), 769–779. doi:10.22092/ari.2021.355928.1738
- Hefferon, K. (2017). Reconceptualizing cancer immunotherapy based on plant production systems. *Future Sci. OA* 3 (3), FSO217. doi:10.4155/fsoa-2017-0018
- Heib, T., Gross, C., Muller, M. L., Stegner, D., and Pleines, I. (2021). Isolation of murine bone marrow by centrifugation or flushing for the analysis of hematopoietic cells - a comparative study. *Platelets* 32 (5), 601–607. doi:10.1080/09537104.2020.1797323
- Heinrich, J., Drewniok, C., Neugebauer, E., Kellner, H., and Wiegert, T. (2019). The YoaW signal peptide directs efficient secretion of different heterologous proteins fused to a StrepII-SUMO tag in *Bacillus subtilis*. *Microb. Cell Fact.* 18 (1), 31. doi:10.1186/s12934-019-1078-0
- Hillary, L. S., Farkas, K., Maher, K. H., Lucaci, A., Thorpe, J., Distaso, M. A., et al. (2021). Monitoring SARS-CoV-2 in municipal wastewater to evaluate the success of lockdown measures for controlling COVID-19 in the UK. *Metabolic engineering of *Saccharomyces cerevisiae*: A key cell factory platform for future biorefineries.* *Cell. Mol. Life Sci. Cell. Mol. Life Sci.* 20069 (16), 1172142671–1172142690. doi:10.1016/j.watres.2021.117214Hong10.1007/s00018-012-0945-1
- Hong, K. K., and Nielsen, J. (2012). Metabolic engineering of *Saccharomyces cerevisiae*: A key cell factory platform for future biorefineries. *Cell. Mol. Life Sci.* 69 (16), 2671–2690. doi:10.1007/s00018-012-0945-1
- Huang, L. P., Lu, Y. H., Wei, Y. W., Guo, L. J., Wu, H. L., Zhang, F. Y., et al. (2011). Construction and biological characterisation of recombinant porcine circovirus type 2 expressing the V5 epitope tag. *Virus Res.* 161 (2), 115–123. doi:10.1016/j.virusres.2011.05.015
- Hunt, I. (2005). From gene to protein: A review of new and enabling technologies for multi-parallel protein expression. *Protein Expr. Purif.* 40 (1), 1–22. doi:10.1016/j.pep.2004.10.018
- Imagawa, T., Ito, M., Matsuda, M., Nakashima, K., Tokunaga, Y., Ohta, I., et al. (2021). Virus-like particles with FLAG-tagged envelope protein as a tetravalent dengue vaccine candidate. *Sci. Rep.* 11 (1), 17542. doi:10.1038/s41598-021-97038-4
- Ing-Simmons, E., and Vaquerizas, J. M. (2019). Visualising three-dimensional genome organisation in two dimensions. *Development* 146 (19), dev177162. doi:10.1242/dev.177162
- Ivanov, I. G., Saraffova, A., Alexandrova, R., and AbouHaidar, M. G. (1993). Expression of human alpha 1 interferon genes in vectors containing tandemly located promoters recognized by two different RNA polymerases (*Escherichia coli* and T7). *FEMS Microbiol. Lett.* 108 (2), 231–236. doi:10.1111/j.1574-6968.1993.tb06104.x
- Jhamb, K., and Sahoo, D. K. (2012). Production of soluble recombinant proteins in *Escherichia coli*: Effects of process conditions and chaperone co-expression on cell growth and production of xylanase. *Bioresour. Technol.* 123, 135–143. doi:10.1016/j.biortech.2012.07.011
- Jiang, N., Ding, X., and Lu, Y. (2021). Development of a robust *Escherichia coli*-based cell-free protein synthesis application platform. *Biochem. Eng. J.* 165, 107830. doi:10.1016/j.bej.2020.107830
- Jing, S. Y., Shi, C., Leong, H. Y., Yuan, J. J., Gao, D., Wang, H. B., et al. (2021). A novel twin-column continuous chromatography approach for separation and enrichment of monoclonal antibody charge variants. *Eng. Life Sci.* 21 (6), 382–391. doi:10.1002/elsc.202000094
- Johar, S. S., and Talbert, J. N. (2017). Strep-tag II fusion technology for the modification and immobilization of lipase B from *Candida Antarctica* (CALB). *J. Genet. Eng. Biotechnol.* 15 (2), 359–367. doi:10.1016/j.jgeb.2017.06.011
- Juturu, V., and Wu, J. C. (2018). Heterologous protein expression in *Pichia pastoris*: Latest research progress and applications. *ChemBiochem* 19 (1), 7–21. doi:10.1002/cbic.201700460
- Karami, M., Shahraky, M. K., Ranjbar, M., Tabandeh, F., Morshedi, D., and Aminzade, S. (2021). Preparation, purification, and characterization of low-molecular-weight hyaluronic acid. *Biotechnol. Lett.* 43 (1), 133–142. doi:10.1007/s10529-020-03035-4
- Karbalaei, M., Rezaee, S. A., and Farsiani, H. (2020). *Pichia pastoris*: A highly successful expression system for optimal synthesis of heterologous proteins. *J. Cell. Physiol.* 235 (9), 5867–5881. doi:10.1002/jcp.29583
- Kaur, J., Kumar, A., and Kaur, J. (2018). Strategies for optimization of heterologous protein expression in *E. coli*: Roadblocks and reinforcements. *Int. J. Biol. Macromol.* 106, 803–822. doi:10.1016/j.ijbiomac.2017.08.080
- Kawaguchi, N., Ogawa, H., and Date, K. (2019). Preparation and purification of active recombinant human pancreatic lipase in *Escherichia coli*. *Bio. Protoc.* 9 (13), e3286. doi:10.21769/BioProtoc.3286
- Keshavarz, R., Babaeipour, V., Mohammadpour-Aghdam, M., and Deldar, A. A. (2021). Overexpression, overproduction, purification, and characterization of rhGH in *Escherichia coli*. *Biotechnol. Appl. Biochem.* 68 (1), 122–135. doi:10.1002/bab.1902
- Kesidis, A., Depping, P., Lodé, A., Vaitopoulou, A., Bill, M. R., Goddard, D. A., et al. (2020). Expression of eukaryotic membrane proteins in eukaryotic and prokaryotic hosts. *Methods* 180, 3–18. doi:10.1016/j.ymeth.2020.06.006
- Khazi, M. I., Demirel, Z., Liaqat, F., and Dalay, M. C. (2020). Analytical grade purification of phycocyanin from *Cyanobacteria*. *Methods Mol. Biol.* 1980, 173–179. doi:10.1007/978-1-4939-9218-2\_10
- Kielkopf, C. L., Bauer, W., and Urbatsch, I. L. (2021). Preparation of cell extracts for purification of proteins expressed in *Pichia pastoris*. *Cold Spring Harb. Protoc.* 2021 (1), pdb.prot102186. doi:10.1101/pdb.prot102186
- Kim, D. S., Kim, S. W., Song, J. M., Kim, S. Y., and Kwon, K. C. (2019). A new prokaryotic expression vector for the expression of antimicrobial peptide abaein using SUMO fusion tag. *BMC Biotechnol.* 19 (1), 13. doi:10.1186/s12896-019-0506-x
- Kim, H. J., Lee, J. H., Lee, K. B., Shin, J. W., Kwon, M. A., Lee, S., et al. (2021). Transglutaminase 2 crosslinks the glutathione S-transferase tag, impeding protein-protein interactions of the fused protein. *Exp. Mol. Med.* 53 (1), 115–124. doi:10.1038/s12276-020-00549-9
- Kimia, Z., Hosseini, S. N., Ashraf Talesh, S. S., Khatami, M., Kavianpour, A., and Javidanbardan, A. (2019). A novel application of ion exchange chromatography in recombinant Hepatitis B vaccine downstream processing: Improving recombinant HBsAg homogeneity by removing associated aggregates. *J. Chromatogr. B* 1113, 20–29. doi:10.1016/j.jchromb.2019.03.009
- Kinrade, B., Davies, P. L., and Vance, T. D. R. (2020). Bacterial sugar-binding protein as a one-step affinity purification tag on dextran-containing resins. *Protein Expr. Purif.* 168, 105564. doi:10.1016/j.pep.2019.105564
- Kou, G., Shi, S., Wang, H., Tan, M., Xue, J., Zhang, D., et al. (2007). Preparation and characterization of recombinant protein ScFv(CD11c)-TRP2 for tumor therapy from inclusion bodies in *Escherichia coli*. *Protein Expr. Purif.* 52 (1), 131–138. doi:10.1016/j.pep.2006.08.007
- Labrou, N. E. (2021). Protein purification technologies. *Methods Mol. Biol.* 2178, 3–10. doi:10.1007/978-1-0716-0775-6\_1
- Labus, K., Wiśniewski, Ł., Cieńska, M., and Bryjak, J. (2020). Effectivity of tyrosinase purification by membrane techniques versus fractionation by salting out. *Chem. Pap.* 74, 2267–2275. doi:10.1007/s11696-020-01060-1
- Lacki, K. M., and Riske, F. J. (2020). Affinity chromatography: An enabling technology for large-scale bioprocessing. *Biotechnol. J.* 15 (1), e1800397. doi:10.1002/biot.201800397
- Lahue, C., Madden, A. A., Dunn, R. R., and Smukowski Heil, C. (2020). History and domestication of *Saccharomyces cerevisiae* in bread baking. *Front. Genet.* 11, 584718. doi:10.3389/fgene.2020.584718
- Lemaitre, R. P., Bogdanova, A., Borgonovo, B., Woodruff, J. B., and Drechsel, D. N. (2019). FlexiBAC: A versatile, open-source baculovirus vector system for protein expression, secretion, and proteolytic processing. *BMC Biotechnol.* 19 (1), 20. doi:10.1186/s12896-019-0512-z
- Li, S., Jendresen, C. B., Grunberger, A., Ronda, C., Jensen, S. I., Noack, S., et al. (2016). Enhanced protein and biochemical production using CRISPRi-based growth switches. *Metab. Eng.* 38, 274–284. doi:10.1016/j.ymben.2016.09.003
- Li, Y. J., Zeng, W. H., Li, Y. L., Fan, W. R., Ma, H., Fan, X. J., et al. (2019). Structure determination of the CAMP factor of *Streptococcus agalactiae* with the aid of an MBP tag and insights into membrane-surface attachment. *Acta Crystallogr. D. Struct. Biol.* 75 (Pt 8), 772–781. doi:10.1107/S205979831901057X
- Li, Y., Zeng, Q. H., Liu, G., Peng, Z., Wang, Y., Zhu, Y., et al. (2021). Effects of ultrasound-assisted basic electrolyzed water (BEW) extraction on structural and functional properties of Antarctic krill (*Euphausia superba*) proteins. *Ultrason. Sonochem.* 71, 105364. doi:10.1016/j.ultsonch.2020.105364
- Li, Z., Huang, X. H., Tang, Q. Y., Ma, M. H., Jin, Y. G., and Sheng, L. (2022a). Functional properties and extraction techniques of chicken egg white proteins. *Foods* 11 (16), 2434. doi:10.3390/foods11162434



- Li, Z. J., Zhang, Z. X., Xu, Y., Shi, T. Q., Ye, C., Sun, X. M., et al. (2022b). CRISPR-based construction of a BL21 (DE3)-derived variant strain library to rapidly improve recombinant protein production. *ACS Synth. Biol.* 11 (1), 343–352. doi:10.1021/acssynbio.1c00463
- Liang, X. N., Qian, G. L., Sun, J., Yang, M., Shi, X. Y., Yang, H., et al. (2021). Evaluation of antigenicity and nutritional properties of enzymatically hydrolyzed cow milk. *Sci. Rep.* 11 (1), 18623. doi:10.1038/s41598-021-98136-z
- Lichty, J. J., Malecki, J. L., Agnew, H. D., Michelson-Horowitz, D. J., and Tan, S. (2005). Comparison of affinity tags for protein purification. *Protein Expr. Purif.* 41 (1), 98–105. doi:10.1016/j.pep.2005.01.019
- Lin, Y., Liu, Y., Li, J. J., Zhao, Y., He, Q. Z., Han, W. J., et al. (2010). Evaluation and optimization of removal of an acid-insoluble surfactant for shotgun analysis of membrane proteome. *Electrophoresis* 31 (16), 2705–2713. doi:10.1002/elps.201000161
- Liu, C., Hao, L. H., Chen, F. S., and Zhu, T. W. (2020a). The mechanism of extraction of peanut protein and oil bodies by enzymatic hydrolysis of the cell wall. *J. Oleo Sci.* 69 (11), 1467–1479. doi:10.5650/jos.ess20148
- Liu, H. N., Dong, W. H., Lin, Y., Zhang, Z. H., and Wang, T. Y. (2022). The effect of microRNA on the production of recombinant protein in CHO cells and its mechanism. *Front. Bioeng. Biotechnol.* 10, 832065. doi:10.3389/fbioe.2022.832065
- Liu, M., Chen, Z. Y., Huang, S. S., Chu, S. H., Issaro, N., Tian, H., et al. (2018). Effective protection on acute liver injury by halo tag-flanked recombinant fibroblast growth factor 7. *Biotechnol. J.* 13 (7), e1700411. doi:10.1002/biot.201700411
- Liu, M., Wang, B., Wang, F., Yang, Z., Gao, D., Zhang, C. Y., et al. (2019). Soluble expression of single-chain variable fragment (scFv) in *Escherichia coli* using superfolder green fluorescent protein as fusion partner. *Appl. Microbiol. Biotechnol.* 103 (15), 6071–6079. doi:10.1007/s00253-019-09925-6
- Liu, X. B., Liu, M., Tao, X. Y., Zhang, Z. X., Wang, F. Q., and Wei, D. Z. (2015). Metabolic engineering of *Pichia pastoris* for the production of dammarenediol-II. *J. Biotechnol.* 216, 47–55. doi:10.1016/j.jbiotec.2015.10.005
- Loh, H. S., Green, B. J., and Yusibov, V. (2017). Using transgenic plants and modified plant viruses for the development of treatments for human diseases. *Curr. Opin. Virol.* 26, 81–89. doi:10.1016/j.coviro.2017.07.019
- Lojewski, E., Kowalczyk, T., Olejniczak, S., and Sakowicz, T. (2016). Extraction and purification methods in downstream processing of plant-based recombinant proteins. *Protein Expr. Purif.* 120, 110–117. doi:10.1016/j.pep.2015.12.018
- Lomonosoff, G. P., and D'Aoust, M. A. (2016). Plant-produced biopharmaceuticals: A case of technical developments driving clinical deployment. *Science* 353 (6305), 1237–1240. doi:10.1126/science.aaf6638
- London, A. S., Mackay, K., Lihon, M., He, Y., and Alabi, B. R. (2014). Gel filtration chromatography as a method for removing bacterial endotoxin from antibody preparations. *Biotechnol. Prog.* 30 (6), 1497–1501. doi:10.1002/btpr.1961
- Lu, J., Zhao, Y., and Zhang, J. (2018). High-level expression of *Aerococcus viridans* pyruvate oxidase in *Escherichia coli* by optimization of vectors and induction conditions. *Lett. Appl. Microbiol.* 67 (3), 262–269. doi:10.1111/lam.13013
- Ma, Q. Y., Liang, M. M., Limjunyawong, N., Dan, Y., Xing, J. C., Li, J. M., et al. (2020). Osteoclast-derived apoptotic bodies show extended biological effects of parental cell in promoting bone defect healing. *Theranostics* 10 (15), 6825–6838. doi:10.7150/thno.45170
- Ma, X., Wang, C. Y., Guo, H. X., Wang, Z. F., Sun, N., Huo, P. F., et al. (2022). Novel dopamine-modified cellulose acetate ultrafiltration membranes with improved separation and antifouling performances. *J. Mat. Sci.* 57 (11), 6474–6486. doi:10.1007/s10853-022-07024-y
- Mamat, U., Wilke, K., Bramhill, D., Schromm, A. B., Lindner, B., Kohl, T. A., et al. (2015). Detoxifying *Escherichia coli* for endotoxin-free production of recombinant proteins. *Microb. Cell Fact.* 14, 57. doi:10.1186/s12934-015-0241-5
- Masuda, Y., Tsuda, M., Hashikawa-Muto, C., Takahashi, Y., Nonaka, K., and Wakamatsu, K. (2019). Cation exchange chromatography performed in overloaded mode is effective in removing viruses during the manufacturing of monoclonal antibodies. *Biotechnol. Prog.* 35 (5), e2858. doi:10.1002/btpr.2858
- Matulis, D. (2016). Selective precipitation of proteins. *Curr. Protoc. Protein Sci.* 83, 41–44. doi:10.1002/0471140864.ps0405s83.5.37
- Mazi, B. G., Hamamci, H., Ogrydzak, D. M., and Dungan, S. R. (2016). Single-step partial purification of intracellular  $\beta$ -galactosidase from *Kluyveromyces lactis* using microemulsion droplets. *Appl. Biochem. Biotechnol.* 180 (5), 1000–1015. doi:10.1007/s12010-016-2148-y
- McElwain, L., Phair, K., Kealey, C., and Brady, D. (2022). Current trends in biopharmaceuticals production in *Escherichia coli*. *Biotechnol. Lett.* 44 (8), 917–931. doi:10.1007/s10529-022-03276-5
- Medema, G., Heijnen, L., Elsinga, G., Italiaander, R., and Brouwer, A. (2020). Presence of SARS-Coronavirus-2 RNA in sewage and correlation with reported COVID-19 prevalence in the early stage of the epidemic in The Netherlands. *Environ. Sci. Technol. Lett.* 7 (7), 511–516. doi:10.1021/acsclett.0c00357
- Menegotto, A. L. L., Fernandes, I. A., Steffens, J., and Valduga, E. (2021). Protein purification of *Arthrosira platensis* using aqueous two-phase system composed of polyethylene glycol and potassium phosphate/sodium citrate. *J. Appl. Phycol.* 34, 311–320. doi:10.1007/s10811-021-02652-4
- Mi, S. Y., Tang, Y. J., Dari, G., Shi, Y. Y., Zhang, J. N., Zhang, H. L., et al. (2021). Transcriptome sequencing analysis for the identification of stable lncRNAs associated with bovine *Staphylococcus aureus mastitis*. *J. Anim. Sci. Biotechnol.* 12 (1), 120. doi:10.1186/s40104-021-00639-2
- Mishra, V. (2020). Affinity tags for protein purification. *Curr. Protein Pept. Sci.* 21 (8), 821–830. doi:10.2174/1389203721666200606220109
- Mohammadi, M., Taheri, R. A., Bemani, P., Hashemzadeh, M. S., Farnoosh, G., and Amini, R. (2022). Utilization of SUMO tag and freeze-thawing method for high level expression and solubilization of recombinant human angiotensin-converting enzyme 2 (rhACE2) protein in *E. coli*. *Protein Pept. Lett.* 29 (7), 605–610. doi:10.2174/0929866529666220715101357
- Moinpour, M., Fracassi, A., Brea, R. J., Salvador-Castell, M., Pandey, S., Edwards, M. M., et al. (2022). Controlling protein enrichment in lipid sponge phase droplets using SNAP-tag bioconjugation. *ChemBiochem.* 23 (5), e202100624. doi:10.1002/cbic.202100624
- Muhmed, S. A., Nor, N. A. M., Jaafar, J., Ismail, A. F., Othman, M. H. D., Rahman, M. A., et al. (2019). Emerging chitosan and cellulose green materials for ion exchange membrane fuel cell: A review. *Energy Ecol. Environ.* 5, 85–107. doi:10.1007/s40974-019-00127-4
- Mukherjee, S., Ura, M., Hoey, R. J., and Kossiakoff, A. A. (2015). A new versatile immobilization tag based on the ultra high affinity and reversibility of the calmodulin-calmodulin binding peptide interaction. *J. Mol. Biol.* 427 (16), 2707–2725. doi:10.1016/j.jmb.2015.06.018
- Muller, C., Zhang, L., Zipfel, S., Topitsch, A., Lutz, M., Eckert, J., et al. (2022). Molecular interplay of an assembly machinery for nitrous oxide reductase. *Nature* 608 (7923), 626–631. doi:10.1038/s41586-022-05015-2
- Muthunayake, N. S., Al-Husini, N., and Schrader, J. M. (2020). Differential centrifugation to enrich bacterial ribonucleoprotein bodies (BR bodies) from *Caulobacter crescentus*. *Star. Protoc.* 1 (3), 100205. doi:10.1016/j.xpro.2020.100205
- Nagai, H., Masuda, A., Toya, Y., Matsuda, F., and Shimizu, H. (2018). Metabolic engineering of mevalonate-producing *Escherichia coli* strains based on thermodynamic analysis. *Metab. Eng.* 47, 1–9. doi:10.1016/j.ymben.2018.02.012
- Nallamsetty, S., and Waugh, D. S. (2006). Solubility-enhancing proteins MBP and NusA play a passive role in the folding of their fusion partners. *Protein Expr. Purif.* 45 (1), 175–182. doi:10.1016/j.pep.2005.06.012
- Nasukawa, T., Uchiyama, J., Taharaguchi, S., Ota, S., Ujihara, T., Matsuzaki, S., et al. (2017). Virus purification by CsCl density gradient using general centrifugation. *Arch. Virol.* 162 (11), 3523–3528. doi:10.1007/s00705-017-3513-z
- Nigi, I., Fairall, L., and Schwabe, J. W. R. (2017). Expression and purification of protein complexes suitable for structural studies using mammalian HEK 293F cells. *Curr. Protoc. Protein Sci.* 90 (5), 1–15. doi:10.1002/cpps.4428.16
- Nickerson, J. L., Baghalabadi, V., Dang, Z. H., Miller, V. A., Little, S. L., and Doucette, A. A. (2022). Organic solvent-based protein precipitation for robust proteome purification ahead of mass spectrometry. *J. Vis. Exp.* 180, e63503. doi:10.3791/63503
- Nishida, T., Kubota, S., and Takigawa, M. (2017). Production of recombinant CCN2 protein by mammalian cells. *Methods Mol. Biol.* 1489, 95–105. doi:10.1007/978-1-4939-6430-7\_10
- Nosaki, S., Terada, T., Nakamura, A., Hirabayashi, K., Xu, Y. Q., Bui, T. B. C., et al. (2021). Highlighting the potential utility of MBP crystallization chaperone for *Arabidopsis* BIL1/BZR1 transcription factor-DNA complex. *Sci. Rep.* 11 (1), 3879. doi:10.1038/s41598-021-83532-2
- O'Connor, B. F., and Cummins, P. M. (2017). Hydrophobic interaction chromatography. *Methods Mol. Biol.* 1485, 355–363. doi:10.1007/978-1-4939-6412-3\_18
- Oganesyan, N., Ankoudinova, I., Kim, S. H., and Kim, R. (2007). Effect of osmotic stress and heat shock in recombinant protein overexpression and crystallization. *Protein Expr. Purif.* 52 (2), 280–285. doi:10.1016/j.pep.2006.09.015
- Owczarek, B., Gerszberg, A., and Hnatuszko-Konka, K. (2019). A brief reminder of systems of production and chromatography-based recovery of recombinant protein biopharmaceuticals. *Biomed. Res. Int.* 2019, 1–13. doi:10.1155/2019/4216060

- Öztel, M. D., Kuleyin, A., and Akbal, F. (2020). Treatment of zinc plating wastewater by combination of electrocoagulation and ultrafiltration process. *Water Sci. Technol.* 82 (4), 663–672. doi:10.2166/wst.2020.357
- Öztürk, S., and Demir, N. (2021). Development of a novel IMAC sorbent for the identification of melamine in dairy products by HPLC. *J. Food Compos. Analysis* 100, 103931. doi:10.1016/j.jfca.2021.103931
- Padayachee, E. R., Adeola, H. A., Van Wyk, J. C., Nsola Biteghe, F. A., Chetty, S., Khumalo, N. P., et al. (2019). Applications of SNAP-tag technology in skin cancer therapy. *Health Sci. Rep.* 2 (2), e103. doi:10.1002/hsr2.103
- Palombarini, F., Ghirga, F., Boffi, A., Macone, A., and Bonamore, A. (2019). Application of crossflow ultrafiltration for scaling up the purification of a recombinant ferritin. *Protein Expr. Purif.* 163, 105451. doi:10.1016/j.pep.2019.105451
- Park, K. Y., and Wi, S. J. (2016). Potential of plants to produce recombinant protein products. *J. Plant Biol.* 59 (6), 559–568. doi:10.1007/s12374-016-0482-9
- Park, S. T., and Kim, J. (2016). Trends in next-generation sequencing and a new era for whole genome sequencing. *Int. Neurol.* 20, S76–S83. doi:10.5213/inj.1632742.371
- Penha, C. B., Falcao, H. G., Ida, E. I., Speranza, P., and Kurozawa, L. E. (2020). Enzymatic pretreatment in the extraction process of soybean to improve protein and isoflavone recovery and to favor aglycone formation. *Food Res. Int.* 137, 109624. doi:10.1016/j.foodres.2020.109624
- Periasamy, P., Rajandran, S., Ziegman, R., Casey, M., Nakamura, K., Kore, H., et al. (2021). A simple organic solvent precipitation method to improve detection of low molecular weight proteins. *Proteomics* 21 (19), e2100152. doi:10.1002/pmic.202100152
- Pfaunmiller, E. L., Paulemond, M. L., Dupper, C. M., and Hage, D. S. (2013). Affinity monolith chromatography: A review of principles and recent analytical applications. *Anal. Bioanal. Chem.* 405 (7), 2133–2145. doi:10.1007/s00216-012-6568-4
- Piovan, A., Filippini, R., Argenti, C., Moro, S., Giusti, P., and Zusso, M. (2022). The effect of C-phycocyanin on microglia activation is mediated by toll-like receptor 4. *Int. J. Mol. Sci.* 23 (3), 1440. doi:10.3390/ijms23031440
- Radhakrishnan, M., Palayam, M., Altemimi, A. B., Karthik, L., Krishnasamy, G., Cacciola, F., et al. (2022). Leucine-rich, potent anti-bacterial protein against *Vibrio cholerae*, *Staphylococcus aureus* from *Solanum trilobatum* leaves. *Molecules* 27 (4), 1167. doi:10.3390/molecules27041167
- Rasala, B. A., and Mayfield, S. P. (2015). Photosynthetic biomanufacturing in green algae; production of recombinant proteins for industrial, nutritional, and medical uses. *Photosynth. Res.* 123 (3), 227–239. doi:10.1007/s11120-014-9994-7
- Rathnapala, E. C. N., Ahn, D. U., and Abeyrathne, S. (2021). Functional properties of ovotransferrin from chicken egg white and its derived peptides: A review. *Food Sci. Biotechnol.* 30 (5), 619–630. doi:10.1007/s10068-021-00901-3
- Rivera, M. C., Maguire, B., and Lake, J. A. (2015). Purification of 70S ribosomes. *Cold Spring Harb. Protoc.* 2015 (3), pdb.prot081356–302. doi:10.1101/pdb.prot081356
- Rosano, G. L., and Ceccarelli, E. A. (2014). Recombinant protein expression in *Escherichia coli*: Advances and challenges. *Front. Microbiol.* 5, 172. doi:10.3389/fmicb.2014.00172
- Rosano, G. L., Morales, E. S., and Ceccarelli, E. A. (2019). New tools for recombinant protein production in *Escherichia coli*: A 5-year update. *Protein Sci.* 28 (8), 1412–1422. doi:10.1002/pro.3668
- Royce, J., Liderfelt, J., and Robinson, C. (2018). Chapter 15-Filtration methods for use in recovery processes. *Biopharm. Process.*, 295–315. doi:10.1016/b978-0-08-100623-8.00015-3
- Ruan, A., Ren, C., and Quan, S. (2020). Conversion of the molecular chaperone Spy into a novel fusion tag to enhance recombinant protein expression. *J. Biotechnol.* 307, 131–138. doi:10.1016/j.jbiotec.2019.11.006
- Santoso, A., Herawati, N., and Rubiana, Y. (2012). Effect of methanol induction and incubation time on expression of human erythropoietin in Methylophilic Yeast *Pichia pastoris*. *MAKARA Technol. Ser.* 16 (1), 29–34. doi:10.7454/mst.v16i1.1041
- Santry, L. A., Jacquemart, R., Vandersluis, M., Zhao, M., Domm, J. M., McAusland, T. M., et al. (2020). Interference chromatography: A novel approach to optimizing chromatographic selectivity and separation performance for virus purification. *BMC Biotechnol.* 20 (1), 32. doi:10.1186/s12896-020-00627-w
- Saraswat, M., Musante, L., Ravid, A., Shortt, B., Byrne, B., and Holthofer, H. (2013). Preparative purification of recombinant proteins: Current status and future trends. *Biomed. Res. Int.* 2013, 1–18. doi:10.1155/2013/312709
- Schiermeyer, A. (2020). Optimizing product quality in molecular farming. *Curr. Opin. Biotechnol.* 61, 15–20. doi:10.1016/j.copbio.2019.08.012
- Schmidt, P. M., Sparrow, L. G., Attwood, R. M., Xiao, X., Adams, T. E., and McKimm-Breschkin, J. L. (2012). Taking down the FLAG! How insect cell expression challenges an established tag-system. *PLoS One* 7 (6), e37779. doi:10.1371/journal.pone.0037779
- Schmidt, T. G. M., Batz, L., Bonet, L., Carl, U., Holzapfel, G., and Kiem, K. (2013). Development of the Twin-Strep-tag® and its application for purification of recombinant proteins from cell culture supernatants. *Protein Expr. Purif.* 92 (1), 54–61. doi:10.1016/j.pep.2013.08.021
- Schuchner, S., Behm, C., Mudrak, I., and Ogris, E. (2020). The Myc tag monoclonal antibody 9E10 displays highly variable epitope recognition dependent on neighboring sequence context. *Sci. Signal.* 13 (616), eaax9730. doi:10.1126/scisignal.aax9730
- Scinto, S. L., Reagle, T. R., and Fox, J. M. (2022). Affinity Bioorthogonal Chemistry (ABC) tags for site-selective conjugation, on-resin protein-protein coupling, and purification of protein conjugates. *Angew. Chem. Int. Ed. Engl.* e202207661. doi:10.1002/anie.202207661
- Scopes, R. K. (2001). Overview of protein purification and characterization. *Curr. Protoc. Protein Sci.* 00, Unit 1.1. Chapter 1 Unit 1.1. doi:10.1002/0471140864.ps0101s00
- Sellaturay, P., Nasser, S., and Ewan, P. (2021). Polyethylene glycol-induced systemic allergic reactions (Anaphylaxis). *J. Allergy Clin. Immunol. Pract.* 9 (2), 670–675. doi:10.1016/j.jaip.2020.09.029
- Sharma, P. R., Sharma, S. K., Lindström, T., and Hsiao, B. S. (2020). Nanocellulose-enabled membranes for water purification: Perspectives. *Adv. Sustain. Syst.* 4 (5), 1900114. doi:10.1002/adsu.201900114
- Shaw, M. M., and Riederer, B. M. (2003). Sample preparation for two-dimensional gel electrophoresis. *Proteomics* 3 (8), 1408–1417. doi:10.1002/pmic.200300471
- Shendure, J., and Lieberman Aiden, E. (2012). The expanding scope of DNA sequencing. *Nat. Biotechnol.* 30 (11), 1084–1094. doi:10.1038/nbt.2421
- Shirley, M., and Taha, M. K. (2018). MenB-FHbp meningococcal group B vaccine (Trumenb®): A review in active immunization in individuals aged ≥ 10 years. *Drugs* 78 (2), 257–268. doi:10.1007/s40265-018-0869-7
- Sina, M., Farajzadeh, D., and Dastmalchi, S. (2015). Effects of environmental factors on soluble expression of a humanized anti-TNF-α scFv antibody in *Escherichia coli*. *Adv. Pharm. Bull.* 5 (4), 455–461. doi:10.15171/apb.2015.062
- Sun, Q. M., Chen, L. L., Cao, L., Fang, L., Chen, C., and Hua, Z. C. (2005). An improved strategy for high-level production of human vasostatin120–180. *Biotechnol. Prog.* 21 (4), 1048–1052. doi:10.1021/bp049583x
- Syamani, F. A. (2020). Cellulose-based membrane for adsorption of dye in batik industry wastewater. *Int. J. Hydrology* 4 (6), 281–283. doi:10.15406/ijh.2020.04.00255
- Szelechowski, M., Bergeron, C., Gonzalez-Dunia, D., and Klonjowski, B. (2013). Production and purification of non replicative canine adenovirus type 2 derived vectors. *J. Vis. Exp.* (83), 50833. doi:10.3791/50833
- Tachioka, M., Sugimoto, N., Nakamura, A., Sunagawa, N., Ishida, T., Uchiyama, T., et al. (2016). Development of simple random mutagenesis protocol for the protein expression system in *Pichia pastoris*. *Biotechnol. Biofuels* 9, 199. doi:10.1186/s13068-016-0613-z
- Tahara, N., Tachibana, I., Takeo, K., Yamashita, S., Shimada, A., Hashimoto, M., et al. (2021). Boosting auto-induction of recombinant proteins in *Escherichia coli* with glucose and lactose additives. *Protein Pept. Lett.* 28 (10), 1180–1190. doi:10.2174/0929866528666210805120715
- Tang, R., Yang, S., Nagel, G., and Gao, S. (2021). mem-iLID, a fast and economic protein purification method. *Biosci. Rep.* 41 (7), BSR20210800. doi:10.1042/BSR20210800
- Tang, W. L., Zhang, M., and Fang, Z. X. (2015). Optimization of ultrasound-assisted-extraction of porcine placenta water-soluble proteins and evaluation of the antioxidant activity. *J. Food Sci. Technol.* 52 (7), 4042–4053. doi:10.1007/s13197-014-1444-1
- Tekoah, Y., Shulman, A., Kizhner, T., Ruderfer, I., Fux, L., Nataf, Y., et al. (2015). Large-scale production of pharmaceutical proteins in plant cell culture—the protalix experience. *Plant Biotechnol. J.* 13 (8), 1199–1208. doi:10.1111/pbi.12428
- Tesfaw, A., and Assefa, F. (20142014). Current trends in bioethanol production by *Saccharomyces cerevisiae*: Substrate, inhibitor reduction, growth variables, coculture, and immobilization. *Int. Sch. Res. Not.* 2014, 1–11. doi:10.1155/2014/532852
- Thakur, G., Masampally, V., Kulkarni, A., and Rathore, A. S. (2022). Process analytical technology (PAT) implementation for membrane operations in continuous manufacturing of mAbs: Model-based control of single-pass tangential flow ultrafiltration. *AAPS J.* 24 (4), 83. doi:10.1208/s12248-022-00731-z

- Thammasena, R., Fu, C. W., Liu, J. H., and Liu, D. C. (2020). Evaluation of nutrient content, physicochemical and functional properties of desalted duck egg white by ultrafiltration as desalination. *Anim. Sci. J.* 91 (1), e13339. doi:10.1111/asj.13339
- Tomás-Gamisans, M., Andrade, C. C. P., Maresca, F., Monforte, S., Ferrer, P., and Albiol, J. (2020). Redox engineering by ectopic overexpression of NADH kinase in recombinant *Pichia pastoris* (*Komagataella phaffii*): Impact on cell physiology and recombinant production of secreted proteins. *Appl. Environ. Microbiol.* 86 (6), e02038–e02019. doi:10.1128/AEM.02038-19
- Traore, E. S., Li, J. S., Chiura, T., Geng, J., Sachla, A. J., Yoshimoto, F., et al. (2021). Heme binding to HupZ with a C-terminal tag from group A *Streptococcus*. *Molecules* 26 (3), 549. doi:10.3390/molecules26030549
- Tremante, E., Sibilio, L., Centola, F., Knutti, N., Holzapfel, G., Manni, I., et al. (2021). Toolbox: StrepTagged nanoassemblies of antibodydrugconjugates (ADC) for modular and conditional cancer drugging. *Oncol. Rep.* 45 (5), 77. doi:10.3892/or.2021.8028
- Tripathi, N. K. (2016). Production and purification of recombinant proteins from *Escherichia coli*. *ChemBioEng Rev.* 3 (3), 116–133. doi:10.1002/cben.201600002
- Tripathi, N. K., and Shrivastava, A. (2019). Recent developments in bioprocessing of recombinant proteins: Expression hosts and process development. *Front. Bioeng. Biotechnol.* 7, 420. doi:10.3389/fbioe.2019.00420
- Trombetta, C. M., Marchi, S., and Montomoli, E. (2022). The baculovirus expression vector system: A modern technology for the future of influenza vaccine manufacturing. *Expert Rev. Vaccines* 21 (9), 1233–1242. doi:10.1080/14760584.2022.2085565
- Turkanoglu Ozcelik, A., Yilmaz, S., and Inan, M. (2019). *Pichia pastoris* promoters. *Methods Mol. Biol.* 1923, 97–112. doi:10.1007/978-1-4939-9024-5\_3
- Vargas-Cortez, T., Morones-Ramirez, J. R., Balderas-Renteria, I., and Zarate, X. (2017). Production of recombinant proteins in *Escherichia coli* tagged with the fusion protein CusF3H. *Protein Expr. Purif.* 132, 44–49. doi:10.1016/j.pep.2017.01.006
- Vatanpour, V., Pasaoglu, M. E., Barzegar, H., Teber, O. O., Kaya, R., Bastug, M., et al. (2022). Cellulose acetate in fabrication of polymeric membranes: A review. *Chemosphere* 295, 133914. doi:10.1016/j.chemosphere.2022.133914
- Verma, V., Kaur, C., Grover, P., Gupta, A., and Chaudhary, V. K. (2018). Biotin-tagged proteins: Reagents for efficient ELISA-based serodiagnosis and phage display-based affinity selection. *PLoS One* 13 (1), e0191315. doi:10.1371/journal.pone.0191315
- Viala, J. P. M., and Bouveret, E. (2017). Protein-protein interaction: Tandem affinity purification in bacteria. *Methods Mol. Biol.* 1615, 221–232. doi:10.1007/978-1-4939-7033-9\_18
- Vilar, L., Vilar, C. F., Lyra, R., and Freitas, M. D. C. (2019). Pitfalls in the diagnostic evaluation of hyperprolactinemia. *Neuroendocrinology* 109 (1), 7–19. doi:10.1159/000499694
- Vyas, P., Wood, M. B., Zhang, Y. Y., Goldring, A. C., Chakir, F. Z., Fuchs, P. A., et al. (2020). Characterization of HA-tagged  $\alpha 9$  and  $\alpha 10$  nAChRs in the mouse cochlea. *Sci. Rep.* 10 (1), 21814. doi:10.1038/s41598-020-78380-5
- Walsh, G. (2018). Biopharmaceutical benchmarks 2018. *Nat. Biotechnol.* 36 (12), 1136–1145. doi:10.1038/nbt.4305
- Wang, A. N., Liu, X. Y., Wu, L. G., and Xu, S. B. (2008a). Summary of extraction, purification and properties of proteins. *China Food Ind.* 6, 56–58. doi:10.3969/j.issn.1006-6195.2008.06.023
- Wang, A. P., Wang, Y. J., Wu, S., Zuo, W. Y., Guo, C. M., Hong, W. M., et al. (2017). Efficient production of an avian adeno-associated virus vector using insect cell/baculovirus expression system. *J. Virol. Methods* 240, 26–31. doi:10.1016/j.jviromet.2016.11.005
- Wang, H. Y., Qian, L. Q., Shang, Z., Wang, Z. Y., Zhang, Y., Cao, C. X., et al. (2022). Immobilized titanium (IV) ion affinity chromatography contributes to efficient proteomics analysis of cellular nucleic acid-binding proteins. *J. Proteome Res.* 21 (1), 220–231. doi:10.1021/acs.jproteome.1c00788
- Wang, W. J., Archbold, T., Lam, J. S., Kimber, M. S., and Fan, M. Z. (2019). A processive endoglucanase with multi-substrate specificity is characterized from porcine gut microbiota. *Sci. Rep.* 9 (1), 13630. doi:10.1038/s41598-019-50050-1
- Wang, W., Tai, F. J., and Chen, S. N. (2008). Optimizing protein extraction from plant tissues for enhanced proteomics analysis. *J. Sep. Sci.* 31 (11), 2032–2039. doi:10.1002/jssc.200800087
- Watanabe, M., Maeda, I., Koyama, M., Nakamura, K., and Sasano, K. (2015). Simultaneous recovery and purification of rice protein and phosphorus compounds from full-fat and defatted rice bran with organic solvent-free process. *J. Biosci. Bioeng.* 119 (2), 206–211. doi:10.1016/j.jbiosc.2014.07.009
- Weigel, T., Soliman, R., Wolff, M. W., Reichl, U., Williams, J. D., Kampmeier, F., et al. (2019). Optimal his-tag design for efficient [ $^{99m}\text{Tc}(\text{CO})_3$ ] $^{+}$  and [ $^{188}\text{Re}(\text{CO})_3$ ] $^{+}$  labeling of proteins for molecular imaging and radionuclide therapy by analysis of peptide Arrays. *Wichmann, C., Rosch, P., and Popp, J.* (2021). Isolation of bacteria from artificial bronchoalveolar lavage fluid using density gradient centrifugation and their accessibility by Raman spectroscopy. *Bioconj. Chem. Anal. Bioanal. ChemBioconj Chem.* 111741332 (207), 10351931242–11752001254. doi:10.1016/j.jchromb.2019.03.03710.1007/s00216-021-03488-010.1021/acs.bioconjchem.0c00561. (2021). Optimal His-tag design for efficient [ $^{99m}\text{Tc}(\text{CO})_3$ ] $^{+}$  and [ $^{188}\text{Re}(\text{CO})_3$ ] $^{+}$  labeling of proteins for molecular imaging and radionuclide therapy by analysis of peptide arrays
- Wichmann, C., Rosch, P., and Popp, J. (2021). Isolation of bacteria from artificial bronchoalveolar lavage fluid using density gradient centrifugation and their accessibility by Raman spectroscopy. *Anal. Bioanal. Chem.* 413 (20), 5193–5200. doi:10.1007/s00216-021-03488-0
- Williams, R. M., Harvey, J. D., Budhathoki-Uprety, J., and Heller, D. A. (2020). Glutathione-S-transferase fusion protein nanosensor. *Nano Lett.* 20 (10), 7287–7295. doi:10.1021/acs.nanolett.0c02691
- Wu, X. L., Xiong, E. H., Wang, W., Scali, M., and Cresti, M. (2014). Universal sample preparation method integrating trichloroacetic acid/acetone precipitation with phenol extraction for crop proteomic analysis. *Nat. Protoc.* 9, 362–374. doi:10.1038/nprot.2014.022
- Wyborski, D. L., Bauer, J. C., Zheng, C. F., Felts, K., and Vaillancourt, P. (1999). An *Escherichia coli* expression vector that allows recovery of proteins with native N-termini from purified calmodulin-binding peptide fusions. *Protein Expr. Purif.* 16 (1), 1–10. doi:10.1006/prep.1999.1064
- Xie, X., Wu, P., Huang, X. C., Bai, W. F., Li, B., and Shi, N. (2022). Retro-protein XXA is a remarkable solubilizing fusion tag for inclusion bodies. *Microb. Cell Fact.* 21 (1), 51. doi:10.1186/s12934-022-01776-7
- Xie, Y., Han, X., and Miao, Y. S. (2018). An effective recombinant protein expression and purification system in *Saccharomyces cerevisiae*. *Curr. Protoc. Mol. Biol.* 123 (1), e62. doi:10.1002/cpmb.62
- Xiong, J., He, J. Q., Xie, W. P., Hinojosa, E., Ambati, C. S. R., Putluri, N., et al. (2019). Rapid affinity purification of intracellular organelles using a twin strep tag. *J. Cell Sci.* 132 (24), jcs235390. doi:10.1242/jcs.235390
- Xu, S., Zhang, G. Y., Zhang, H., Kitajima, T., Nakanishi, H., and Gao, X. D. (2016). Effects of Rho1, a small GTPase on the production of recombinant glycoproteins in *Saccharomyces cerevisiae*. *Microb. Cell Fact.* 15 (1), 179. doi:10.1186/s12934-016-0575-7
- Yang, L. L., Cui, L. F., Ma, S. M., Zuo, Q. Q., and Huang, Q. L. (2022). A gene transfer-positive cell sorting system utilizing membrane-anchoring affinity tag. *Front. Bioeng. Biotechnol.* 10, 930966. doi:10.3389/fbioe.2022.930966
- Ye, S. H., Pan, F. P., Yao, L. N., Fang, H. L., Cheng, Y. Q., Zhang, Z. X., et al. (2022). Isolation, characterization of bamboo leaf flavonoids by size exclusion chromatography and their antioxidant properties. *Chem. Biodivers.* 19 (9), e202200506. doi:10.1002/cbdv.202200506
- Yeliseev, A., van den Berg, A., Zoubak, L., Hines, K., Stepnowski, S., Williston, K., et al. (2020). Thermostability of a recombinant G protein-coupled receptor expressed at high level in mammalian cell culture. *Sci. Rep.* 10 (1), 16805. doi:10.1038/s41598-020-73813-7
- Yeliseev, A., Zoubak, L., and Schmidt, T. G. M. (2017). Application of Strep-Tactin XT for affinity purification of Twin-Strep-tagged CB2, a G protein-coupled cannabinoid receptor. *Protein Expr. Purif.* 131, 109–118. doi:10.1016/j.pep.2016.11.006
- Zhai, Y. J., Zhang, D. Y., Yu, L. Y., Sun, F., and Sun, F. (2019). SmartBac, a new baculovirus system for large protein complex production. *J. Struct. Biol. X* 1, 100003. doi:10.1016/j.jysbx.2019.100003
- Zhang, B. H., Zhao, X. R., Wang, Z. W., Wang, H. Z., Zhou, J. W., Du, G. C., et al. (2021a). Efficient secretory expression and purification of food-grade porcine myoglobin in *Komagataella phaffii*. *J. Agric. Food Chem.* 69 (35), 10235–10245. doi:10.1021/acs.jafc.1c04124
- Zhang, C., Ku, Z. Q., Liu, Q. W., Wang, X. L., Chen, T., Ye, X. J., et al. (2015). High-yield production of recombinant virus-like particles of enterovirus 71 in *Pichia pastoris* and their protective efficacy against oral viral challenge in mice. *Vaccine* 33 (20), 2335–2341. doi:10.1016/j.vaccine.2015.03.034
- Zhang, J., Cai, Y. F., Xiao, T. S., Lu, J. M., Peng, H. Q., Sterling, S. M., et al. (2021). Structural impact on SARS-CoV-2 spike protein by D614G substitution. *Science* 372 (6541), 525–530. doi:10.1126/science.abc2303
- Zhang, Y. Y., Ye, F., Zhang, T. T., Lv, S. Y., Zhou, L. P., Du, D. H., et al. (2021b). Structural basis of ketamine action on human NMDA receptors. *Nature* 596 (7871), 301–305. doi:10.1038/s41586-021-03769-9

- Zhang, Z. W., Wu, X. D., Cao, L. L., Zhong, Z. D., and Zhou, Y. (2016). Generation of glucagon-like peptide-2-expressing *Saccharomyces cerevisiae* and its improvement of the intestinal health of weaned rats. *Microb. Biotechnol.* 9 (6), 846–857. doi:10.1111/1751-7915.12412
- Zhang, Z. X., Wang, Y. Z., Nong, F. T., Xu, Y., Ye, C., Gu, Y., et al. (2022). Developing a dynamic equilibrium system in *Escherichia coli* to improve the production of recombinant proteins. *Appl. Microbiol. Biotechnol.* 106 (18), 6125–6137. doi:10.1007/s00253-022-12145-0
- Zhao, X. Y., Li, G. S., and Liang, S. F. (2013). Several affinity tags commonly used in chromatographic purification. *J. Anal. Methods Chem.* 2013, 581093. doi:10.1155/2013/581093
- Zhou, H. H., Zhang, A. X., Zhang, Y., and Zhu, D. Y. (2012). Cloning, expression, and purification of a recombinant Tat-HA-NR2B9c peptide. *Protein Expr. Purif.* 85 (2), 239–245. doi:10.1016/j.pep.2012.08.011
- Zhou, L. X., Liu, Z. Y., Xu, G. Y., Li, L. H., Xuan, K., Xu, Y., et al. (2020). Expression of melittin in fusion with GST in *Escherichia coli* and its purification as a pure peptide with good bacteriostatic efficacy. *ACS Omega* 5 (16), 9251–9258. doi:10.1021/acsomega.0c00085
- Zielinski, M., Romanik-Chruscielewska, A., Mikiewicz, D., Lukasiewicz, N., Sokolowska, I., Antosik, J., et al. (2019). Expression and purification of recombinant human insulin from *E. coli* 20 strain *Protein Expr. Purif.* 157, 63–69. doi:10.1016/j.pep.2019.02.002



# Frontiers in Bioengineering and Biotechnology

Accelerates the development of therapies,  
devices, and technologies to improve our lives

A multidisciplinary journal that accelerates the  
development of biological therapies, devices,  
processes and technologies to improve our lives  
by bridging the gap between discoveries and their  
application.

## Discover the latest Research Topics

See more →

### Frontiers

Avenue du Tribunal-Fédéral 34  
1005 Lausanne, Switzerland  
[frontiersin.org](https://frontiersin.org)

### Contact us

+41 (0)21 510 17 00  
[frontiersin.org/about/contact](https://frontiersin.org/about/contact)



Frontiers in  
Bioengineering  
and Biotechnology

